2020

Influence of osmotic suction on the shear strength of root-permeated soil

Balagalla Ralalage Pubudu Manora Jayathilaka
University of Wollongong

UNIVERSITY OF WOLLONGONG AUSTRALIA

Influence of osmotic suction on the shear strength of root-permeated soil

Balagalla Ralalage Pubudu Manora Jayathilaka
[BSc. Eng. (Hons)]

Supervisors:
Distinguished Professor Buddhima Indraratna
Dr Ana Heitor

This thesis is presented as part of the requirement for the conferral of the degree:
Doctor of Philosophy

This research has been conducted with the support of the
Australian Government Research Training Program Scholarship

University of Wollongong
School of Civil, Mining and Environmental Engineering

June 2020

ABSTRACT

Most civil infrastructure is built on and remain under unsaturated conditions for most of its service life, so the longevity of those structures depends on the actual strength or bearing capacity of the subgrade soil. Incorporating unsaturated soil mechanics into construction practices has become challenging due to lack of understanding, especially of the mostly saline soils prevalent along the coastal belt of Australia. Omitting the benefits of salinity based osmotic suction and the influence of tree roots can lead to undue design conservatism. Previous studies have proven that the matric suction and root reinforcement influence the shear strength of natural or compacted soil, however the number of studies that focussed on the role of osmotic suction with or without the influence of tree roots are limited.

The concept of green corridor or the use of native vegetation in the railway industry has become more popular over the past few decades because they are sustainable, environmentally friendly, cost-effective, long-lasting, and provide wind protection and noise barriers. Most importantly, tree roots can significantly increase the shear strength of soil because of the additional matric suction induced by root water uptake, and root reinforcement. However, the contribution that tree roots has on the shear strength of soil under coastal environmental conditions (or with osmotic suction) is yet to be investigated and discussed comprehensively.

In this study, a series of small scale direct shear tests was carried out at various levels of osmotic (0, 910, 1790, 2700, 3690, 4650 and 9560 kPa) and matric (0, 25, 100, 200, 500, 1000 and 1500 kPa) suctions to investigate the influence that osmotic suction has on the shear strength of compacted soil. The integrated behaviour of osmotic suction and root reinforcement on the shear strength of unsaturated soil was also investigated through a

series of large scale direct shear tests carried out at various levels of osmotic (0, 910, 1790, 2700, 3690, 4650 and 9560 kPa) and matric (0, 100 and 200 kPa) suction. The peak shear stress of soil increased as the osmotic suction increased under all matric suction conditions, whereas the contribution that root reinforcement has on the peak shear stress decreased due to osmotic suction or osmotic stress. The change in peak stress due to osmotic suction only was defined mathematically employing a new parameter χ_2, which is a function of the electrical conductivity ratio (*ECR*) and degree of saturation. The influence that osmotic suction has on tree roots and hence on shear strength was defined by another new parameter RAR_π, which is a function of *ECR* and the root area ratio at π = 0 kPa. The model predictions were in good agreement with the laboratory results, given that the proposed assumptions were still valid. Furthermore, electrical resistivity determinations were introduced to predict the soil water characteristic curve (SWCC) of specimens of undisturbed soil or in situ. Interestingly, the proposed electrical resistivity technique was able to capture the variation of suction and moisture variation of soil specimens due to root water uptake and transpiration.

The performance of an embankment for given subgrade conditions was monitored numerically using the finite element software PLAXIS 2D (2018) with regards to the changing osmotic and matric suction, and with and without the influence of tree roots. The equivalent parameters related to the change in peak shear stress due to matric suction, osmotic suction, and tree roots were estimated based on the proposed new models. All the analyses were carried out on a plain strain model with an axial load of 25 tonnes which would mimic a typical modern freight car. The stability of the embankment was investigated by means of the safety factor and settlement. The influence of osmotic suction and tree roots, when considered as separate components, increased the factor of safety and decreased the vertical deformation. However, in an integrated system, osmotic

suction had a negative effect on the growth of tree roots and hence reduced the contribution of tree roots on the shear strength of a soil system. The effect of the clearance length on the stability of the embankment was investigated; basically, the stability of the embankment decreased. Based on this numerical investigation, the optimum clearance length for a usual railway section was 25 m.

ACKNOWLEDGEMENT

Executing a doctoral thesis successfully is not due to an individual contribution or commitment; rather it takes place in a social context and includes several persons, whom I would like to thank sincerely.

First and foremost, I would like to express my sincere gratitude to my supervisor Distinguished Professor Buddhima Indraratna, for his unconditional support, invaluable suggestions, continuous encouragement and excellent guidance throughout this doctoral study. I would also like to acknowledge my co-supervisor Dr Ana Heitor, for her continuous assistance and insightful guidance provided during my PhD. Returning to full time academics after complete five years was itself challenging for me to cope with necessary studies, however the patience guidance and precious advice provided by my supervisors made my stay far more comfortable.

I am grateful for the financial assistance provided by the Australian Government Research Training Program Scholarship to carry out this research study. Also, the continuous support provided by the UOW technical staff Richard Berndt, Ritchie McLean and Duncan Best is highly appreciated. Further, I would like to extend my sincere thanks to all academic and administrative staff in the faculty of Engineering and Information Sciences and all colleagues at the University of Wollongong. Moreover, I am thankful to all my friends in Wollongong and suburbs for making this academic life far more enjoyable.

I would like to extend my sincere gratitude to my parents Balagalla Ralalage Jayathilaka and Chithra Piyaseeli for everything that they have done unconditionally in my life. Also, I would like to further extend my deepest gratitude to my parents in law, Anthony

Sarathchandra Peramuna and Anna Saparamadu for their continuous blessings and encouragements.

Last but not least, I would like to extend my sincere thanks to my loving wife Chesmin Melani Peramuna for her unconditional love, encouragement and care throughout this journey, and my son Sindun Sanumitha Jayathilaka and daughter Senaya Uvindi Jayathilaka for their beautiful smiles and for being with me all the time.

CERTIFICATION

I, Balagalla Ralalage Pubudu Manora Jayathilaka, declare that this thesis submitted in fulfilment of the requirement for the conferral of the degree Doctor of Philosophy, in the School of Civil, Mining and Environmental Engineering, Faculty of Engineering and Information Sciences, University of Wollongong, is wholly my own work unless otherwise referenced or acknowledged. The document has not been submitted for qualification at any other academic institution.

……..

B. R. P. M. Jayathilaka

20th June 2020

LIST OF PUBLICATIONS AND AWARDS

PUBLICATIONS

1. Jayathilaka, P, Indraratna, B & Heitor, A 2019, 'Influence that Osmotic Suction and Tree Roots has on the Stability of Coastal Soils', Geotechnics for Transportation Infrastructure, Springer, pp. 669-80.

2. Jayathilaka, P, Indraratna, B & Heitor, A. 'Influence of salinity based osmotic suction on the shear strength of a compacted clay', ASCE Journal of Geomechanics (Under Review)

3. Jayathilaka, P, Indraratna, B & Heitor, A. 'Coupled contribution of root reinforcement and osmotic stress on the shear strength of root-permeated soil'. (In Preparation)

AWARDS

1. Coffey-UOW Award for the Best Postgraduate performance in Geo-Technical Research, 2018.

2. IESL NSW Chapter Engineering Excellence Award (2018) in Best Paper Catogory – Highly Commended Award.

3. AGS NSW Research Award 2019: Got selected for the final four and presented in the finals (https://www.linkedin.com/feed/update/urn:li:activity:6563938141001089024/)

LIST OF SYMBOLS

Letters

A_D	:	A constant
A	:	Salinity threshold
A'	:	Cross sectional area
$(A-R)$	:	Net inter-particle stress generated due physicochemical effects
A_{S_i}	:	Average circumferential area of the cylindrical shape soil annulus for i^{th} root class
a	:	Experimental coefficient
B_D	:	A constant
B	:	Slope of the yield graph
B_{r/sl_i}	:	Bond stress between root and soil of the i^{th} root during pure slipping (no root breaking involved)
B_{r/sa_i}	:	Bond stress between root and soil of the i^{th} root during pulling out with a soil annulus
b	:	Experimental coefficient
C_c	:	Cation concentration
C	:	Sum of molar concentrations of all anions and cations in the solution
c	:	Experimental coefficient
c'	:	Effective cohesion
D	:	Diffusion coefficient
d_r	:	Root diameter
ECR	:	Ratio of electrical conductivity
EC	:	Electrical conductivity of saturated soil
$\mathrm{ECR_c}$	:	Minimum ECR value where χ_2 reaches its maximum or critical ECR
E	:	Young's modulus
EA	:	Axial stiffness
e_o	:	Initial void ratio
$F(T_p(t))$	:	Potential transpiration factor
$f(\psi(t))$	:	Soil suction factor
$G(\beta(t))$	:	Root density factor
h	:	Water pressure head
i	:	Root diameter class
K'	:	Geometric factor
k_1	:	Experimental coefficient
k_4	:	Experimental coefficient
k_z	:	Permeability function along the vertical direction
L	:	Length
n	:	Number of tree roots for the given diameter class
n_1	:	Number of roots that slipped without breaking during shearing
n_2	:	Number of broken roots during shearing

n_3	:	Number of roots slipped with the soil annulus during shearing
OP_{fc}	:	Osmotic potential of the soil water extracted from root zone at field capacity
p_v	:	Partial pressure of water vapour
p_{vo}	:	Saturation pressure of pure water vapour
R	:	Universal gas constant
R_T	:	Total resistance
R_m	:	Radius of curvature of the meniscus
R_e	:	Retardation coefficient
RAR	:	Root area ratio
RAR^0	:	Root area ratio when the osmotic stress is 0 kPa
RAR_π	:	RAR with respect to pore water salinity or osmotic stress
s	:	Matric suction
S	:	Rate of tree root water uptake
S_{max}	:	Maximum of rate of tree root water uptake
S_r	:	Degree of saturation
S_{res}	:	Degree of saturation at residual state
S_{sat}	:	Degree of saturation at full saturation
T	:	Absolute temperature
T_c	:	Surface tension of the air water interface
T_p	:	Potential transpiration
T_R	:	Tensile strength of a root
T_{r/st_i}	:	Maximum root tensile strength for the i^{th} root (root tensile strength at
t	:	Time
t_R	:	Additional tensile strength due to tree roots per unit area of soil
u_w	:	Pore water pressure
u_a	:	Pore air pressure
u_y	:	Vertical deformation
V	:	Electric potential
VD_R	:	Root influenced maximum vertical displacement
w	:	Molecular mass of water vapour
x_{DDL}	:	Distance from the electrically charged surface
Y_r	:	Relative yield
z	:	Vertical direction

Greek Letters

α_1	:	Positive empirical coefficient that depend on type species
α_2	:	Positive empirical coefficient that depend on type species
β	:	Deformed root orientation to the sharing plane
β_R	:	Root density
θ	:	Volumetric water content
θ_c	:	Contact angle of the meniscus with capillary tube to the vertical direction
θ_d	:	Minimum moisture content when $S = S_{max}$
θ_r	:	Residual volumetric water content
θ_s	:	Volumetric water content at saturation
θ_{sat}	:	Saturated moisture content
θ_w	:	wilting point moisture content
λ_1	:	Experimental coefficient
λ_2	:	Experimental coefficient
ν	:	Poisson's ratio
π	:	Osmotic suction
ρ	:	Resistivity of the material which is considered as a material specific
ρ_{app}	:	Apparent resistivity
ρ_w	:	Density of water
σ	:	Total stress
σ'	:	Effective stress
τ'	:	Shear strength of saturated soil
τ_f'	:	Shear stress on the failure envelope
$\Delta\tau_R$	:	Additional increase in shear strength due to root permeation
$\Delta\tau_s$	:	Additional increase in shear strength due to soil matric suction
τ_U'	:	Shear strength of unsaturated soil
τ_{US}'	:	Shear strength of unsaturated-saline soil
v	:	Specific volume of water
v_D	:	Darcy velocity
ϕ'	:	Effective friction angle
ϕ^b	:	Angle with respect to change in matric suction or basic friction angle
ϕ_d	:	Dilatancy angle
χ_1	:	Effective stress parameter which depends on the matric suction
$\chi_{2_{max}}$	:	Maximum theoretical value of χ_2
χ_m	:	Ratio of sectional area of meniscus water to that of the soil mass
ψ	:	Suction
ψ_{an}	:	Lowest value of ψ
ψ_{max}	:	Maximum value of ψ
ψ_w	:	Suction at wilting point

Abbreviations

AEV	:	Air entry value
CW	:	Constant water content
DDL	:	Diffuse Double Layer
DST	:	Direct shear test
DLVO	:	Derjaguin-Landau-Verwey-Overbeek
LVDT	:	Linear variable differential transformer
LDST	:	Large scale direct shear test
MDD	:	Maximum dry density
OMC	:	Optimum moisture content
RH	:	Relative humidity
SWCC	:	Soil water characteristic curve
UTM	:	Universal Testing Machine

TABLE OF CONTENTS

ABSTRACT i

ACKNOWLEDGEMENT iv

CERTIFICATION vi

LIST OF PUBLICATIONS AND AWARDS vii

LIST OF SYMBOLS viii

TABLE OF CONTENTS xii

LIST OF FIGURES xvii

LIST OF TABLES xxv

CHAPTER 1: Introduction 1

1.1 Background 1

1.1.1 Railway network in Australia 1

1.1.2 Native vegetation as a geotechnical approach 3

1.2 Research Motivation 4

1.3 Research objectives 5

1.4 Thesis Outline 6

CHAPTER 2: Literature review 8

2.1 Background 8

2.2 Behaviour of unsaturated soil 8

2.2.1 Overview of unsaturated soil 8

2.2.2 Soil suction 9

2.2.2.1 Matric suction 9

2.2.2.2 Osmotic suction 12

2.2.2.3 Suction measurement 12

2.2.3 Soil water characteristic curve 13

2.2.4 Shear strength 15

2.3 Physiochemical influence in soil 17

2.3.1 Overview of physiochemical interaction with soil 17

2.3.2 Diffusive double layer and zeta potential....18
2.3.3 Physiochemical influence on soil water interaction....20
2.3.4 Influence of osmotic suction on shear strength....21
2.4 Use of bio-engineering for geo-engineering....22
2.4.1 Mechanism of root water and nutrient uptake....23
2.4.1.1 Root water uptake....23
2.4.1.2 Nutrient uptake....29
2.4.2 Influence of pore water salinity on tree roots....30
2.4.3 Root systems....32
2.4.4 Influence of root water uptake on SWCC....33
2.4.5 Soil reinforcement by tree roots....37
2.5 Using electrical resistivity in geotechnical engineering....40
2.5.1 Electrical resistivity with soil salinity....44
2.6 Summary....46
CHAPTER 3: Experimental procedure....48
3.1 Background....48
3.2 Preliminary experiments....49
3.2.1 Soil sampling....49
3.2.2 Preliminary tests....50
3.2.3 Filter paper test to determine SWRC....50
3.2.4 Use of WP4C potentiometer to measure osmotic suction....52
3.2.5 Using an SR-2 resistivity meter to measure electrical conductivity....53
3.3 Determining the influence of osmotic suction on the shear strength of soil (without roots)....54
3.3.1 Soil specimen preparation....54
3.3.2 Small scale direct shear test....55
3.4 Determining how osmotic suction influences on the shear strength of root permeated soil....57
3.4.1 Selection of plant species....57
3.4.2 Soil specimen preparation....58
3.4.3 Large scale direct shear test (LDST)....60

3.5 Root are ratio (RAR) and Root tensile strength test 64
3.6 Electrical resistivity in vegetated soil 65
3.7 Variation of matric suction in soil with tree roots 66
3.8 Summary 67
CHAPTER 4: Results and discussion 68
4.1 Background 68
4.2 Preliminary soil properties 68
4.3 Influence of osmotic suction on the shear strength of soil (without roots) 72
4.3.1 Influence of osmotic suction under saturated conditions 72
4.3.2 Influence of osmotic suction in unsaturated conditions 74
4.3.3 Peak shear stress 78
4.4 Influence of osmotic suction on the shear strength of root permeated soil 80
4.4.1 Influence of osmotic suction on root-only shear strength 86
4.5 Root tensile strength 88
4.6 Root area ratio 91
4.7 Influence of tree root induced suction on SWCC 92
4.8 Electrical conductivity and soil suction 95
4.9 Summary 96
CHAPTER 5: Development of a new shear strength model 98
5.1 Background 98
5.2 Shear strength model considering the role of osmotic suction 99
5.2.1 Sensitivity analysis of χ_2 101
5.2.2 Experimental determination of χ_2 106
5.2.3 Model calibration and validation 107
5.3 Shear strength model for root permeated soil 112
5.3.1 Sensitivity analysis of $\boldsymbol{RAR_\pi}$ 116
5.3.2 Model prediction of shear strength contribution by tree roots 119
5.3.3 Model calibration and validation 125
5.3.4 Limitations of the model 127

5.4 Summary 127
CHAPTER 6: Numerical simulation on a practical application 129
6.1 Background 129
6.2 Analysis using PLAXIS 130
6.2.1 Material model in FEM 131
6.2.2 Generation of element mesh in PLAXIS 2D 131
6.2.3 Root simulation 132
6.3 Rail embankment simulation using PLAXIS 2D 133
6.3.1 Model geometry 133
6.3.2 Initial calibration of the model 135
6.4 Simulating the field application 137
6.4.1 Properties of tree roots 138
6.4.2 Properties of subgrade soil and the embankment 139
6.4.3 Track geometry and material properties of the super structure 140
6.4.4 Loading 141
6.5 Results and discussion 142
6.5.1 Vertical deformation 142
6.5.2 Factor of safety 151
6.5.3 Influence of clearance length to the tree 157
6.5.3.1 Change in vertical deformation due to clearance length 159
6.5.3.2 Change in the factor of safety due to clearance length 162
6.6 Summary 165
CHAPTER 7: Conclusions and recommendations 167
7.1 Background 167
7.2 Specific observations 168
7.2.1 Development of a new model ($\boldsymbol{\chi_2}$) on saline shear strength 168
7.2.2 Development of a new model ($\boldsymbol{RAR_\pi}$) to characterise the influence of osmotic stress on root growth 170
7.2.3 Suction variation in a saline-vegetated environment 172
7.2.4 Numerical modelling with a FEM software PLAXIS 2D 173

7.3 Limitations of the study 175
7.4 Recommendations for future work 176
REFERENCES 177
APPENDIX A: Previous models for the shear strength of unsaturated soil 198
APPENDIX B: Determination of optimum electrode spacing 205

LIST OF FIGURES

Figure 1.1 Australian rail map (Source: Australian Railway Association (ARA), 2014) 2

Figure 1.2 Forested environment in Australia (Scarth et al. 2019).....2

Figure 1.3 Schematic diagram of a train line with vegetation 3

Figure 2.1 Capillary tube.....10

Figure 2.2 Capillary water and bulk water.....11

Figure 2.3 Soil water characteristic curve (SWCC) (Modified after Pasha et al. (2016)) 14

Figure 2.4 Extended Mohr-Coulomb failure criterion for unsaturated soil (Adopted from Fredlund et al., (1978)).....16

Figure 2.5 Cation interaction on a negatively charged clay surface 18

Figure 2.6 Diffusive double layer 19

Figure 2.7 Shear strength of a clay soil (Fully-saturated) with distilled water and saline water (Tiwari & Ajmera 2014) 21

Figure 2.8 Lateral migration of subgrade moisture and subsequent root water uptake and transpiration.....22

Figure 2.9 The process of root water uptake (Adopted from McElrone et al. (2013)) ..24

Figure 2.10 Root water uptake with respect to the volumetric moisture content (Adopted from Feddes et al. (1976)).....29

Figure 2.11 Major root systems (a) tap root, and (b) fibrous root 32

Figure 2.12 Common types of root architecture, (a) to (j) by Lynch (1995) and (k) by Ghestem et al. (2011) 33

Figure 2.13 Comparison of desorption SWCC between bare soil and vegetated soil (Modified after Leung, AK et al. (2015)) 34

Figure 2.14 Distribution of change of matric suction with distance from the centre of the tree trunk for different depths (Adopted from Pathirage et al. (2017))..... 35
Figure 2.15 Distribution of change of osmotic suction with distance from the centre of the tree trunk for different depths (Adopted from Pathirage et al. (2017))..... 36
Figure 2.16 Distribution of tensile strength with respect to root diameter for *Ulex europaeus L. (Ue)* (Adopted from Boldrin et al. (2017))..... 38
Figure 2.17 Increase of shear strength due to tree roots (Adopted from Pallewattha et al. (2019))..... 40
Figure 2.18 General electrode configuration for a typical four electrodes method 42
Figure 2.19 Current flow and equipotential surfaces for homogeneous and inhomogeneous subsurface (Modified after Herman (2001))..... 43
Figure 2.20 Distribution of electrical resistivity with volumetric water content 45
Figure 2.21 Distribution of electrical resistivity with volumetric water content for different levels of saline pore water (Modified after Kalinski and Kelly (1993)) 46
Figure 3.1 Sampling location, Wollongong NSW Australia (Adopted from, Maps of World (2013))..... 49
Figure 3.2 Filter paper test (Contact method) 51
Figure 3.3 WP4C Dewpoint Potentiometer 52
Figure 3.4 SR2 resistivity meter from Tinker and Rasor..... 53
Figure 3.5 Direct shear box (60 x 60 x 40 mm), (a) schematic diagram with instrumentation and (b) an image of the direct shear box..... 55
Figure 3.6 Modified top cap of the DST and the miniature pore water pressure transducer used to measure the matric suction 57
Figure 3.7 Schematic diagram of the soil box with plant 58
Figure 3.8 Soil compaction and planting in the soil box 60

Figure 3.9 Schematic diagram of LDST (Adopted from Pallewattha et al. (2019)).....62
Figure 3.10 Arrangement of sensor cables into the data logger.....63
Figure 3.11 Moisture evaporation control using cling wrap and wet gunny sacks.....63
Figure 3.12 Tensile strength test set up.....64
Figure 3.13 Resistivity tests set up with SR2 resistivity meter.....66
Figure 4.1 Particle size distribution curve.....69
Figure 4.2 Soil water characteristic curve (SWCC).....70
Figure 4.3 Distribution of electrical conductivity of saturated soil specimens with respect to pore water salinity.....71
Figure 4.4 Distribution of (a) shear stress and (b) vertical displacement, with horizontal displacement for saturated conditions (σ_N' = 10 kPa) 73
Figure 4.5 Distribution of shear stress with horizontal displacement for different initial matric suctions at various osmotic suctions (a) 0 kPa (b) 1790 kPa (c) 3690 kPa and (d) 9560 kPa osmotic suctions (σ_N' = 10 kPa).....75
Figure 4.6 Distribution of vertical displacement with horizontal displacement for different initial matric suctions at (a) 0 kPa (b) 1790 kPa (c) 3690 kPa and (d) 9560 kPa osmotic suctions (σ_N' = 10 kPa) 76
Figure 4.7 Distribution of maximum vertical displacement with respect to osmotic suction for different initial matric suctions (σ_N' = 10 kPa) 77
Figure 4.8 Distribution of peak shear stress with respect to osmotic suction for different initial matric suctions (σ_N' = 10 kPa).....79
Figure 4.9 Distribution of shear stress of soil specimens with tree roots (σ_N' = 10 kPa)81
Figure 4.10 Distribution of peak shear stress with and without tree roots.....82
Figure 4.11 The vertical displacement of vegetated soil specimens.....84

Figure 4.12 Distribution of maximum vertical displacement with respect to osmotic suction with and without the influence of tree roots 85
Figure 4.13 Distribution of root influenced peak shear stress with respect to osmotic suction for various initial matric suction 86
Figure 4.14 Distribution of root influenced vertical displacement with respect to osmotic suction for various initial matric suction 88
Figure 4.15 Tensile strength of tree roots with respect to root diameter 89
Figure 4.16 Distribution of maximum root diameter and maximum root tensile strength with respect to osmotic suction 90
Figure 4.17 Distribution of average root area ratio with respect to osmotic suction 92
Figure 4.18 Change of SWCC with and without the influence from tree roots (π = 0 kPa) 93
Figure 4.19 Comparison of SWCC under vegetated conditions for different osmotic suctions and non-vegetated conditions with 0 kPa osmotic suction 94
Figure 4.20 Distribution of electrical conductivity of soil specimens with tree roots, with respect to matric suction for different osmotic suctions 95
Figure 5.1 Sensitivity analysis of $\chi 2$ with respect to a 101
Figure 5.2 Sensitivity analysis of $\chi 2$ with respect to b 102
Figure 5.3 Distribution of critical ECR (ECR_c) with respect to coefficient b 103
Figure 5.4 Sensitivity analysis of $\chi 2$ with respect to c 104
Figure 5.5 Distribution of $\chi 2max$ with respect to coefficient c 105
Figure 5.6 Sensitivity analysis of $\chi 2$ with respect to the degree of saturation 106
Figure 5.7 Model calibration with s_i = 0 kPa, s_i = 200 kPa and s_i = 500 kPa (σ'_N = 20 kPa) 108

Figure 5.8 Experimental and model prediction results of $\chi 2$ for different initial matric suctions where a = 0.003, b = 0.0375 and c = 2.0, (a) $\sigma'_N = 10kPa$ and (b) $\sigma'_N = 40kPa$ 109

Figure 5.9 The experimental and model peak shear stress for different initial matric suctions and saturated osmotic suctions, (a) $\sigma'_N = 10kPa$ and (b) $\sigma'_N = 40kPa$.....111

Figure 5.10 Distribution of RAR with respect to ECR 114

Figure 5.11 Most common root failure patterns, a) slipping b) breaking and c) coupled with soil annulus (Pallewattha et al. 2019) 115

Figure 5.12 Sensitivity of $RAR\pi$ with respect to λ_1.....117

Figure 5.13 Sensitivity of $RAR\pi$ with respect to λ_2.....118

Figure 5.14 Sensitivity of $RAR\pi$ with respect to RAR^0.....119

Figure 5.15 Model prediction of root induced shear strength with respect to ECR for roots deformed at different angles.....120

Figure 5.16 Model prediction of root induced shear strength with the angle of deformed root for different osmotic stresses 122

Figure 5.17 Model prediction of root induced shear strength with ECR for different root diameters 123

Figure 5.18 Model prediction of root induced shear strength with root diameters for different osmotic stresses 124

Figure 5.19 Comparison of experimental and model results of root induced shear strength 125

Figure 5.20 Experimental and model prediction of root induced shear strength 126

Figure 6.1 Schematic diagram of the rail section of the study.....129

Figure 6.2 Mesh options in PLAXIS 131

Figure 6.3 Types of elements in PLAXIS 2D, (a) 15 nodes elements, and (b) 6 nodes elements.....132
Figure 6.4 Nodes and stress points in a geogrid element.....133
Figure 6.5 Diagram of PLAXIS 2D model.....134
Figure 6.6 Shear stress distribution of numerical model vs experimental results (s = 200 kPa and π = 4650 kPa).....137
Figure 6.7 Schematic diagram of a typical section of rail with the user defined embankment section.....138
Figure 6.8 Schematic diagram of the super structure and the embankment.....138
Figure 6.9 Graphical view of the distribution of vertical deformation, (a) π = 0 kPa and (b) π = 9560 kPa, for fully saturated conditions (without roots).....142
Figure 6.10 Graphical view of the distribution of vertical deformation, (a) π = 0 kPa and (b) π = 9560 kPa, for s = 100 kPa (without roots).....143
Figure 6.11 Graphical view of the distribution of vertical deformation, (a) π = 0 kPa and (b) π = 9560 kPa, for s = 200 kPa (without roots).....144
Figure 6.12 Change in maximum vertical deformation with respect to osmotic suction for different matric suctions (without roots).....145
Figure 6.13 Graphical view of vertical deformation (Fully-saturated), (a) without roots (π = 0 kPa), (b) with roots (π = 0 kPa) and (c) with roots (π = 95600 kPa).....146
Figure 6.14 Distribution of maximum vertical deformation (Fully-saturated) due to osmotic suction with and without roots.....147
Figure 6.15 Graphical view of vertical deformation (s = 100 kPa), (a) without roots (π = 0 kPa), (b) with roots (π = 0 kPa), and (c) with roots (π = 95600 kPa).....148
Figure 6.16 Graphical view of vertical deformation (s = 200 kPa), (a) without roots (π = 0 kPa), (b) with roots (π = 0 kPa), and (c) with roots (π = 95600 kPa).....149

Figure 6.17 Distribution of maximum vertical deformation due to osmotic suction with and without roots 150
Figure 6.18 Graphical view of the variation of incremental deformation ($|\Delta u|$) without roots (Fully-saturated), π = 0 kPa and (b) π = 9560 kPa 151
Figure 6.19 Distribution of factor of safety with respect to matric suction for various osmotic suctions (Without roots) 152
Figure 6.20 Graphical view of the change of $|\Delta u|$ (Fully-saturated), (a) without roots and (b) with roots 153
Figure 6.21 Graphical view of the distribution of $|\Delta u|$ (s = 100 kPa), (a) π = 0 kPa (without roots), (b) π = 0 kPa (with roots), (c) π = 9560 kPa (without roots) and (d) π = 9560 kPa (With roots) 154
Figure 6.22 Graphical view of the distribution of $|\Delta u|$ (s = 200 kPa), (a) π = 0 kPa (without roots), (b) π = 0 kPa (with roots), (c) π = 9560 kPa (without roots) and (d) π = 9560 kPa (With roots) 155
Figure 6.23 Factor of safety with respect to osmotic suction with and without roots .. 156
Figure 6.24 Factor of safety due to roots with respect to osmotic suction for various matric suctions 157
Figure 6.25 Schematic diagram of a rail track with different clearance lengths 158
Figure 6.26 Generated mesh diagram for various clearance lengths, (a) 5 m (b) 10 m (c) 15 m and (d) 25 m 158
Figure 6.27 The point of analysis for vertical deformation while determining the influence of clearance length 159
Figure 6.28 Graphical view of the distribution of vertical deformation (when s = 0 kPa and (kPa= 0 kPa) for various clearance lengths, (a) 5 m (b) 10 m (c) 15 m and (d) 25 m 160

Figure 6.29 3D distribution of vertical deformation with respect to clearance length and osmotic suction (Saturated).....161
Figure 6.30 Distribution of maximum vertical deformation with respect to osmotic suction for various clearance lengths (Saturated) 162
Figure 6.31 Graphical view of the distribution of $|u|$ (when s = 0 kPa and π = 0 kPa) due to changing clearance length, (a) 5 m (b) 10 m (c) 15 m and (d) 25 m 163
Figure 6.32 Distribution of factor of safety with respect to the clearance length (Fully-saturated).....164
Figure 6.33 Distribution of factor of safety with respect to osmotic suction (Fully-saturated).....165

LIST OF TABLES

Table 2.1 Suction measurement techniques (Adopted from Murray and Sivakumar (2010)) 13

Table 2.2 Salinity tolerance of some Australian native species (Adopted from Marcar et al. (1995)) 31

Table 2.3 Electrical resistivity depending parameters 41

Table 4.1 Measured osmotic suction of saturated soil specimens for different amounts of pore water concentrations 71

Table 6.1 Properties of input parameters for the DSS test in PLAXIS 2D 136

Table 6.2 Parameters for the root zone 139

Table 6.3 Properties of the subgrade soil (After Fatahi et al. (2010)) 140

Table 6.4 Properties of the embankment (Esmaeili et al. 2013) 140

Table 6.5 Material properties for the super structure (Indraratna et al. 2017) 141

CHAPTER 1: Introduction

1.1 Background

Over the past few decades, the increase in population has been driving research to find new approaches for optimising the development of infrastructure constructed on weak soils. This increasing demand for new methods has inspired geotechnical engineers to consider and plan for more durable, reliable and cost-effective techniques, including more environmentally friendly ground improvement techniques. Given the current trends towards decarbonisation, it is important to consider more sustainable techniques for stabilising soil, which is why native vegetation for soil stabilization has become an increasingly popular practice, in contrast to chemical treatment of soil. Most rail lines in Australia are driven along vegetated coastal areas; however current geotechnical design codes have not incorporated the influence of osmotic suction and root reinforcement.

1.1.1 Railway network in Australia

Australia has an extensive rail network covering over 44262 km of passenger, freight, interstate, and suspended services across standard, narrow, and broad gauges (Australian Railway Association (ARA), 2014) (Figure 1.1). Most of those rail lines are driven along fully or partly covered by native vegetation, especially along the eastern side of Australia that receives a relatively high annual rainfall (Figure 1.2). Due to the complexity and lack of knowledge of coastal-vegetated soil, the design codes focus mainly on foundation soil or subgrade, which means the benefits of root reinforcement and osmotic suction are underestimated, and therefore the cost of construction is higher.

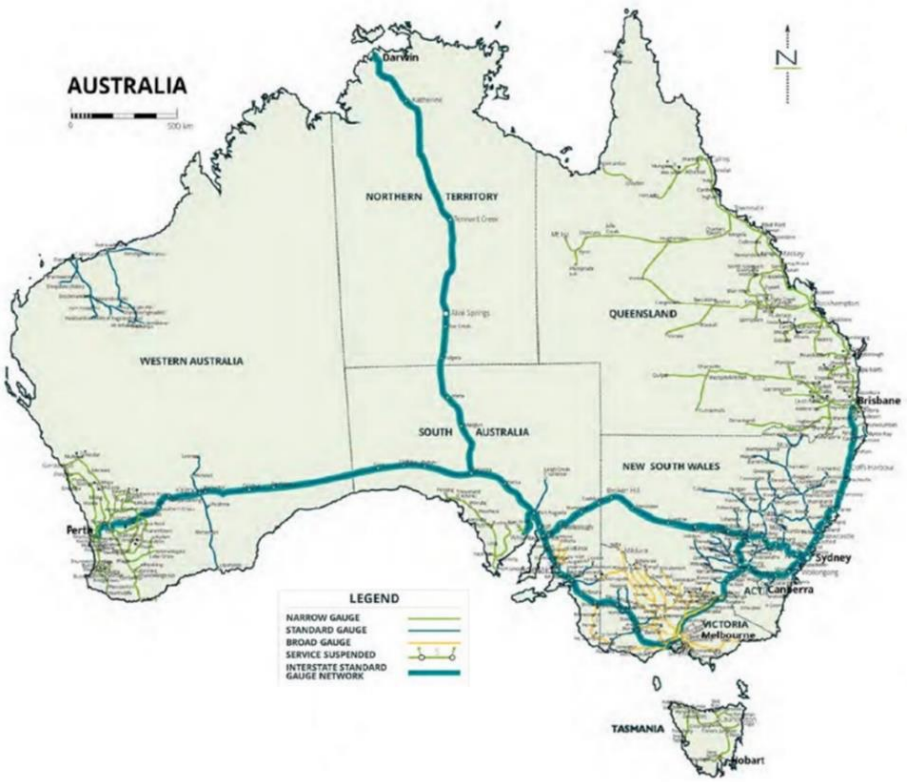

Figure 1.1 Australian rail map (Source: Australian Railway Association (ARA), 2014)

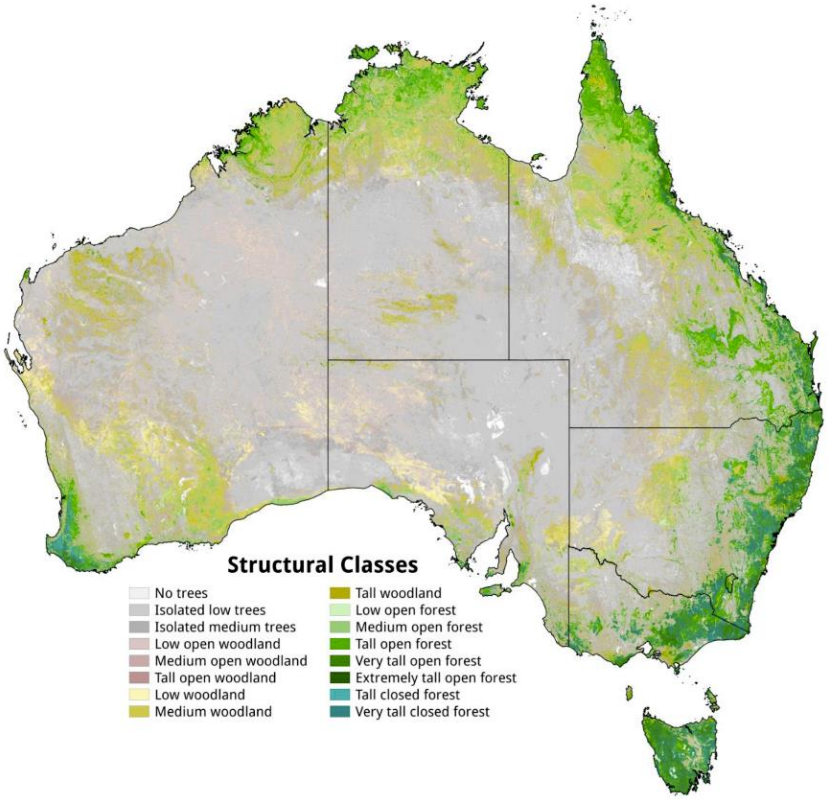

Figure 1.2 Forested environment in Australia (Scarth et al. 2019)

1.1.2 Native vegetation as a geotechnical approach

The use of native vegetation to stabilise soil slopes, embankments, earth retaining walls, and foundations, especially beside the rail lines (Figure 1.3) has been common practice since ancient times. However, due to the inception of rapid industrialisation during the 19th century, manmade materials such as concrete and steel have become increasingly popular. Over the last few decades, the importance of tree roots for ground improvement has become an emerging discipline in geotechnical engineering due to its favourable carbon footprint, low establishment costs, and insignificant maintenance. However, the lack of qualitative and quantitative knowledge on the mechanism of root water uptake and the strong interaction between roots and soil make this bioengineering approach a challenging topic in terms of computational efforts and design practices.

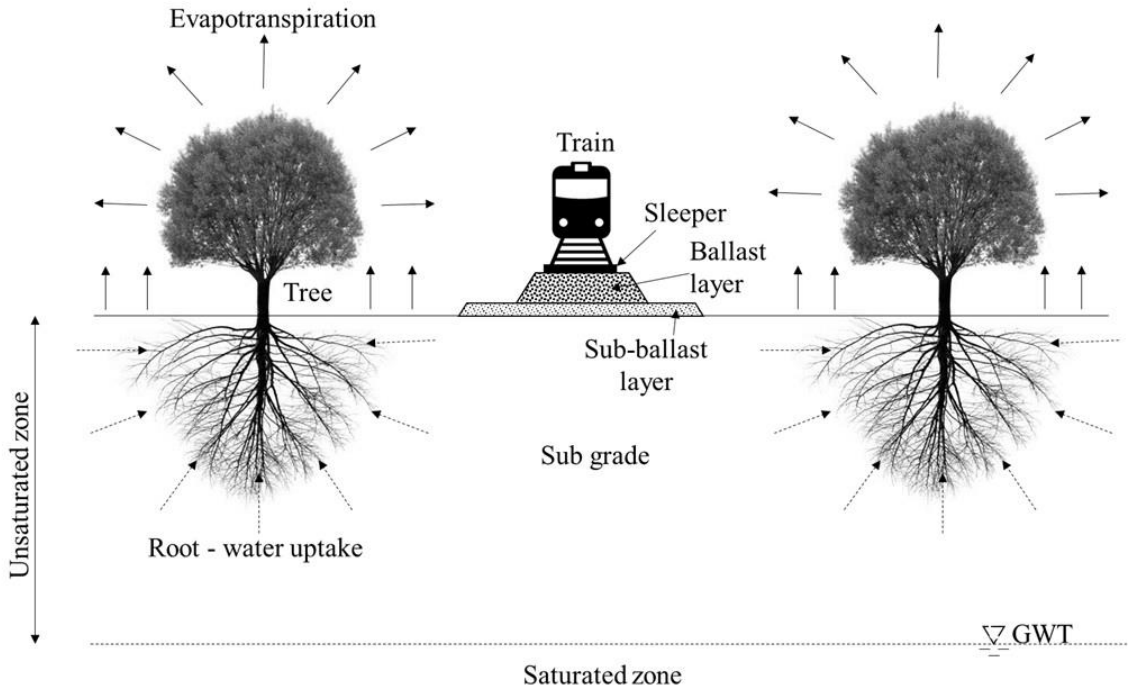

Figure 1.3 Schematic diagram of a train line with vegetation

Furthermore, conventional design practices do not consider the role of native vegetation and the osmotic influence caused by pore water salinity. These two components cannot be easily separated in a vegetated environment. Therefore, comprehensive research is crucial to characterise and quantify the contributions made by tree roots and osmotic suction. While most of past studies only considered the mechanical reinforcement of soil structure by the tree roots, some researchers have examined the role of water uptake mechanisms. However, to the writer's knowledge, no significant effort has been put into analysing the role of native vegetation combined with the effect of osmotic suction.

1.2 Research Motivation

Most types of civil infrastructure are built on and remain under unsaturated conditions for much of their service life, and therefore their long term stability depends on the shear strength of the foundation soil (subgrade). Extensive studies into the use of geosynthetics, prefabricated vertical drains with vacuum preloading, and chemical treatments have been carried out to enhance the shear strength of soil. However, most of these techniques are neither economically attractive nor considered the influence of osmotic suction. Moreover, neglecting the benefits of salinity and associated osmotic suction, especially along the coastal belt of Australia can lead to undue design conservatism after underestimating the actual bearing capacity or the strength of coastal soil. Some previous studies (Di Maio et al. 2004; Di Maio & Scaringi 2016; Fritz & Marine 1983; Tiwari & Ajmera 2014) have considered the effect of osmotic suction, but quantifying the role of osmotic suction on the stress-strain behaviour of unsaturated soil and the corresponding shear strength have further scope for advancement.

In most past studies on vegetated environments, the behaviour of soil is often characterised by (a) the intrinsic strength of soil fabric, (b) the reinforcement provided by the tree roots, and (c) the additional induced suction due to root uptake and associated

evapotranspiration. Previous reserchers (Docker & Hubble 2001; Fan & Su 2008; Pallewattha et al. 2019) have focused on the mechanical strengthening of subsurface soil due to tree roots, while others (Fatahi et al. 2014; Indraratna et al. 2006) have accounted for the strengthening of subsurface soil attributed to induced matric suction by evapotranspiration. However, only a few of these studies have analysed how pore water salinity or osmotic suction can affect the traditional soil water characteristic curve (SWCC) and the shear strength of the soil. This study, therefore, aims to examine the changes in the stress-strain behaviour of unsaturated saline soil (osmotically induced) as influenced by tree roots in contrast to saturated soils and those traditionally analysed with matric suction alone.

1.3 Research objectives

The main objective of this study is to introduce a new fundamental model that can capture the increase in shear strength of saturated and unsaturated soil due to osmotic suction and tree roots to enhance the geotechnical design. Two distinct series of small scale and large scale direct shear tests (with and without tree roots) subjected to varying levels of osmotic suction were carried out to investigate the influence of osmotic suction on the stress-strain behaviour of soil permeated with roots. The newly proposed shear strength model was independently calibrated and validated by experimental data. Commercially available finite element modelling software PLAXIS 2D (2018) was used to numerically simulate the influence of osmotic suction induced by tree roots in relation to a field application.

The specific objectives of this study are as follows;

1. Improve the understanding of the mechanisms associated with plant and soil interactions with and without osmotic suction in saturated and unsaturated soil.
2. Analyse the effect of osmotic suction on the shear strength and deformation of saturated and unsaturated soil.
3. Analyse the effect of osmotic suction on the efficiency of root systems (expressed in terms of the root area ratio (RAR)).
4. Monitor the variation in matric suction due to root water uptake with and without the influence of osmotic suction.
5. Develop a new theoretical model that captures the above mentioned concepts and mechanisms.
6. Numerically simulate the soil stress-strain behaviour with and without the influence of tree roots, where PLAXIS 2D being adopted to investigate the optimum distance between the toe of a rail embankment and the tree line (optimum clearance length).

1.4 Thesis Outline

This thesis is organised in seven chapters, as follows;

Chapter 1 introduces the research background, the scope and scientific challenges, and the principal objectives leading to an original PhD thesis.

Chapter 2 offers a critical and comprehensive literature review of previous studies with respect to the shear strength of soil under the influence of osmotic suction and root effects, corresponding to saturated and unsaturated soil conditions.

Chapter 3 presents the experimental program of a series of small scale (60 x 60 x 40 mm) direct tests used to determine how osmotic suction influences the stress-strain behaviour

of saturated and unsaturated silty clay. The variations of peak shear stress and deformation due to osmotic suction are discussed.

Chapter 4 describes a series of large scale (300 x 300 x 200 mm) direct tests used to determine the influence of tree roots and osmotic suction. It discusses the behaviour of peak shear stress and deformation as influenced by osmotic suction and tree roots.

Chapter 5 introduces two new theoretical models to capture soil shear strength. The first model primarily considers unsaturated-saline conditions where a new shear strength parameter (χ_2) is introduced in terms of electrical conductivity. The second model can capture the shear strength induced by tree roots due to osmotic suction under both saturated and unsaturated conditions. The way tree roots are distributed is described in terms of a new semi-empirical model, i.e. osmotically induced root area ratio (RAR_π).

Chapter 6 presents a numerical simulation of a field-based application using the finite element modelling software, PLAXIS 2D (2018). The variations of deformation and the factor of safety due to osmotic suction and root reinforcement are numerically simulated and analysed. Moreover, the effect of the tree line clearance length on the stability of a rail embankment is also presented.

Chapter 7 concludes the salient findings of this study and provides recommendations for future studies for advancing this field of research further.

CHAPTER 2: Literature review

2.1 Background

The focus of this chapter is to critically evaluate the current state of research related to the unsaturated behaviour of compacted clay using shear strength, water retention characteristics, root influence and physiochemical influence. The chapter begins with an introduction on the fundamentals of unsaturated soil, and different types and measurements of suction. Subsequently, a review of constitutive models available to describe the unsaturated shear strength of soil is presented. Thereafter, the micro-scale mechanisms and interactions between moisture and soil particles are discussed especially those relevant to saline conditions. Moreover, the role of native vegetation on strength and the water retention of soil is discussed. Finally, based on the current literature review, the expected contribution through this study is outlined.

2.2 Behaviour of unsaturated soil

2.2.1 Overview of unsaturated soil

Most types of infrastructure are built and remain under unsaturated conditions for most of their service life. Even though the mechanical behaviour of saturated soil has been well established using Terzaghi's (1936) theory of effective stress, the mechanical behaviour of unsaturated soil is still under investigation. In unsaturated soil, the voids are filled with air and water which can lead to distinct changes in the volume, strength, and hydraulic properties. The stresses acting on the soil skeleton mainly control the level of deformation and the failure mechanism, and hence the prediction of this settlement and deformation of infrastructure during service plays a major role in the construction industry

(Karube & Kawai 2001). Moreover, these stresses are primarily affected by the pore water and the capillary tension between soil particle and meniscus water which enhances bonding by inducing internal stress (Karube & Kawai 2001). This is why identifying the influence of pore water on the shear strength of unsaturated soil is critical for any further analysis of soil stability (Karube & Kawai 2001).

2.2.2 Soil suction

Soil suction is the potential energy of water with respect to pure water, which quantifies the potential of soil to adsorb and/or retain pore water (Likos & Lu 2003; Wagner et al. 1994); it is also referred to as total suction. Soil suction results from capillarity action, and the presence of ions, and its salt concentration in pore water (Bulut & Leong 2008). Ridley et al. (2003) pointed out that the effects of suction are common in all the ground conditions of soils that remain above the water table. The matric suction and osmotic suction are the most common components of affecting the magnitude of total suction, and also these two components are additive (Leong et al. 2007; Tang et al. 1997; Thyagaraj & Salini 2015).

$$\psi_T = s + \pi \tag{2.1}$$

where ψ_T is the total suction, s is the matric suction and π is the osmotic suction.

2.2.2.1 Matric suction

Matric suction is the most common parameter used in unsaturated soil mechanics, and it is influenced by capillarity effect, relative compaction, particle size, degree of saturation and soil particle texture. Fredlund et al. (2012) suggested that the matric suction can be defined as the equivalent suction measured from the partial pressure of the water vapour equilibrated with soil water in reference to that equilibrated with an identical composition of the solution to the soil water.

$$s = -\frac{RT}{vw}\ln(\frac{p_v}{p_{vo}}) \tag{2.2}$$

where s is the matric suction, p_v is the partial pressure of water vapour, p_{vo} is the saturation pressure of pure water vapour, R is the universal gas constant, T is the absolute temperature, v is the specific volume of water, and w is the molecular mass of water vapour.

The matric suction can be represented by the difference between pore water pressure and pore air pressure. In considering equilibrium at the air and water interface the difference in pressure across the meniscus of the capillary tube is a physical representation of the magnitude of matric suction (Figure 2.1).

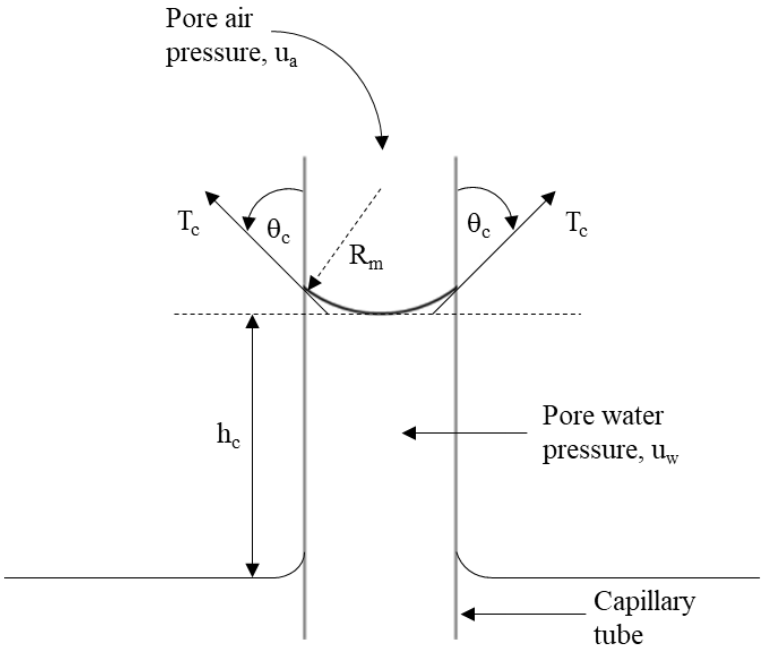

Figure 2.1 Capillary tube

$$s = (u_a - u_w) = h_c\rho_w g = \frac{2T_c}{R_m} \tag{2.3}$$

where R_m is the radius of curvature of the meniscus, T_c is the surface tension of the air-water interface, ρ_w is the density of water, θ_c is the contact angle of the meniscus with the capillary tube to the vertical direction, u_w is the pore water pressure, and u_a is the pore air pressure.

The pore water within soil particles can be classified as capillary water, adsorbed water (Zhou et al. 2016), and bulk water (Karube & Kawai 2001) (Figure 2.2). Under highly unsaturated conditions the pore water present at the contact points of the soil particles is called meniscus or capillary water (Karube & Kawai 2001). The contact stress of soil particles will be directly influenced by the presence of capillary water (Baker & Frydman 2009; Fuentesc & Triantafyllidisc 2013; Konrad & Lebeau 2015), which is why capillary is a major contributor to the shear behaviour of unsaturated soil. However adsorbed water has a negligible effect under unsaturated conditions (Baker & Frydman 2009; Konrad & Lebeau 2015; Lu et al. 2010; Xu 2004), because under an applied load, the bulk water can easily be drained out (Karube & Kawai 2001).

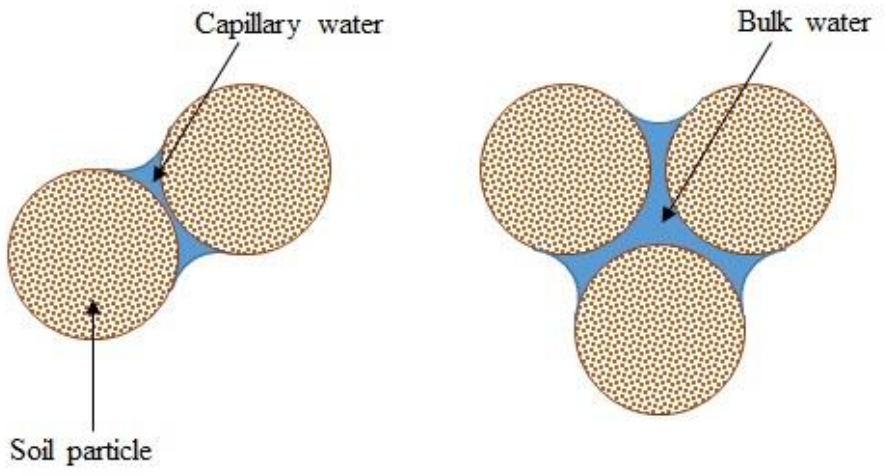

Figure 2.2 Capillary water and bulk water

2.2.2.2 Osmotic suction

The osmotic suction is generated due to the presence of salts in soil water (Agus & Schanz 2005; Krahn & Fredlund 1972; Thyagaraj & Rao 2010). The salt migrates into the soil by processes such as natural weathering of rock and soil, chemical spillage, infiltration from landfill leachate, and infiltration from brine ponds (Gidigasu 1974). Therefore, since salt can be present in the pore water under saturated and unsaturated conditions, the effect of osmotic suction must be considered for any moisture condition (Fredlund et al. 2012; Guimarães et al. 2013). Aitchison (1964) was the first to have a reasonable definition of osmotic suction, which is the equivalent suction measured out of the partial pressure of water vapour in equilibrium with a solution of identical composition to soil water (p_{v1}), compared to water vapour in equilibrium with pure water.

$$\pi = -\frac{RT}{vw}\ln(\frac{p_{v1}}{p_{vo}}) \tag{2.4}$$

Babu et al. (2005) pointed out that the general contribution of osmotic suction would be 25-60% of the total, therefore in notably saline soil (i.e. coastal soil) the contribution of osmotic suction on the strength of soil can be significant than matric suction.

2.2.2.3 Suction measurement

Over the last few decades, a number of experiments and techniques have been introduced to effectively quantify the suction in the soil. The range of measurements and their equilibration time are shown in Table 2.1.

Table 2.1 Suction measurement techniques

(Adopted from Murray and Sivakumar (2010))

Instrument	Measured Suction Component	Typical Range (kPa)	Equilibration Time
Pressure Plate	Matric	0 – 1,500	Several hours to days
Tensiometers and Suction probes		0 – 1,500	Several minutes
Thermal conductivity sensors		1 – 1,500	Several hours to days
Electrical conductivity sensors		50 – 1,500	Several hours to weeks
Filter paper contact		0 – 10,000 or greater	2 – 57 days
Filter paper non -contact	Total	1,000 – 10,000 or greater	2 – 14 days
Thermocouple psychrometers		100 – 8,000	Several minutes to several hours
Transistor psychrometers		100 – 70,000	About 1 hour
Chilled mirror psychrometers		1 – 60, 000	3 – 10 minutes
Electrical conductivity of extracted pore water by squeezing	Osmotic	Entire range	-

2.2.3 Soil water characteristic curve

The soil water characteristic curve (SWCC) can be defined as the relationship between a given amount of water in the soil pores expressed in terms of weight (gravimetric water content) or volume (volumetric water content) (Bai & Liu 2012; Fredlund et al. 2011), which can adequately describe the hydraulic properties and volumetric behaviour of unsaturated soil. The use of SWCC plays an important role in the characterisation of unsaturated soil such as the volume change characteristics, permeability, the coefficient of diffusion, and the adsorption and shear strength

(Fredlund & Rahardjo 1993; Frydman & Baker 2009; Li et al. 2007; Pham et al. 2005; Vanapalli, SK et al. 1996; Wissmeier & Barry 2008; Xiao et al. 2009). The SWCC primarily depends on the type of soil, the degree of compaction, the initial water content, the soil structure, texture, confining stress, density, stress history and mineralogy (Likos & Lu 2004; Marinho 2005; Ng & Pang 2000; Sreedeep & Singh 2008; Thakur et al. 2006; Thu et al. 2007; Vanapalli et al. 1999). Three major zones are defined in a conventional SWCC, the boundary effect zone, the transition zone, and the residual zone (Figure 2.3); moreover, the SWCC has two different paths, drying curve and the wetting curve. Only the drying curve will be considered in this study, and the hysteresis between wetting and drying curves will not be discussed. From this point onwards, the term soil water characteristic curve or SWCC will be used to indicate the drying path of the SWCC, unless stated otherwise.

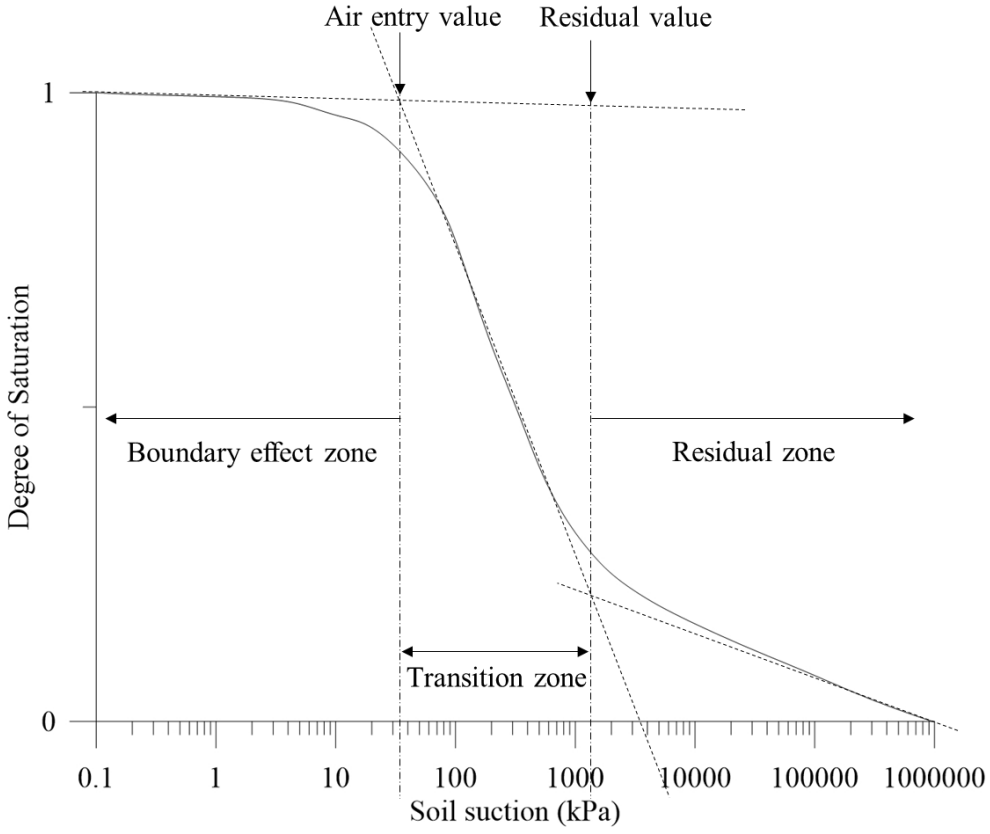

Figure 2.3 Soil water characteristic curve (SWCC) (Modified after Pasha et al. (2016))

The main parameters of the SWCC are the air entry value (AEV), the fully saturated water content, the residual water content, and the residual suction. The suction where the air starts to move into the largest pores in the soil on the drying path is called the air entry value. The water content of the soil at optimum saturation is designated as the saturated water content. The residual water content is the amount of water that does not decrease as the suction increases. This level of suction at the residual water content is designated as residual suction. The shape of the SWCC depends on the soil structure (Vanapalli, SK et al. 1996), the type of soil, and the particle size distribution (Fredlund et al., 2002).

2.2.4 Shear strength

Terzaghi's (1936) effective stress principle was applied for saturated conditions when pore space was filled only with water (Karube & Kawai 2001).

$$\sigma' = \sigma - u_w \tag{2.5}$$

where σ' is the effective stress, σ is the total stress and u_w is the pore water pressure.

Bishop (1959) studied the mechanical behaviour of unsaturated soil using suction controlled tri-axial compression tests and observed the behaviour of net normal stress and the suction component. The effective stress is a summation of the contribution made by externally applied stress and internally generated fluid pressure that can be used to transform the actual multi-stress and multi-phase state porous medium into a mechanically equivalent single stress and single-phase state continuum where the principle solid mechanics can be applied (Bishop 1959).

$$\sigma_{ij}' = \sigma_{ij} + \chi_m(u_a - u_w) \tag{2.6}$$

where $\sigma_{ij}{}'$ is the effective stress of a point on a solid skeleton, σ_{ij} is the total stress in the porous medium at the point, u_a is the pore air pressure, χ_m is the ratio of the sectional area of meniscus water to the soil mass, and u_w is the pore water pressure.

Bishop (1959) further reported that Equation 2.6 can be coupled with Terzaghi (1936)'s Mohr-Coulomb failure criterion on effective stress. This combination of effective stress and the Mohr-Coulomb failure criterion was further extended by Fredlund et al. (1978), and it is often referred as "extended Mohr-Coulomb failure envelope" (Figure 2.4).

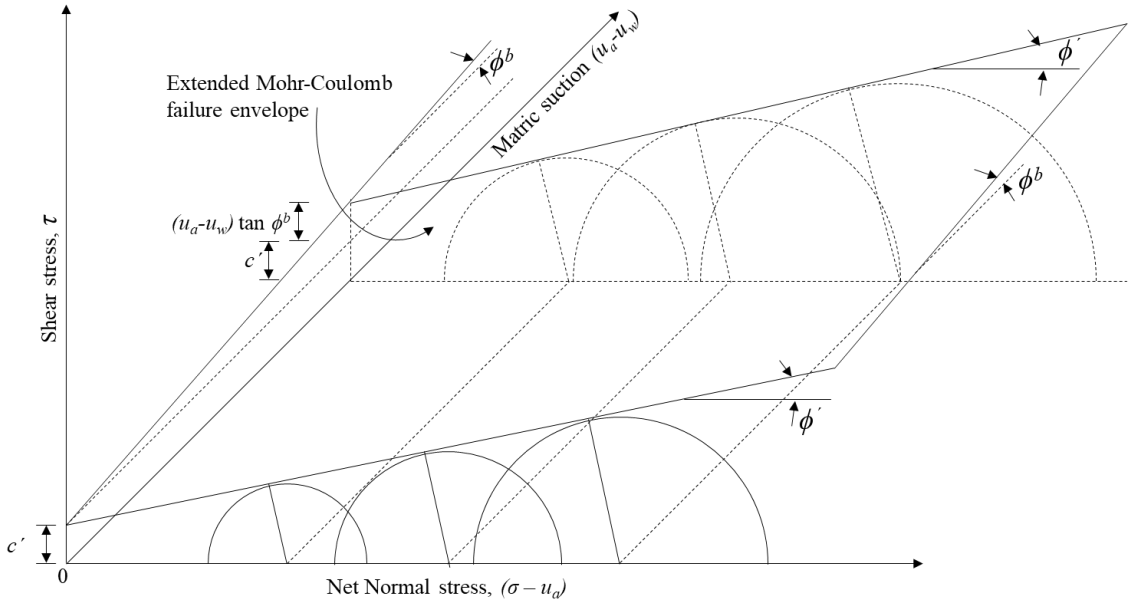

Figure 2.4 Extended Mohr-Coulomb failure criterion for unsaturated soil

(Adopted from Fredlund et al., (1978))

$$\tau_f' = c' + \sigma' tan\, \phi' + (u_a - u_w) tan\, \phi^b \quad (2.7)$$

where τ_f' is the shear stress on the failure envelope, c' is the effective cohesion, σ' is the effective normal stress, ϕ' is the effective friction angle and ϕ^b is the angle with respect to the change in matric suction or basic friction angle.

Oloo and Fredlund (1996) reported that the characterisation of ϕ^b is complex, time consuming, and not readily available. Therefore, Vanapalli, SK et al. (1996) extended the Fredlund et al. (1978)'s shear strength model by keeping the traditional Mohr-Coulomb framework with just one equivalent friction angle.

$$\tau' = c' + \sigma' \tan \phi' + (u_a - u_w) \tan \phi' \left(\frac{\theta - \theta_r}{\theta_s - \theta_r}\right) \quad (2.8)$$

where θ_r is the residual volumetric water content and θ_s is the volumetric water content at saturation.

Murray and Sivakumar (2010) demonstrated that the soil shear strength depends on the cohesion, the applied normal stress, and the suction components. To capture the actual unsaturated shear strength of soil, a number of researchers have introduced different shear strength models (Appendix-A), but the studies that have considered the influence of osmotic suction or the pore water chemistry on the shear strength are limited.

2.3 Physiochemical influence in soil

2.3.1 Overview of physiochemical interaction with soil

The surface of clay particles is negatively charged, due to imperfections on their surfaces, isomorphous substitution, and unsatisfied valence charges on the edges of the particles. Electrostatic forces are generated between the negative surfaces and cations in the solution (Yong et al. 1992), so once clay particles come into contact with the fluid an ionic counter charge accumulates at the surface of the clay particle to maintain electric

neutrality (Schmitz 2006). This electrically neutral ionic surface around the clay particle is called the Diffuse Double Layer (DDL). Based on this theory, the distribution of ions at the clay surface is shown in Figure 2.5.

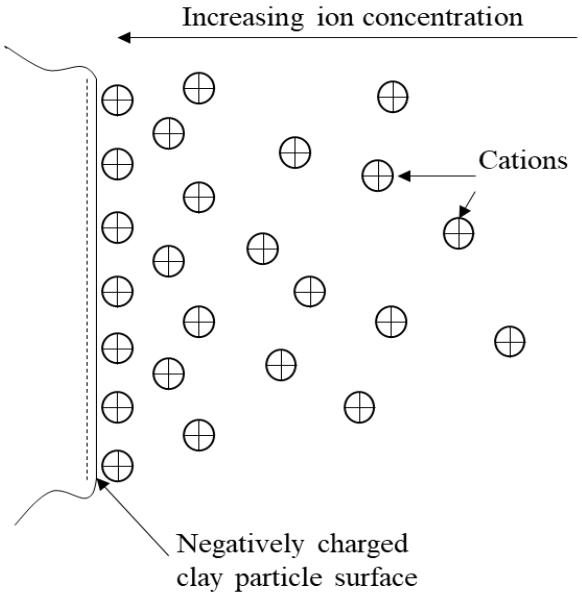

Figure 2.5 Cation interaction on a negatively charged clay surface

2.3.2 Diffusive double layer and zeta potential

The interaction of counterions with negatively charged clay particles forms a layer of electrically neutral ions called the Diffuse Double Layer (DDL) or Double Electric Layer (DEL) (Khamehchiyan et al. 2007; Mishra et al. 2009) (Figure 2.6), which is a combination of two layers, i.e. stern layer and diffusive layer. The potential difference between the inner surface of the stern layer and the outer surface of the diffusive layer is called the Zeta Potential. Ayenu-Prah (2004) reported that the thickness of the DDL would be less than 10^{-6} cm. In addition, Gouy (1910) also proposed a model for the thickness of the DDL as a function of electrolyte concentration at a constant surface potential.

$$x = A_D - B_D \ln C_c \tag{2.9}$$

where, C_c is the cation concentration, x is the distance from the electrically charged surface, and A_D and B_D are constants.

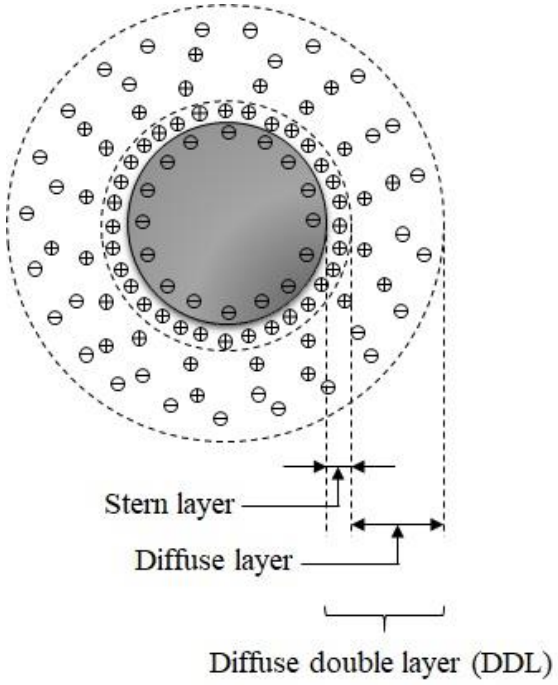

Figure 2.6 Diffusive double layer

Sudnitsyn et al. (2012) pointed out that the cations that contribute to the formation of DDL are spread all around but they retained tightly by the electrostatic attraction of a layer of counter ions, which generates an ion atmosphere nucleus. These cations form an osmotic force that would retain and absorb water into the soil surface due to cation hydration. This hydration energy or osmotic force can even reach to higher values and also can be influenced by the valency (Sudnitsyn et al. 2012). The magnitude of this energy would significantly surpass the hydrogen bonds and Van der Waals bonds in water molecules (Sudnitsyn et al. 2012). Also, Sudnitsyn et al. (2012) mentioned that the hydration energy of a solution with a different mix of solvents, will be collective.

2.3.3 Physiochemical influence on soil water interaction

The thickness of the DDL is directly proportional to the value of dielectric constant and inversely proportional to the concentration of salt (Schmitz 2006). The osmotic suction of a soil solution also depends on the concentration of salt, so there should be a distinct correlation to the DDL theory of pore fluid of a certain solution with the solution osmotic suction. Schmitz (2006) mentioned that all the individual particles are geometrically attached by electrostatic forces that strongly depend on the chemistry of the pore fluid and the particle surface charge. Van Olphen (1977) and Mansouri et al. (2013) mentioned that adding salt to the solution will have a negative effect on the electrokinetic mobility and diffuse double layer thickness, due to the decrease in repulsive forces between the clay particles. Therefore, the pore fluid chemistry can significantly contribute to the interparticle mobility and ion cloud. This can be illustrated by the Equation 2.9 where the spread of ions decreases as a result of increasing ion concentration. The effect of flocculation will be dominant if inter particle attractive forces exist (Van Olphen 1977). The most common attractive component is considered to be van der Waal's forces but they are generally small in magnitude and decay rapidly. When there is a collection of particles, the combined effect of attractive forces is the summation of all the van der Waal's forces, so for a bulky sample, the magnitude of van der Waal's forces is very high and will not decay rapidly (Van Olphen 1977). Therefore, clays with salt solutions will increase the aggregative stability of the particles and coagulate to reduce their volume, moisture capacity (Sudnitsyn et al. 2012). The possibility of clay soil being swelled, is higher in pure water than in salty solutions (Ayenu-Prah 2004; Gleason et al. 1997; Moore 1991; Shackelford et al. 2000; Sudnitsyn et al. 2012; Sumner & Naidu 1998), which is why the chemistry of pore water appears to be a controlling parameter of the stress-strain behaviour of soil.

2.3.4 Influence of osmotic suction on shear strength

The physiochemical properties of pore water affect heavily on the hydraulic and mechanical properties of soil. Fritz and Marine (1983) reported that the higher the cation exchange capacity and hence the lower the porosity, which then cause the osmotic suction to increase the strength of the soil. This was further validated by Rao and Thyagaraj (2007), Di Maio and Scaringi (2016) and Zhang et al. (2016). The experimental study on natural clays by Tiwari and Ajmera (2014) showed a significant increase in the shear strength as the salinity of pore water or osmotic suction increased (Figure 2.7).

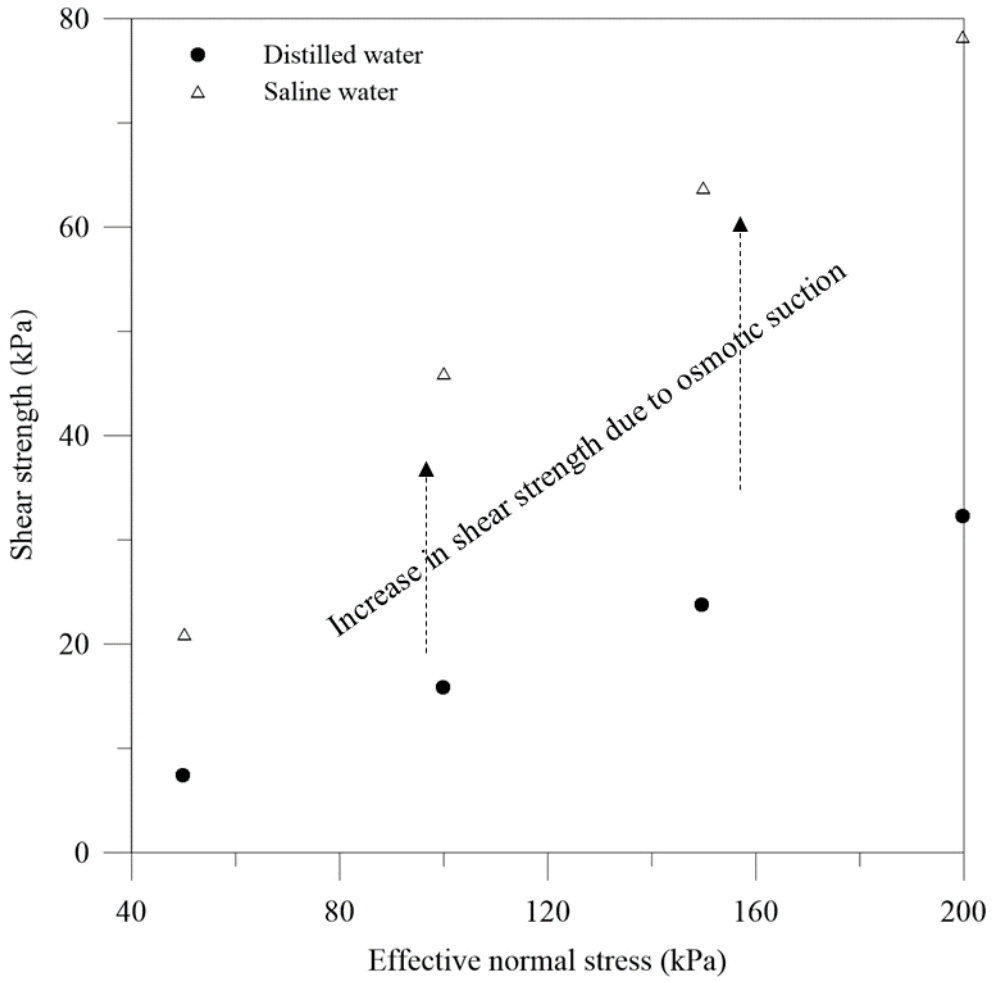

Figure 2.7 Shear strength of a clay soil (Fully-saturated) with distilled water and saline water (Tiwari & Ajmera 2014)

2.4 Use of bio-engineering for geo-engineering

Vegetation growing in the vicinity of rail tracks can assist in reducing the amount of moisture within the soil, by means of root water uptake and evapotranspiration (i.e. evaporation + transpiration) (Figure 2.8). Potter (2006) found that the soil suction under rail tracks with tree roots was higher than without tree roots, which is why the resilient modulus, the stiffness and strength of the underlying subgrade of rail track with tree roots were higher than the rail tracks without tree roots. Therefore, vegetation is a desirable way of reducing the moisture content of soil and increase its strength, however the use of vegetation as a soil strengthening mechanism has not yet been properly addressed.

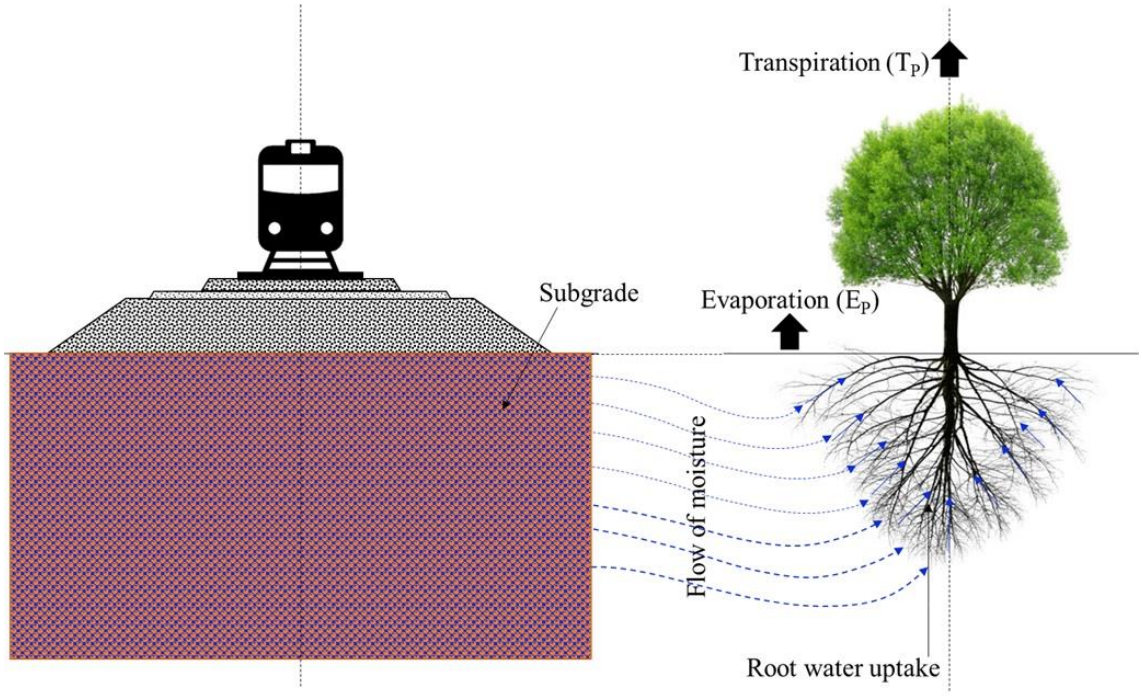

Figure 2.8 Lateral migration of subgrade moisture and subsequent root water uptake and transpiration

A number of past studies identified the effects of native vegetation with respect to enhancing the stability of soil (Fan & Chen 2010; Fatahi et al. 2015; Woon et al. 2011). Fan and Su (2008) classified the beneficial effects of native vegetation on soil stability as;

- Root reinforcement
- Soil moisture depletion
- Buttressing and arching

The root reinforcement mechanism and related qualitative and quantitative determinations have been broadly discussed previously (Docker & Hubble 2001; Gray & Leiser 1982; Indraratna et al. 2006; Ng, C et al. 2016). The tensile strength of roots can contribute an increase in the strength of the soil and therefore vegetated soil exhibits higher strength than soil without tree roots. In addition to root reinforcement, the root water uptake and transpiration also contribute to further increase in matric suction (Ng et al. 2013) and osmotic suction (Pathirage et al. 2017). While past research focused on the variation of matric suction due to root water uptake and transpiration (Leung, AK et al. 2015; Pallewattha et al. 2019), limited studies have been carried out to evaluate the role of tree roots on the shear strength of soil considering the influence from osmotic suction.

2.4.1 Mechanism of root water and nutrient uptake

Trees naturally absorb water and nutrients from the soil, and this mechanism is called root water and nutrient uptake.

2.4.1.1 Root water uptake

Water absorption by plant roots depends on the potential gradient between soil and root xylem (Figure 2.9). Kramer (1932) suggested that the potential gradient is characterised

by two major mechanisms based on the rate of transpiration, such as active absorption (driven by osmotic suction, due to nutrient uptake) and passive absorption (driven by matric suction).

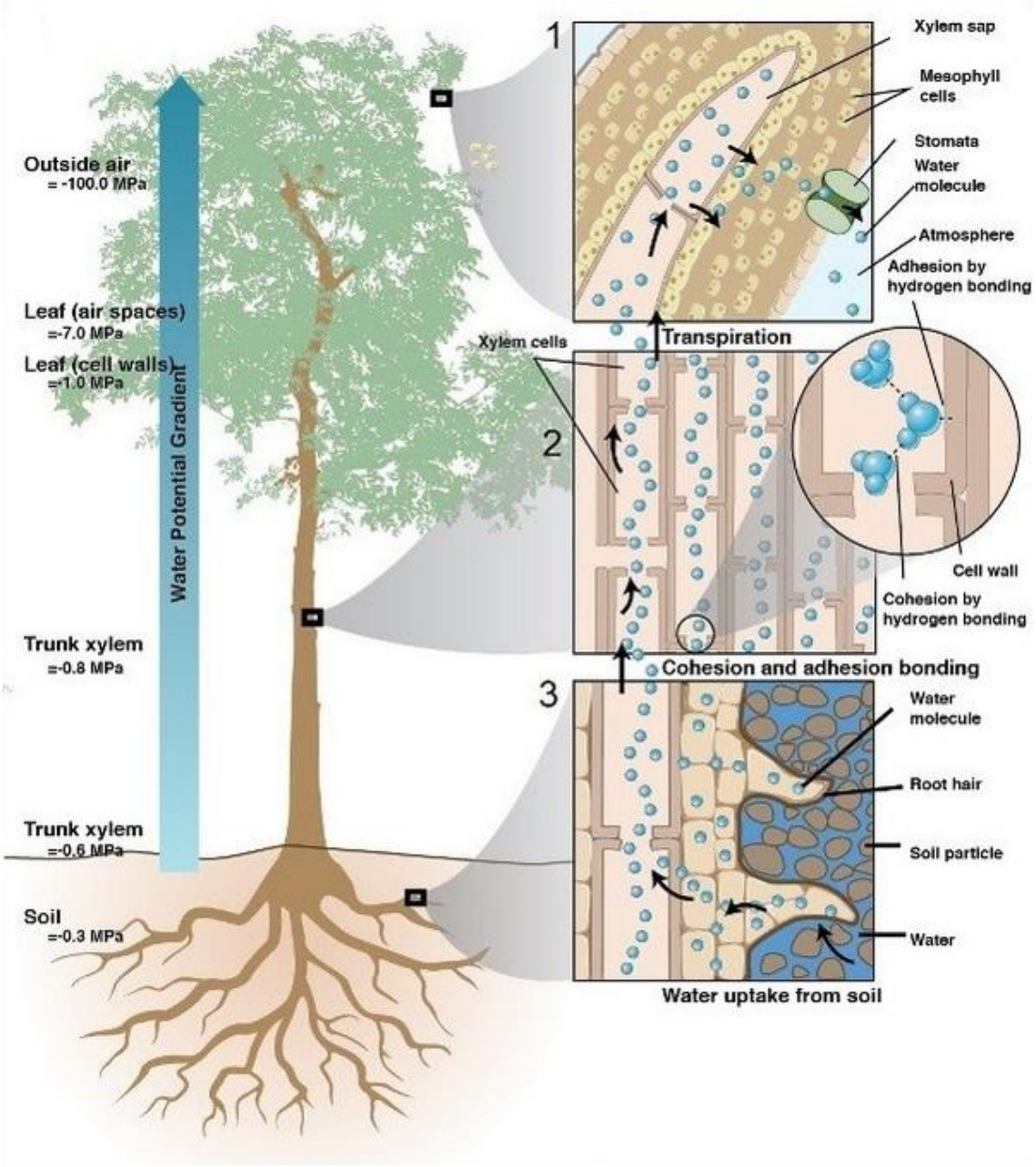

Figure 2.9 The process of root water uptake
(Adopted from McElrone et al. (2013))

Active absorption occurs when plants have a slow rate of transpiration such as during night time or on cloudy days, whereas passive absorption occurs when plants have a rapid transpiration rate such as during the day time. The mechanism of water uptake by plant roots is physically similar to the mechanism for extracting water on a pressure cell extractor where water flows until it reaches equilibrium with a certain pressure difference (Czyż & Dexter 2013). The only difference is the geometrical behaviour such as in the case of a pressure cell extractor where the water uptake is planar (soil sample) and in plant roots where the water uptake is considered to be an array of thin connected cylinders (Czyż & Dexter 2013). Measuring and evaluating the movement of water in soil with tree roots has been addressed in numerous past studies (Busscher & Fritton 1978; Fiscus 1975; Fiscus & Kramer 1975; Hillel & Talpaz 1976; Kleidon & Heimann 1998; Landsberg & Fowkes 1978; Milly 1997; Newman 1976; Protopapas & Bras 1993; Sanderson 1983; Zeng et al. 1998). Since the water potential is higher in soil than in root hair, soil is considered to be hypotonic and the root is considered to be hypertonic. The effect of osmosis takes place from a hypotonic medium to a hypertonic medium, and hence water translocate from the soil into the root. Water absorbed from soil is transferred to the xylem by an apoplast movement and a symplast movement. In addition, water can move by transcellular pathways, which is primarily because of the osmotic suction.

Water that is transported through the xylem vessels to the plant leaves can be described by Darcy's law, by assuming that the xylem is a porous medium (Siau 1984).

$$v = -k_x i_{r/l} \tag{2.10}$$

where v is the velocity of water, k_x is the water permeability of xylem and $i_{r/l}$ is the hydraulic gradient between the roots and leaves.

$$i_{r/l} = \frac{(h_l - h_r) + (l_r - l_{ps})}{(l_{ps} + l_r)} \tag{2.11}$$

where h_l is the hydraulic head of plant leaves, h_r is the hydraulic head in roots, l_r is the length of the roots, and l_{ps} is the length of the plant stem.

The total length of the water uptake is $l_{ps} + l_r$, and it can be determined by capillary theory (Nobel 2009). The capillary rise model proposed by Fredlund and Rahardjo (1993) can be used to determine the capillary height of the plant (assuming the contact angle of the plant cell wall is 0^0 and the temperature is 20^0.)

$$h_c = \frac{1.49 * 10^{-5}}{R_{xv}} \tag{2.12}$$

where R_{xv} is the radius of xylem vessel.

Based on the Capillary theory (Equation 2.12) the root water uptake for shorter plants (< 2 m) can be described by considering that the average xylem radius varies from 8 to 500 μm. However, trees can grow up to 100 m high or more, and yet the root water uptake still takes place. Hence, in addition to capillary theory, there should be some other mechanisms to lift water from the roots to much longer lengths. Hopkins (1999) proposed two mechanisms that facilitate root water uptake, one method was cohesion-adhesion theory and the other was root pressure. Here,

- Cohesive force is the attraction force between identical particles such as water-water molecules.
- Adhesive force is the attraction force between different particles such as water and lignin.

When the water molecules are lost by the stomata in the bottom surface of the leaf, water moves up to occupy that shortage of water. Since water molecules attract each other by

hydrogen forces (cohesively or adhesively), and are aided by capillary action, water is continuously pulled up by a process called transpiration. Weatherley (1970) and Radcliffe et al. (1980) pointed out that the percentage of water required for photosynthesis is considered to be negligible compared to total root water uptake, therefore it is reasonable to consider that the amount of moisture released by transpiration is equal to the total root water uptake by the plant.

Trees absorb water through their roots from the sub surface so that photosynthesis and transpiration process can take place, and hence the subsurface soil moisture content decreases. This water deficit generates a movement of water into the tree roots that results in an increase in matric suction, but this induced matric suction cannot be easily distinguished (Pallewattha et al. 2019). The root water uptake can be significantly influenced by the soil density (Ng et al. 2013), architecture and density of the roots (Feddes et al. 1978; Taylor & Klepper 1975), and the spatial distribution of root system (Kutílek & Nielsen 1994; Perrochet 1987; Prasad 1988). Fine roots are better of absorbing water and nutrients from the sub surface soil (Gwenzi et al. 2011), because the fine roots can penetrate the soil easily and increase the root-soil contact area, which is highly beneficial for root water uptake.

Considering all these factors, Indraratna et al. (2006) proposed an equation for estimating the rate of tree root water uptake (S).

$$S\,(x, y, z, t) = G(\beta(t))F(T_p(t))f(\psi(t)) \tag{2.13}$$

where, $G(\beta(t))$ is the root density factor, $F(T_p(t))$ is the potential transpiration factor, $f(\psi(t))$ is the soil suction factor.

$$G(\beta) = \frac{\tanh(k_1\beta(t))}{\int \tanh(k_1\beta(t))dV} \tag{2.14}$$

where, k_1 is an experimental coefficient.

$$F(T_p(t)) = \frac{T_p(t)(1 - k_4 z_{max} + k_4 z)}{\int G(\beta)(1 - k_4 z_{max} + k_4 z)dV} \tag{2.15}$$

where, k_4 is an experimental coefficient depends on depth in the rate of transpiration.

$$f(\Psi) \begin{cases} f(\psi) = 0 & \psi < \psi_{an} \\ f(\psi) = 1 & \psi_{an} \leq \psi < \psi_{max} \\ f(\psi) = \frac{\psi_w - \psi}{\psi_w - \psi_{max}} & \psi_{max} \leq \psi < \psi_w \\ f(\psi) = 0 & \psi_w \leq \psi \end{cases} \tag{2.16}$$

where, ψ_w is the suction at wilting point, ψ_{max} is the maximum value of ψ and ψ_{an} is the lowest value of ψ.

The volumetric change in moisture within the soil can be estimated by Richard's continuity equation.

$$\frac{\partial\theta}{\partial t} = \left[\nabla(k_z \nabla\psi) - \frac{\partial h}{\partial z}\right] - S(x, y, z, t) \tag{2.17}$$

where θ is the volumetric water content, k_z is the permeability function in a vertical direction, h is the water pressure head, z is the vertical direction, and t is the elapsed time.

Feddes et al. (1976) proposed a model to capture the change of root water uptake with respect to the volumetric water content in soil (Figure 2.10). The model clearly shows the

transition range of root water uptake and the maximum possible uptake range. Figure 2.10 shows that the rate of root water uptake gradually increases from zero to its maximum (S_{max}) as the moisture content increases from θ_w (the wilting point moisture content) to θ_d (the minimum moisture content when $S = S_{max}$). Note that the root water uptake is minimal when the soil is fully saturated.

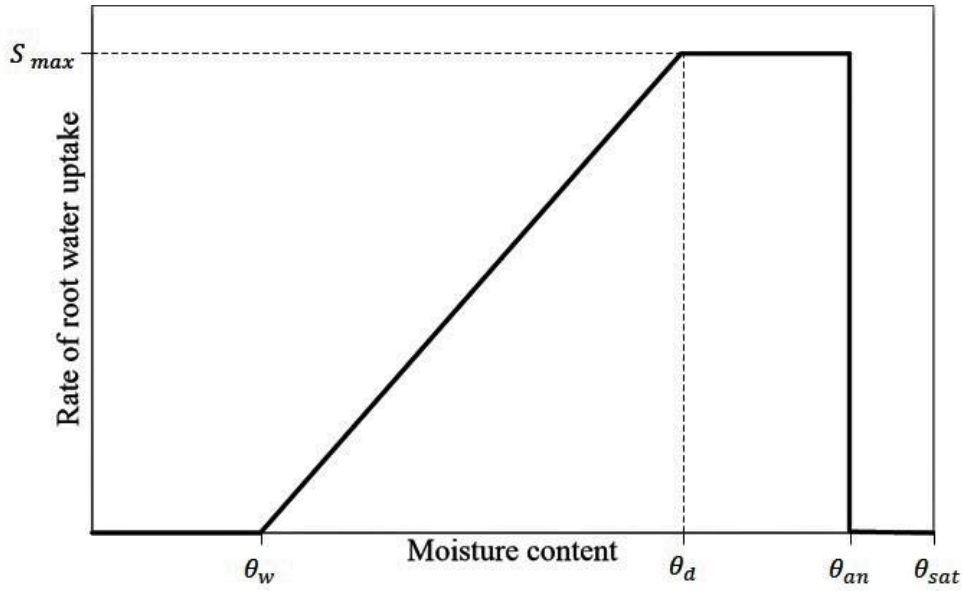

Figure 2.10 Root water uptake with respect to the volumetric moisture content (Adopted from Feddes et al. (1976))

2.4.1.2 Nutrient uptake

There are two major mechanisms that control the rate at which trees absorb minerals. In the passive drag mechanism the mineral concentration in the soil is higher than the root system and therefore minerals move by diffusion, whereas the active drag mechanism takes place when the mineral concentration is low compared to the root system, which is called convection. The most common mechanism is convection which induces an additional osmotic suction due to nutrient uptake. This nutrient behaviour of tree roots from soil can be described by Richard's advection and dispersion equation.

$$\frac{\partial(\theta R_e C)}{\partial t} = \nabla\left[\theta D \frac{\partial C}{\partial z} - v_D C\right] \tag{2.18}$$

where R_e is the retardation coefficient, C is the sum of molar concentrations of all anions and cations in the solution, D is the diffusion coefficient, and v_D is the Darcy velocity.

The nutrient uptake by the tree roots can generate an ion concentration gradient between root and soil, hence an additional osmotic suction can be induced. The intensity of this induced osmotic suction depends on the rate of nutrient uptake, height of the tree and the soil degree of saturation.

2.4.2 Influence of pore water salinity on tree roots

The presence of salinity in pore water or osmotic suction has been reported as a negative component on tree roots. According to the botanical investigations, osmotic stress has a negative impact on plant physiology (Colmer et al. 2006; Minhas et al. 2020; Shalhevet & Bernstein 1968), which is why the osmotic stress of tree roots has been monitored by previous researchers to identify the growth of species (root growth, leaf growth and shoot growth) in saline soil especially for agricultural purposes (Maas & Hoffman 1977; Shalhevet & Bernstein 1968; Skaggs et al. 2006; Memon et al. 2010; Qados 2011; Yilmaz & Kina 2008). For instance, Maas and Hoffman (1977) proposed a piecewise linear response function (Equation 2.19) for plant yield based on the osmotic potential.

$$Y_r = 100 - B(OP_{fc} - A) \tag{2.19}$$

where Y_r is the relative yield, OP_{fc} is the osmotic potential of the soil water extracted from root zone at field capacity, A is the salinity threshold expressed in bars and B is the slope expressed in percentage per bar.

In fact selecting a saline tolerant native species would be a challenge. Marcar et al. (1995) has listed some native plants in Australia with their surviving salinity levels (Table 2.2).

Table 2.2 Salinity tolerance of some Australian native species

(Adopted from Marcar et al. (1995))

Slight (2-4 dS/m)	**Moderate (4-8 dS/m)**	**Severe (8-16 dS/m)**	**Extreme (>16 dS/m)**
Acacia Mearnsii	All Luehmannii	Acacia Salicina	Acacia Ampliceps
Acacia Melanoxylon	All Verticillata	Casuarina Cristata	Acacia Stenophylla
Eucalyptus Aggregata	Casuarina Cunningghamiana	Casuarina Glauca	Casuarina Obesa
Eucalyptus Camphora	Eucalyptus Astringens	Eucalyptus Campaspe	Eucalyptus Kondininensis
Eucalyptus Cinerea	Eucalyptus Botryoides	Eucalyptus Occidentalis	
Eucalyptus Cladocalyx	Eucalyptus Brockwayi	Eucalyptus Sargentii	
Eucalyptus Cornut	Eucalyptus Camaldulensis	Eucalyptus Spathulata	
Eucalyptus Crenulata	Eucalyptus Coolabah	Melaleuca Leucadendra	
Eucalyptus Dumosa	Eucalyptus Largiflorens	Melaleuca Quinquenervia	
Eucalyptus Elata	Eucalyptus Leucoxylon		
Eucalyptus Globulus	Eucalyptus Melliodora		
Eucalyptus Grandis	Eucalyptus Moluccana		
Eucalyptus Ovata	Eucalyptus Platypus		
	Eucalyptus Polybractea		
	Eucalyptus Robust		
	Eucalyptus Rudis		
	Eucalyptus Tereticornis		
	Melaleuca Styphelioides		

2.4.3 Root systems

The shape, size, and spatial distribution of root systems have a significant influence on the root water uptake. In general, root system can differ based on the type of tree species. Two major root systems have been identified, a tap and a fibrous root system (Figure 2.11).

Figure 2.11 Major root systems (a) tap root, and (b) fibrous root

In addition to the root system and root size, the root architecture can also influence the water and nutrient uptake mechanism. The most common types of root architectures are shown in Figure 2.12. The type of root system and its architecture depends on the type of species, the soil texture and structure, the temperature, availability of moisture, and tree spacing, all of which can significantly influence the root water and nutrient uptake.

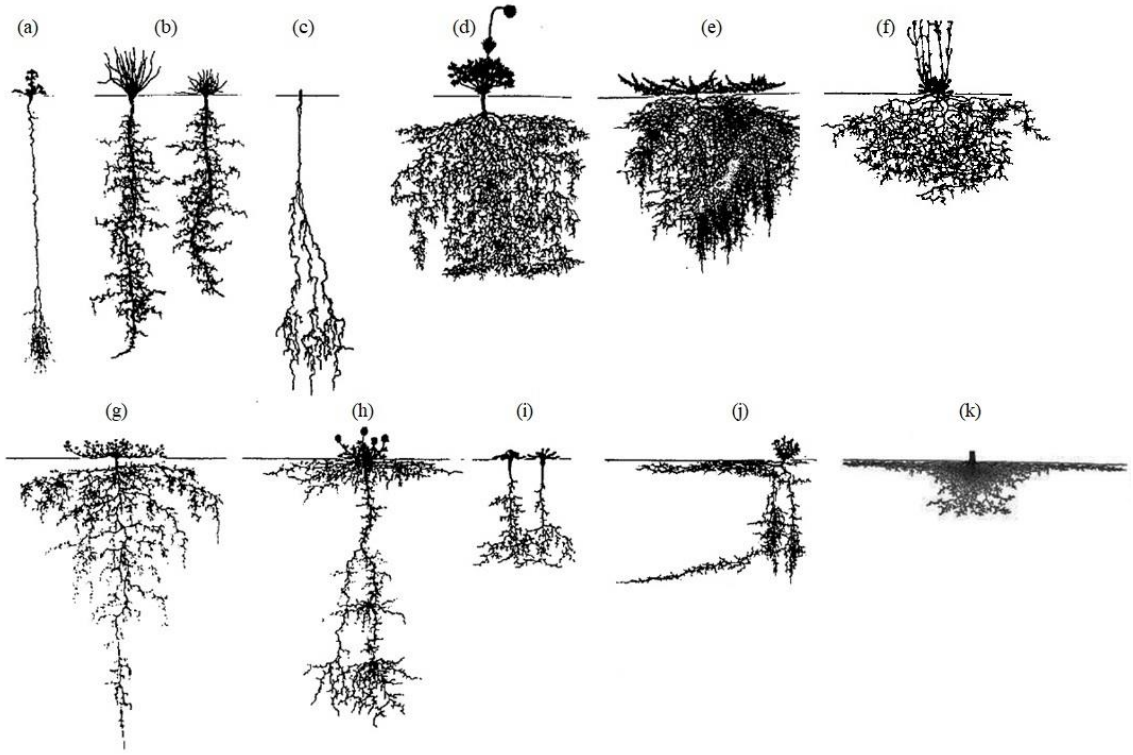

Figure 2.12 Common types of root architecture, (a) to (j) by Lynch (1995) and (k) by Ghestem et al. (2011)

2.4.4 Influence of root water uptake on SWCC

Extensive amounts of research have been carried out to investigate the effect of root water uptake on soil suction as it relates to slope applications (Ng et al. 2013; Rahardjo et al. 2014). All the researchers pointed out that plant roots can directly affect the hydraulic properties of soil, especially for the SWCC. The change of SWCC with the influence of tree roots depends on the type of species (Leung, A et al. 2015), the planting density (Ng, CWW, Ni, J, et al. 2016) , the soil density (Ng et al. 2013), and the leaf and root indices (Ng, CWW, Garg, A, et al. 2016). In addition, the factors that would affect the growth of trees such as weather conditions and pore water chemistry should also be considered to have an accurate SWCC for vegetated environments.

Leung, AK et al. (2015) considered the change of hydrological behaviours of completely decomposed granite (CDG) with a *Schefflera heptaphylla* species (Figure 2.13). Leung, AK et al. (2015)'s work concluded with three key points with SWCC when influenced by the tree root water uptake.

- The drying SWCC of bare soil is always below that of vegetated soil.
- AEV of bare soil is always less than vegetated soil.
- The rate of desorption is not affected by the influence of tree roots.

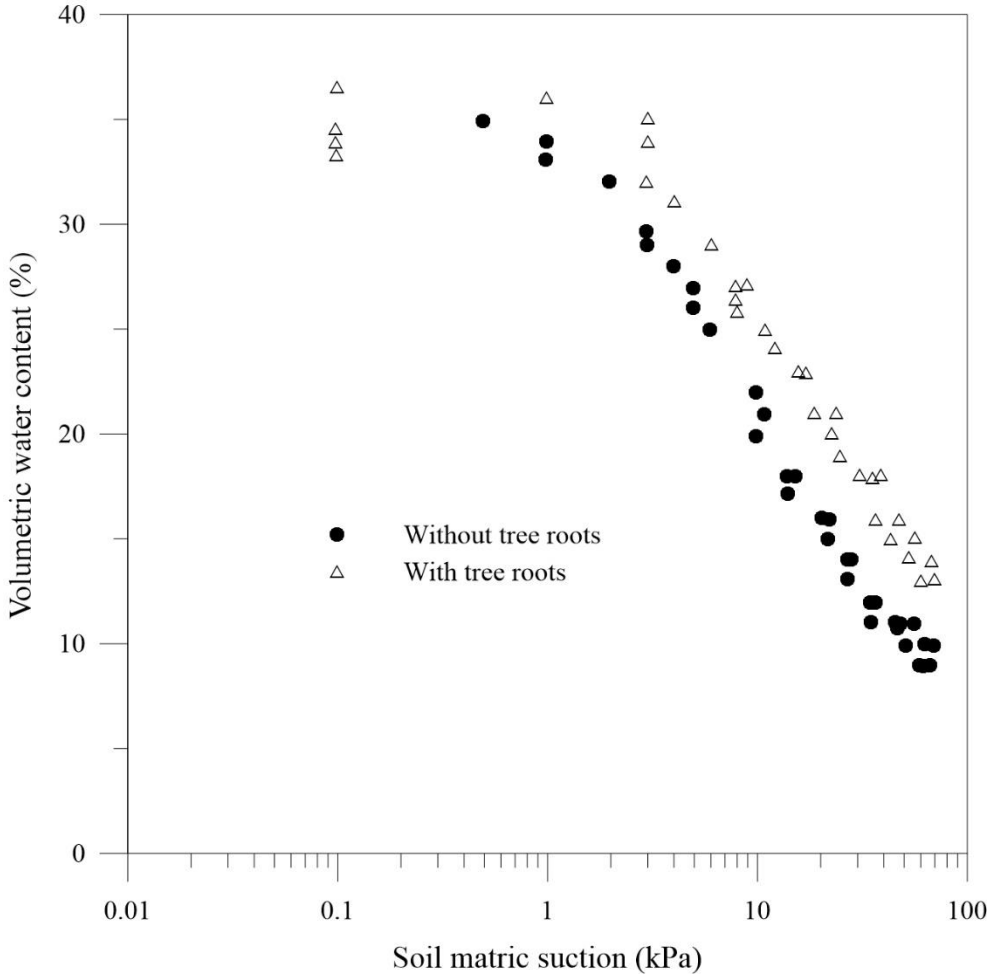

Figure 2.13 Comparison of desorption SWCC between bare soil and vegetated soil (Modified after Leung, AK et al. (2015))

Figure 2.13 shows that SWCC of soil with tree roots remains above the SWCC of soil without tree roots, hence it is evident that soil with tree roots retains higher soil matric

suction than soil without tree roots for the same moisture content. Furthermore, this root water uptake has increased the AEV. The suction variation along the spatial distribution of a root system is necessary to have a better understand about the highest induced suction and its location of a root system. Pathirage et al. (2017) mathematically investigated the behaviour of different suction components close to and away from the tree, and at various depths. The distribution of change of matric suction with respect to the distance from the centre of the tree trunk for different depths is shown in Figure 2.14.

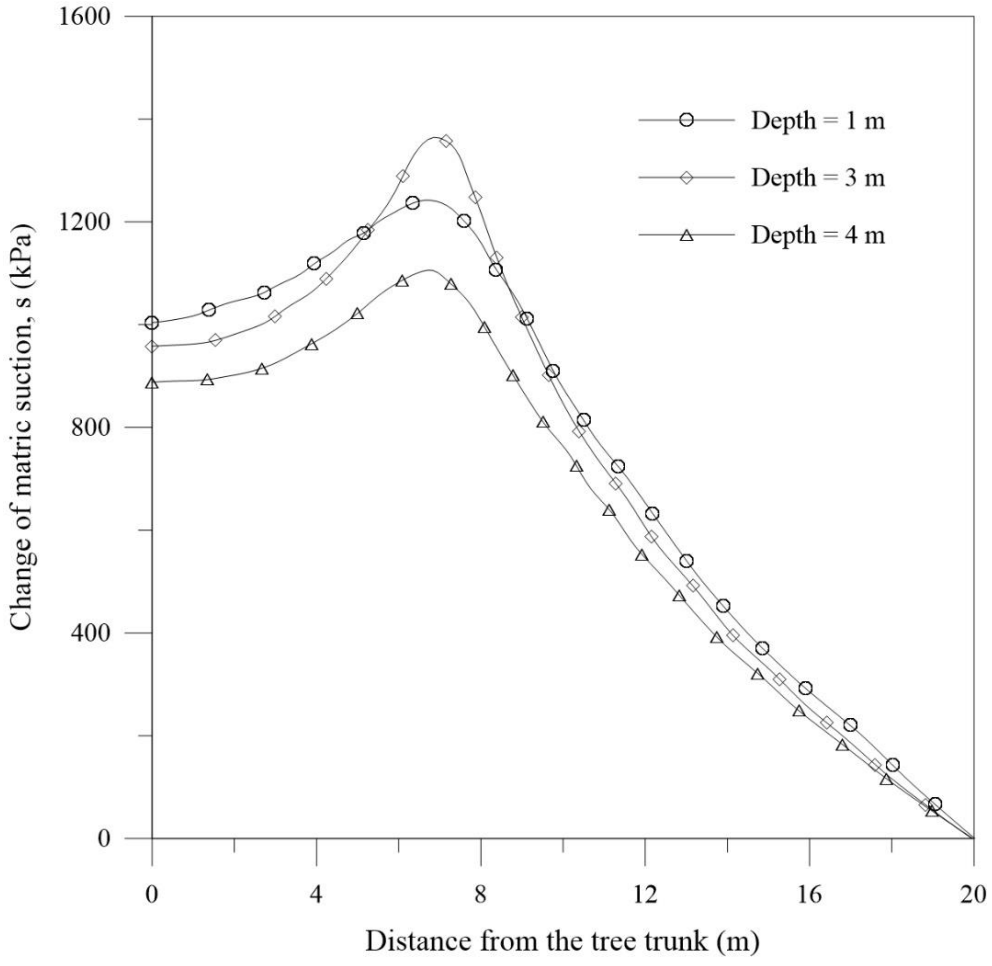

Figure 2.14 Distribution of change of matric suction with distance from the centre of the tree trunk for different depths (Adopted from Pathirage et al. (2017))

Pathirage et al. (2017) observed that the highest variation of matric suction is not exactly underneath the tree, it is around 7 m away from the tree trunk and 3 m from the ground

surface; this is because the highest density of fine roots are exist within this region. In addition, the change of matric suction increases further away from tree trunk until it reaches a maximum, and then it decreases again. In addition to the matric suction, Pathirage et al. (2017) pointed out that root uptake can influence the osmotic suction, and the corresponding change of osmotic suction with distance from tree trunk is shown in Figure 2.15.

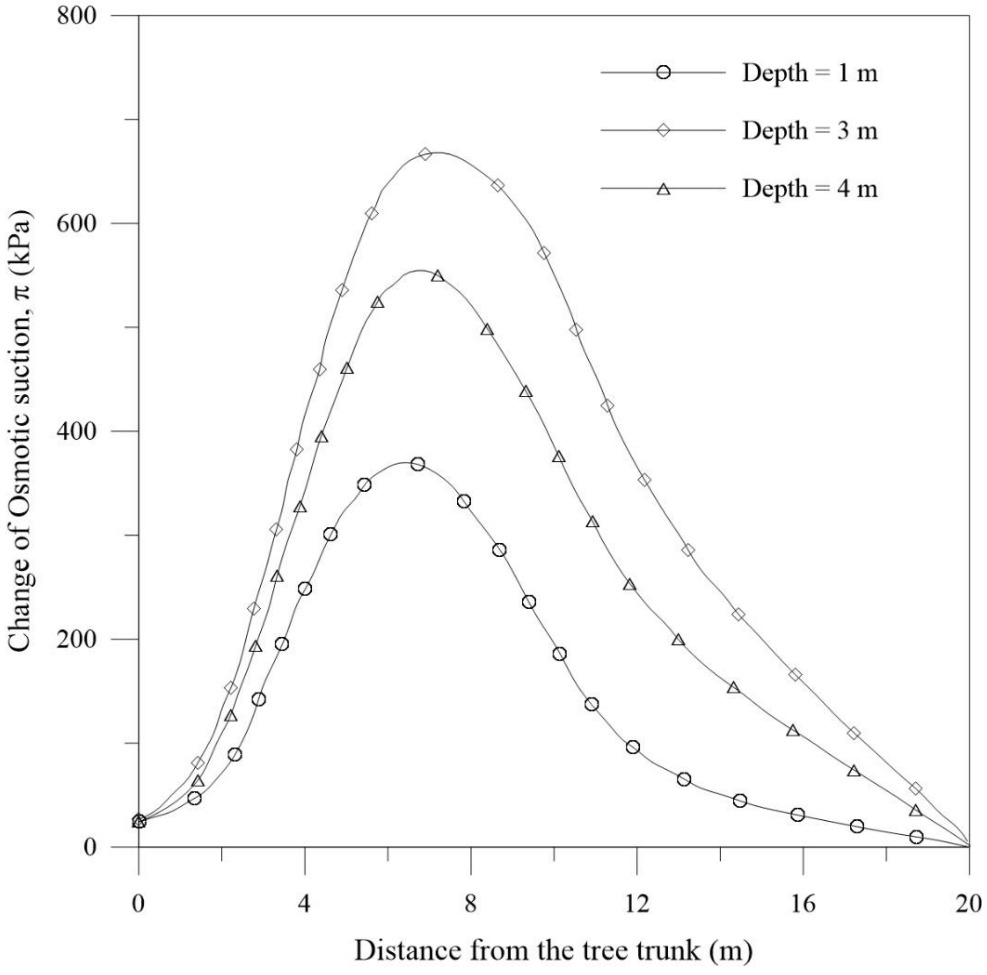

Figure 2.15 Distribution of change of osmotic suction with distance from the centre of the tree trunk for different depths (Adopted from Pathirage et al. (2017))

The highest change in osmotic suction was also occurred at the point where the highest matric suction change was predicted. Pathirage et al. (2017)'s study suggested that tree roots can induce a variation of matric and osmotic suction due to root water and nutrient

uptake, respectively. This study also reports that the highest change of suction is where the fine root are most dense.

2.4.5 Soil reinforcement by tree roots

It is anticipated that the tree roots can reinforce the soil. Docker and Hubble (2001) reported that both larger and smaller roots can help to reinforce soil. Waldron (1977) described that the additional shear strength generated by the tensile strength of tree roots can be directly added to the Mohr Coulomb model, because the soil friction angle is not affected by tree roots. Therefore, the additional strength generated by tree roots can be considered as an apparent cohesion component which can be directly added to the Mohr Coulomb model, having the same friction angle.

$$\tau' = \tau'_{soil} + \Delta\tau_R \tag{2.20}$$

where, τ'_{soil} is the shear strength of soil only, $\Delta\tau_R$ is the additional increase in shear strength due to root permeation, and τ' is the total shear strength of a root permeated soil.

Gray and Leiser (1982) proposed a simple model to predict the additional tensile strength generated by tree roots (Equation 2.21), based on root area ratio.

$$t_R = T_R RAR \tag{2.21}$$

where t_R is the additional tensile strength due to tree roots per unit area of soil, T_R is the tensile strength of a root and RAR is the root area ratio.

Gray and Leiser (1982)'s model is valid as long as the root diameter remains the same. However, in reality the diameters of root are not uniform. Previous studies have reported that the distribution of tensile strength of tree roots with root diameter can be represented by the power decay law (Gray & Sotir 1996; Leung, FT et al. 2015; Mao et al. 2012; Mattia et al. 2005).

$$T_R = \alpha_1 {d_r}^{-\alpha_2} \tag{2.22}$$

where, d_r is the root diameter, and α_1 and α_2 are positive empirical coefficients that depend on the type of species.

Boldrin et al. (2017) observed the distribution of tensile strength of tree roots with respect to root diameter and noted that the power decay law only applies for certain species. Boldrin et al. (2017) proved that the species such as *Euonymus europaeus L. (Ee)* and *Ulex europaeus L. (Ue)* showed a power decay law, whereas *Buxus sempervirens L. (Bs), Corylus avellana L. (Ca), Crataegus monogyna Jacq (Cm), Cytisus scoparius L. Link (Cs), Ilex aquifolium L. (Ia), Ligustrum vulgare L. (Lv), Prunus spinose L. (Ps) and Salix viminalis L. (Sa)* did not. The distribution of tensile strength of *Ulex europaeus L. (Ue)* with respect to root diameter is shown in Figure 2.16 where the corresponding α_1 and α_2 are 16.61 and 0.46 respectively.

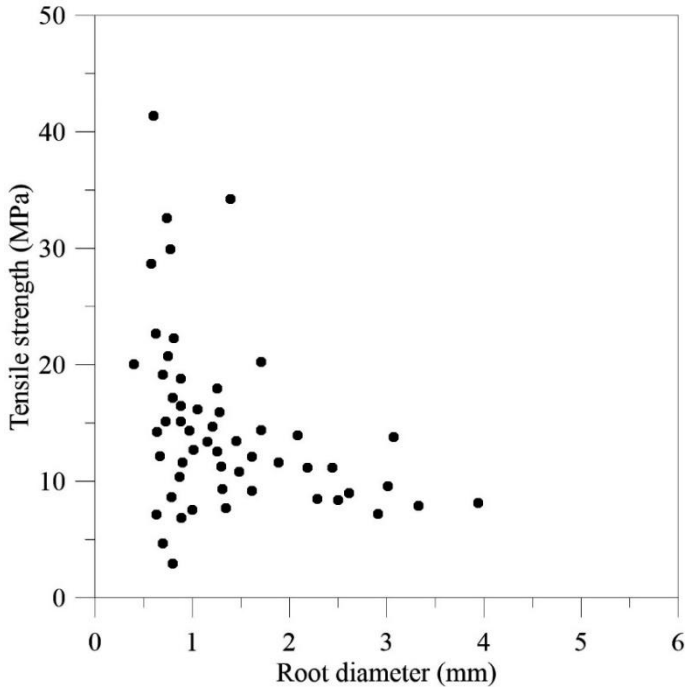

Figure 2.16 Distribution of tensile strength with respect to root diameter for *Ulex europaeus L. (Ue)* (Adopted from Boldrin et al. (2017))

Interestingly, not only the tensile strength, Young's modulus of the two species follows the same power decay law but with different α_1 and α_2. Therefore, the tensile strength of roots, root architecture, root density, degree of saturation or moisture content of soil, and the rate of transpiration can be considered as controlling parameters to characterise the strength of vegetated soil.

Pallewattha et al. (2019) conducted a series of direct shear tests on vegetated soil specimens with different soil matric suction. In this study, all other factors such as type of species, degree of compaction, the chemical composition of soil, and the temperature and environmental conditions were kept constant. The experimental results showed that the peak shear strength increased because of the root reinforcement of tree roots (Figure 2.17). Pallewattha et al. (2019)'s experimental investigations reported that the contribution of root induced shear strength increased as the matric suction increased. However, the matric suction measured during the experiments was considered to be a combination of the soil initial matric suction based on availability of moisture, and the induced matric suction due to root water uptake.

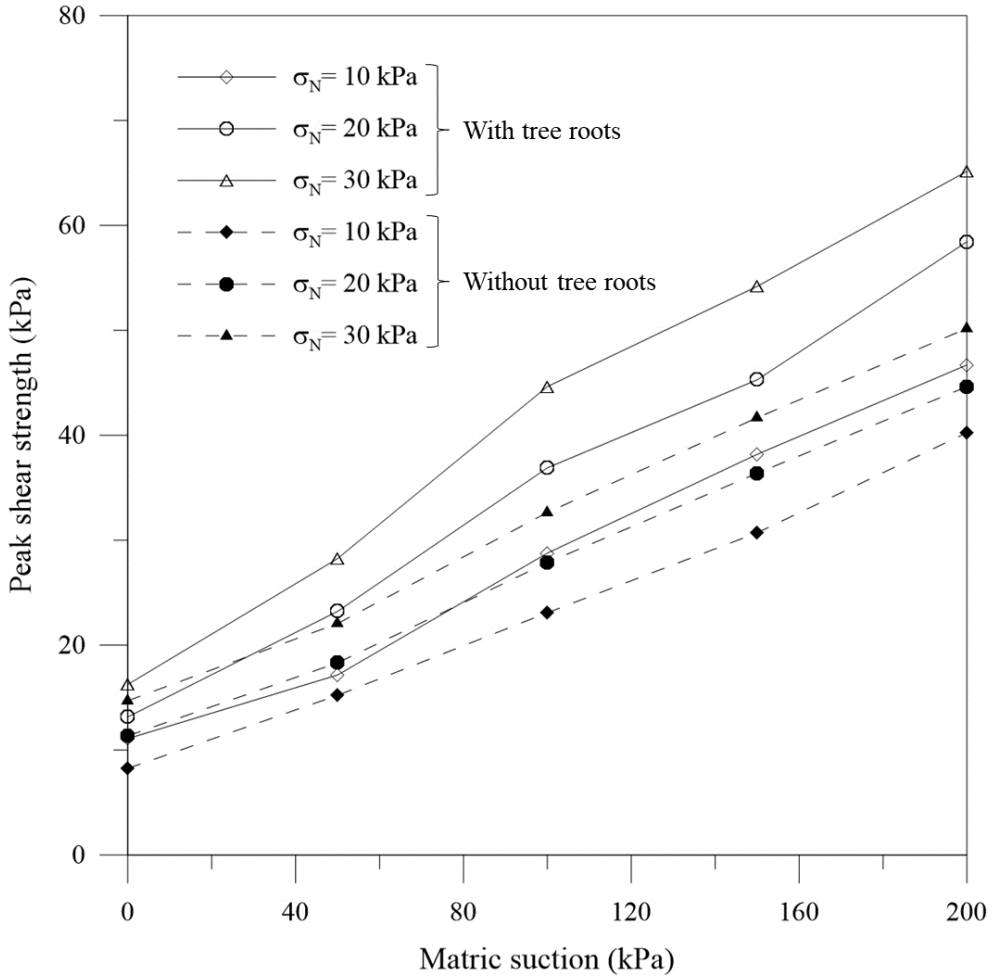

Figure 2.17 Increase of shear strength due to tree roots

(Adopted from Pallewattha et al. (2019))

2.5 Using electrical resistivity in geotechnical engineering

Electrical resistivity is typically measured using a current flow through the sub surface medium with different materials at various individual levels of resistivity (Reynolds 2011; Telford et al. 1990). Herman (2001) pointed out that the resistivity would change significantly with the type of material and the material properties. Generally, the resistivity of a good conductor would be in the order of $\approx 10^{-8}$ Ωm, the resistivity of an intermediate conductor such as top soil would be in the order of $\approx$ 10 Ωm, and the resistivity of a poor conductor would be in the order of $\approx 10^{8}$ Ωm. A summary of parameters that control electrical resistivity are given in Table 2.3.

Table 2.3 Electrical resistivity depending parameters

Author/s	Parameter/s
Keller and Frischknecht (1966),Ward (1990), Adam et al. (2012)	Percentage of clay, moisture content of soil, pore water concentration of soil, void ratio, and temperature
Yan et al. (2012)	Moisture content of soil, temperature, void ratio, electrical conductivity of pore fluid, composition of the solids, saturation, salinity, and shape and arrangement of particles
Arulanandan and Muraleetharan (1988), Thevanayagam (1993), Abu-Hassanein et al. (1996)	Void ratio and pore structure, electrical conductivity of the pore fluid, solids, saturation, shape and arrangement of particles.
Sudduth et al. (2003), Jiao-Jun et al. (2007)	Moisture content of soil, pore water salinity, temperature, texture
Sheets and Hendrickx (1995), Mori et al. (2003)	Pore water salinity, percentage and mineralogy of clay, cation exchange capacity, void ratio and pore distribution, moisture content of soil, and temperature
Rhoades et al. (1976)	Bulk liquid phase conductivity (free salt in the liquid filled pores), and bulk surface conductivity (exchangeable ions at the solid/liquid interface)
Abu-Hassanein et al. (1996)	Porosity, pore fluid electrical resistivity, solid composition, degree of saturation, and shape and arrangement of particles, and pore structure.

The total resistance (R_T) for a particular material can be measured using Ohm's law;

$$R_T = \rho \frac{L}{A'} \tag{2.23}$$

where ρ is the resistivity of the material which is considered as a material specific constant, L is the length, and A' is the cross sectional area.

The equation 2.23 can be rewritten as;

$$\rho = \rho_{app} K' \tag{2.24}$$

where ρ_{app} is the apparent resistance and K' is the geometric factor.

The resistivity of soil can be measured using either two or four electrodes; with the four electrodes method being the most popular because of its high accuracy. The general configuration for a typical electrical survey is shown in Figure 2.18, where the outer two electrodes (A and B) will control the current flow while the inner two electrodes (M and N) are used to measeure the voltage potential difference (Reshma et al. 2004).

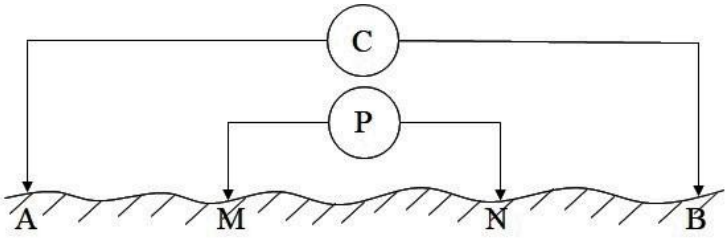

Figure 2.18 General electrode configuration for a typical four electrodes method (Modified after Herman (2001))

The flow of current and the corresponding equipotential lines through homogeneous and inhomogeneous medium are shown in Figure 2.19. This clearly shows how resistivity varies with the subsurface properties.

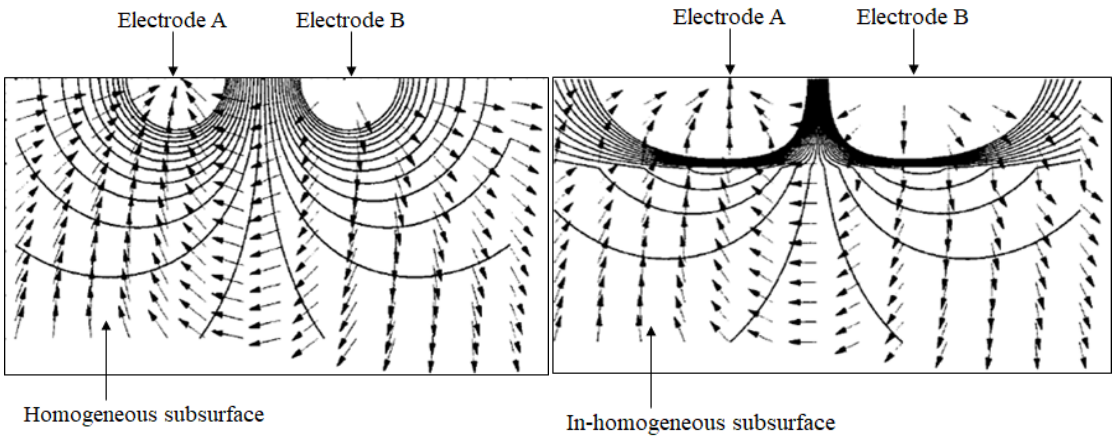

Figure 2.19 Current flow and equipotential surfaces for homogeneous and inhomogeneous subsurface (Modified after Herman (2001))

Different configurations have been introduced such as the Wenner configuration, the Schlumberger configuration and the Dipole-Dipole configuration. The main difference between the three configurations is the spacing between the electrodes. Jiao-Jun et al. (2007) pointed out that the spacing between the electrodes might influence the spatial variability of soil properties. When the electrodes are far apart most of the current would pass through the low resistivity layer and occupy deeper depths, and when the electrodes are closer to each other, the current flow will occupy shorter depths (Herman 2001).

A general equation can be developed to measure the electric potential difference (V_{MN}) with respect to electrode spacing, based on Figure 2.19, and hence determine the electrical resistivity of subsurface material.

$$V_{MN} = (V_M - V_N) = \frac{\rho L}{2\pi}\left[\left(\frac{1}{AM} - \frac{1}{MB}\right) - \left(\frac{1}{AN} - \frac{1}{NB}\right)\right] \quad (2.25)$$

$$\rho = \frac{V_{MN}}{I} K \tag{2.26}$$

2.5.1 Electrical resistivity with soil salinity

Abu-Hassanein et al. (1996) recognised that geophysical methods such as electrical resistivity are the most effective and efficient techniques for investigating large scale volumes of soil. Therefore, the concept of electrical resistivity and its applications have been spread throughout a vast range of geo technical applications such as the soil water content, soil salinity, saturation, liquefaction potential, earthing resistance, soil freezing, degree of compaction, hydraulic conductivity, geomembrane failures, corrosive effects, and the formation factor and the electro osmosis phenomenon (Butterfield & Johnston 1980; Gunnink & El-Jayyousi 1993; McCarter 1984; McCollum & Logan 1913; Reshma et al. 2004; Rhoades et al. 1976; Shea & Luthin 1961). For instance, electrical resistivity ground surveys were used to establish the SWCC (Higginbottom 1976; Mualem & Friedman 1991; Parkhomenko 2012; Yan et al. 2012). Also, Perez et al. (2009) pointed out that as the soil matric suction increased electrical resistivity of soil increased for a given dry density of soil. Moreover, the change of electrical resistivity of different clay types with respect to the volumetric water content has been investigated by Yan et al. (2012), Perez et al. (2009), McCarter (1984), Michot et al. (2003) and Fukue et al. (1999), and the results are shown in Figure 2.20. For all types of clay, the electrical resistivity decreases with increasing volumetric water content. Therefore, electrical resistivity can be considered as a proper parameter to define the change of moisture content in soil (Figure 2.20).

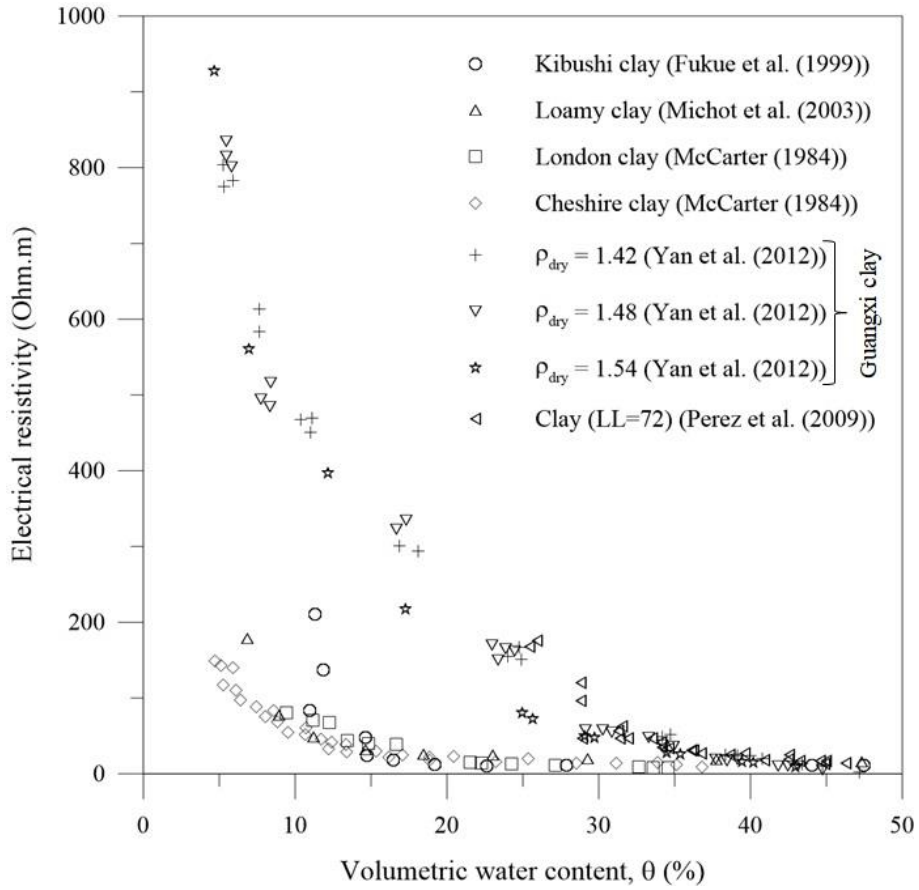

Figure 2.20 Distribution of electrical resistivity with volumetric water content

Moreover, electrical resistivity theory has also been used to estimate the salinity of soil. For instance, Bernstone et al. (2000) used electrical resistivity for the purpose of landfill structures, Rodriguez et al. (1997) used electrical resistivity to investigate the ground water pollution in the field, and Kalinski and Kelly (1993) experimentally investigated the distribution of electrical resistivity of pore water with different degrees of salinity (Figure 2.21). Figure 2.21 showed that electrical resistivity decreases as the salinity or the ion concentration of pore water solution increases. Based on these observations, electrical resistivity is a proper parameter to define the salinity of pore water, and hence the osmotic suction.

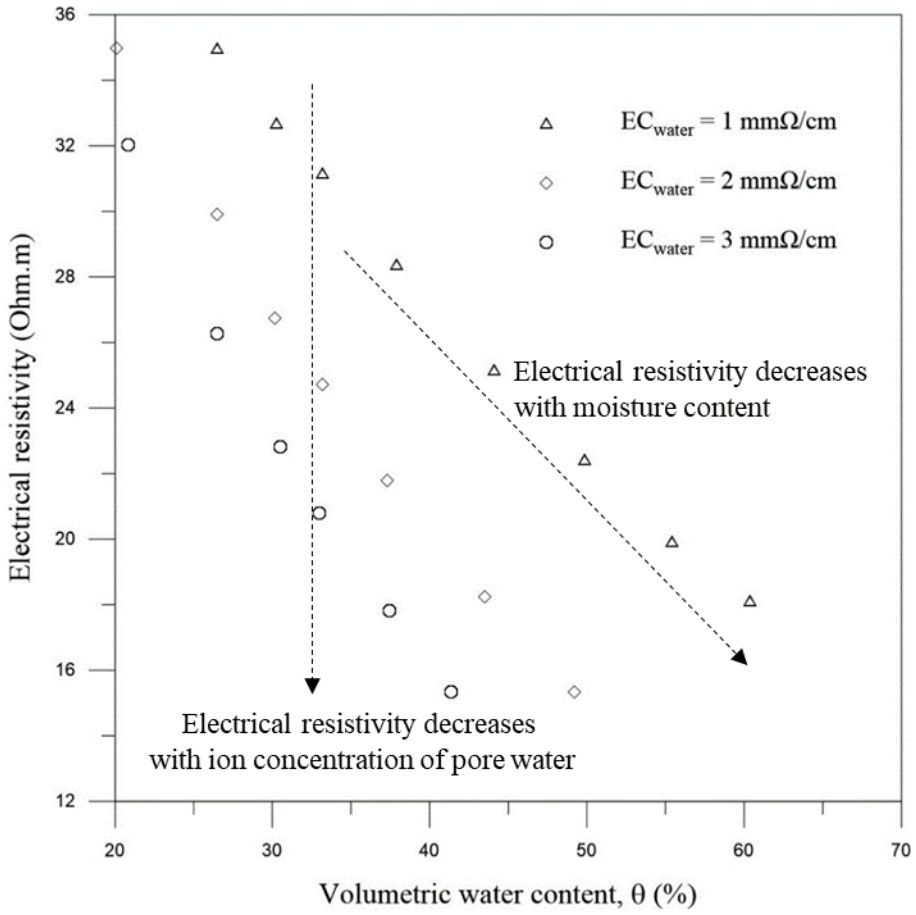

Figure 2.21 Distribution of electrical resistivity with volumetric water content for different levels of saline pore water (Modified after Kalinski and Kelly (1993))

2.6 Summary

The previous sections summarise the important conclusions acquired by reviewing past literature relating to soil stabilisation under unsaturated conditions. Even though most of the geotechnical applications analysed are based on saturated conditions, the actual soil conditions present in those structures are unsaturated, where suction (matric and osmotic suction) plays a significant role. For example, rail structures are driven on unsaturated soil with tree roots. The presence of tree roots can significantly increase the shear strength of soil. Moreover, the root water and nutrient uptake from tree roots can induce an additional matric and osmotic suction respectively, which would

further contribute to increase the soil shear strength. However, these induced components of suction cannot be separated from usual soil suction during measurements. The determination of matric suction and the contribution of tree roots on shear strength are very well established. However, an accurate determination of osmotic suction in the field has been a challenge which is why the incorporation of electrical conductivity would be a satisfactory method to measure the osmotic suction. Most previous studies associated with soil shear strength only focused on the unsaturated or saturated behaviour of soil with or without the influence of tree roots, whereas a combination of all those components such as saturated, unsaturated, saline (osmotically influenced) and rooted, have not yet been considered. Therefore, this study focused on evaluating the change of unsaturated shear strength of vegetated soil with osmotic suction.

CHAPTER 3: Experimental procedure

3.1 Background

The shear strength of soil is directly influenced by the physical and chemical properties of its structure. While a great deal of research has gone into investigating how physical properties such as the moisture content affects the shear strength of soil, only a limited number of research has been conducted to monitor the influence of chemical properties on shear strength, because of the complexity of particle interaction in saline solutions. The influence of pore water chemistry, especially salinity, on the shear strength of soil has been considered, but only under saturated conditions; this is why an experimental investigation of the shear strength of soil with salinity under unsaturated or partially saturated conditions was necessary.

A conventional small scale shear box was modified in-house to accommodate a miniature pore water pressure transducer (measure the variation of matric suction), and the tests were conducted at various pore water salinities (osmotic suctions), and matric suctions. The apparatus used for these tests, as well as soil sampling, remoulding, loading, the variation of osmotic suction and matric suction, and data acquisition are discussed in the subsequent sections. The mechanical strengthening of vegetated soil due to root water uptake and root reinforcement under saturated and unsaturated conditions (matric suction only) has already been discussed in previous studies. To the best of the writer's knowledge, no previous research studies had considered the effect that osmotic suction has on the shear strength of vegetated soil. The experimental results from small scale direct shear box show that the soil shear strength has been significantly influenced by the osmotic suction. Therefore, a series of large scale direct shear tests with vegetated

soil specimens was conducted under different osmotic suction conditions and matric suctions, to observe the combined contribution of tree roots and osmotic suction. Further, the electrical conductivity was determined with respect to soil matric suction as a non-destructive technique to establish the corresponding SWCC of soil, for both vegetated and non-vegetated environments.

3.2 Preliminary experiments

3.2.1 Soil sampling

The soil used for this study obtained from Wollongong (NSW, Australia) (Figure 3.1). First it was air dried and pulverized with a rubber mallet, and then organic content (i.e. pieces of decayed wood) was discarded. The soil was then sieved through 2 mm sieve to achieve a uniform sample.

Figure 3.1 Sampling location, Wollongong NSW Australia

(Adopted from, Maps of World (2013))

3.2.2 Preliminary tests

The soil was mechanically sieved in accordance with AS1289.3.6.1 (2009) and the Malvern particle size analyser was used for the fraction smaller than 75 μm. The consistency limits of the soil were measured based on AS1289.3.1.1 (2009) and AS1289.3.2.1 (2009). Compaction characteristics such as the maximum dry density (MDD) and optimum moisture content (OMC) of the soil were determined based on AS1289.5.1.1 (2009). The specific gravity of the soil was determined based on AS1289.3.5.2 (2009).

3.2.3 Filter paper test to determine SWRC

A filter paper test based on the standard test method for measurement of soil potential (suction) using filter paper (ASTM_D5298 2003) was carried out using Whatman No 42 filter paper to determine the as compacted matric suction of soil. Thirteen different samples of soil were mixed with different amount of distilled water and contained in air sealed polythene bags for seven days in a temperature and humidity controlled room (20 ± 2^{o}C, 30% RH). The soil samples were then subsequently compacted to 85% of MDD into a 50 mm diameter cylindrical mould, as shown in Figure 3.2(a) to a height of 60 mm. For each soil specimen, the initial degree of saturation was calculated.

The extruded soil specimen was then cut into two equal-size pieces. The filter papers were dried in an oven and then stored in a desiccant to enable the temperature of the filter paper to return to room temperature without absorbing any moisture. A stack of three filter papers was placed between the two soil specimens, as shown in Figure 3.2(c). The 3 mm diameter inner filter paper was measured to the nearest 0.0001 g and then used for the matric suction measurements, whereas the two, 4 mm diameter outer filter papers were used to prevent the soil from contaminating the inner filter paper. The soil specimens with

filter papers were then placed in an air-sealed container. The lid and the container contact area were sealed with insulation tape. Then the soil specimen was stored in an insulated chest (Esky box) in a temperature and humidity control room (20 ± 2°C, 30% RH) for seven days. A measurement process was quickly carried out to minimise the loss of moisture when transferring the filter paper from the container to an aluminium cup resting on the scale.

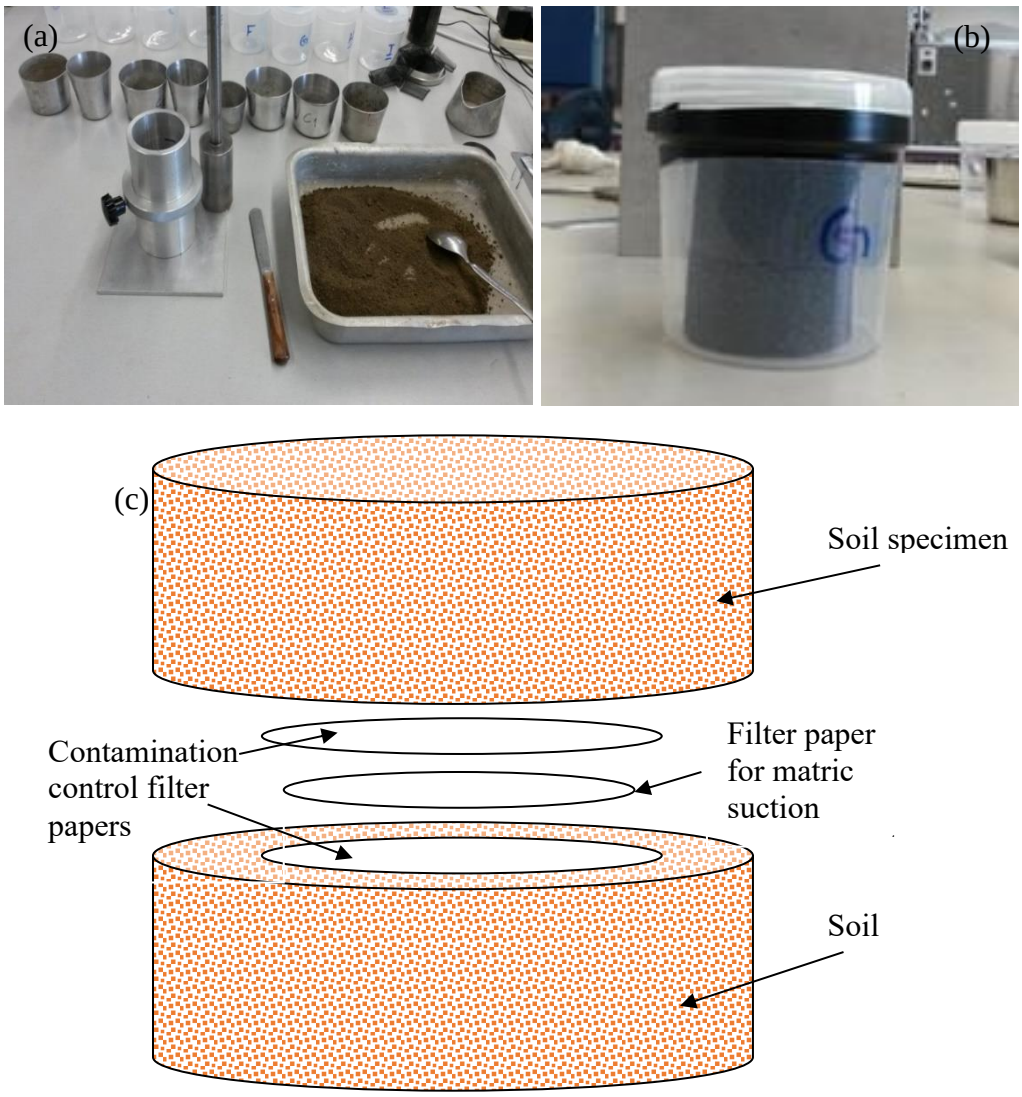

Figure 3.2 Filter paper test (Contact method)

3.2.4 Use of WP4C potentiometer to measure osmotic suction

A WP4C (Decagon Devices, Inc.) potentiometer (range 0 to -300 MPa) (Figure 3.3) generally uses vapour pressure to measure total suction of soil specimens. However, for this study, the osmotic suction was measured using fully saturated soil specimens of different pore water concentrations of NaCl.

Figure 3.3 WP4C Dewpoint Potentiometer

Seven different solutions were prepared by mixing crystallised NaCl with distilled water. Although the soil contains a constant ion content, the pore water salinity likely to increase due to soil moisture decrease (i.e. rise in global temperature induced by climate change). Therefore, it is appropriate to consider a wide range of salinity values. Therefore, seven soil samples were fully saturated with solutions having NaCl concentrations of 0.0, 0.2, 0.4, 0.6, 0.8, 1.0 and 2.0 mol/L, where the maximum salinity of the studied soil was three times more than the maximum salinity of sea water (i.e. 35 g/L). The soil specimens were then air-sealed in polythene bags to have hydraulically and chemically equilibrated soil specimens, which were then stored in a temperature and humidity controlled room (20 $\pm$ 2^{o}C, 30% RH) for 24 hours. The measuring cups for the WP4C potentiometer were half-filled with soil and tested using the pre-calibrated WP4C potentiometer in a precise

(p) mode for more accurate results. The osmotic suction of these soil specimens was checked for repeatability by subjecting three samples of soil with the same concentrated pore water with NaCl.

3.2.5 Using an SR-2 resistivity meter to measure electrical conductivity

An SR-2 resistivity meter (±0.1 Ωcm accuracy- Tinker and Rasor) is shown in Figure 3.4(a), was used to measure the electrical resistivity of soil; the electrical resistivity (ER) was then converted to electrical conductivity (EC) using Equation 3.1.

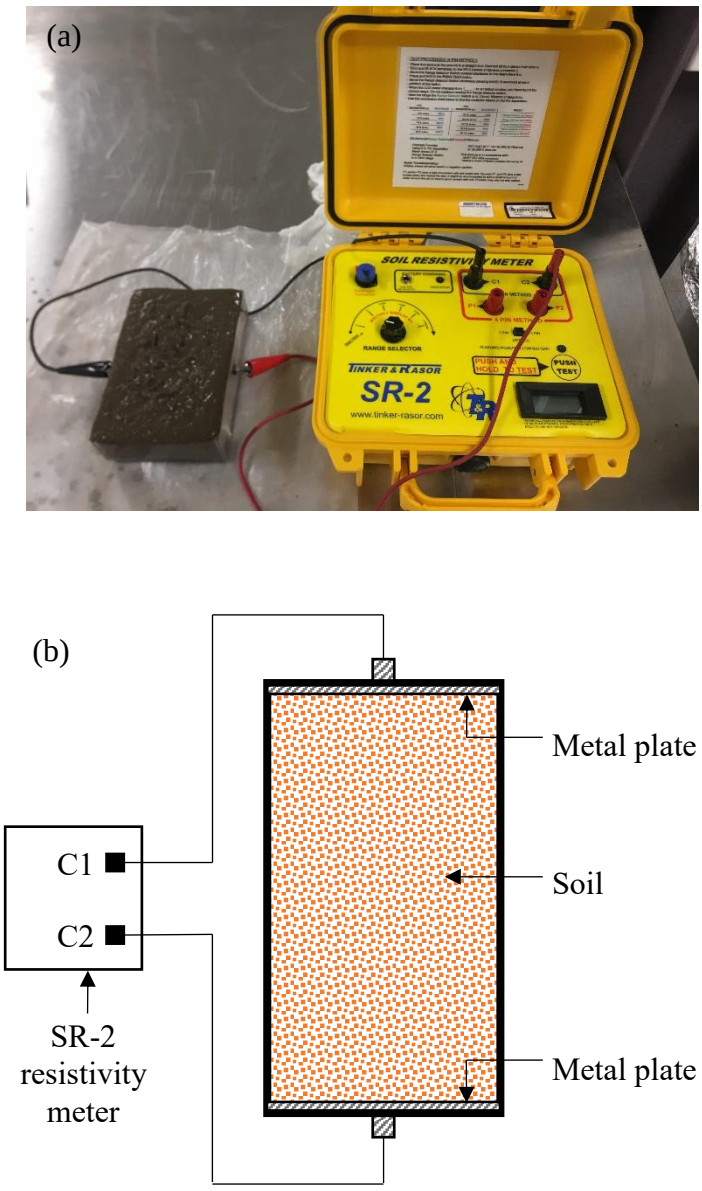

Figure 3.4 SR2 resistivity meter from Tinker and Rasor

$$EC = \frac{1}{ER} \tag{3.1}$$

A standard electrical resistivity soil box (38 x 101.5 x 152.3 mm) was used with the two-pin method. A standard two-pin electrical resistivity soil box is made from hard and transparent plastic with two metal plates, as shown in Figure 3.4(b). Seven solutions were prepared by first mixing crystallised NaCl with distilled water and then with soil to achieve fully saturated soil samples described in section 3.2.3. These soil samples were then placed inside air sealed polythene bags and stored in a temperature and humidity controlled room for 24 hours to facilitate the moisture and chemical equilibration process. The soil samples were then compacted into a standard electrical resistivity soil box to 85% of MDD.

3.3 Determining the influence of osmotic suction on the shear strength of soil (without roots)

3.3.1 Soil specimen preparation

Different amounts of commercially available crystallised NaCl in weight were mixed with distilled water to have solutions of 0, 0.2, 0.4, 0.6, 0.8, 1 and 2 mol/L NaCl concentrations with seven different osmotic suctions. Only the distilled water was used to replicate the 0 mol/L NaCl condition or zero osmotic suction. The soil was then mixed with the NaCl solution at different moisture contents to achieve seven different initial matric suctions (0, 25, 100, 200, 500, 1000 and 1500 kPa). The amount of moisture needed for relevant initial matric suction was calculated from the soil water characteristic curve (SWCC). The samples of soil mixed into a solution were contained in air-tight polythene bags and stored in a temperature and humidity control room (20 ± 2^{o}C, 30% RH) for seven days for moisture and chemical equilibration. This overall

process ensures the uniform mixing of soil and NaCl solution. The soil was compacted to 85% of MDD, and then the compacted specimens were extruded into a shear box.

3.3.2 Small scale direct shear test

A direct shear test program using conventional shear box apparatus (60 x 60 x 40 mm) was carried out based on AS1289.6.2.2 (2009), to determine the mechanical behaviour of compacted soil (Figure 3.5).

(a)

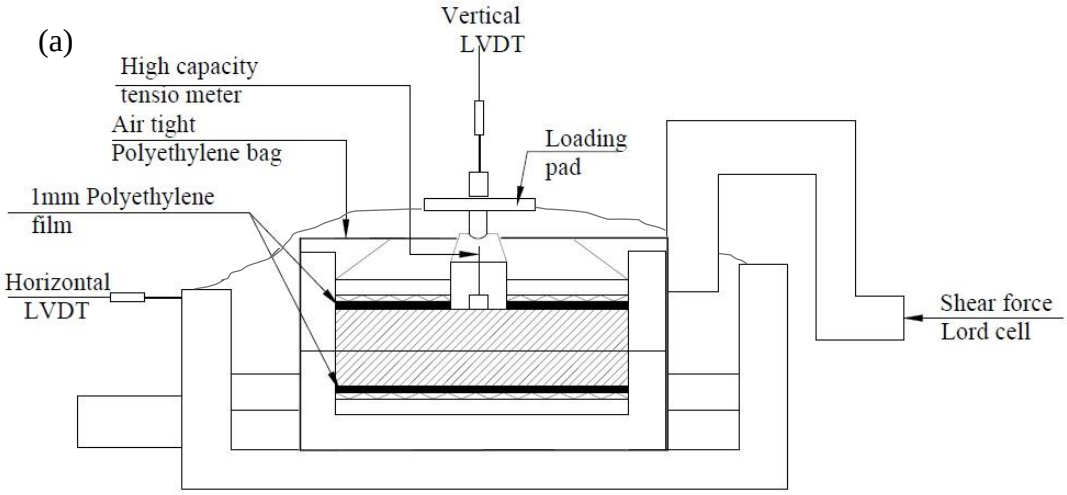

(b)

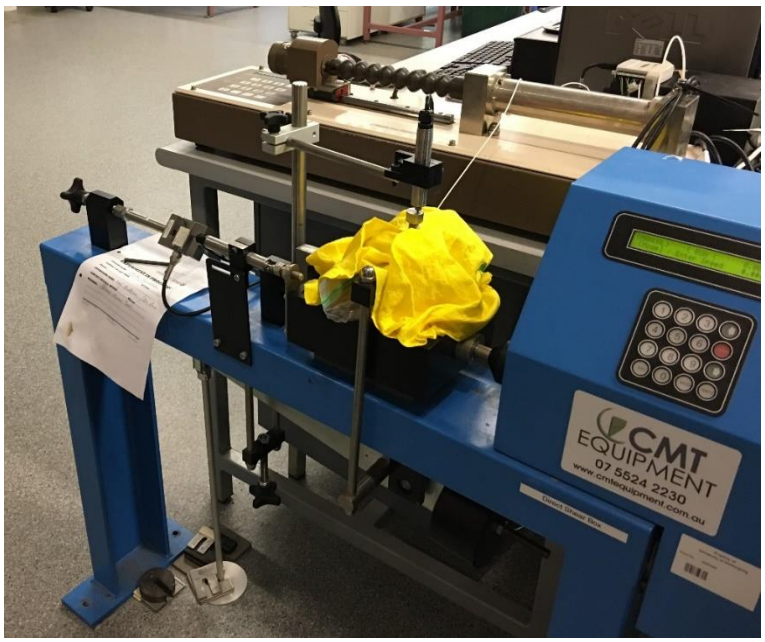

Figure 3.5 Direct shear box (60 x 60 x 40 mm), (a) schematic diagram with instrumentation and (b) an image of the direct shear box

Based on the particle size distribution curve (Figure 4.1), the maximum particle size of the soil specimen was 2 mm. Therefore, using a 60 x 60 x 40 mm shear box is reasonable enough to observe the strength of the selected soil specimen. The samples carriage of the direct shear box was mounted on two parallel sets of roller bearings to enable the free horizontal movement. A step motor drive unit is connected to the shear box by a shaft to apply a constant rate of horizontal displacement. Two LVDT (Linear variable differential transformer) displacement transducers (accuracy = ±0.001 mm) and a load cell (accuracy = ±0.001 kN) were used to measure the horizontal displacement, vertical displacement and the horizontal shear force. A lever arm loading mechanism with a beam ratio of 10:1 was used to apply a vertical load with a top cap. The top cap was modified to accommodate a miniature pore water pressure transducer to measure the matric suction variation during shearing (Figure 3.6). A National Instruments card (NI USB-6009) with eight input channels and an in-house coded program with LabVIEW software were used to acquire data in every 60 seconds.

All the direct shear tests were carried out under CW conditions; therefore the evaporation of moisture was minimised by carrying out the compression and shearing stages in a temperature and humidity-controlled (20 ± 2^{o}C, 30% RH) room. Moreover, the entire direct shear box assembly was covered with an airtight polythene bag to isolate the air around the soil specimen further. The top and bottom surfaces of the soil specimen were covered with two, 1 mm thick files of polythene. Moreover, the space between the top and bottom sliding halves were sealed with silicone grease. The airtight polyethene cover was then covered with a moist cloth to minimise any air temperature variation inside the polythene bag. The soil specimens were then subjected to a compression stage consisting of three vertical stresses (i.e. 10, 20 and 40 kPa) for 24 hrs, during which time the vertical displacement was monitored (For this study, the maximum vertical tree root length was

considered as 3 m. When there is no surcharge pressure, only the soil overburden pressure contributes for the deformation. Therefore low vertical stresses such as 10, 20 and 40 kPa are suitable for analysis.). For fully saturated conditions (at 0 kPa initial matric suction), the compacted soil specimens were submerged for 24 hours in a relevant solution that depends on expected osmotic suction, before shearing. The specimens were sheared at a relatively low horizontal displacement rate of 0.006 mm/min to allow for redistribution of any additional matric suction within the soil specimen during shearing. The soil specimens were allowed to shear until they achieve a maximum horizontal displacement of 12.0 mm.

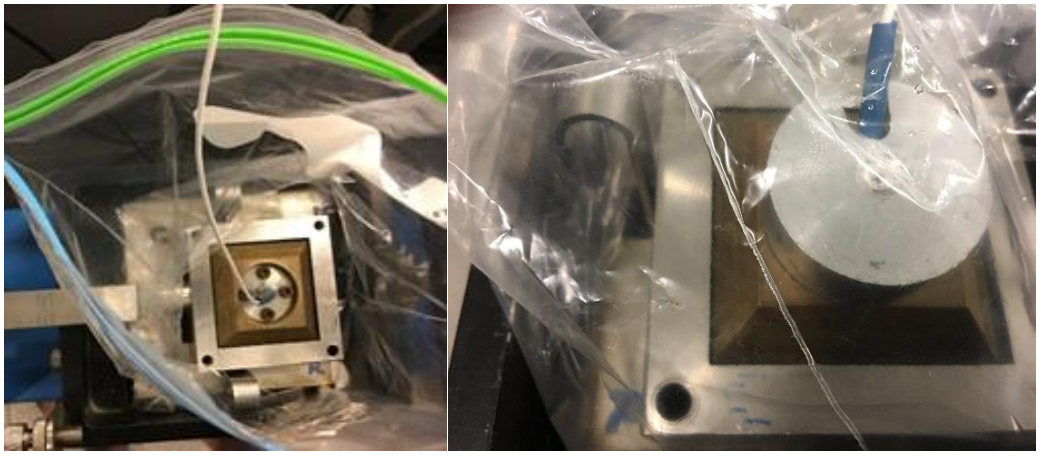

Figure 3.6 Modified top cap of the DST and the miniature pore water pressure transducer used to measure the matric suction

3.4 Determining how osmotic suction influences on the shear strength of root permeated soil

3.4.1 Selection of plant species

Acacia Stenophylla (River Cooba), is a highly drought and salinity tolerant species, so it was selected for this study. Based on Marcar et al. (1995)'s salinity tolerant chart

(Table 2.2), *Acacia Stenophylla* is considered to be in the extreme (> 16 dS/m) category of salinity tolerance. Moreover, *Acacia Stenophylla* is an evergreen native (especially in eastern Australia) with a conical shape tap-rooted system. According to Boxshall and Jenkyn (2001), *Acacia Stenophylla* is a small tree (shrub) that grows to an average height of about 20 m. The plants required for this study were purchased from a nursery in NSW. The plants were almost the same height (300 ± 50 mm); they came from the same planting batch and had almost the same stem diameter.

3.4.2 Soil specimen preparation

The plants were grown in wooden boxes made from water-resistant form ply; the internal dimensions were 300 x 300 x 200 mm, as shown in Figure 3.7 (a).

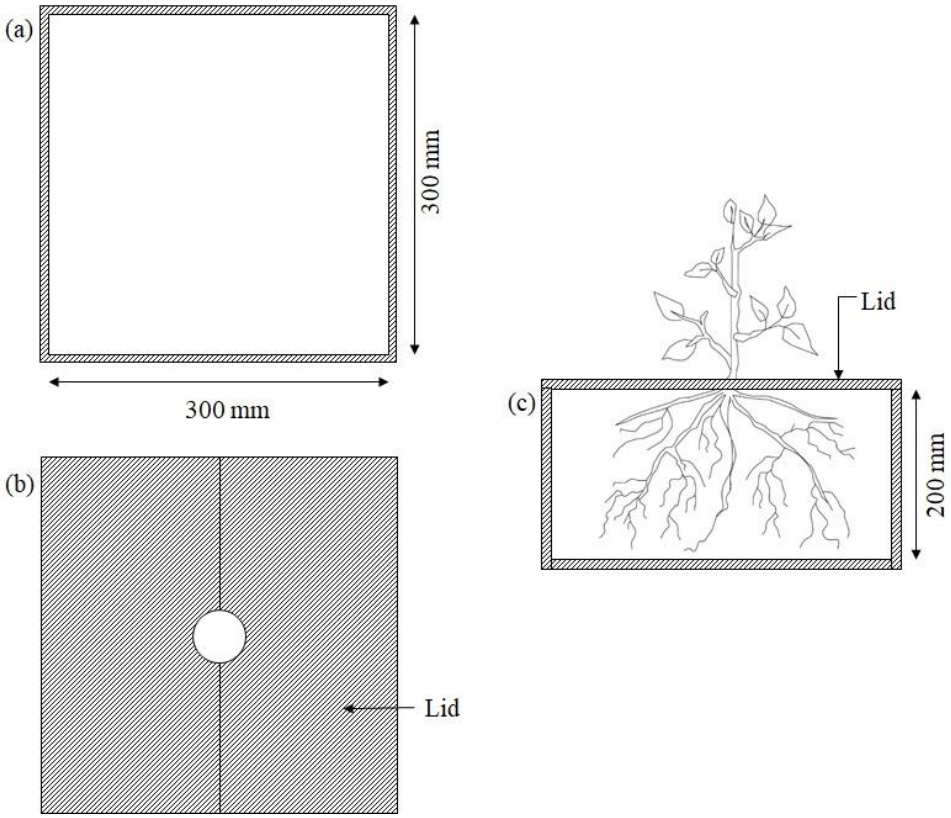

Figure 3.7 Schematic diagram of the soil box with plant

The boxes were then lined with Polyurethane sealer to control deterioration due to water, temperature or changes in the weather. Further, a lid with an aperture in the middle was prepared for each box to minimize the precipitation and soil surface evaporation [Figure 3.7 (b)]. The soil required for this study was prepared as described in Section 3.3.1, and then mixed with solutions of NaCl to the required moisture content. The same concentrations of NaCl (i.e. 0, 0.2, 0.4, 0.6, 0.8, 1 and 2 mol/L NaCl) described in Section 3.3.1 were used to achieve the same osmotic suctions. The moisture content of the soil samples was varied to enable three different initial matric suctions (0 kPa, 100 kPa and 200 kPa). The moisture content for the corresponding matric suction was selected from the SWCC (Figure 4.2). The moistened soil samples prepared at the selected level of moisture were then sealed in labelled polythene bags and stored in a temperature and humidity controlled room (20 ± 2^{o}C, 30% RH) for seven days.

The soil was subsequently compacted into the wooden boxes in three 66.7 mm (= 200/3) thick layers using a 300 x 300 mm steel plate and applying a predetermined number of blows (i.e. 25 blows). Ng et al. (2013) reported that increasing the degree of compaction can significantly reduce the growth of tree roots and also the effect of roots on water retention was high when the degree of compaction was exceeded 80%. Therefore, the expected degree of compaction selected was 85% of MDD (15.58 kN/m^3), which was 13.24 kN/m^3. The plants were then uprooted from the commercially provided plant seedling trays. The root section with soil was submerged in distilled water for about one hour to enable the soil particles to release the roots without causing any damage (Barber and Martin, 1976). The roots of the uprooted plants were then washed with distilled water, and then the plants were transplanted in the middle of the compacted soil box, by burring the rooted section to a depth of 50 mm as a reference point [Figure 3.8 (b)]. The soil boxes with the plant were then labelled, placed in a dry area and

covered with lids to control any evaporation and precipitation [Figure 3.8 (d)]. The plants remained in these positions for more than two years to enable the tree roots to grow.

Figure 3.8 Soil compaction and planting in the soil box

3.4.3 Large scale direct shear test (LDST)

The large scale direct shear setup (300 x 300 x 200 mm, which was the largest direct shear box size in University of Wollongong) was used to determine the stress-strain behaviour of large scale soil specimens with tree roots. The mechanism of the LDST was similar to the conventional direct shear test. A schematic diagram of the LDST is shown in Figure 3.9. The top and bottom halves of the shear box are made from brass. The top half was fixed, and the bottom half was driven by a mechanical motor. The vertical and horizontal

displacements were measured during shearing by dial gauges. The horizontal force generated by soil friction was measured by a calibrated load ring (proving ring) and a dial gauge. The top cap on the soil specimen was designed in house to avoid disturbing the plant stem during tests, and a normal load was applied onto the top cap using a loading arm. The LDSTs were carried out at three different levels of initial matric suctions such as 0 kPa (fully saturated), 100 kPa and 200 kPa. The moisture content and the soil matric suction were measured by an EC5 moisture sensor and an MPS2 matric suction sensor, while the data from these two sensors were recorded by a Procheck data logger (Decogon Devices) (Figure 3.10). The sensors were installed closer to the shear zone, while the cables were laid along the surface of the soil and then out of the hole in the middle of the top plate. Under fully saturated conditions, the entire soil specimen is inundated by the relevant solution, for which the soil specimen had previously been prepared. In all the matric suction conditions, the test setup was covered with cling wrap and wet gunny sacks until it reached the desired matric suction value (Figure 3.11). Shear tests were carried out at three different normal stresses: 10, 20 and 40 kPa. Shear tests were carried out at every osmotic suction and initial matric suction at each normal stress. Before shearing, all the specimens were compressed to the corresponding normal stress. The change in vertical displacement during compression process was measured by the vertical displacement dial gauge shown in Figure 3.9 and 3.11 (b). Once the soil specimens were sufficiently consolidated (i.e. no visible change in vertical displacement dial gauge), the soil specimens were sheared at the slowest strain rate the motor could achieve, 2.5 mm/min. Two separate direct shear tests at different strain rates (i.e. 0.006 mm/min and 2.5 mm/min) were conducted with the small direct shear box (60 x 60 x 40 mm). The results showed that the peak shear stress was not sensitive to the deformation rate. This is consistent to the study conducted by Ribeiro Heitor (2013). The soil specimens were

allowed to shear until they achieve a maximum horizontal displacement of 32.5 mm. After every shear test, the shear force and the change of vertical displacement with respect to horizontal displacement were recorded. The characterisation of root failure patterns, determination of the root area ratio (RAR) and experimental evaluation of root tensile strength were recorded after every shear test.

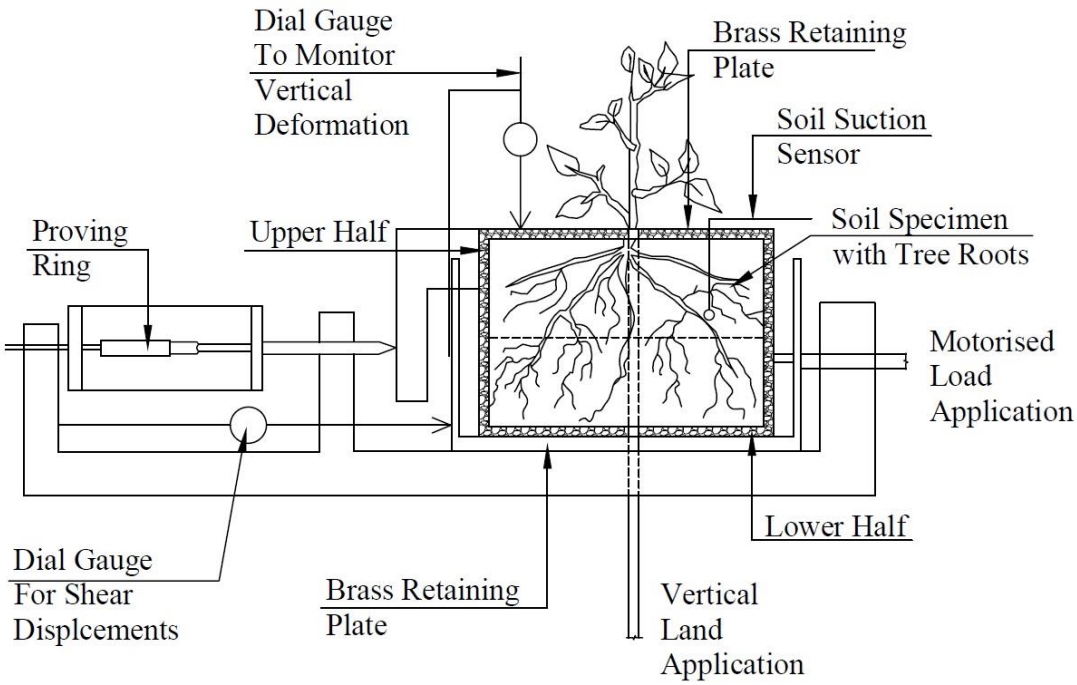

Figure 3.9 Schematic diagram of LDST (Adopted from Pallewattha et al. (2019))

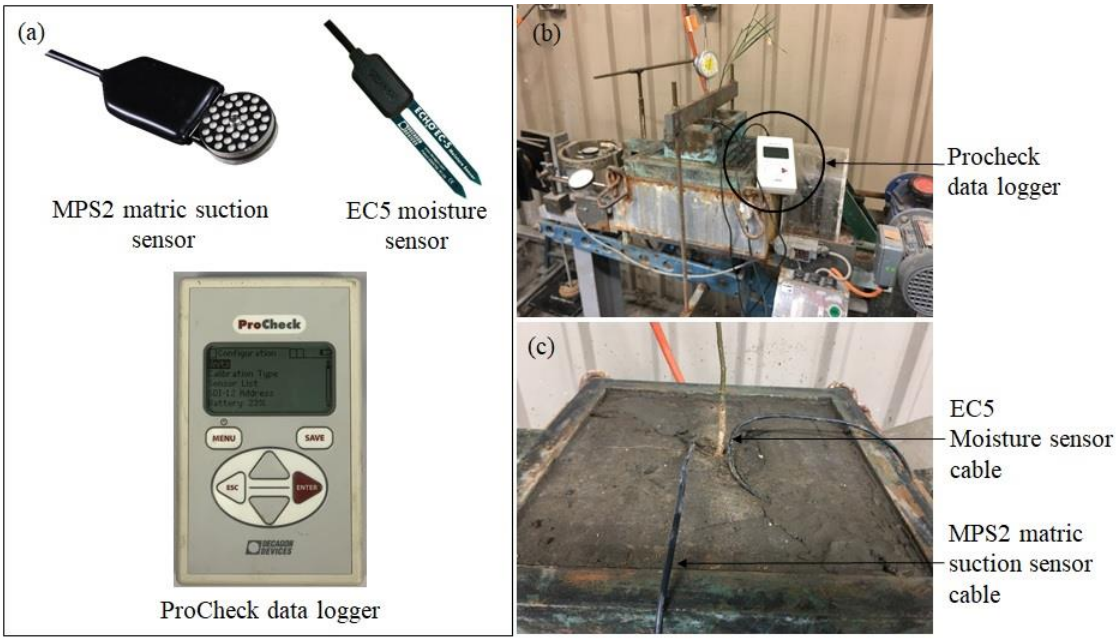

Figure 3.10 Arrangement of sensor cables into the data logger

Figure 3.11 Moisture evaporation control using cling wrap and wet gunny sacks

3.5 Root are ratio (RAR) and Root tensile strength test

At the end of each direct shear test, the two halves of the shear box were separated and the diameter of each root at the shear plane was measured and recorded. The root area is the proportion of the cross sectional area of the roots to the cross sectional area of soil. Roots less than 1 mm in diameter cannot be separated from soil without disturbance and they cannot be easily identified. Since measuring smaller roots can be inaccurate, roots smaller than 1 mm in diameter were not considered for this analysis. Roots that are more than 1 mm in diameter were selected to determine their plant root tensile strength using the Universal Testing Machine (UTM) from Instron.

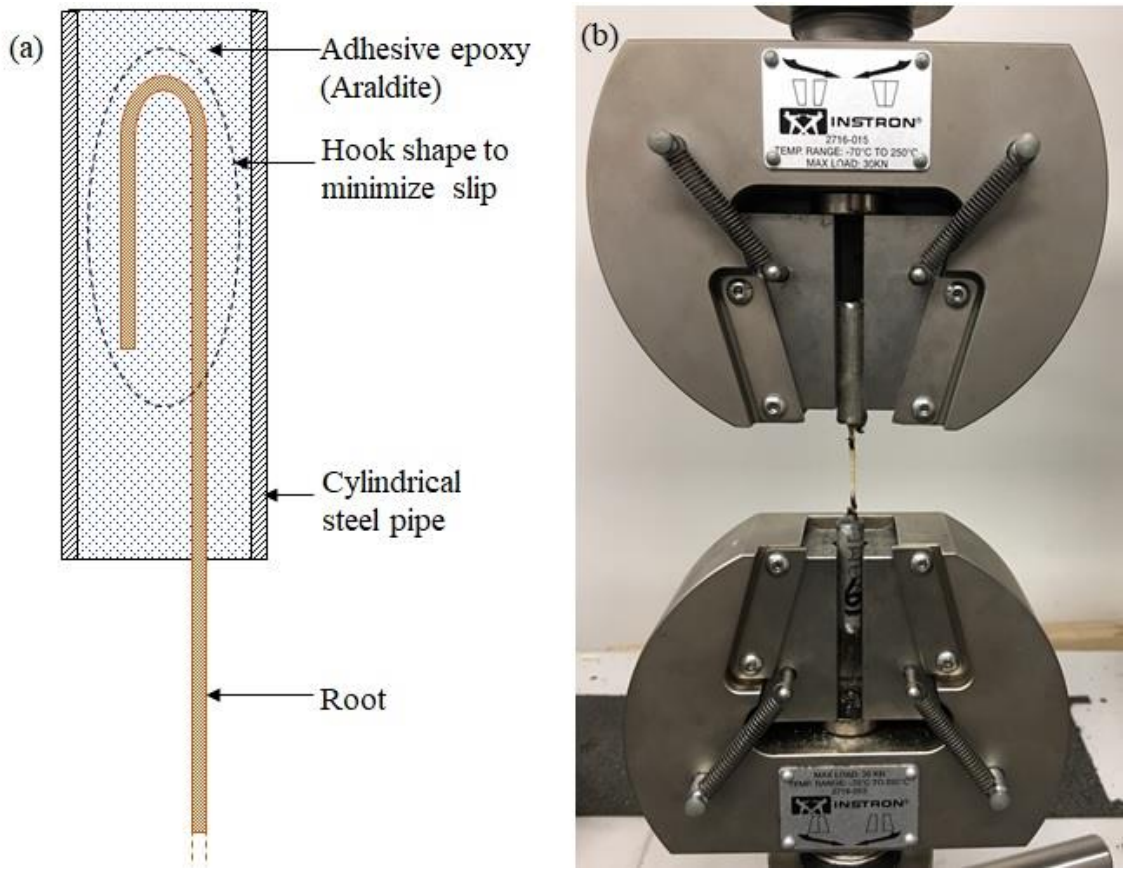

Figure 3.12 Tensile strength test set up

The diameters of roots of equal length (i.e. 125 mm) were measured. Each end of the root was bent into a hook, as shown in Figure 3.12 (a), and then insert into the cylindrical steel pipe. The steel pipe was then filled with an adhesive epoxy (Araldite) and then allowed to harden with the root inside. The hook shape was introduced to have extra resistance and to minimize the slip the root during the tensile strength tests. The prepared root sample was fixed into the top and bottom jaws of the UTM for the tensile strength test [Figure 3.12 (b)]. The tensile strength test of plant roots was carried out at a constant 1 mm/min rate of elongation until the root snapped. During these experiments, the root tensile force was recorded as the elongation of the root.

3.6 Electrical resistivity in vegetated soil

Seven soil specimens with plants as described in Section 3.4.2, were used to determine the electrical conductivity. The initial gravimetric moisture content of all seven soil specimens was kept constant (35.5 w% ± 0.5). The soil surfaces of all the specimens were covered with aluminium foil to minimise evaporation from the surface, and hence only transpiration dominated. All the soil specimens were then stored in a temperature and humidity-controlled (20 ± 2^{o}C, 30% RH) room and allowed to grow for about twelve months. The plants were watered at regular intervals; the wind speed was kept at zero, and a constant light intensity was provided by cool white fluorescent lamps. A resistivity meter (±0.1 Ωcm accuracy-Tinker and Razor (SR2)) was used to measure the electrical resistivity of soil specimens, and then convert to electrical conductivity (Equation 3.1). The Wenner configuration is one of four-point methods; it was used because of its high accuracy. Once the optimum electrode spacing had been calculated based on Appendix B, the electrodes were fixed, as shown in Figure 3.13. The A and B electrodes were used

to apply a current to the soil specimen, and M and N electrodes were used to measure the potential.

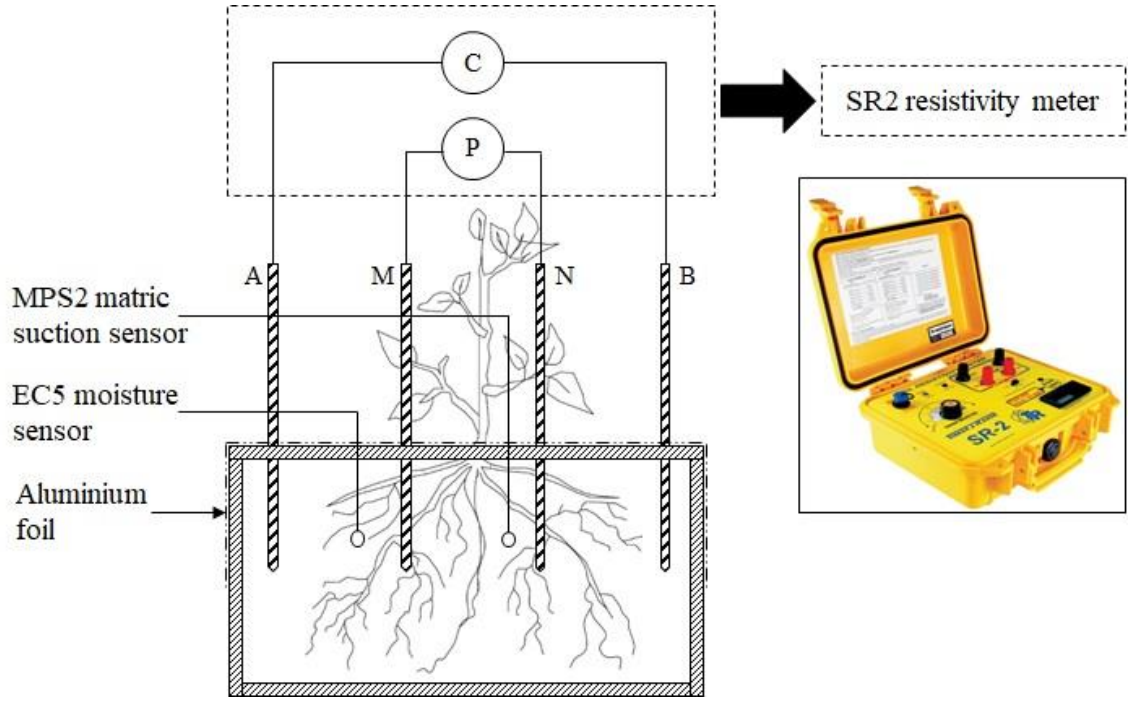

Figure 3.13 Resistivity tests set up with SR2 resistivity meter

3.7 Variation of matric suction in soil with tree roots

The soil specimens with the same species used for Section 3.6 were used to determine the change of matric suction and moisture in the soil due to root water uptake and transpiration. An MPS2 matric suction sensor and an EC5 moisture sensor were installed, as shown in Figure 3.13 to determine the change of matric suction and moisture. The ProCheck data logger shown in Figure 3.10 (a) was used for logging and recording the data. As discussed in Section 3.6, the plants were allowed to grow for about twelve months, after which continuous data recording commenced.

3.8 Summary

A series of small and large scale direct shear tests were carried out to determine how the role of osmotic suction affected the shear strength of unsaturated soil with and without root permeation. Small scale direct shear tests took place under constant water content conditions on remoulded silty clay with seven osmotic suctions (i.e. 0, 910, 1790, 2700, 3690, 4650 and 9560 kPa), and seven initial matric suctions (i.e. 0, 25, 100, 200, 500, 1000 and 1500 kPa). The soil specimens with 0 kPa osmotic suction were prepared by mixing soil with distilled water. The direct shear box assembly was covered with an airtight polyethene bag to isolate the air around the soil specimen. The soil specimens were loaded with three different normal stresses (i.e. 10, 20 and 40 kPa) and sheared at a very low strain rate of 0.006 mm/min. Large scale direct shear tests were carried out on soil specimens with tree roots. The remoulded soil samples with same seven different osmotic stresses (as in small scale DST) were compacted (85% of MDD) into the wooden boxes. Then the selected species (*Acacia Stenophylla* (River Cooba)) were potted and allowed to grow for about two years. They were then transferred into a large scale direct shear box setup and instrumented with an EC5 moisture sensor and an MPS2 matric suction sensor to observe any variations of moisture and matric suction during shearing. The soil specimens were subjected to three normal stresses (i.e. 10, 20 and 40 kPa) and allowed to compress; they were then sheared until a maximum displacement of 32.5mm was achieved. The plants were extruded from all the sheared soil specimens, and the roots were subjected to tensile strength analysis. The tensile strength of all the plants with different osmotic stresses was determined, and the variations of electrical conductivity, soil matric suction, soil moisture content and root area ratio were observed.

CHAPTER 4: Results and discussion

4.1 Background

This chapter presents the results and discussion of two separate series of small scale (60 x 60 x 40 mm) and large scale (300 x 300 x 200 mm) direct shear box tests, as well as several other preliminary tests. The small scale direct shear tests were carried out to determine how the role of osmotic suction affected the stress-strain behaviour of soil specimens without the influence of tree roots, whereas the large scale direct shear box tests considered the influence of tree roots. The shear stresses and vertical displacements for different matric and osmotic suctions were then compared with and without the influence of tree roots. Furthermore, the preliminary properties of soil such as soil classification, SWCC, compaction properties, and consistency limits were discussed. The properties of roots such as root tensile strength, root area ratio, and root induced matric suction were monitored with respect to the osmotic suction.

4.2 Preliminary soil properties

The particle size distribution of the soil is shown in Figure 4.1 where the soil contains 48% of sand, 36% of silt and 16% of clay. The liquid limit and plastic limit are 46.8% and 27.7%. The soil is classified as CL (Lean clay with sand) based on the ASTM Unified Soil Classification system (ASTM_D2487 2010).

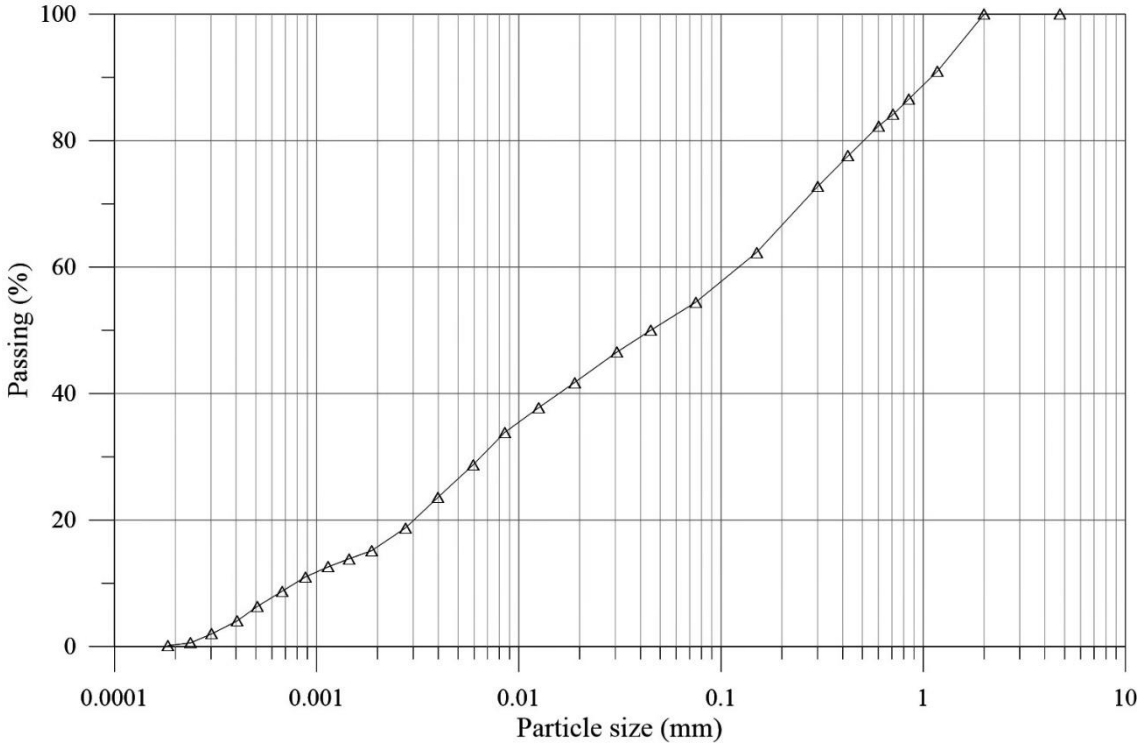

Figure 4.1 Particle size distribution curve

The specific gravity of the soil is 2.62. The maximum dry density (MDD) and optimum moisture content (OMC) are 15.58 kN/m^3 and 27.2% respectively. The soil water characteristic curve (SWCC) determined according to section 3.2.2 is shown in Figure 4.2. The experimental results have been interpolated with the van Genuchten (1980) model, whose fitting parameters are m = 0.306, n = 1.44 and α = 0.008 (initial void ratio is 0.79). As per the experimental results shown in Figure 4.2, the soil has an air entry value (AEV) of around 50 kPa.

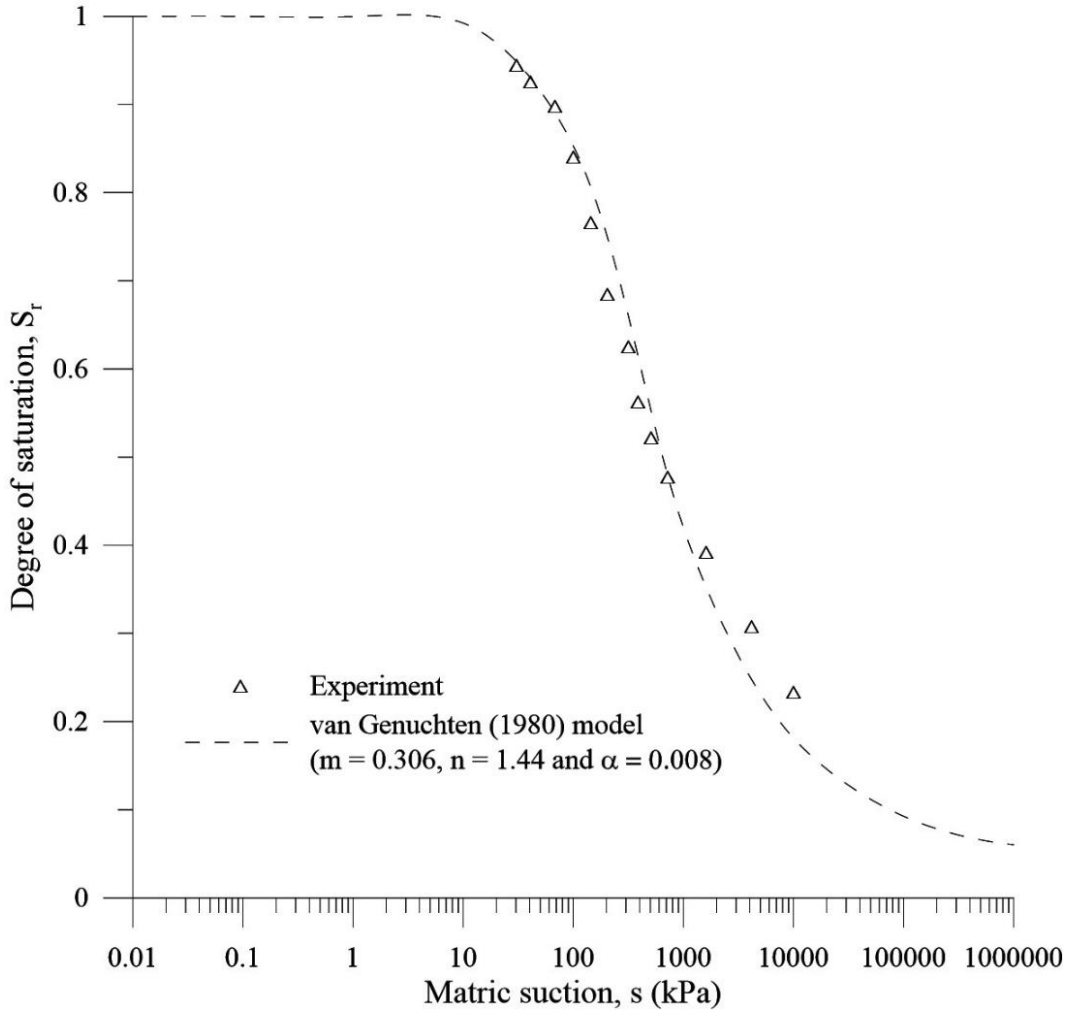

Figure 4.2 Soil water characteristic curve (SWCC)

The osmotic suctions of the specimens of saturated soil remoulded with NaCl solutions (as described in Section 3.2.4) are summarised in Table 4.1.

The electrical conductivity of these saturated soil specimens shown in Figure 4.3 indicates that the electrical conductivity increases with increasing concentrations of pore water.

Table 4.1 Measured osmotic suction of saturated soil specimens for different amounts of pore water concentrations

Concentration (mol/L)	Measured osmotic suction (kPa)
0.0	0.0
0.2	910
0.4	1790
0.6	2700
0.8	3690
1.0	4650
2.0	9560

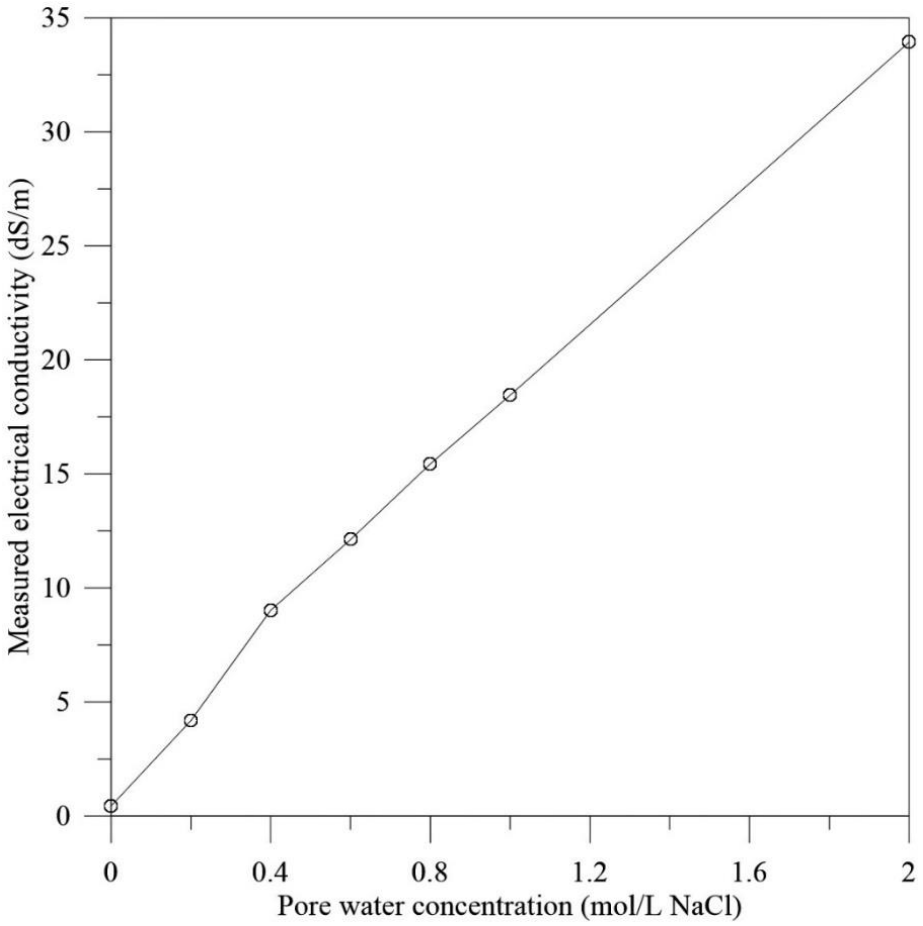

Figure 4.3 Distribution of electrical conductivity of saturated soil specimens with respect to pore water salinity

4.3 Influence of osmotic suction on the shear strength of soil (without roots)

The shear stress and displacement of 147 soil samples were measured at three different normal loads for given osmotic suctions and various initial matric suctions. The direct shear test was repeated for selected soil specimens to verify the accuracy of the results. Although the stress-strain behavior of these selected soil specimens was not exactly identical, the peak shear stress and maximum vertical deformation were comparable. The influence of osmotic suction on the peak shear stress was estimated for saturated and unsaturated conditions. The change in saturated peak shear stress without the influence of osmotic suction (π = 0 kPa) was considered as a reference for unsaturated soils where the osmotic suction varied.

4.3.1 Influence of osmotic suction under saturated conditions

The distribution of saturated shear stress with respect to horizontal displacement for various osmotic suctions at a given normal stress (σ'_N = 10 kPa) are shown in Figure 4.4 (a). In this figure, the shear stress increases with the horizontal displacement until it reaches a maximum, after which it shows a residual behaviour at higher horizontal displacements. Moreover, the change in osmotic suction increased the peak shear stress of the soil to a maximum of around 14 kPa [Figure 4.4 (a)]. This is in agreement with the findings reported in previous research works by Fu et al. (2019), El-Aal (2017), Di Maio and Scaringi (2016) and Zhang et al. (2016). Therefore, based on these investigations, it is evident that the osmotic suction can increase the peak shear stress of saturated soil, and since the stress distribution does not show a stable residual stress state, only the peak shear stress conditions were used in this study.

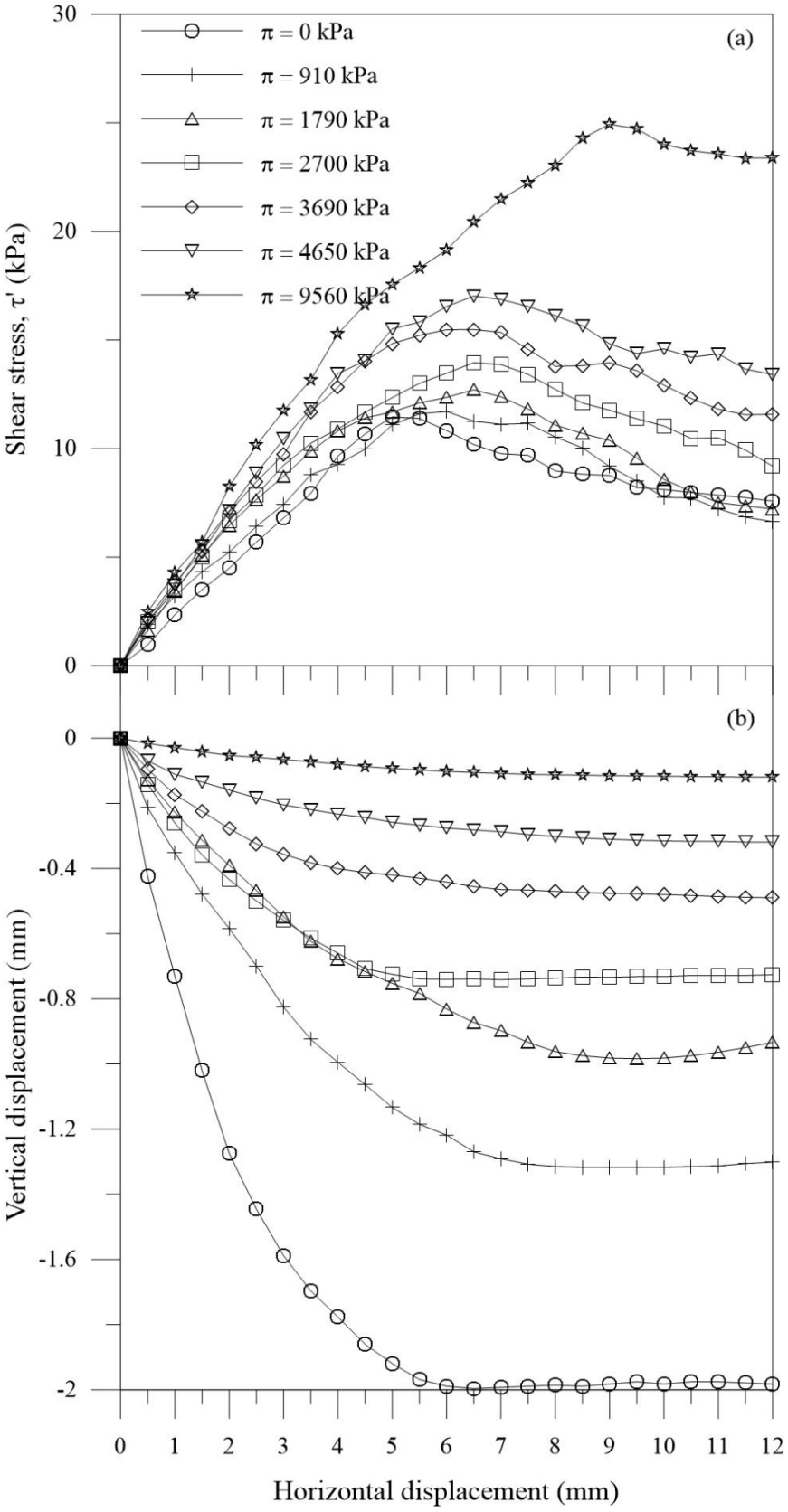

Figure 4.4 Distribution of (a) shear stress and (b) vertical displacement, with horizontal displacement for saturated conditions (σ'_N = 10 kPa)

The osmotic suction also influenced the change in volume of the soil specimen, so in this study, the volumetric change in the soil specimen is discussed in terms of a change in vertical deformation. The influence of osmotic suction on vertical displacement is shown in Figure 4.4 (b). Since the maximum displacement of all the samples decreases as the osmotic suction increases, it appears that osmotic suction can help the specimens generate resistance to deformation during shearing.

4.3.2 Influence of osmotic suction in unsaturated conditions

Based on the critical literature review described under Chapter 2, no study has considered the influence of osmotic suction on the stress-strain behaviour of unsaturated soil. This is why the stress-strain behaviour of unsaturated soil specimens is being analysed for various soil matric suctions. Figure 4.5 shows the distribution of shear stress with respect to horizontal displacement for various initial matric suctions. In saturated conditions the shear stress increased with the horizontal displacement until it reached to a maximum, and then it followed residual behaviour at higher horizontal displacements. Of all the osmotic suction conditions, only four are discussed within this subsection. These four osmotic suctions cover the entire range of osmotic suctions, i.e., low (π = 0 kPa), mid (π = 1790 and 3650 kPa) and high (π = 9560 kPa). The results indicate that the peak shear stress increases ass the initial matric suction increases. The change of peak shear stress with respect to matric suction and osmotic suction is described in Section 3.3.4. The increase in the initial matric suction from a 0 to 1500 kPa facilitated to increase the peak shear stress from 11.46 kPa to 133.10 kPa when there was no influence from osmotic suction (i.e. π = 0 kPa) at a given normal stress (i.e. 10 kPa) (Figure 4.5). This increase in peak shear stress due to matric suction has already been proved by previous researchers such as Toll and Ong (2003), Khalili and Khabbaz (1998), Vanapalli, SK et al. (1996) and Bishop (1959). Moreover, the influence of osmotic suction further increased the peak

shear stress because it increased from 24.4 kPa, with an increase of 9560 kPa of osmotic suction when the initial matric suction was 200 kPa.

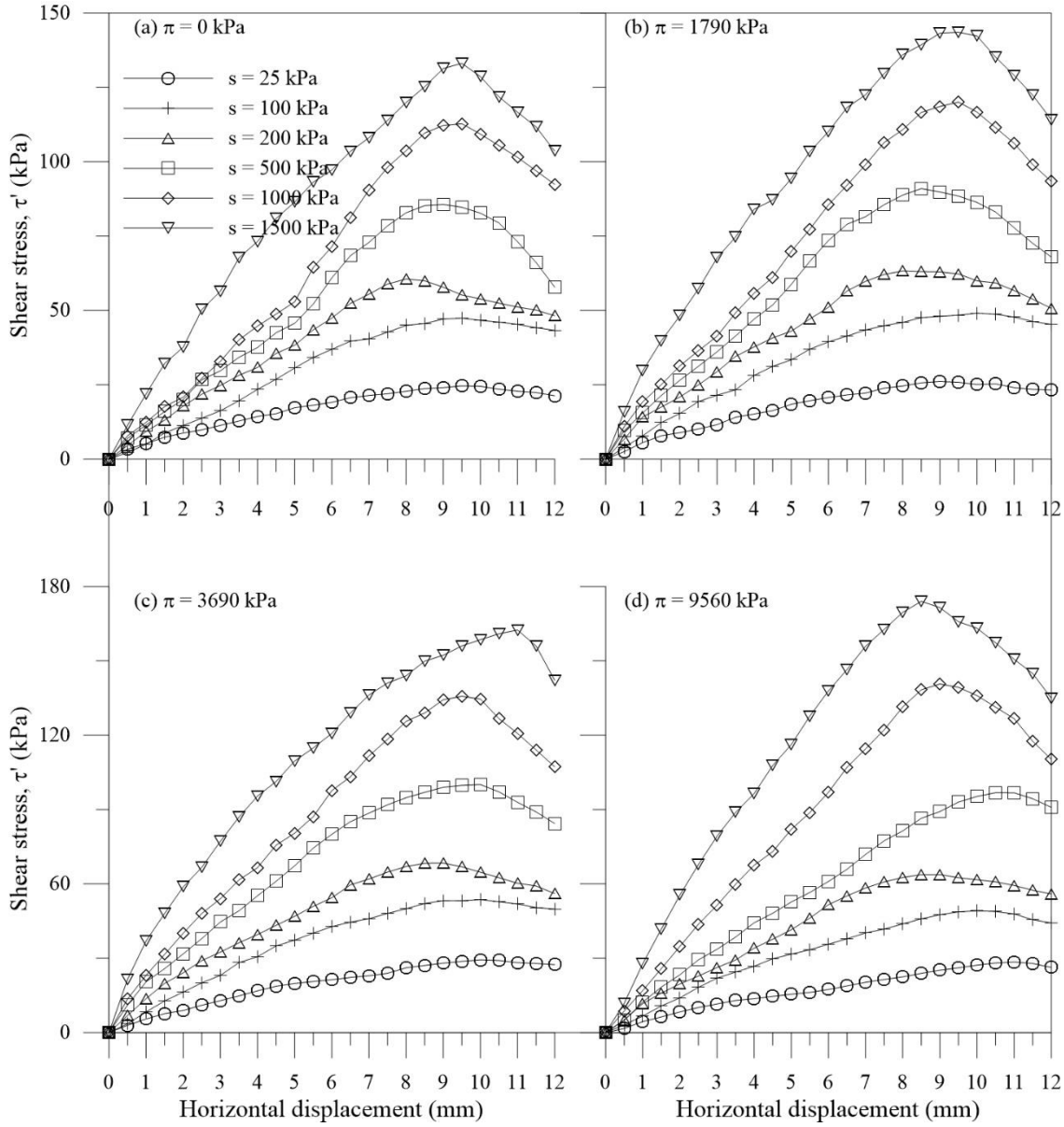

Figure 4.5 Distribution of shear stress with horizontal displacement for different initial matric suctions at various osmotic suctions (a) 0 kPa (b) 1790 kPa (c) 3690 kPa and (d) 9560 kPa osmotic suctions (σ'_N = 10 kPa)

The saturated specimens indicate that osmotic suction also influences vertical deformation, and it is anticipated that vertical deformation decreases due to the influence of matric suction. However, the influence that osmotic suction has on vertical deformation of unsaturated soil has not been established properly and neither has it been discussed. The distribution of vertical displacement with horizontal displacement for various initial matric suctions at four different osmotic suctions is shown by Figure 4.6.

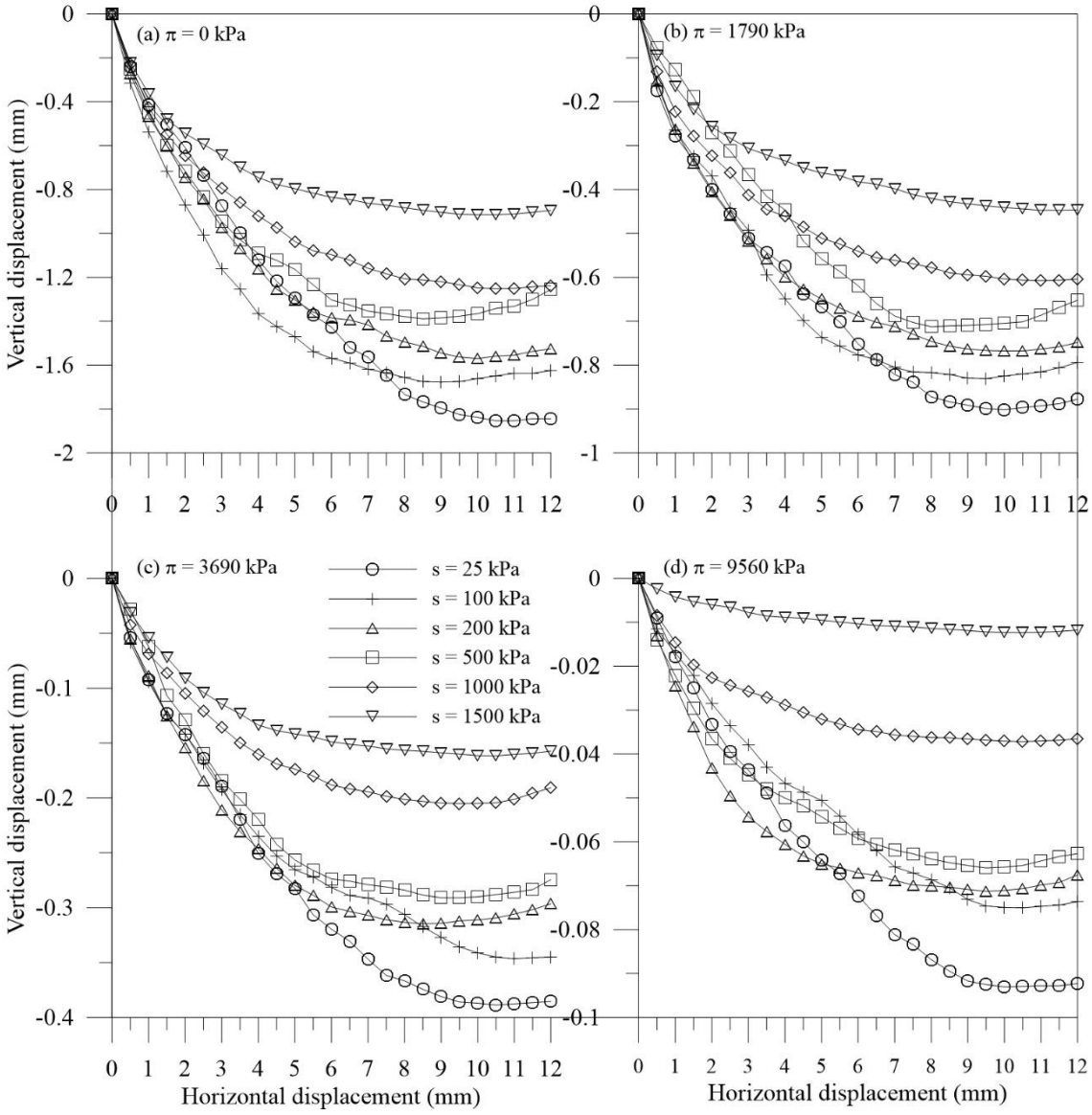

Figure 4.6 Distribution of vertical displacement with horizontal displacement for different initial matric suctions at (a) 0 kPa (b) 1790 kPa (c) 3690 kPa and (d) 9560 kPa osmotic suctions (σ'_N = 10 kPa)

For all osmotic and matric suction conditions, the specimens have contracted. Figure 4.6 also shows that vertical displacement decreased with matric suction and the osmotic suction; this influence also controlled the contractive behaviour of specimens. This deformation due to osmotic and matric suction can be seen in terms of maximum vertical displacement. The maximum vertical displacement is considered to be the lowest vertical displacement reached by the specimen for a given soil and loading condition. The distribution of maximum vertical displacement with respect to osmotic suction for different initial matric suctions is shown in Figure 4.7.

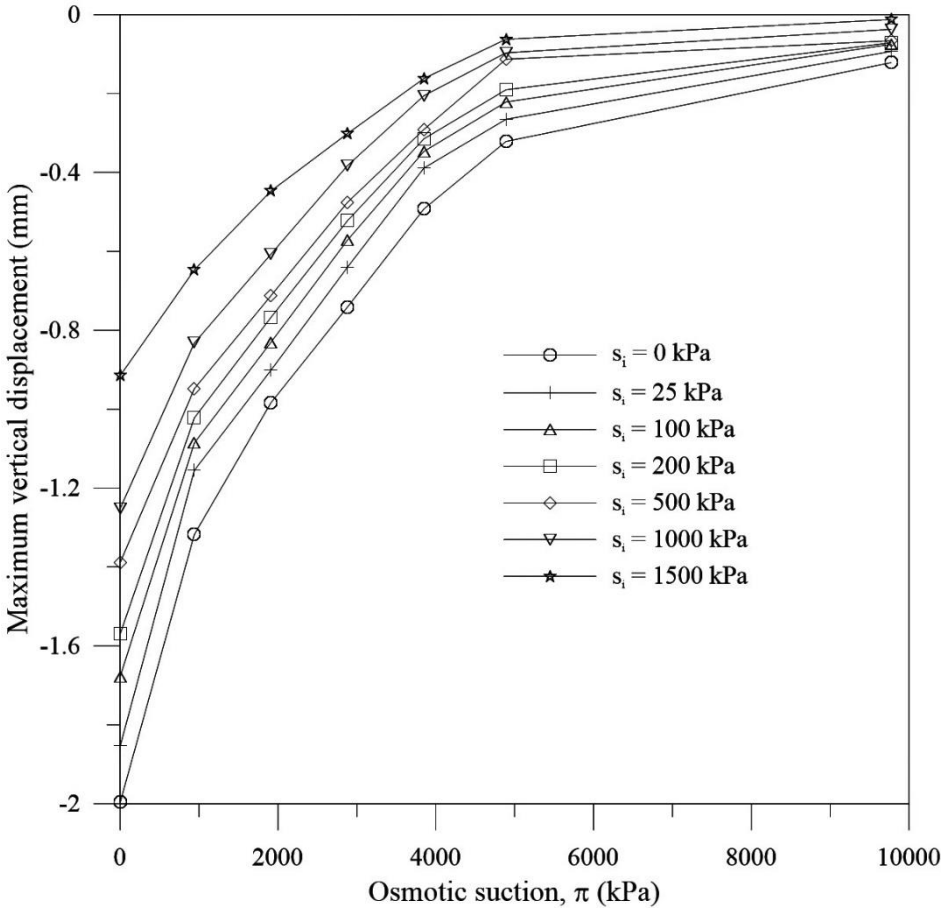

Figure 4.7 Distribution of maximum vertical displacement with respect to osmotic suction for different initial matric suctions (σ'_N = 10 kPa)

The maximum vertical displacement of 2.0 mm resulted from the soil specimens being remoulded with distilled water (π = 0 kPa) under saturated conditions for a given normal stress (i.e. 10 kPa). However, after increasing osmotic suction to 9560 kPa, maximum vertical displacement decreased to 0.12 mm which is an almost 94% decrease. Moreover, by increasing the initial matric suction to 1500 kPa, maximum displacement decreased to 0.91 mm, which is almost a 54.5% decrease. Therefore, it is evident that the increase in the initial matric suction and osmotic suction significantly reduced the maximum vertical displacement. This could be attributed to increase resistance to the relative movement of particles due to the influence of osmotic suction.

4.3.3 Peak shear stress

The peak shear stress or shear strength is significantly influenced by the initial matric suction and osmotic suction. It is in fact anticipated that under unsaturated conditions, additional inter-particle forces are generated by capillary tension, and these additional forces increase the peak shear stress. This study reveals that the peak shear stress has increased significantly as the initial matric suction increased. For example, at a given normal stress (i.e. 10 kPa), the peak shear stress increased to almost 121.64 kPa as the soil matric suction increased from 0 kPa (fully saturated) to 1500 kPa without the influence of osmotic suction (π = 0 kPa). However, the results indicate that the increase of peak shear stress decreases as the matric suction increases; this behaviour of the peak shear stress to the matric suction agrees with the findings by Fredlund et al. (1978). This change in osmotic suction occurs because of the concentration of cations and/or anions changes within the pore water solution. As the concentration of cations around a clay particle increase, the magnitude of the van der Waal attraction force increases and the magnitude of repulsive force decreases. Hence, the bond strength between the clay particles increases as the osmotic suction increases; therefore, the peak shear stress of the

soil must be increased as the osmotic suction increases. The distribution of peak shear stress to osmotic suction at different initial matric suctions is shown in Figure 4.8.

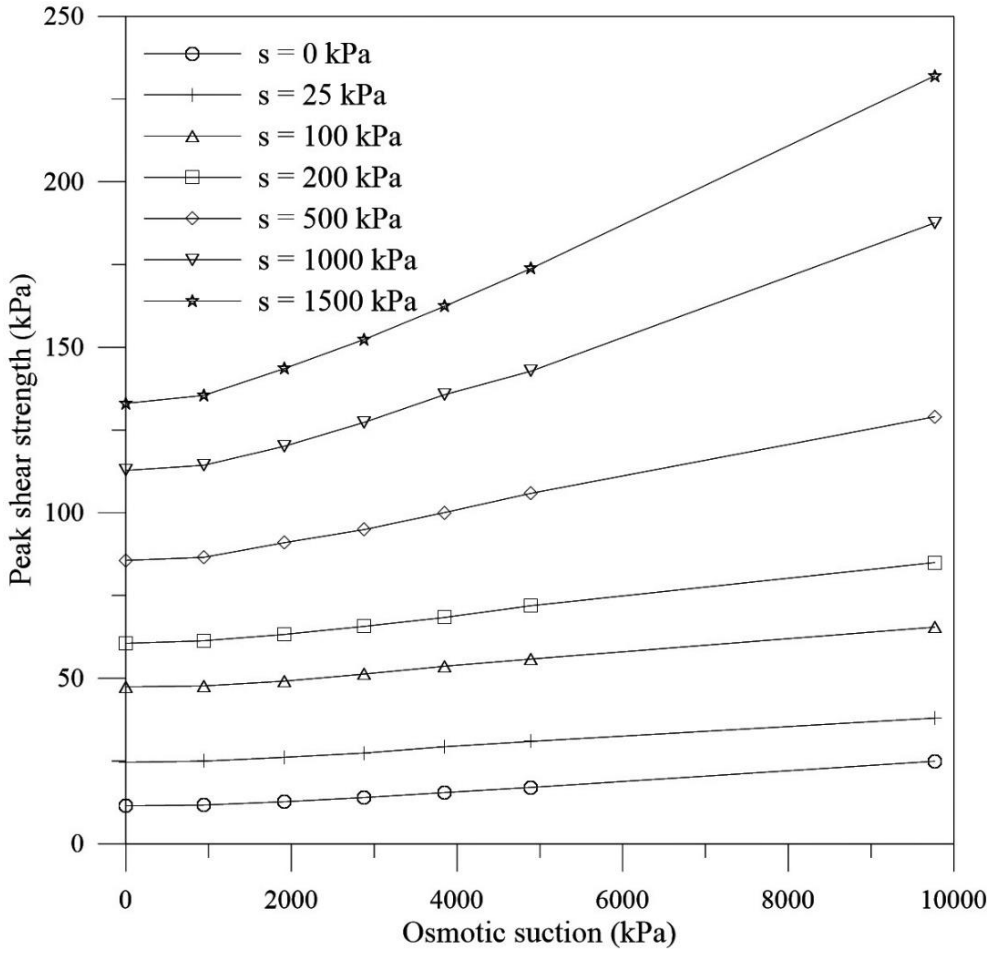

Figure 4.8 Distribution of peak shear stress with respect to osmotic suction for different initial matric suctions (σ'_N = 10 kPa)

This study shows that the peak shear stress increased to almost 15.5 kPa with a 9560 kPa increase in osmotic suction under fully-saturated conditions and for a given normal stress (i.e. 10 kPa). However, given that the normal stress remains unchanged when the soil matric suction increased to 1500 kPa, and the peak shear stress increased to 98.96 kPa for the same increase in osmotic suction. Therefore it is evident that, at higher matric suctions the contribution made by osmotic suction on the peak shear stress is even more significant than under fully-saturated conditions. Furthermore, as with the matric suction, the peak

shear stress shows a non-linear distribution with osmotic suction. Overall, the osmotic suction and initial matric suction can significantly influence the peak shear stress.

4.4 Influence of osmotic suction on the shear strength of root permeated soil

The shear stress and the displacement of 63 specimens of vegetated soil were tested in the large scale direct shear box apparatus under seven osmotic suctions and three matric suctions with three normal stresses. The distribution of shear stress for the specimens of vegetated soil is shown in Figure 4.9. The shear stress of the unsaturated and vegetated (saline) soil with respect to horizontal displacement shows an overall ductile behaviour (Figure 4.9). Even though the shear stress results of unsaturated soil under the influence of osmotic suction (without root permeation) show a distinct post-peak behaviour, the specimens influenced by tree roots do not show a well-defined peak. Similar behaviour was observed in the large scale direct shear box tests carried out by Pallewattha et al. (2019). During their experiments, the writer noted that most of the roots remained within the soil without slipping or breaking during shearing; thus those roots generated an additional resistance to shearing. Therefore, only the vegetated soil specimens showed a distinct post-peak behaviour during shearing. It appears that the influence of tree roots can actually strengthen soil enough to increase the peak shear stress, unlike the soil specimens without tree roots, even with the same conditions such as matric suction and applied normal stress. This is evident when Figure 4.5 (a) and 4.9 are compared without the influence of osmotic suction. However, when the osmotic suction is influenced by tree roots, there is no distinguishable change in the shear stress. While the matric suction and osmotic suction contribute to the shear stress of the soil specimens, the osmotic stress adversely affects the growth of tree roots. The influence of osmotic stress on the growth

of tree roots is discussed in Section 4.6. To observe the contribution on shear strength made by the roots only, the results of the peak shear stress of vegetated soil specimens were compared with non-vegetated soil specimens

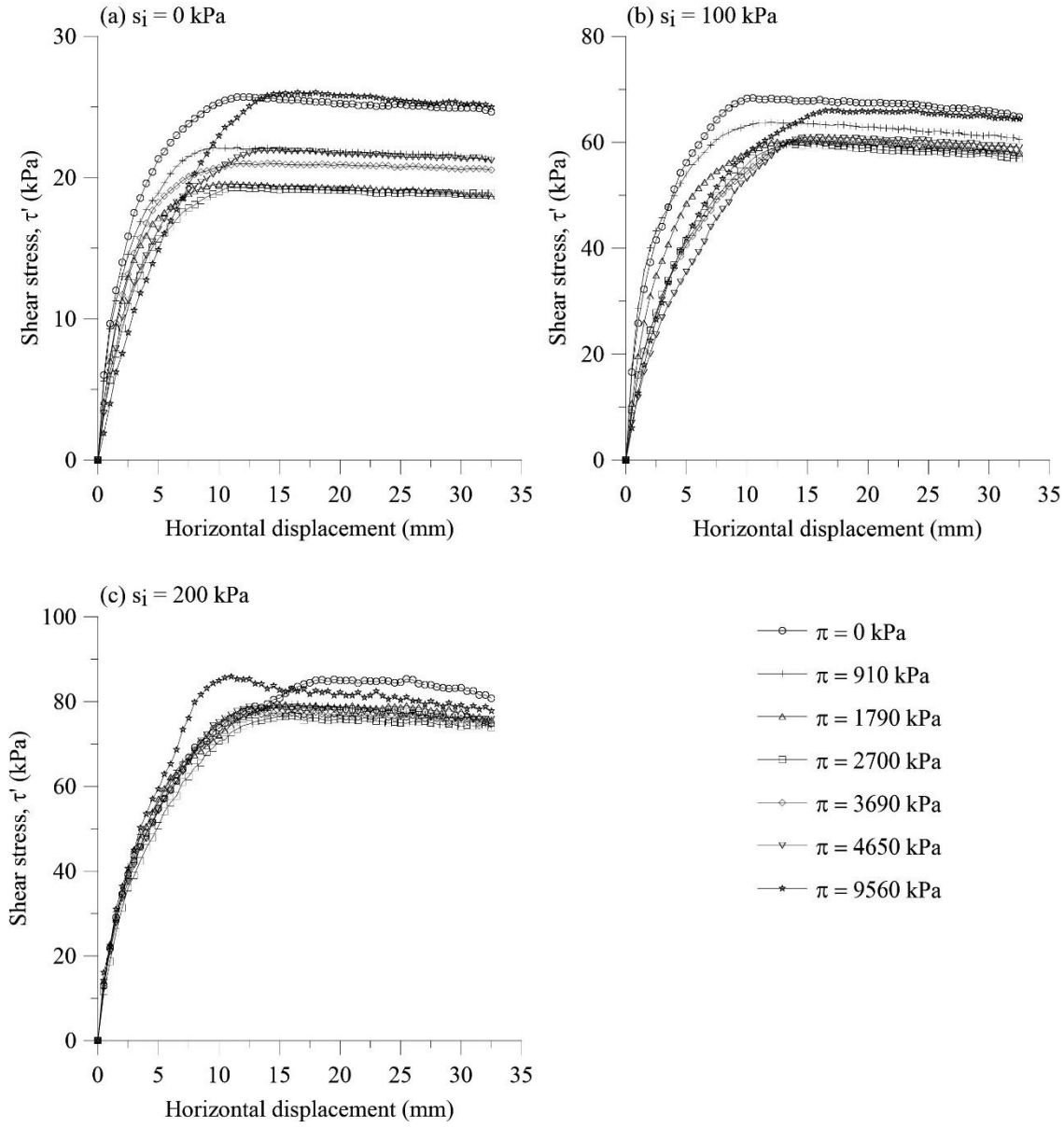

Figure 4.9 Distribution of shear stress of soil specimens with tree roots

(σ'_N = 10 kPa)

The peak shear stress was not sensitive to the deformation rate, therefore the peak shear stress results from with-roots and without-roots direct shear tests can be effectively

compared. The peak shear stress with and without the influence of tree roots for different osmotic suctions and initial matric suction for a given normal stress (σ'_N = 10 kPa) are shown in Figure 4.10.

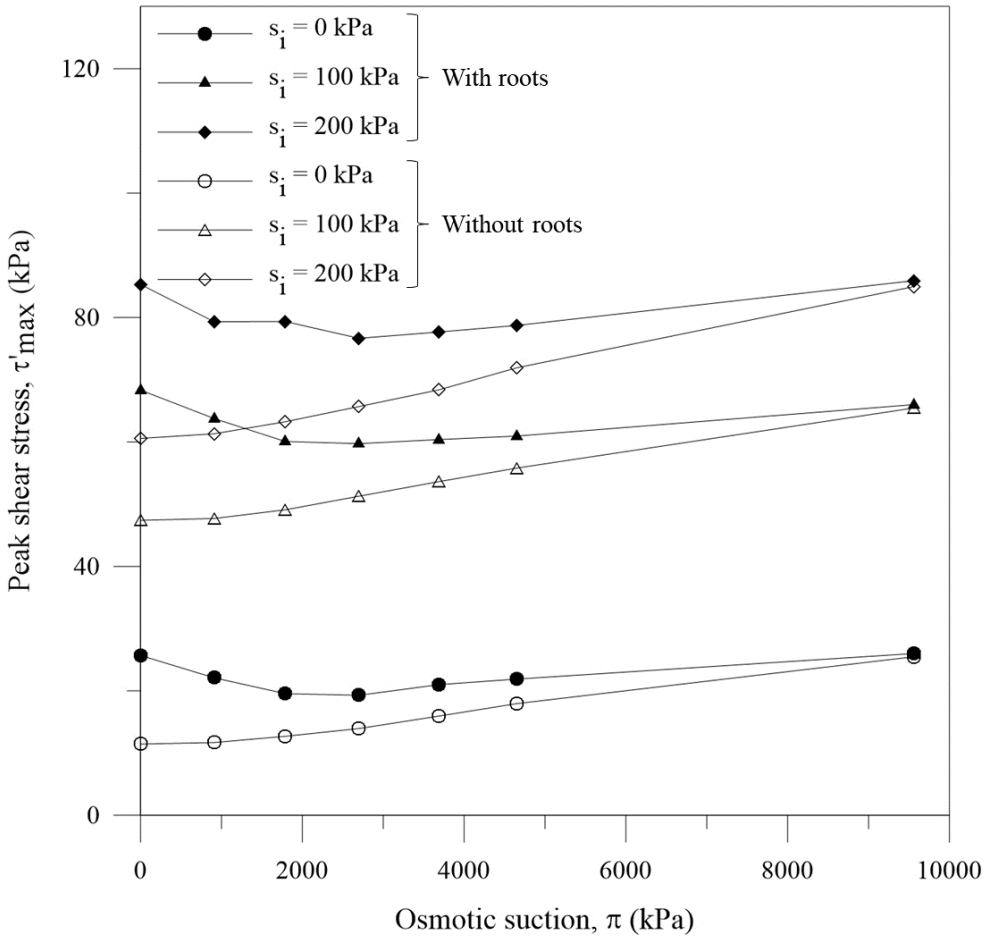

Figure 4.10 Distribution of peak shear stress with and without tree roots

Here, the peak shear stress of vegetated soil specimens is higher than the non-vegetated soil specimens for all the initial matric suctions. Moreover, as described earlier in Section 4.3, the influence of soil matric suction and osmotic suction have increased the peak shear stress, and therefore the matric suction, osmotic suction and tree roots can increase the peak shear stress individually. Moreover, the peak shear stress increased as the initial matric suction for both vegetated and non-vegetated conditions increased, but unlike the matric suction, the osmotic suction or osmotic stress could inhibit the growth

of tree roots. In fact this reduction in growth due to the influence that osmotic stress has on the plants is shown by the change in root area ratio in Section 4.6. In reality, the increase in the peak shear stress of vegetated soil specimen decreases as the osmotic suction increases; this can be seen at very high osmotic suctions where π = 9560 kPa. For example, when the osmotic suction is 9560 kPa for any given normal stress, the peak shear stress of the vegetated soil specimens was almost to the same as the peak shear stress of the non-vegetated soil specimens under all the initial matric suction conditions (Figure 4.10). Therefore, under very high osmotic suction, the influence of tree roots on the peak shear stress is negligible. The influence of tree roots on the peak shear stress with varying osmotic suction is discussed in Section 4.4.1.

Not only the shear stress or peak shear stress, but the vertical deformation of soil specimens with tree roots also changes due to osmotic suction. The vertical displacement of vegetated soil specimens with respect to horizontal displacement for different osmotic suctions at various initial matric suctions is shown in Figure 4.11. As per Section 4.3, the vertical deformation of soil specimens without tree roots decreased due to the matric suction and osmotic suction at any given normal stress. Similarly, the vertical deformation of vegetated soil specimens decreased with the matric suction and osmotic suctions. For example, when the initial matric suction is 100 or 200 kPa, and the osmotic suction is 9560 kPa, there is no significant vertical displacement, therefore, irrespective of vegetated or non-vegetated conditions, vertical displacement decreases as the osmotic suction and matric suction increases. This behaviour can be discussed using the results of maximum vertical displacement.

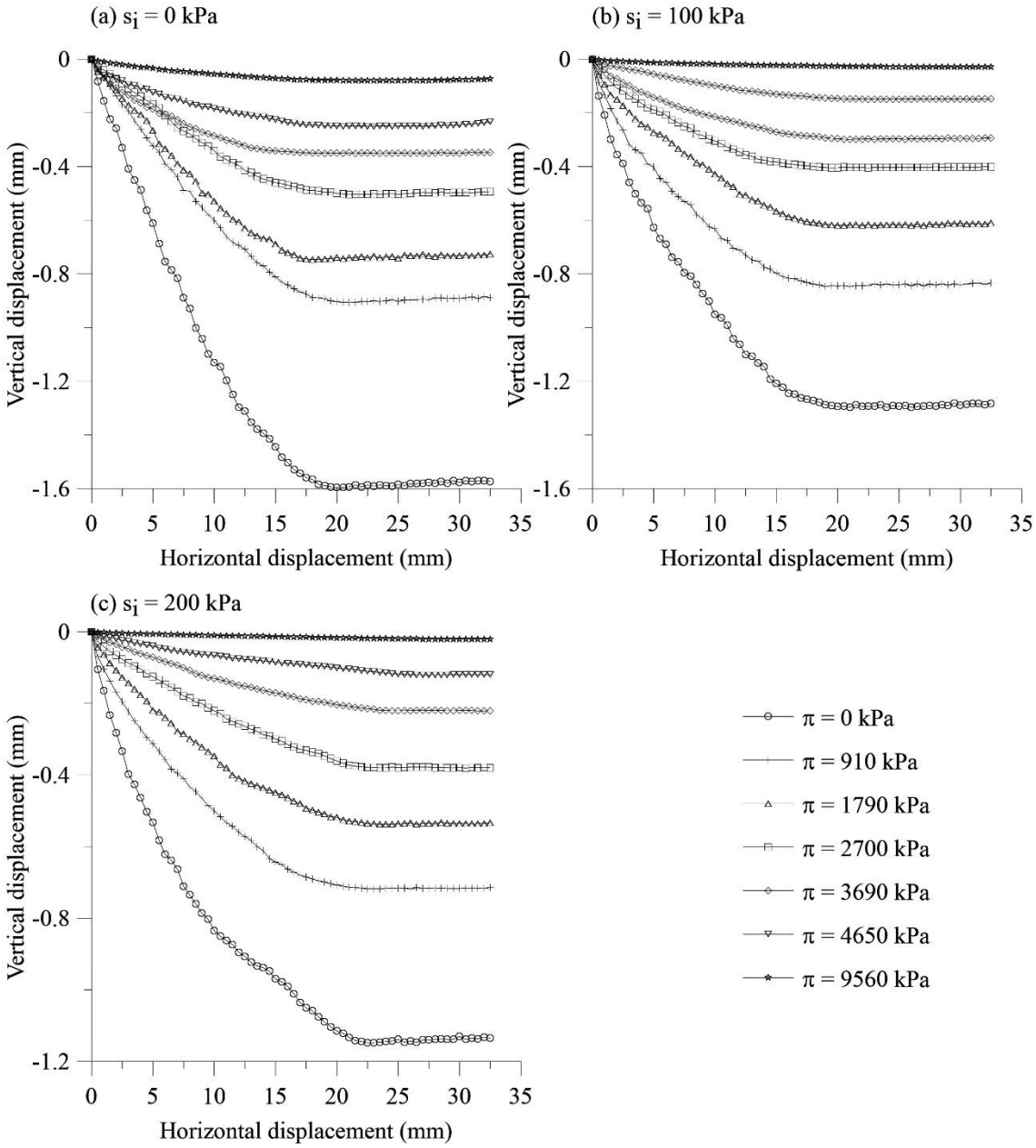

Figure 4.11 The vertical displacement of vegetated soil specimens

To discuss deformation behaviour with respect to the role of osmotic suction played on specimens of vegetated soil, the maximum vertical displacements were compared with and without tree roots and for various osmotic suctions and matric suctions at a given normal stress (σ'_N = 10 kPa). The maximum vertical displacement of soil specimens with and without the tree roots for various osmotic suctions and initial matric suctions are shown in Figure 4.12. The soil specimens with tree roots showed a decrease in maximum

vertical displacement, unlike the soil specimens without tree roots. The roots within the soil specimens with tree roots provide additional root reinforcement, therefore, the settlement or maximum vertical displacement decreases. It is therefore evident that the influence of roots also retards settlement.

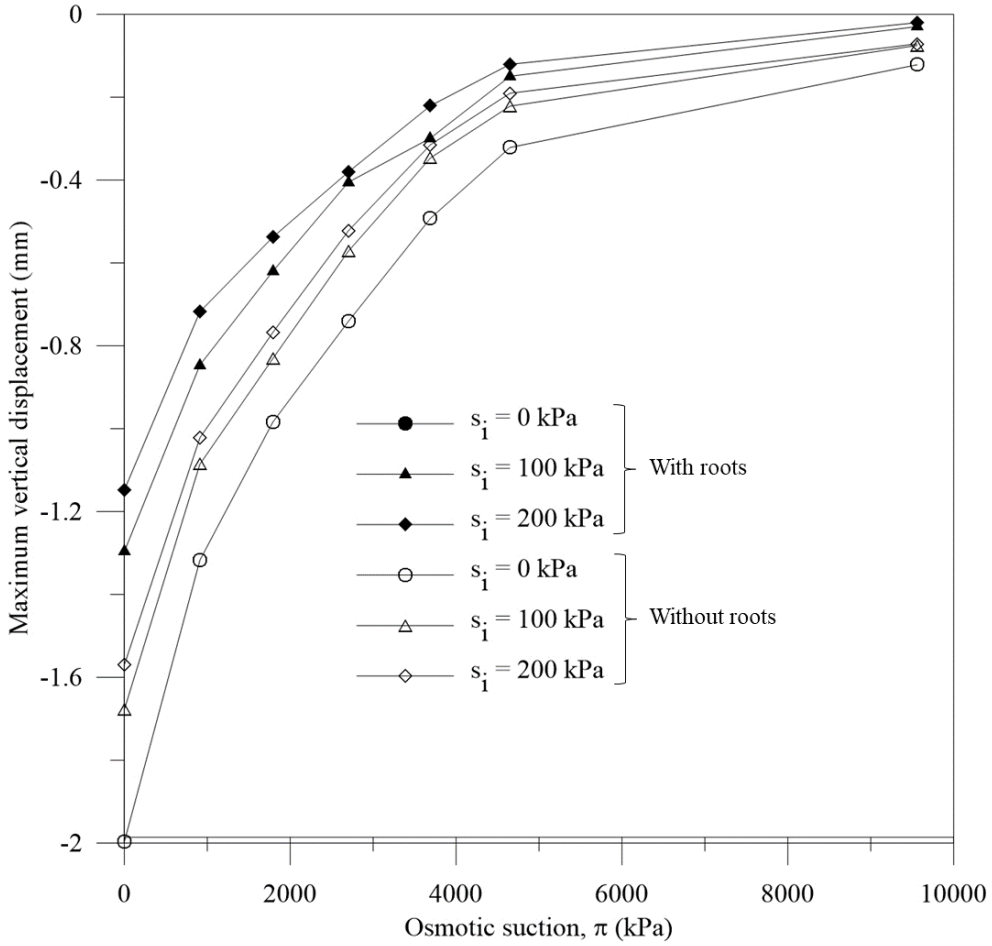

Figure 4.12 Distribution of maximum vertical displacement with respect to osmotic suction with and without the influence of tree roots

Irrespective of vegetated or non-vegetated conditions, the maximum vertical displacement decreased significantly as the osmotic suction increased for all the matric suctions. The findings from Section 4.3 indicate that the maximum vertical displacement of soil specimens without tree roots decreased due to the influence of osmotic suction. At very high osmotic suctions (i.e. π = 9560 kPa), the maximum vertical displacement under all conditions converged to a negligible settlement of a minimum value around 0.1 mm.

However, the contribution made by the roots on maximum vertical displacement should be considered with respect to osmotic suction.

4.4.1 Influence of osmotic suction on root-only shear strength

The influence that the roots have on peak shear stress or shear strength of the soil specimens were calculated based on the direct shear tests of vegetated and non-vegetated specimens. The contribution made by the roots on the peak shear stress with regard to osmotic suction is shown in Figure 4.13. The contribution made by roots on the peak shear stress decreased as the osmotic suction increased for any given normal stress; this behaviour is common for all three initial matric suction conditions.

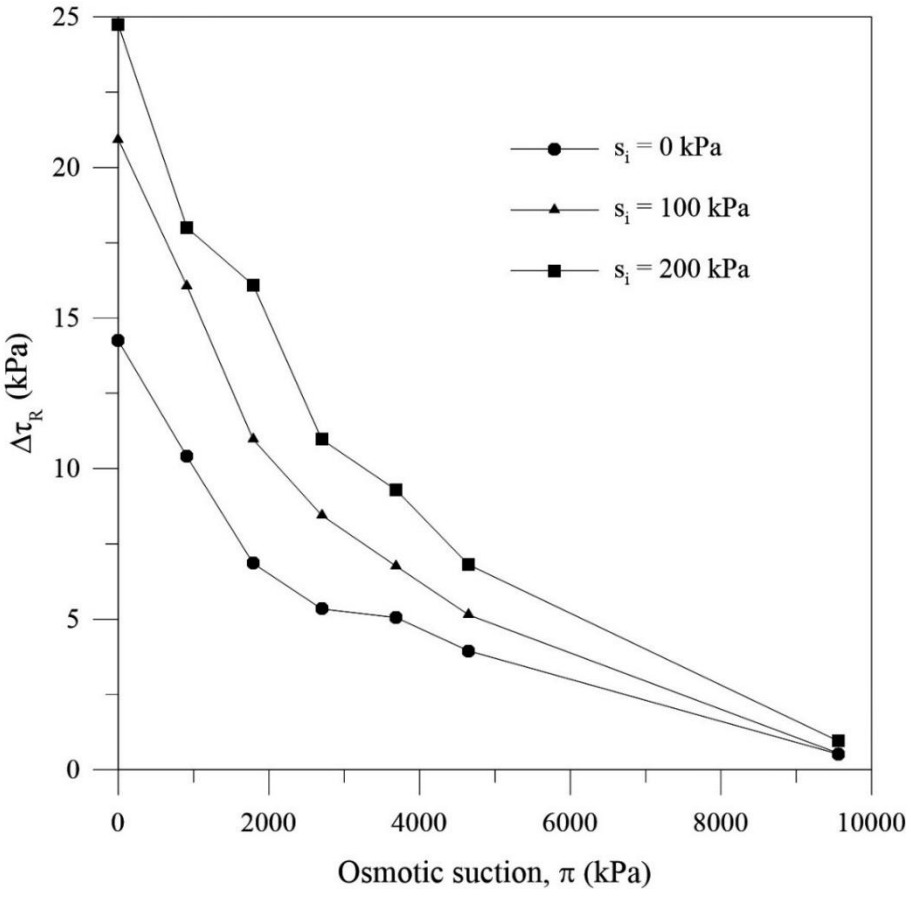

Figure 4.13 Distribution of root influenced peak shear stress with respect to osmotic suction for various initial matric suction

Figure 4.13 also shows that the contribution made by roots on the peak shear stress is negligible at very high osmotic suctions, i.e. 9560 kPa. The contribution made by roots on the peak shear stress under saturated conditions is less than the other two initial matric suctions, because, most of the roots slipped during shearing, so they offered less resistance. The highest contribution made by roots on the peak shear stress was reported to be with 200 kPa initial matric suction. It is evident that as the soil matric suction increases or the degree of saturation decreases, the contact or bonding strength between the root and soil increases. This increasing contact strength was discussed in terms of a series of pull out tests carried out by Galpathage et al. (2019), which showed an increase in the pull-out force as the soil matric suction increased. Moreover, the contribution made only by roots on the peak shear stress decreases with osmotic suction. As discussed above, osmotic stress is due to the presence of salinity in the pore water generated within the roots (or plant cells); therefore the growth of the roots decreases with the degree of osmotic suction or osmotic stress. This condition is even intensified by the unsaturated behaviour of soil, which shows that the root contributes almost the same shear strength for all matric suctions. Similar to the root-only influence on the peak shear stress calculations, the change of vertical displacement of soil specimens was calculated based on vegetated and non-vegetated direct shear test results. The results of root-only influence on maximum vertical displacement (ΔVD_R) is shown in Figure 4.14. Vertical displacement due to tree roots (at maximum vertical displacements) decreases as the osmotic suction increases. There is a scattered distribution of ΔVD_R from 0 kPa to 3690 kPa of osmotic suction, and almost the same ΔVD_R values for all the three initial matric suctions. However, the experimental results indicate there is no distinguishable relationship between ΔVD_R and the initial matric suction.

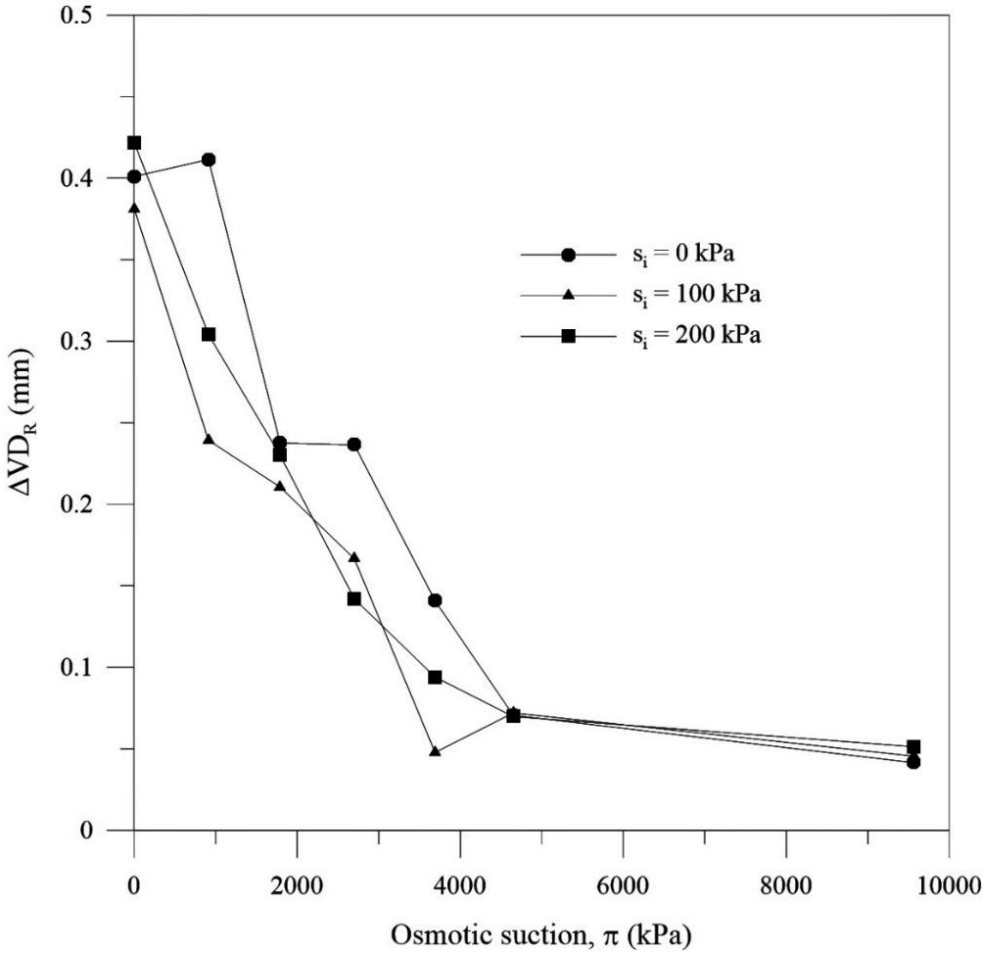

Figure 4.14 Distribution of root influenced vertical displacement with respect to osmotic suction for various initial matric suction

4.5 Root tensile strength

A total of 254 root samples were selected to analyse the tensile strength of roots. The tensile strength (maximum recorded value from the tensile strength test) with respect to root diameter is shown in Figure 4.15. Of the seven osmotic suctions, only four were selected to represent low, medium and high ranges.

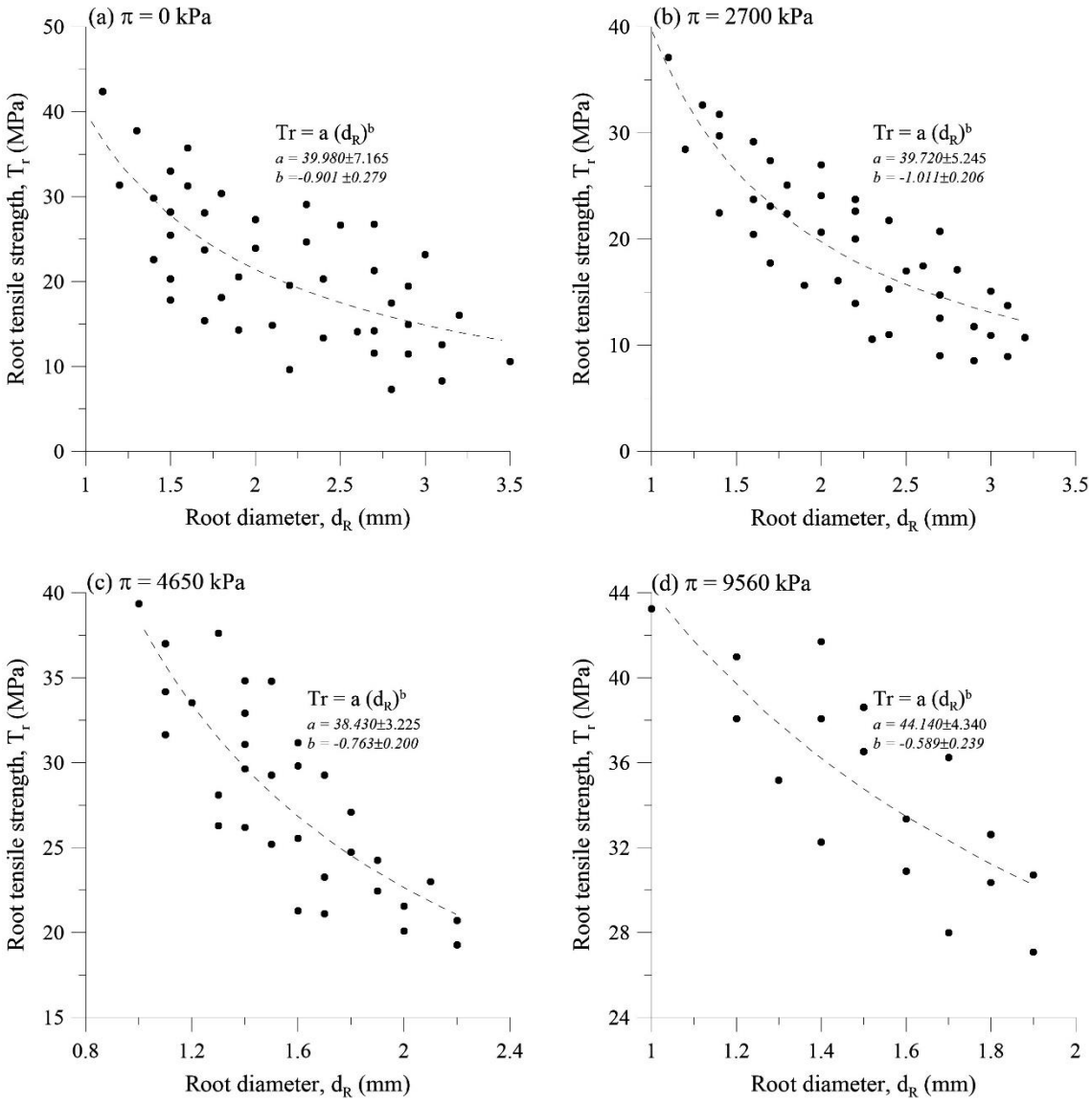

Figure 4.15 Tensile strength of tree roots with respect to root diameter

The tensile strength with respect to root diameter followed the power decay function for all osmotic suctions, which satisfied the previous work carried out by Boldrin et al. (2017), and Operstein and Frydman (2000). It is therefore evident that the tensile strength of roots decreases with their diameter (as per previous research as well). Even though the fitting parameters were changed slightly, the basic function of root tensile strength vs root diameter is not affected by the osmotic suction.

However, as the osmotic suction increased the maximum root diameter and maximum tensile strength showed some variations. Hence, the maximum root diameter and maximum root tensile strength were compared with respect to osmotic suction (Figure 4.16).

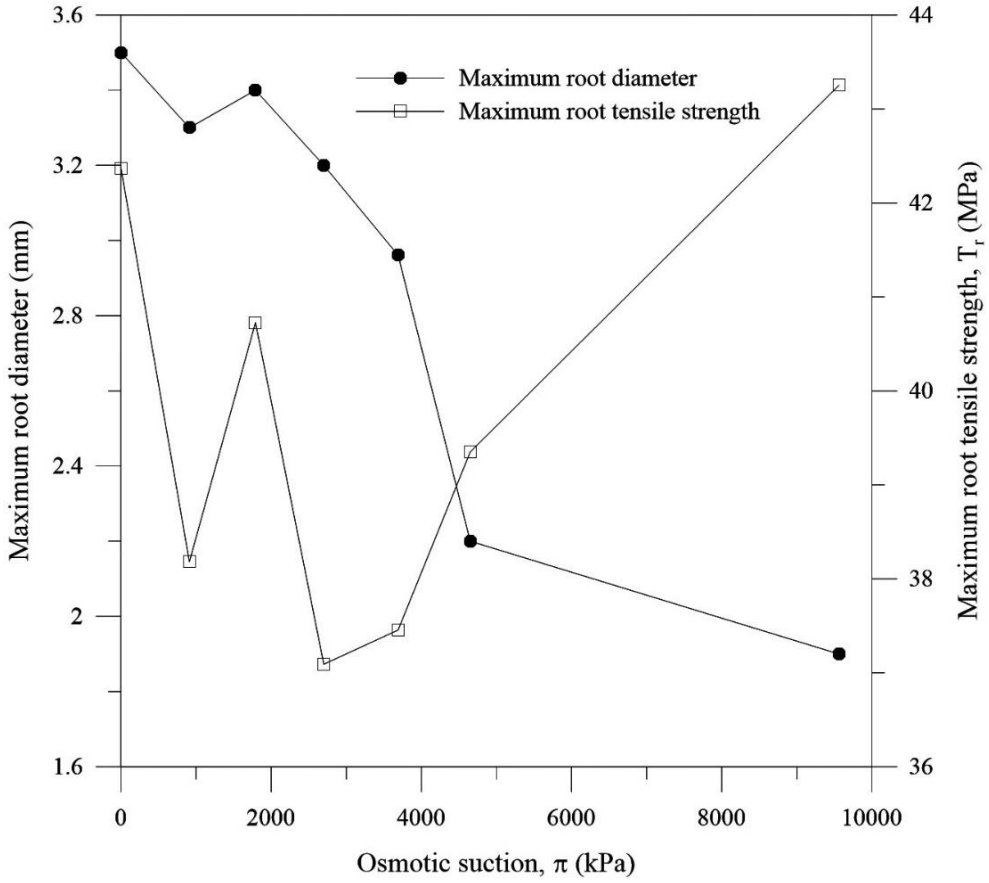

Figure 4.16 Distribution of maximum root diameter and maximum root tensile strength with respect to osmotic suction

In Figure 4.16 the maximum root diameter decreased as the osmotic suction increased, probably because the salinity stress generated within the tree roots controlled any further growth of the roots. However, the maximum tensile strength of roots does not show a noticeable relationship with the osmotic suction variation, and therefore, the maximum root tensile strength can be considered as independent of the osmotic suction.

4.6 Root area ratio

The root area ratio is the ratio between the cumulative cross-sectional area of roots of a shear plane to the cross-sectional area of the soil of the same shear plane. The root cross-sectional area was measured after each direct shear test. When determining the tensile strength, roots that are less than 1 mm in diameter were not considered due to a lack of accuracy during sampling and measuring. The RAR of each soil specimen was measured to one decimal place as a percentage. The average RAR for the same soil conditions (i.e. same osmotic stress or suction) was calculated and then considered to be the RAR for a given soil condition. In the following sections, the term "root area ratio or RAR" refers to the averaged root area ratio. The distribution of root area ratio with respect to osmotic suction is shown in Figure 4.17, where the root area ratio decreases as the osmotic suction increases; it follows a power decay law. It is evident that the RAR is affected by the osmotic stress generated within the tree roots by salinity in the pore water. Therefore, the RAR will be used to analytically model root response with respect to osmotic stress in Chapter 5.

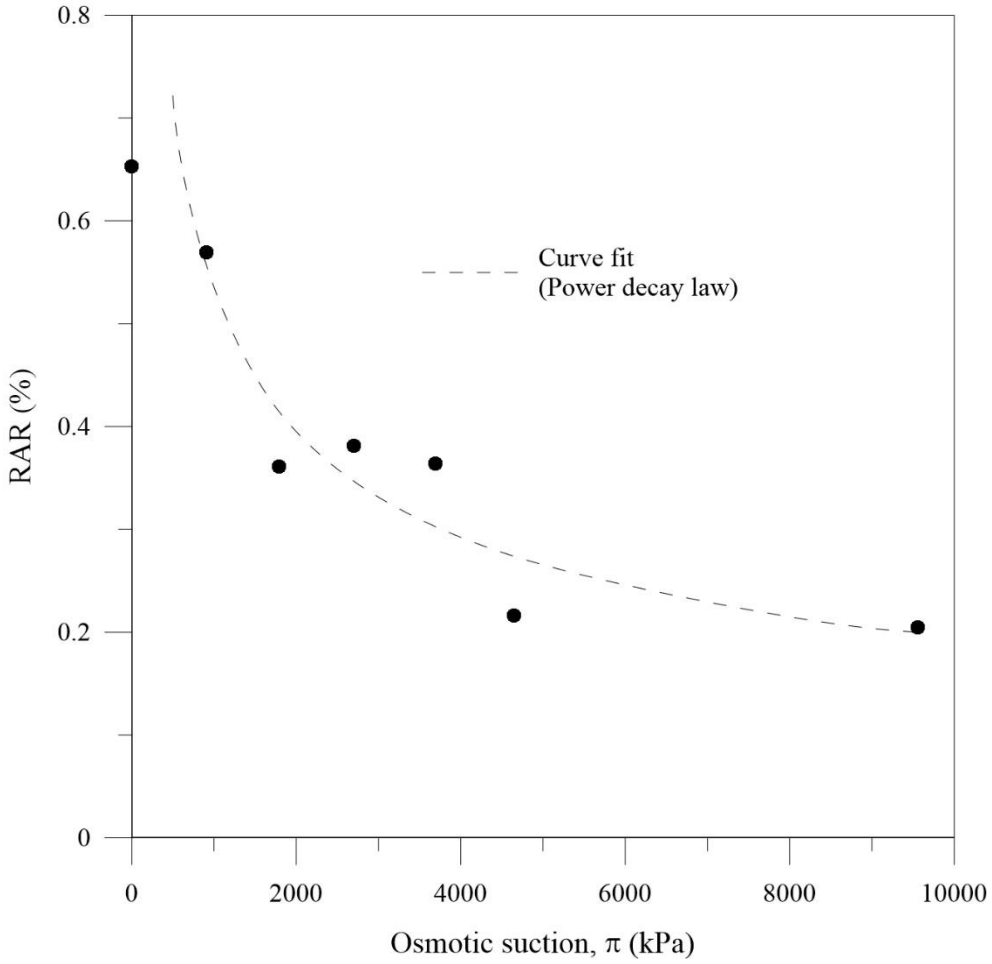

Figure 4.17 Distribution of average root area ratio with respect to osmotic suction

4.7 Influence of tree root induced suction on SWCC

As per the previous studies, the root water uptake and transpiration process can change the soil suction due to changes in the water content. As per unsaturated soil mechanics, the shear strength of soil may increase by this induced soil suction; therefore, it is necessary to understand the behaviour of SWCC with and without the influence of root permeation under variable osmotic stress conditions.

The influence of tree root water uptake on SWCC (specimens prepared with distilled water having negligible osmotic suction) was considered as a reference condition for the other osmotic stresses (Figure 4.18). According to Figure 4.18, the SWCC has clearly shifted up along the y-axis (i.e. volumetric water content). Therefore, soil with trees has

higher matric suction than soil without trees for the same volumetric water content. Also, the AEV of the vegetated soil specimens is higher than soil without tree roots. However, the slope of the SWCC within the transition zone or the rate of desorption remains unchanged. These findings prove that vegetated soil retains a high soil matric suction because of root water uptake and transpiration.

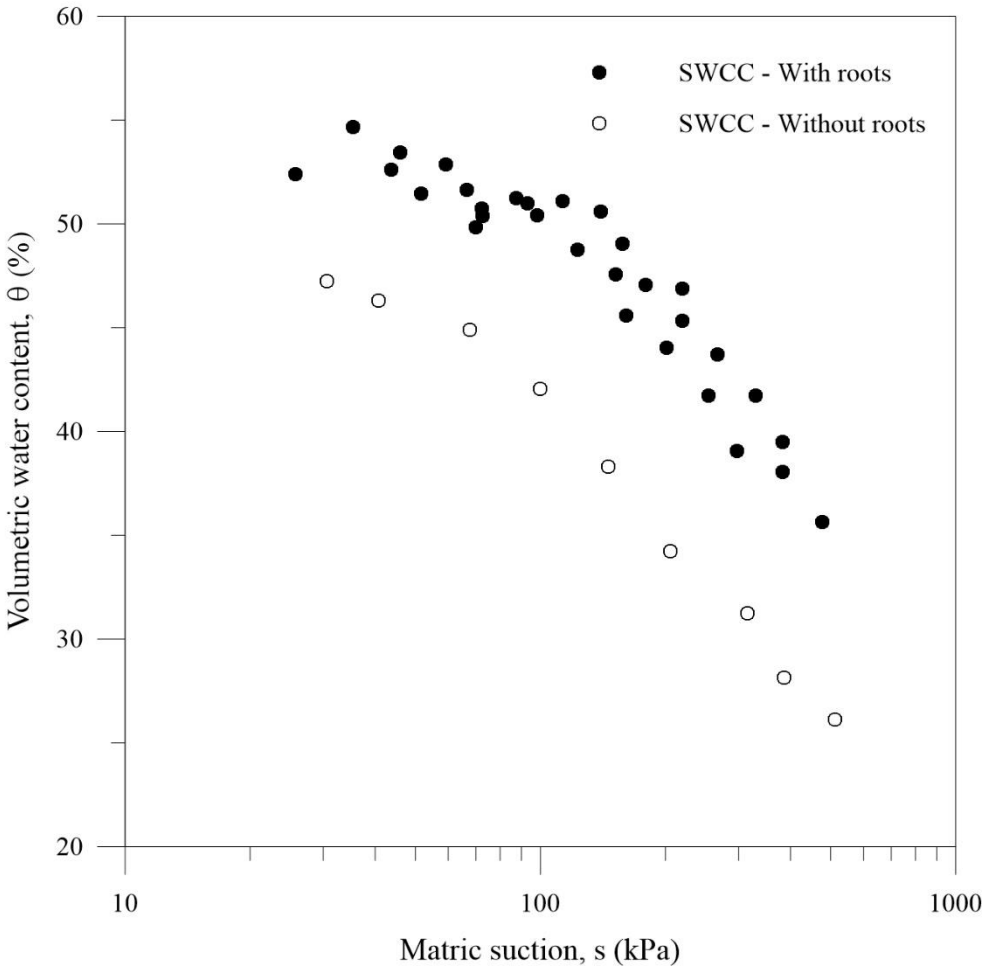

Figure 4.18 Change of SWCC with and without the influence from tree roots (π = 0 kPa)

Based on the previous analysis in Sections 4.5 and 4.6, the maximum root diameter and root area ratio were influenced by the osmotic stress. The change in RAR due to osmotic stress can influence the SWCC of a vegetated soil. Therefore, the change of SWCC in relation to the soil matric suction for various osmotic suctions is shown in Figure 4.19,

where the SWCC has shifted down along the volumetric water content axis due to the influence of osmotic suction. However, the osmotic suction has not affected the rate of desorption. With the influence of osmotic suction, the root water uptake and plant growth have been deteriorated due to the osmotic stress generated between the root and water phases, therefore, as the osmotic suction increases, the vegetated soil specimens show a reduction in the soil matric suction for the same volumetric water content, unlike the vegetated soil specimens with 0 kPa osmotic suction.

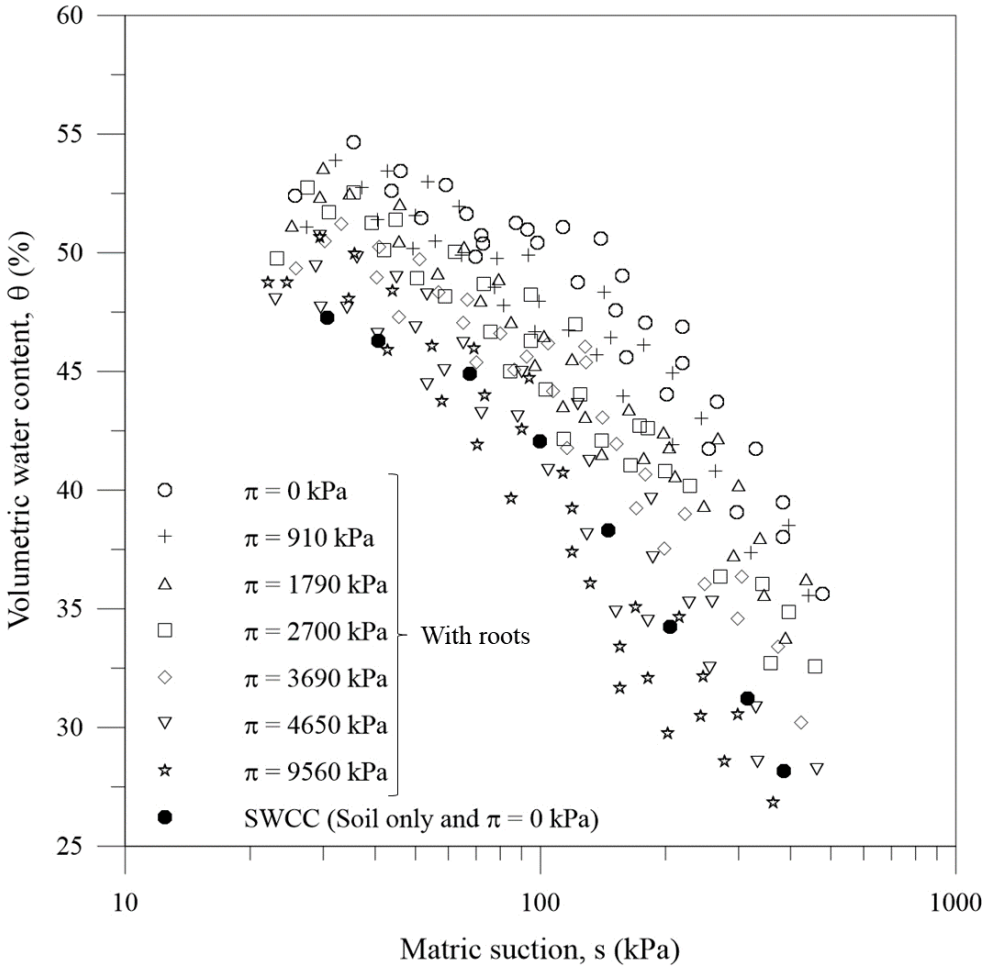

Figure 4.19 Comparison of SWCC under vegetated conditions for different osmotic suctions and non-vegetated conditions with 0 kPa osmotic suction

4.8 Electrical conductivity and soil suction

The change in the moisture content or change in the ion concentration in pore water of a soil specimen can be determined by the theory of electrical conductivity. In this study, the change in electrical conductivity of vegetated soil specimens was based on a four-point electrode method (i.e. Wenner configuration) for different osmotic stress conditions. The electrical conductivity with respect to the soil matric suction for different osmotic suctions is shown in a log-log plot (Figure 4.20).

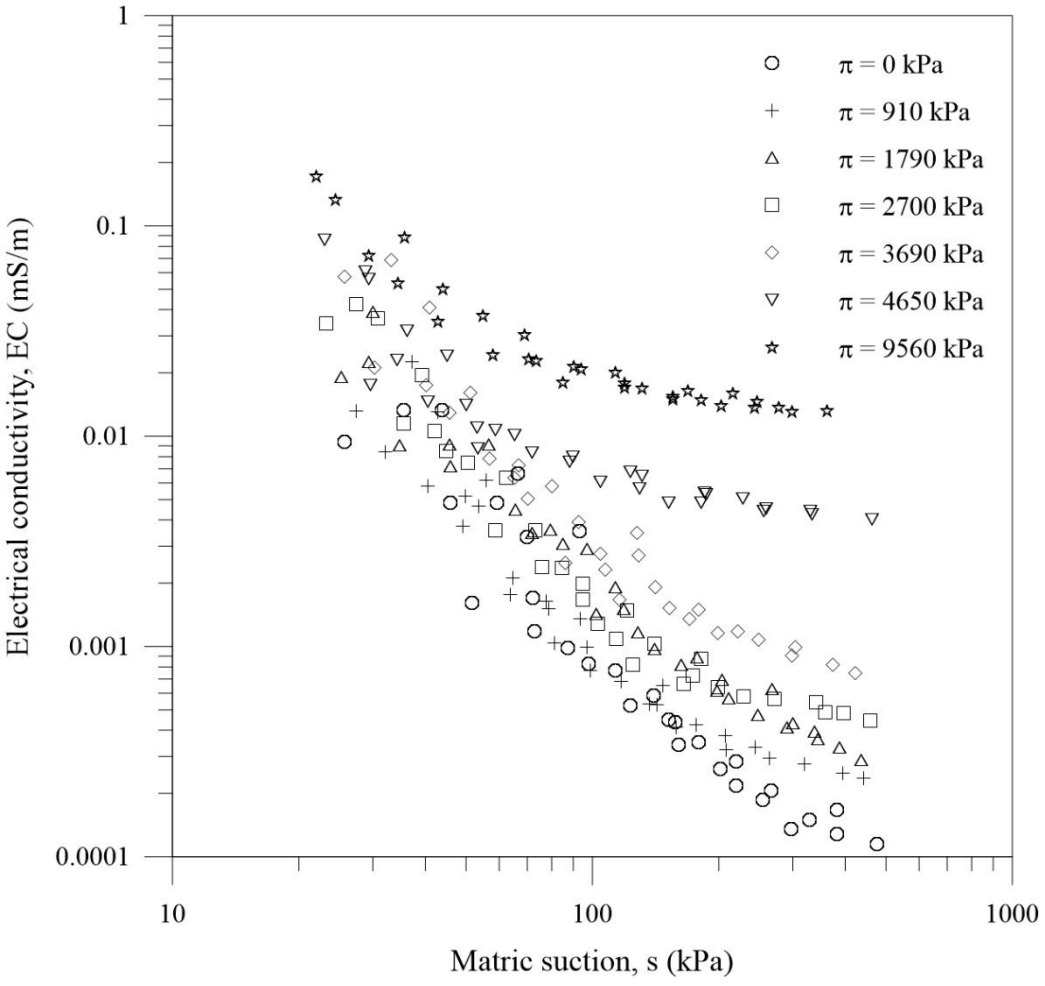

Figure 4.20 Distribution of electrical conductivity of soil specimens with tree roots, with respect to matric suction for different osmotic suctions

When the matric suction increased, the moisture content of the soil specimen decreased and hence the electrical resistivity of the soil increased. Therefore, electrical conductivity decreases as the matric suction increases. However, according to Figure 4.20, the decrease in electrical conductivity with the matric suction is linear (on log-log axis) for the entire matric suction range until the osmotic suction reaches to 2700 kPa. However, when the osmotic suction increases to 2700 kPa or more, the electrical conductivity becomes linear from fully-saturated (s = 0 kPa) condition to about 80 kPa of matric suction, beyond which the electrical conductivity becomes nonlinear.

4.9 Summary

The stress-strain behaviour of unsaturated soil specimens (without the influence of tree roots) with variable osmotic suctions was investigated and analysed with different soil matric suction conditions. The peak shear stress and maximum vertical displacement results were used to compare the influence of osmotic suction and matric suction. As anticipated, the peak shear stress increased, and the maximum vertical displacement decreased as the matric suction increased. In addition, the osmotic suction also increased the peak shear stress and reduced the maximum vertical displacement. A series of large scale direct shear tests was carried out on vegetated soil specimens with seven different osmotic suctions, three different matric suctions, and three different normal stresses, to quantify the role of osmotic suction on the peak shear stress under saturated and unsaturated conditions. The introduction of tree roots significantly increased the peak shear stress of soil and reduced the vertical displacement. Purely, the root contribution has on peak shear stress decreased as the osmotic suction increased, and there was no considerable change in the overall peak shear stress (peak shear stress of soil specimen with tree roots and osmotic suction) with respect to osmotic suction. The decreasing root-only contribution has on peak shear stress could be attributed to the root tensile

strength, the number of roots or RAR, and root-soil contact properties. The increase in osmotic suction retarded the growth of tree roots and also the root area ratio. However, the tensile strength of an individual root was not affected by the influence of osmotic suction, therefore, the primary cause of a decreasing tree root-only contribution to peak shear stress was because of the osmotic suction is root area ratio (RAR). The SWCC shifted along the volumetric water content axis due to the root water uptake that induced an additional matric suction in vegetated soil unlike in soil without tree roots for the same moisture content. However, due to the osmotic suction, the SWCC gradually moved down along the moisture content axis due to a reduction in the growth of tree roots. This growth of tree roots may be controlled by the osmotic stress generated between the root and soil boundary due to salinity in the pore water. A geophysical electrical conductivity test was used as a non-destructive technique to determine the SWCC. The electrical conductivity showed a liner distribution with the soil matric suction on a log-log plot until the osmotic suction reached 2700 kPa. However, as the osmotic suction increased (> 2700 kPa), the electrical conductivity became non-linear at higher matric suctions.

CHAPTER 5: Development of a new shear strength model

5.1 Background

This chapter presents the development of two different theoretical models used to capture the shear strength of unsaturated soil influenced by osmotic suction, with and without tree roots. The first model mainly focuses on unsaturated soil under the influence of osmotic suction where a new shear strength parameter (χ_2) is introduced. The behaviour of saturated soil influenced by the same osmotic suction used as a reference for unsaturated conditions. This parameter is defined in terms of electrical conductivity theories. The shear strength induced by osmotic suction can be explained quantitatively. The second model captures the influence that tree roots play on the shear strength of compacted specimens prepared at different levels of osmotic suction. Even though new models related to tree roots have been developed in terms of osmotic suction, the term osmotic stress has often been used for applications related to tree roots. The results presented in Chapter 4 show that even though the individual tensile strength of a tree root is not affected by the osmotic stress in pore water, it does have a substantial effect on the root area ratio (RAR), and therefore a new empirical model for osmotically induced root area ratio was introduced RAR_{π}. The quantitative determination of the induced shear strength of unsaturated soil in coastal areas with tree roots by the proposed new model is satisfactory. This new model retains the traditional Mohr-Coulomb framework with just a single equivalent friction angle, so engineers and researchers can easily implement this model for further investigations.

5.2 Shear strength model considering the role of osmotic suction

Chattopadhyay (1972) proposed that the influence of net inter-particle physiochemical stresses can be directly added to the effective stress:

$$\sigma_{net} = \sigma^* + (A - R) \tag{5.1}$$

where σ^* is the effective stress and $(A - R)$ is the net interparticle stress generated due to physicochemical effects.

Khalili and Khabbaz (1998) introduced a new parameter, χ_1, which is an effective stress parameter that depends on soil matric suction:

$$\sigma^* = (\sigma_N - u_a) + \chi_1(u_a - u_w) \tag{5.2}$$

where $(\sigma_N - u_a)$ is the effective normal stress, $\chi_1 = \left(\frac{u_a - u_w}{AEV}\right)^{-0.55}$ is the effective stress parameter which depends on the matric suction, $(u_a - u_w)$ is the matric suction, and AEV is the air entry value.

By combining Equations 5.1 and 5.2, the overall effective stress can be defined for unsaturated soil with physicochemical effects:

$$\sigma_{net} = (\sigma_N - u_a) + \chi_1(u_a - u_w) + (A - R) \tag{5.3}$$

By considering the Mohr Coulomb model, the shear strength of the soil can be written as:

$$\tau'_{US} = [(\sigma_N - u_a) + \chi_1(u_a - u_w) + (A - R)] \tan \phi' + c' \tag{5.4}$$

where τ'_{US} is the shear strength of unsaturated-saline soil, ϕ' is the effective friction angle, and c' is the effective cohesion component.

The $(A - R)$ component theoretically depends on interparticle forces which can be defined by the DLVO (Derjaguin-Landau-Verwey-Overbeek) theory (Liang et al. 2007). The cations and anions spread around a clay particle to form a region known as the diffusive layer. The potential difference between the surface of clay particles and the outer surface of the diffusive layer is called the zeta potential. A change in the concentration of

pore water (NaCl) increases the density of cations close to the surface of the clay, and hence the zeta potential also increases; this increase in the zeta potential also reduces the DDL thickness. It is still a challenge to accurately determine the zeta potential of a soil specimen with varying pore solutions, but it can be measured with a lot of limitations and assumptions. Therefore, an accurate determination of $(A - R)$ is difficult.

However, a new definition for $(A - R)$ is introduced by Equation 5.5:

$$(A - R) = \chi_2 \pi \tag{5.5}$$

where π is the osmotic suction (kPa) and χ_2 is a parameter which depends on osmotic suction.

Salinity can be defined as the number of dissolved ions in a known volume of water or solution. Osmotic suction is due to the change in the salinity of pore water, therefore χ_2 may theoretically vary when the number of dissolved ions changes and when the volume of solvent changes. On this basis χ_2 can be assumed to be a parameter that depends on osmotic suction; hence, a new semi-empirical model for χ_2 is introduced.

$$\chi_2 \begin{cases} = 0 & \pi = 0 \\ = \dfrac{a}{S_r^c}\left(1 - \exp\left(-b(ECR)\right)\right) & \pi \neq 0 \end{cases} \tag{5.6}$$

In the above equation, the ratio of electrical conductivity $(ECR) = \frac{\Delta EC}{EC_i}$, $\Delta EC = (EC - EC_i)$, EC is the electrical conductivity of saturated soil for a given concentration of salt in pore water, EC_i is the initial electrical conductivity of saturated soil remoulded with distilled water, S_r is the degree of saturation, and a, b and c are the experimental coefficients.

5.2.1 Sensitivity analysis of χ_2

The sensitivity of χ_2 depends mainly on *a*, *b*, *c* and S_r, so the effect that each coefficient has on the sensitivity of χ_2 will be discussed in this section. To study the effect of *a*, the distribution of χ_2 with respect to ECR was compared for different values of *a*. The maximum theoretical value of χ_2 can be calculated by Equation 5.7.

$$\chi_{2_{max}} = \left(\frac{a}{S_r^c}\right) \tag{5.7}$$

Figure 5.1 shows that an increase in coefficient *a* significantly increases the maximum value of χ_2 or $\chi_{2_{max}}$. According to Equation 5.7, $\chi_{2_{max}}$ depends on two coefficients *a*, *c*, and the degree of saturation of soil. Therefore when the soil approaches its dry state, the $\chi_{2_{max}}$ increases.

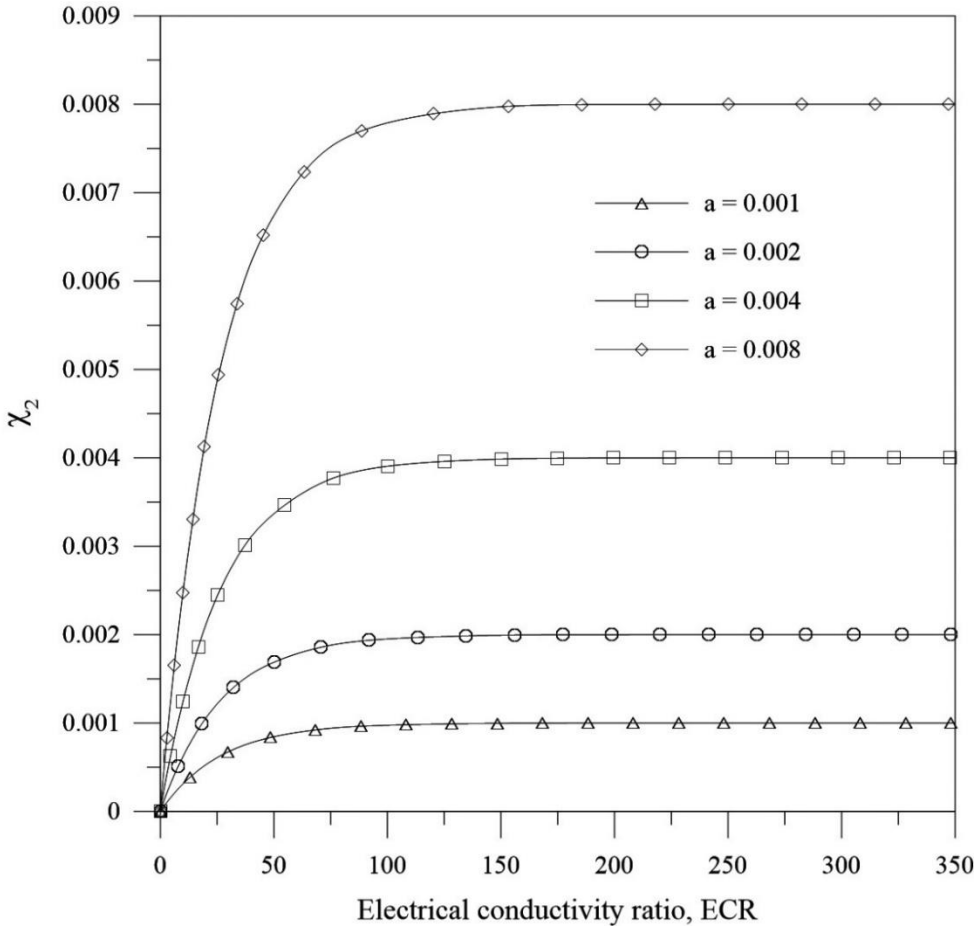

Figure 5.1 Sensitivity analysis of χ_2 with respect to *a*

However, the influence of *a* on critical ECR or ECR_c (the minimum ECR value where χ_2 reaches its maximum) is not significant. To understand the effect that coefficient *b* has on χ_2, the sensitivity of χ_2 with coefficient *b* was compared with different values of *b* (Figure 5.2). Figure 5.2 shows that coefficient *b* does not affect $\chi_{2_{max}}$, but it does have a substantial influence on the ECR_c; essentially, ECR_c decreases as the value of coefficient *b* increases.

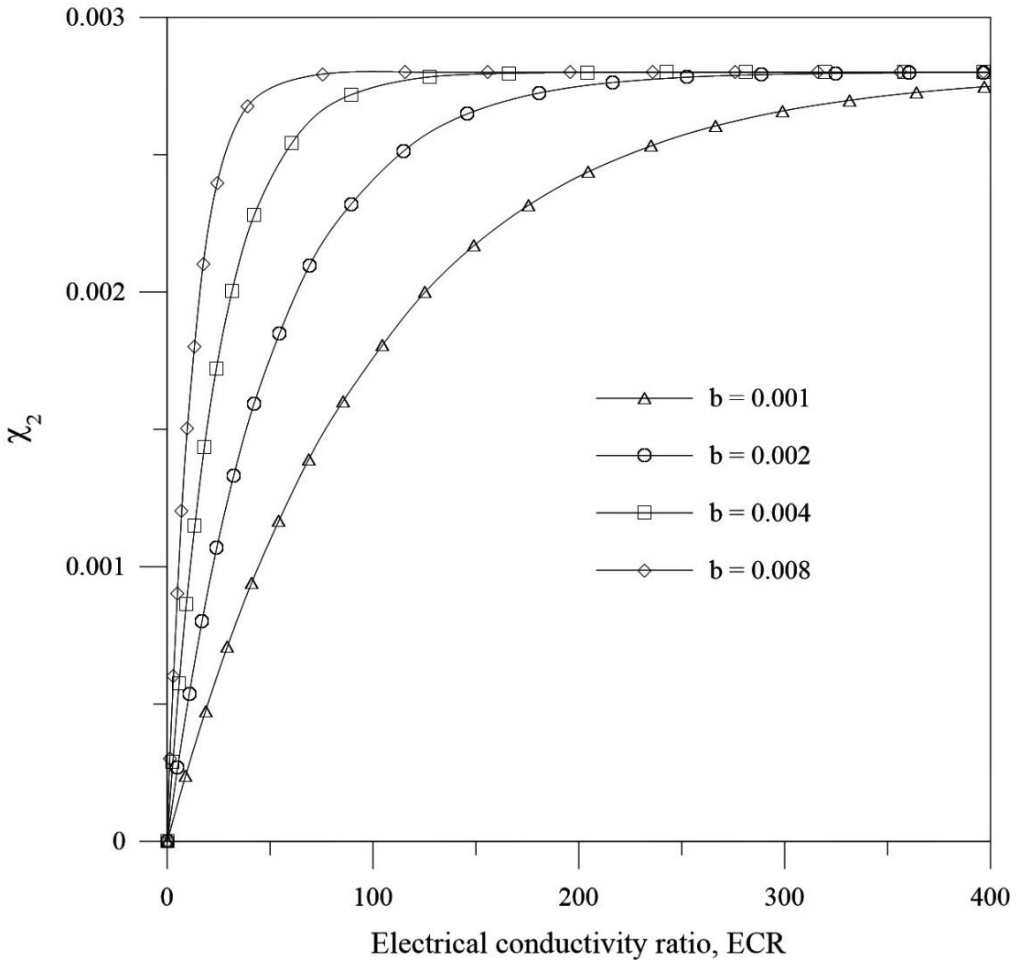

Figure 5.2 Sensitivity analysis of χ_2 with respect to *b*

The distribution of ECR_c can be described based on the power decay law shown in Figure 5.3. With a decreasing degree of saturation ECR_c increases for all the given values of coefficient *b*, but the increase in ECR_c with respect to the degree of saturation decreases

as the coefficient *b* increases. For example, when coefficient *b* increases from 0.01 to 0.08, the ECR_c varies from 750 to 125.

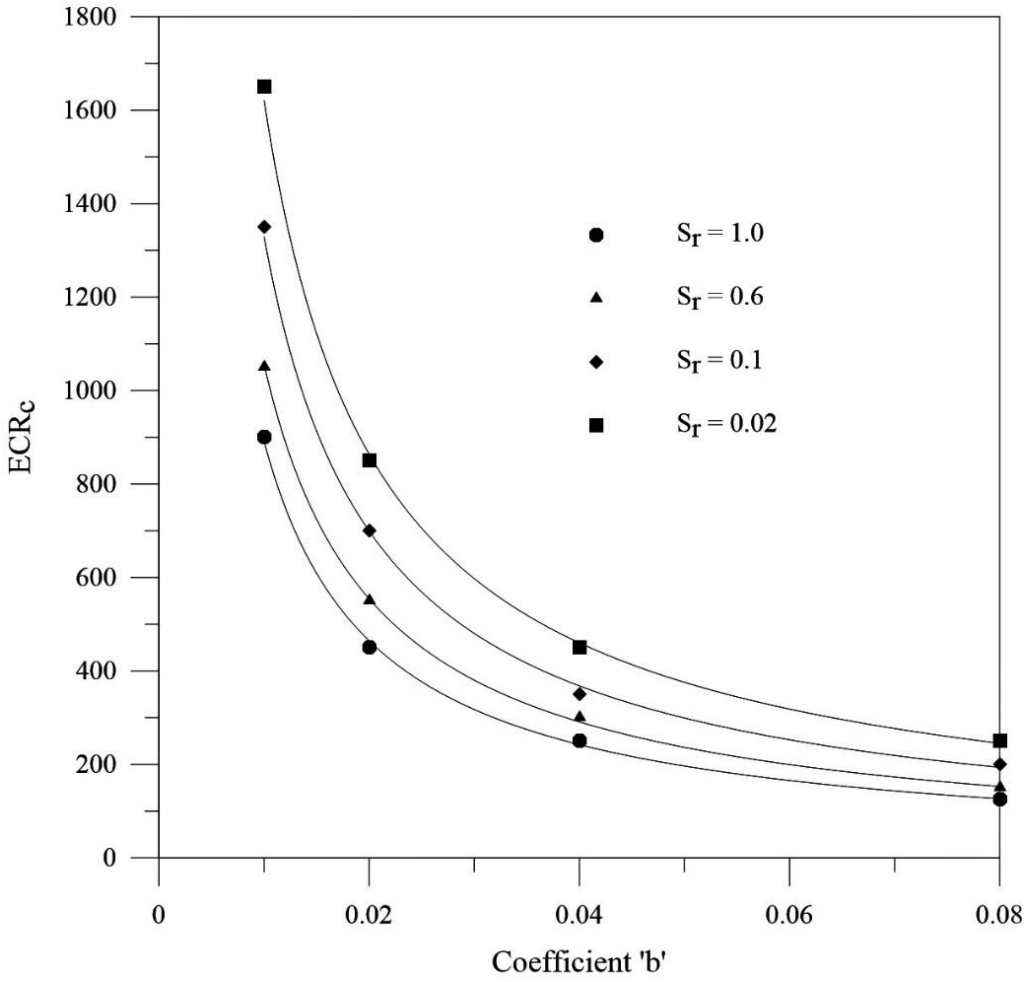

Figure 5.3 Distribution of critical ECR (ECR_c) with respect to coefficient *b*

To determine the influence that coefficient *c* has on χ_2, the sensitivity of χ_2 with respect to ECR was compared with various values of coefficient *c*. Figure 5.4 shows the distribution of χ_2 with relation to ECR for different values of coefficient *c* at two different degrees of saturations, 0.4 and 0.8. Irrespective of the degree of saturation, this increase in coefficient *c* has increased χ_2 [Figure 5.4 (a)], whereas this increase in the degree of saturation has reduced χ_2 [Figure 5.4 (b)].

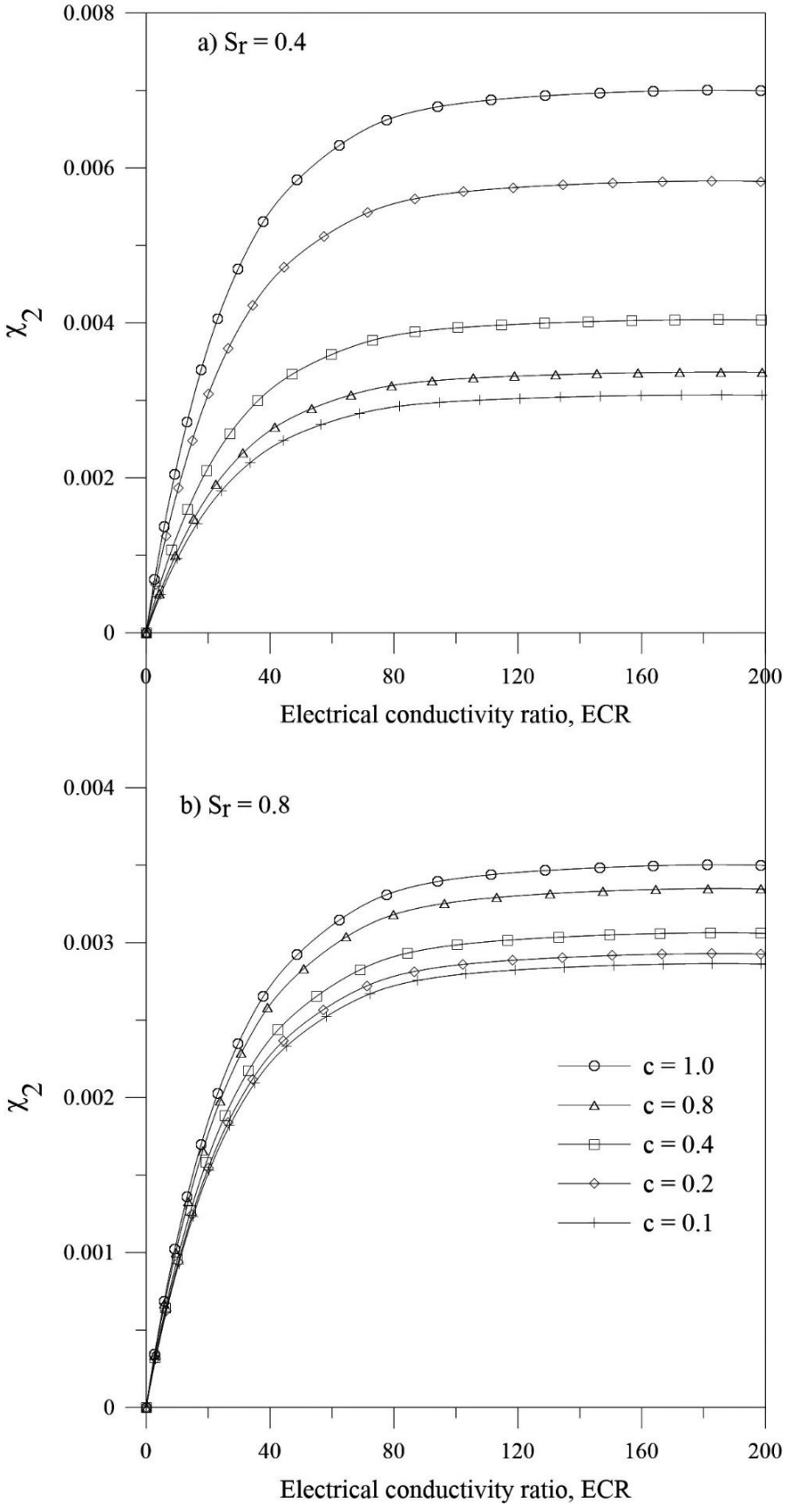

Figure 5.4 Sensitivity analysis of χ_2 with respect to c

The maximum theoretical χ_2 with respect to different values of coefficient *c* for two different degrees of saturations is shown in Figure 5.5. Here, the distribution of $\chi_{2_{max}}$ with respect to coefficient *c* is linear at higher degrees of saturation, but with decreasing degrees of saturation the distribution of $\chi_{2_{max}}$ becomes exponential.

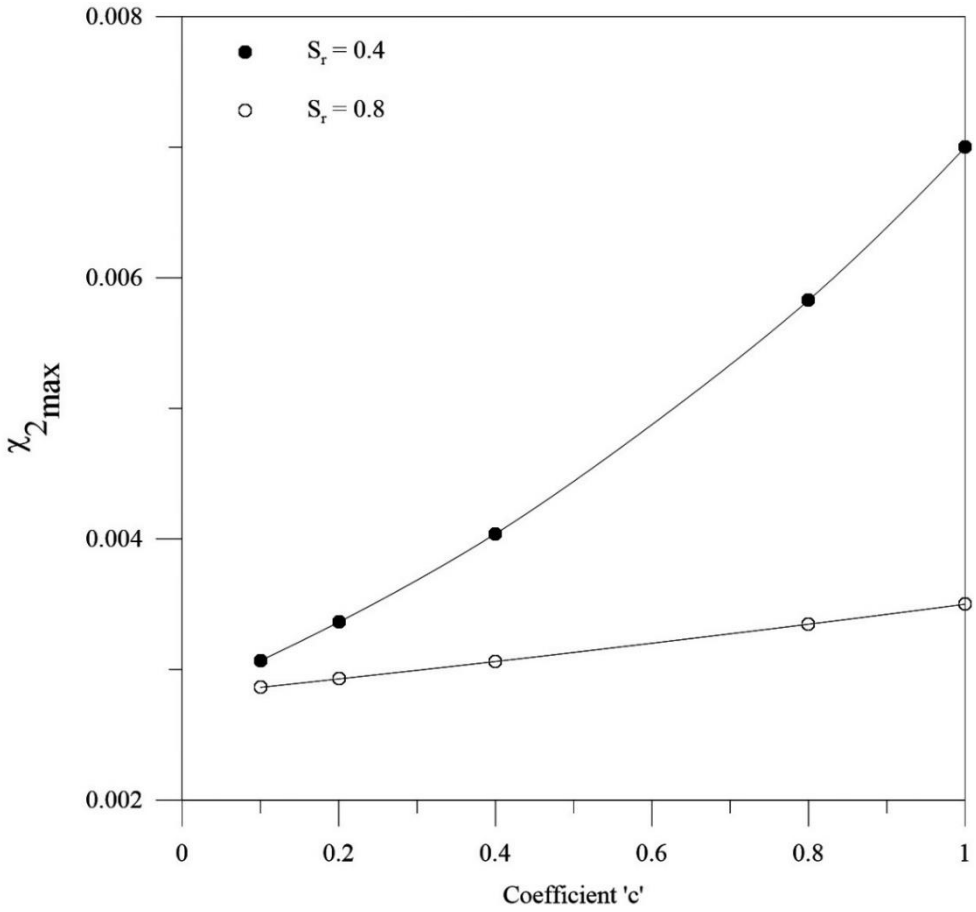

Figure 5.5 Distribution of $\chi_{2_{max}}$ with respect to coefficient *c*

To observe how the degree of saturation affects χ_2, the sensitivity of χ_2 with respect to ECR was compared for various stages of the degree of saturations. The χ_2 decreases as the degree of saturation increases (Figure 5.6). This change in $\chi_{2_{max}}$ is significant at lower degrees of saturation, but it shows a slight change at higher degrees of saturation.

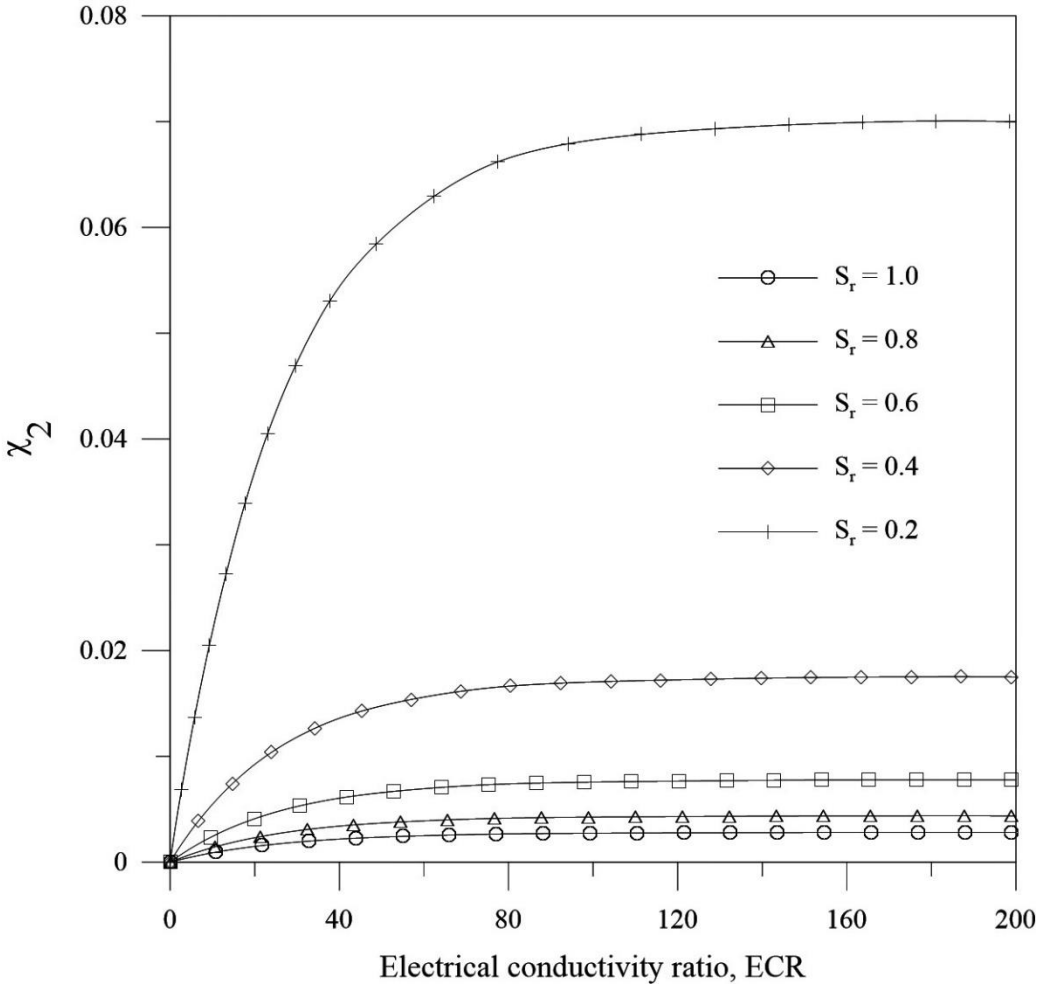

Figure 5.6 Sensitivity analysis of χ_2 with respect to the degree of saturation

5.2.2 Experimental determination of χ_2

By combining Equation 5.4 and 5.5 the shear strength model can be re-written as:

$$\tau'_{US} = [(\sigma_N - u_a) + \chi_1(u_a - u_w) + \chi_2\pi] \tan\phi' + c' \quad (5.8)$$

According to Khalili and Khabbaz (1998) model, the shear strength of unsaturated soil, without the influence of osmotic suction, can be derived by combining Equation 5.2 into the Mohr-Coulomb model.

$$\tau'_U = [(\sigma_N - u_a) + \chi_1(u_a - u_w)] \tan\phi' + c' \quad (5.9)$$

By subtracting Equation 5.9 from Equation 5.8:

$$\chi_2 \pi \tan \phi' = \tau'_{US} - \tau'_U \tag{5.10}$$

The only unknown parameter χ_2 can be estimated as follows:

$$\chi_2 = \left(\frac{\tau'_{US} - \tau'_U}{\pi \tan \phi'} \right) \tag{5.11}$$

5.2.3 Model calibration and validation

The peak shear stress for the various conditions discussed in Section 3.2.3 was calculated using the results of the direct shear test. The saturated soil friction angle (ϕ') was calculated by carrying out direct shear tests under fully-saturated and non-saline conditions. The saturated friction angle was calculated when the soil sample became fully-saturated with distilled water (π = 0 kPa), and then the experimental determination of χ_2 was obtained based on Equation 5.11. The proposed new model for χ_2 (Equation 5.6) was calibrated for three major initial matric suction conditions where s_i = 0 kPa (saturated), s_i = 200 kPa and 500 kPa, with respect to the experimental results for a given normal stress (σ'_N = 20 kPa). The distribution of χ_2 with the electrical conductivity ratio for three different levels of matric suctions is shown in Figure 5.7; this was used to estimate the best-fit parameters which were then used to predict the unsaturated behaviour of soil in conjunction with the degree of saturation for the other independent data sets.

A fully-saturated condition was used to determine the coefficients *a* and *b* when the influence of coefficient *c* was not significant ($S_r = 1$). Parameter *c* was then determined based on the results of the s_i = 200 kPa condition, and then all three parameters were calibrated with s_i = 500 kPa. Of all these determinations, the calibrated experimental

coefficients are a = 0.003, b = 0.0375 and c = 2. A comparison between the experimental results and model distribution to determine the calibrating coefficients is shown in Figure 5.7.

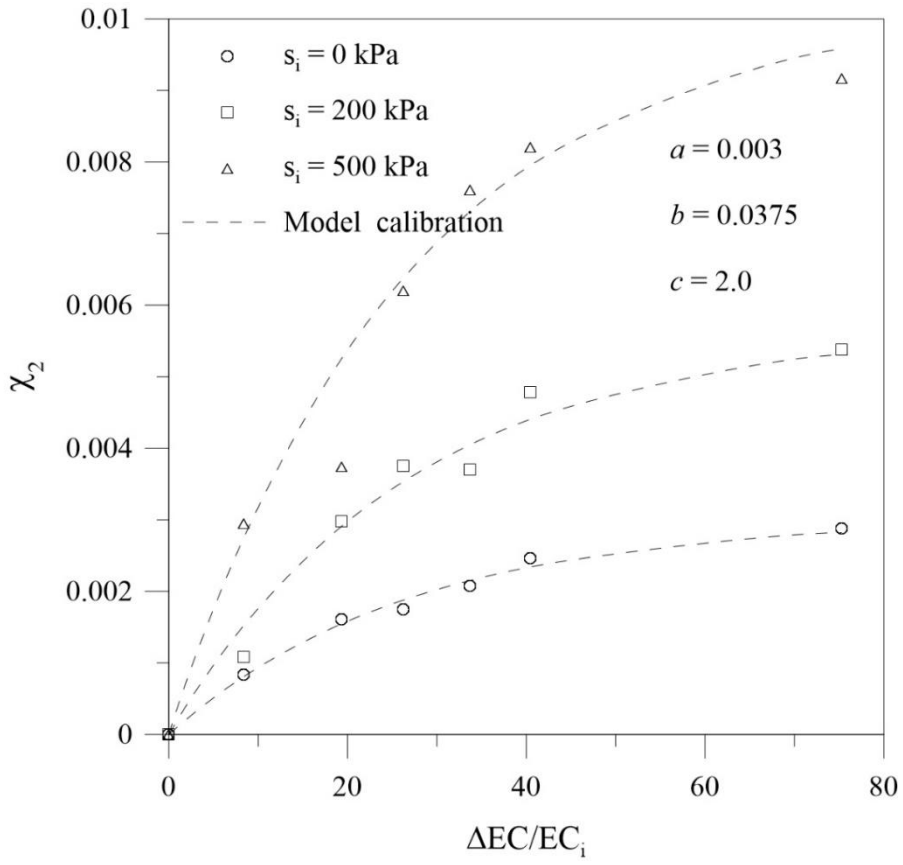

Figure 5.7 Model calibration with s_i = 0 kPa, s_i = 200 kPa and s_i = 500 kPa (σ'_N = 20 kPa)

The calibration coefficients from the above two conditions were used to predict the values for χ_2 for other unsaturated-saline conditions. A comparison between the experimental results and predicted results is shown in Figure 5.8. The model predictions perfectly match the experimental results, and therefore the proposed new model χ_2 is a suitable parameter for predicting the shear strength of unsaturated soil with the influence of osmotic suction.

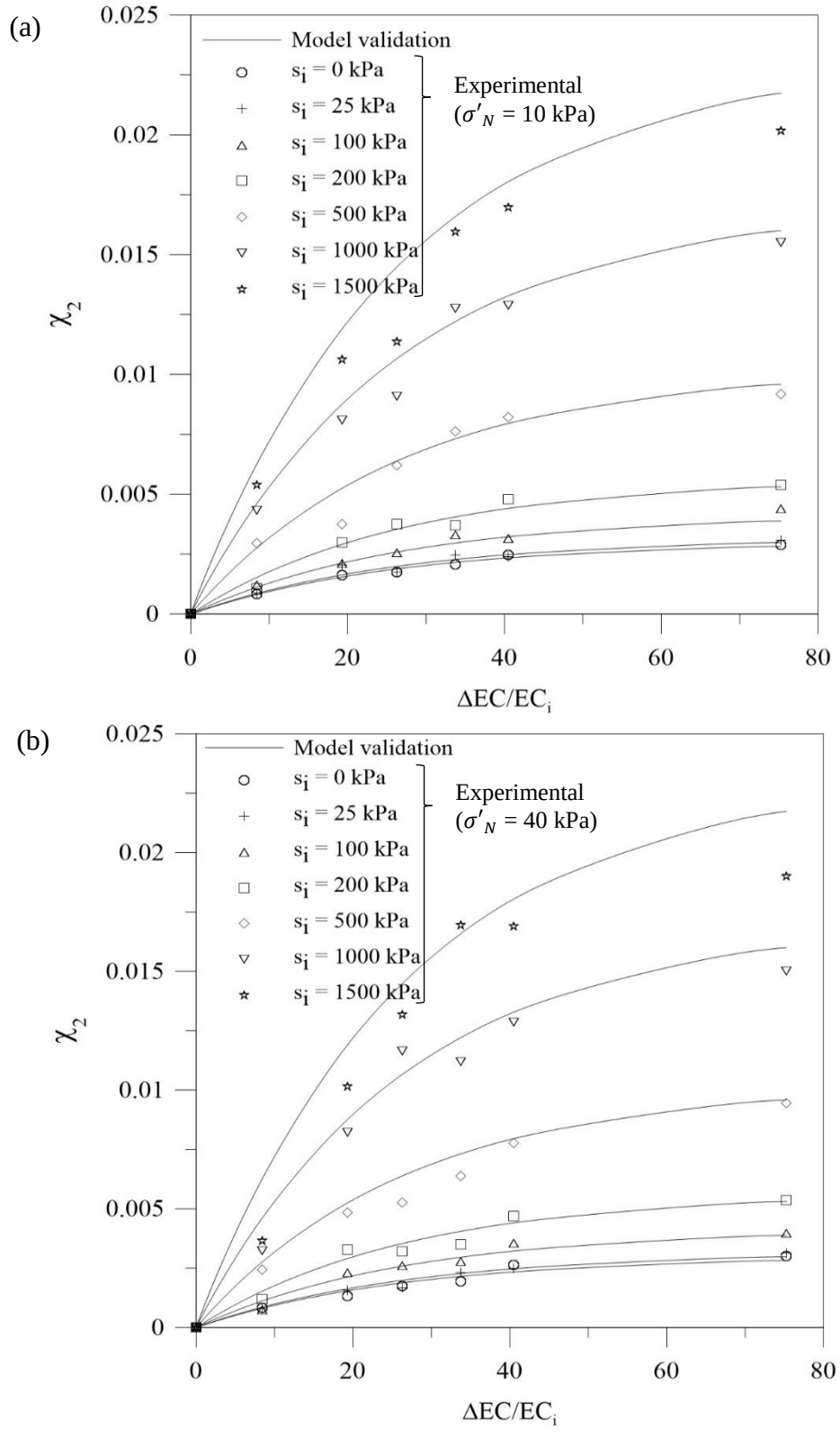

Figure 5.8 Experimental and model prediction results of χ_2 for different initial matric suctions where a = 0.003, b = 0.0375 and c = 2.0, (a) $\sigma'_N = 10kPa$ and (b) $\sigma'_N = 40kPa$

The predicted peak shear stress was calculated based on Equation 5.8 and then the results were compared with the experimental results for two independent normal stress conditions. The corresponding distribution of model prediction and experimental results of peak shear stress are shown in Figure 5.9. The model predictions match the experimental results at lower initial matric suctions (< 500 kPa), giving a maximum deviation of less than 5 kPa, but as the initial matric suction (> 500 kPa) increases, the model shows a slight deviation (5-14.5 kPa) depending on the magnitudes of osmotic suction and matric suction. Overall, the model exhibits an increased deviation from the experimental results at the highest values of osmotic suction and initial matric suction. The maximum deviation of the model with respect to experimental data for any condition was about 14.5 kPa when the osmotic suction increases to 9560 kPa at the highest considered initial matric suction of 1500 kPa.

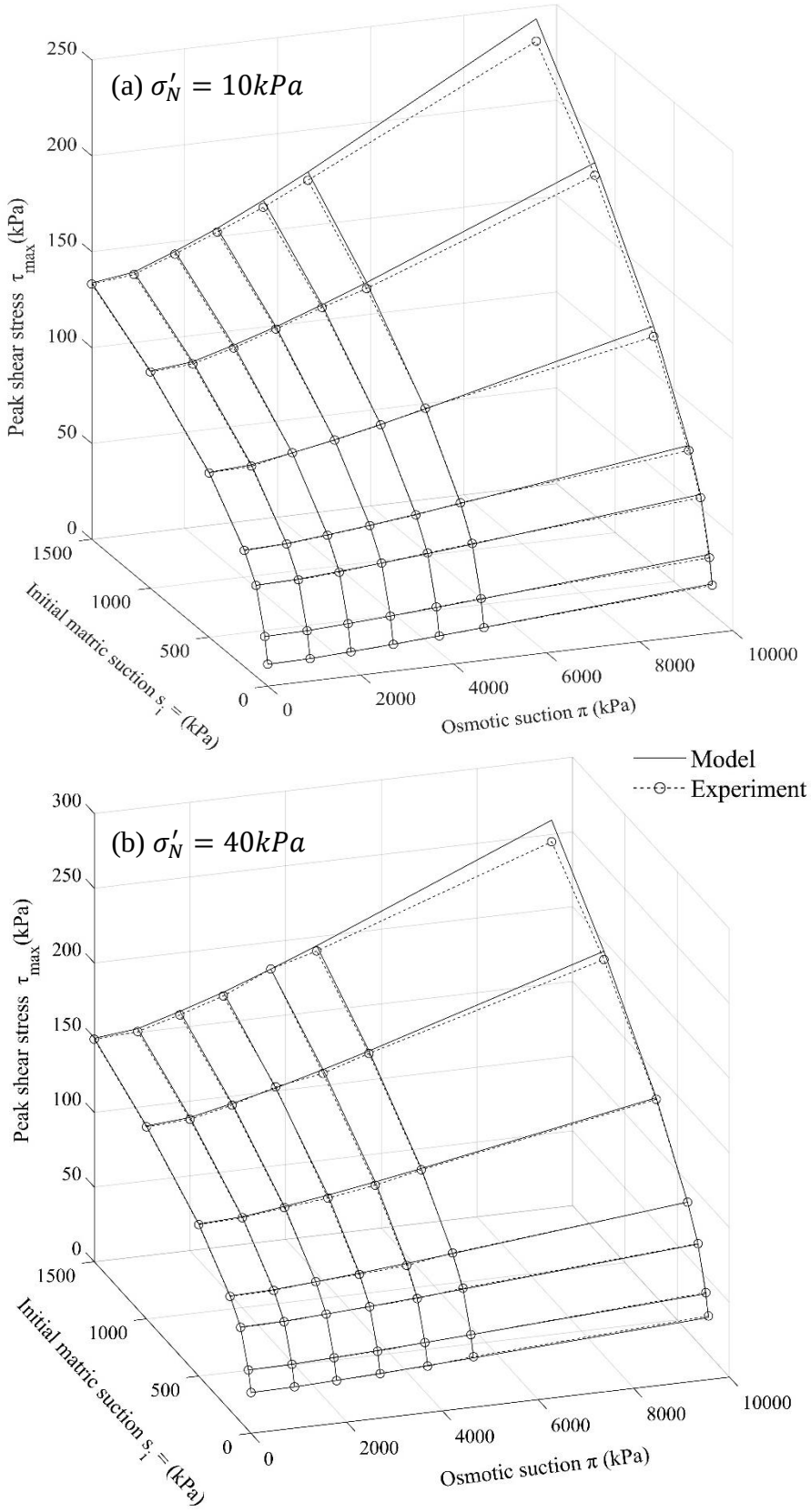

Figure 5.9 The experimental and model peak shear stress for different initial matric suctions and saturated osmotic suctions, (a) $\sigma'_N = 10kPa$ and (b) $\sigma'_N = 40kPa$

5.3 Shear strength model for root permeated soil

The increase in shear strength due to tree roots can be directly added to the Mohr-Coulomb equation as an additional component of cohesion (Pallewattha et al. 2019; Waldron 1977). Therefore, the total shear strength of unsaturated soil permeated with roots can be re-written as follows:

$$\tau' = \tau'_U + \Delta\tau_R \tag{5.12}$$

where $\Delta\tau_R$ is the additional increase in shear strength due to root permeation.

$$\tau'_U = \tau' + \Delta\tau_s \tag{5.13}$$

In the above equation, τ' is the shear strength of saturated soil and $\Delta\tau_s$ is the additional increase in shear strength due to soil matric suction.

According to the Wu (1976) and Waldron (1977) model, the additional shear strength generated by tree roots can be defined as:

$$\Delta\tau_R = t_R(cos\beta + sin\beta tan\phi) \tag{5.14}$$

where t_R is the mobilised tensile strength of roots per unit area of soil, β is the deformed root orientation to the sharing plane, and ϕ is the friction angle of soil.

The mobilised tensile strength of tree roots can be defined by the average root tensile strength per average cross-sectional area (T_r) and the root area ratio (RAR) (Gray & Leiser 1982), hence:

$$t_R = T_r(RAR) \tag{5.15}$$

The average tensile strength decreases with the diameter of the roots, and this behaviour can be described by a simple power decay function (Gray & Sotir 1996), therefore:

$$T_r = \alpha_1 d_R^{-\alpha_2} \tag{5.16}$$

In the above equation, α_1 and α_2 are species dependent empirical constants, and d_R is the root diameter or the average diameter of a diameter class.

Therefore, based on Equations 5.14 to 5.16, a relationship for additional shear strength due to tree roots can be given by considering the variability in root size;

$$\Delta\tau_R = \sum_{i=1}^{n} \alpha_1 d_{R_i}^{-\alpha_2} (RAR_i)(cos\beta_i + sin\beta_i tan\phi) \tag{5.17}$$

where i indicates the diameter class and n is the number of tree roots for the given diameter class.

This model (Equation 5.17) did not consider the influence of salinity on tree roots. As per the results discussed in Chapter 4, the tensile strength of a tree root with the same diameter is not affected by the osmotic stress due to pore water salinity, but it is affected by the RAR. The distribution of RAR is replotted with ECR, and is shown in Figure 5.10. Based on those results, the distribution of RAR with respect to pore water salinity can be described with respect to ECR.

$$RAR_\pi \begin{cases} = RAR^0 & \pi = 0 \\ = RAR^0 * \lambda_1 * (ECR)^{-\lambda_2} & \pi \neq 0 \end{cases} \tag{5.18}$$

where RAR^0 is the root area ratio when the osmotic stress is 0 kPa (when there is no salinity in the pore water), and λ_1 and λ_2 are the experimental coefficients.

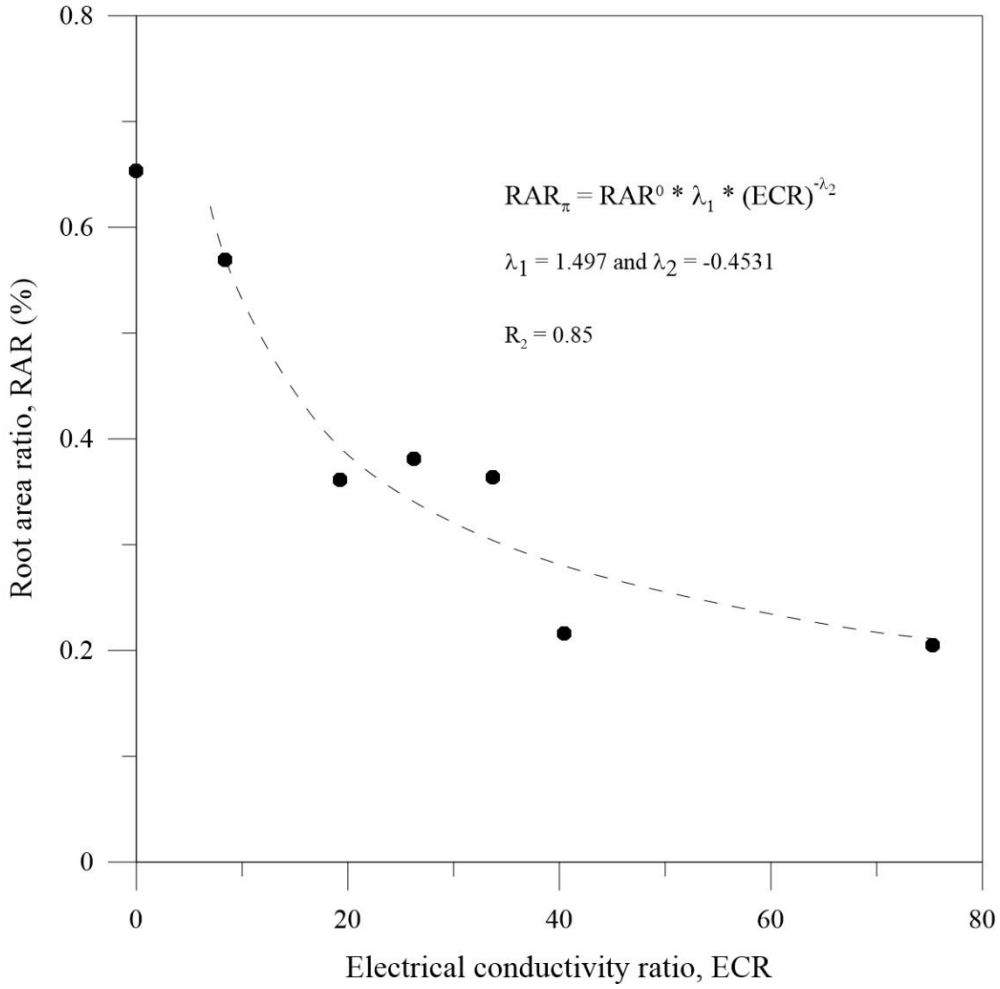

Figure 5.10 Distribution of RAR with respect to ECR

By reorganising Equation 5.17 to include the influence of osmotic stress on the tree RAR, a new equation to determine the additional shear strength generated by the tree roots can be developed.

$$\Delta\tau_R = \sum_{i=1}^{n} \alpha_1 d_{R_i}^{-\alpha_2} (RAR_{\pi_i})(cos\beta_i + sin\beta_i tan\phi) \tag{5.19}$$

Equation 5.19 can be elaborated further by combining it with Equation 5.18.

$$\Delta\tau_R = \sum_{i=1}^{n} \alpha_1 d_{R_i}^{-\alpha_2} (RAR_i^0 \lambda_1 (ECR)^{-\lambda_2})(cos\beta_i + sin\beta_i tan\phi) \tag{5.20}$$

Equation 5.20 can be used to approximate the additional shear strength generated by tree root permeation. This new model is important because it has considered the effects of root inclination, variations of root diameter and pore water chemistry. Three major root failure patterns have been identified, pure slipping, breaking and coupled with soil annulus during shearing (Figure 5.11) as proposed by Pallewattha et al. (2019). To describe these three root failure mechanisms, Equation 5.20 will be rewritten including the tensile strength.

$$\Delta\tau_R = \sum^{n} T_{r_i}(RAR_i^0 \lambda_1 (ECR)^{-\lambda_2})(cos\beta_i + sin\beta_i tan\phi) \qquad (5.21)$$

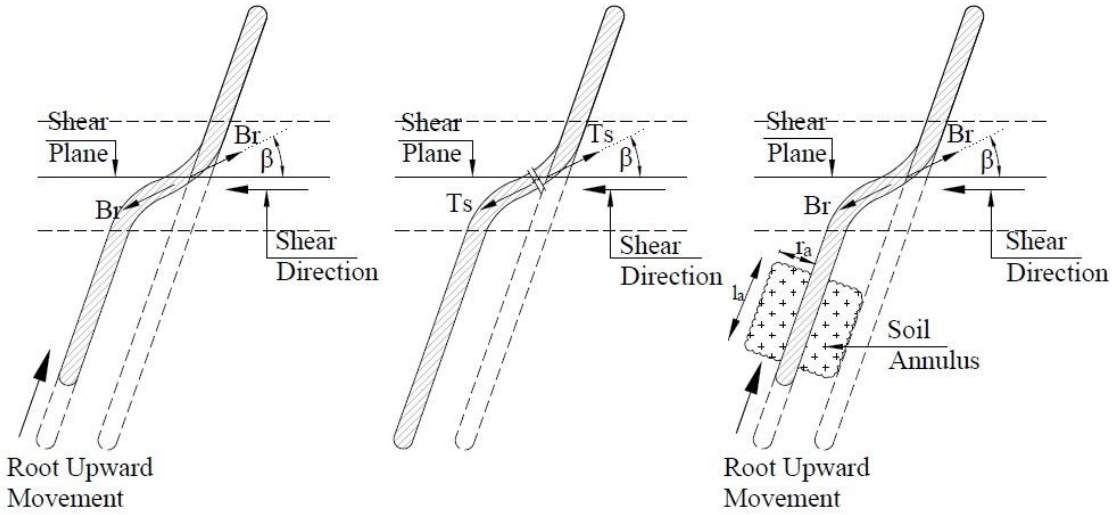

Figure 5.11 Most common root failure patterns, a) slipping b) breaking and c) coupled with soil annulus (Pallewattha et al. 2019)

Pallewattha et al. (2019) derived three different force functions for these three failure patterns, all of which can be revised according to the new model (Equation 5.21). It is assumed here that only the slipping and breaking failure patterns would be affected by the osmotic stress where the tree roots will be directly involved.

$$\Delta\tau_{R_1} = \sum_{i=1}^{n_1} B_{r/sl_i}(RAR_i^0 \lambda_1 (ECR)^{-\lambda_2})(cos\beta_i + sin\beta_i tan\phi) \quad (5.22)$$

$$\Delta\tau_{R_2} = \sum_{i=1}^{n_2} T_{r/st_i}(RAR_i^0 \lambda_1 (ECR)^{-\lambda_2})(cos\beta_i + sin\beta_i tan\phi) \quad (5.23)$$

$$\Delta\tau_{R_3} = \sum_{i=1}^{n_3} B_{r/sa_i}(\frac{A_{S_i}}{A})(cos\beta_i + sin\beta_i tan\phi) \quad (5.24)$$

In the above equation, A_{S_i} is the average circumferential area of the cylindrical shape soil annulus for *i*th root class, and n_1, n_2 and n_3 are the number of roots that slipped without breaking, those that broke and slipped with the soil annulus during shearing, T_{r/st_i} is the maximum root tensile strength for the *i*th root (root tensile strength at breakage), B_{r/sl_i} is the bond stress between root and soil of the *i*th root during pure slipping (no root breaking involved), and B_{r/sa_i} is the bond stress between root and soil of the *i*th root during pulling out with a soil annulus.

Based on Equation 5.22, 5.23 and 5.24, the total shear strength induced by the root permeation can be defined as;

$$\Delta\tau_R = \Delta\tau_{R_1} + \Delta\tau_{R_2} + \Delta\tau_{R_3} \quad (5.25)$$

5.3.1 Sensitivity analysis of RAR_π

Since the sensitivity of RAR_π depends mainly on λ_1 and λ_2, the effect of each coefficient on the sensitivity of RAR_π will be discussed in this section. To study the effect of λ_1, the distribution of RAR_π with respect to ECR was compared for different values of λ_1 (Figure 5.12).

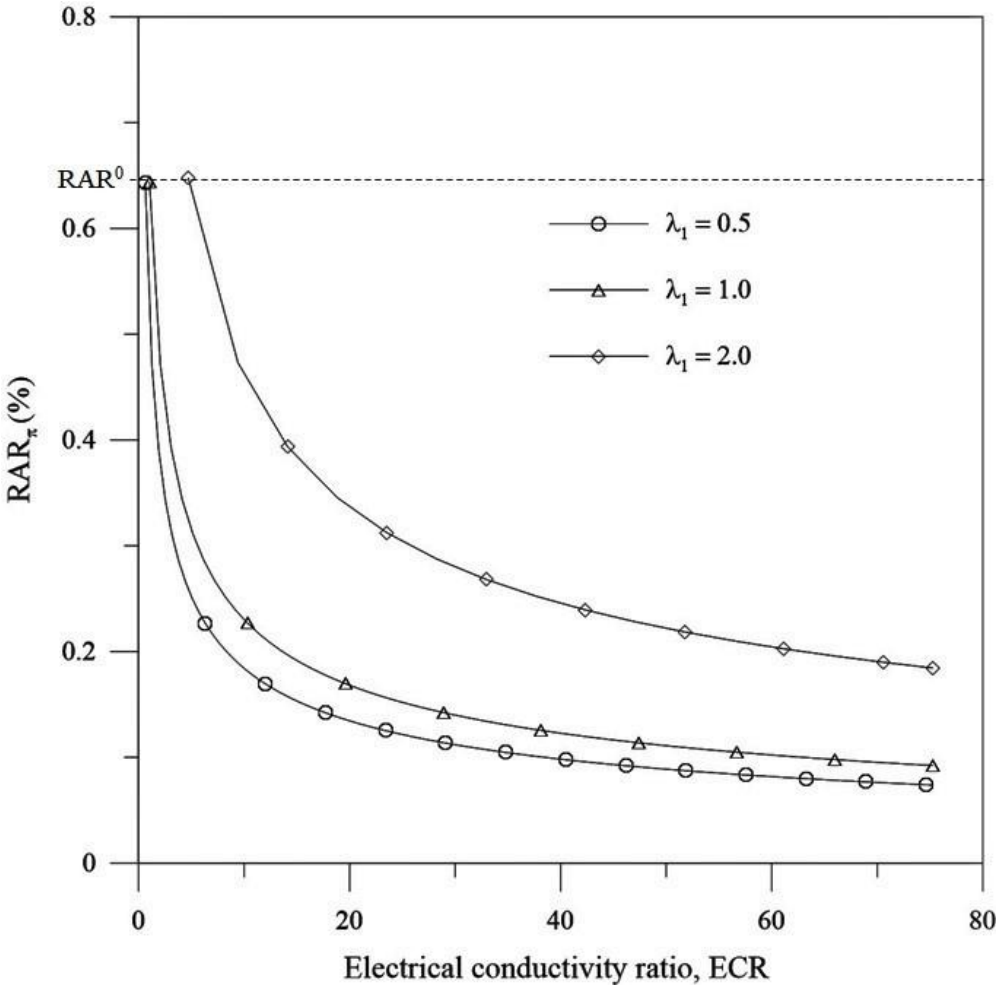

Figure 5.12 Sensitivity of RAR_π with respect to λ_1

Figure 5.12 shows that the minimum value of RAR_π increases with an increasing λ_1 under similar conditions of osmotic stress. This means that with an increasing λ_1, the root system becomes dense or the RAR has increased for the same osmotic stress. In this study the effective range of λ_1 is 0.487 to 2.507. To study the effect of λ_2, the distribution of RAR_π with respect to ECR was compared for different values of λ_2 (Figure 5.13).

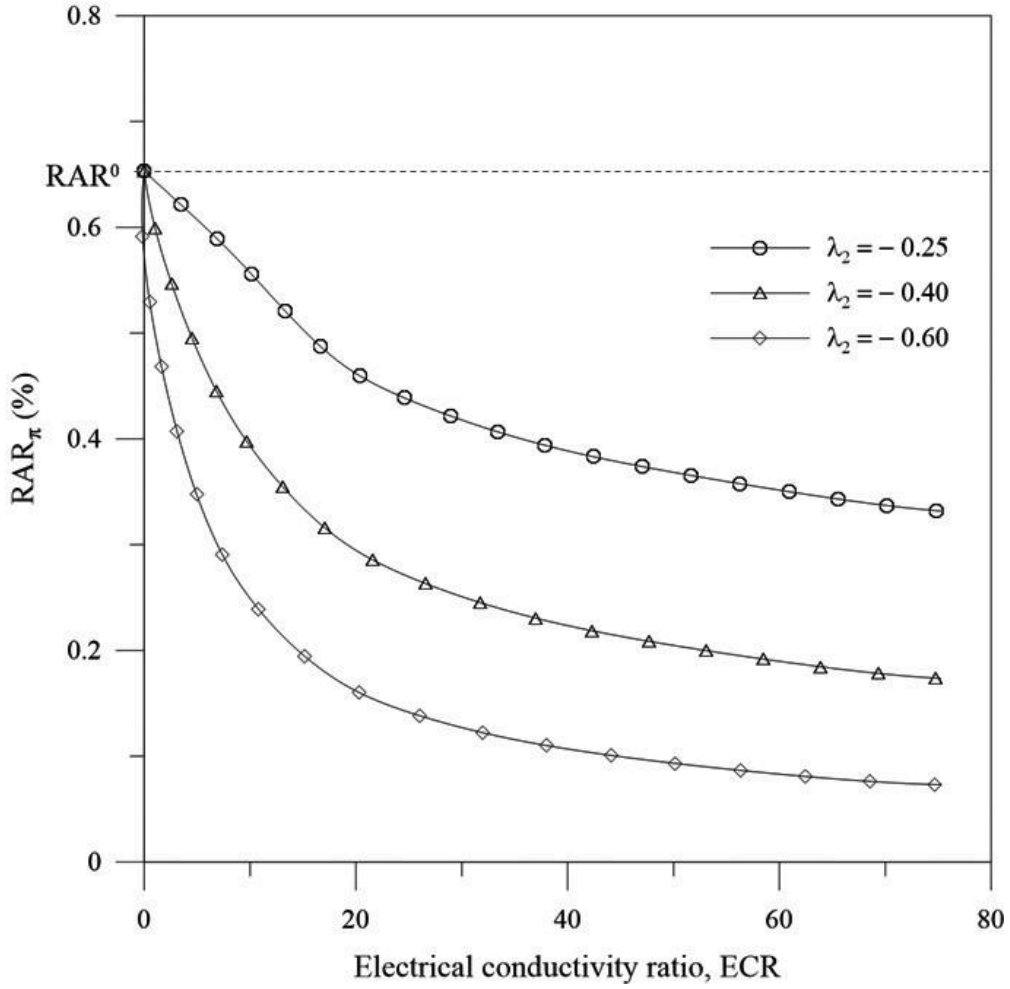

Figure 5.13 Sensitivity of RAR_π with respect to λ_2

Figure 5.13 shows that the minimum value of RAR_π decreases with increasing (negatively) λ_2 for the same osmotic stresses, and this increase in λ_2 negatively accelerates the reach for the corresponding minimum RAR_π. In this study, the effective range of λ_2 is -0.226 to -0.680. To study the effect of RAR^0, the distribution of RAR_π in relation to ECR was compared for different values of RAR^0 (Figure 5.14). The change in RAR^0 can also be considered as a tree ageing or growing.

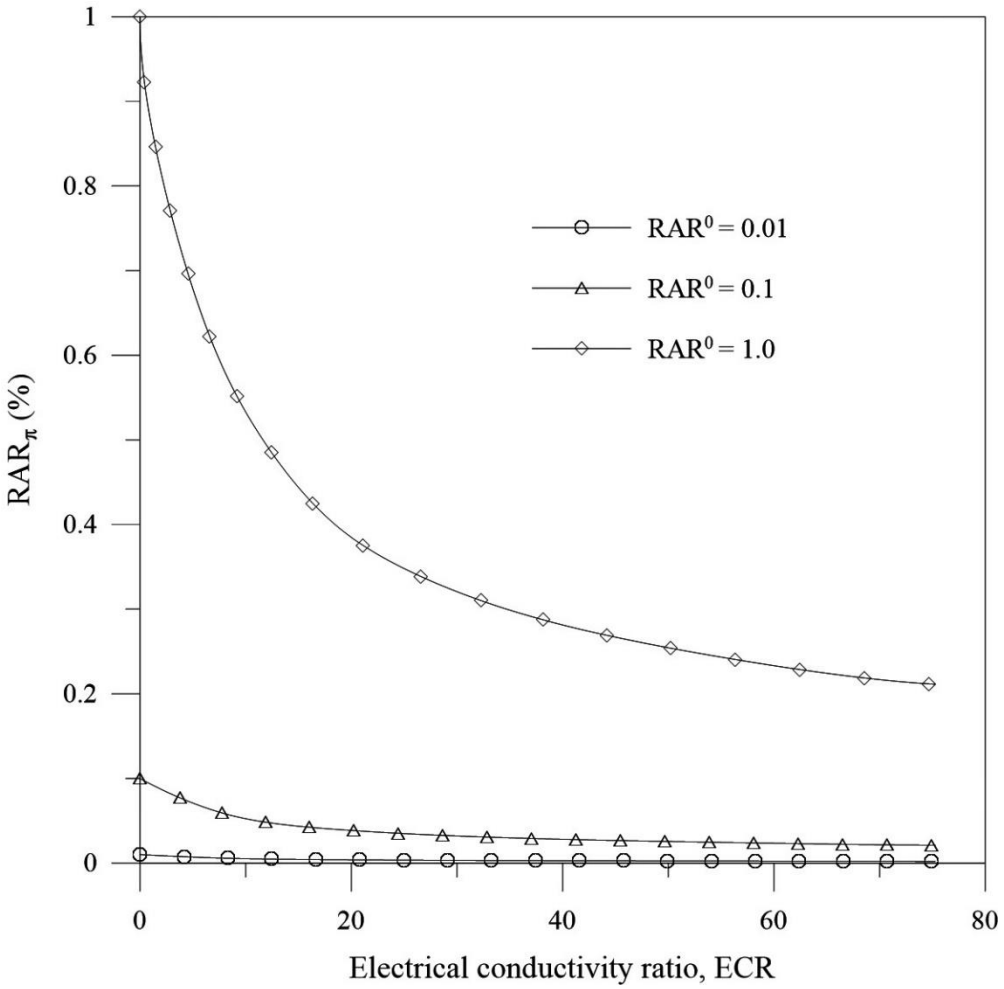

Figure 5.14 Sensitivity of RAR_π with respect to RAR^0

Even with the same λ_1 and λ_2 values, the minimum value of RAR_π increases with an increasing RAR^0 which further proves that the tolerance of trees to osmotic stress increases with the growth of the tree. However, even for a larger tree, the influence of salinity in pore water or the corresponding osmotic stress can still affect its growth.

5.3.2 Model prediction of shear strength contribution by tree roots

Predicting the amount of shear strength contributed by tree roots is very challenging because the following factors will have a significant effect on the accuracy of any prediction;

- Deformed root alignment: Roots can be aligned at different angles, and the same root may have different alignments during shearing.
- Root diameter: The root diameter is not uniform along its length, and therefore the average diameter will not accurately represent the overall dimensions, and
- Root architecture.

Therefore, the root-only contribution to shear strength will be discussed on the basis of different parameters. The results of root induced shear strength predicted by the model with respect to the ECR is shown in Figure 5.15.

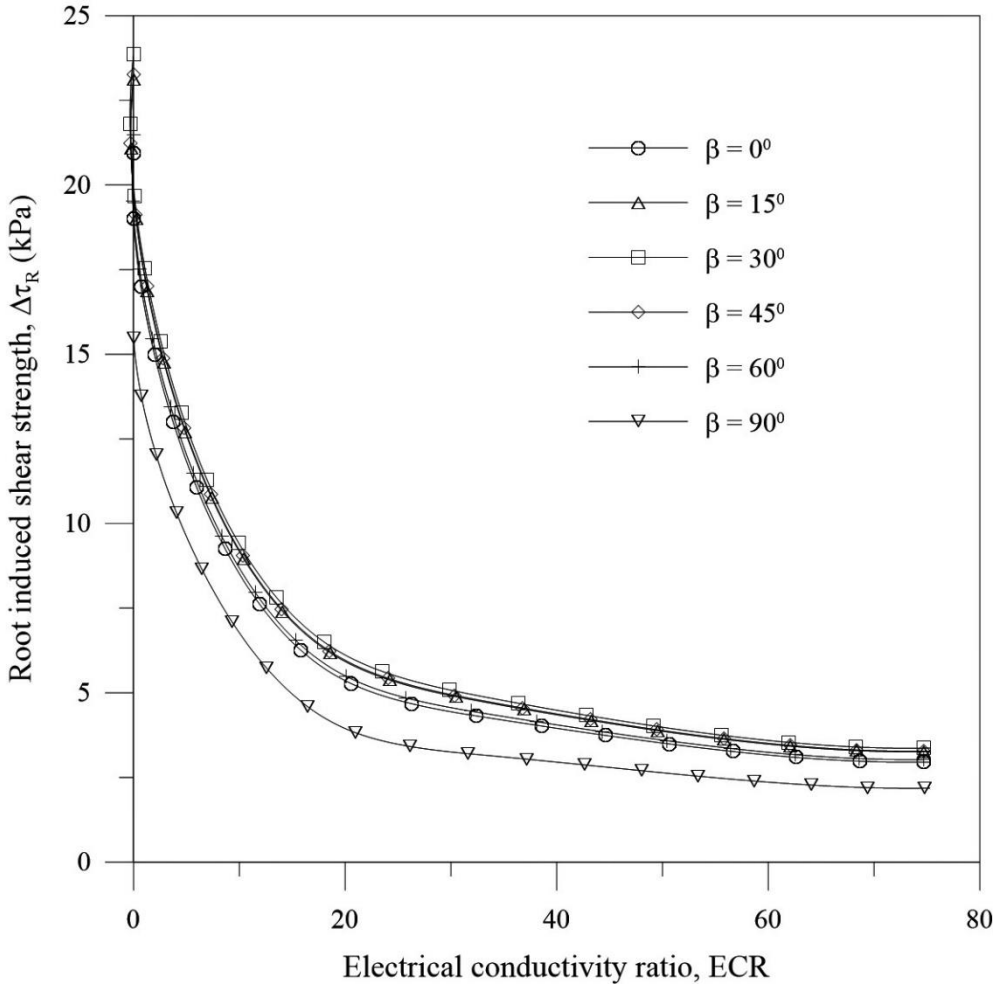

Figure 5.15 Model prediction of root induced shear strength with respect to ECR for roots deformed at different angles

Figure 5.15 shows that the root induced shear strength decreases with an increasing ECR. Irrespective of the angle of deformed roots, the root induced shear strength follows the same power decay law with ECR. There is a rapid decrease in root induced shear strength until about 2700 kPa of osmotic stress, and then (i.e. osmotic stress > 2700 kPa) the root induced shear strength decreases gradually and almost linearly. This implies that after about 2700 kPa of osmotic stress, the roots may start to deteriorate or decay. Plants absorb water by osmosis, which then passes through a semi-permeable membrane from low saline sections to high saline sections; this mechanism continues until all the plant cells are saturated. However, when the pore water becomes more saline, the increasing concentration of salt in the soil media reverses the process. The plants then lose moisture and experience stress within their cells due to lack of sufficient moisture and the plant begins to decay. Figure 5.15 shows the plants had critically stressed by reverse-osmosis until osmotic stress reached 2700 kPa, after which there was no significant increase or decrease in root induced shear strength. This implies that after 2700 kPa of osmotic stress plants cannot release water into the soil or cannot cope with the reverse-osmosis process any further, so they begin to wilt due to the lack of moisture. Figure 5.15 also shows that the rate of wilting was almost the same for all root alignments; therefore, as expected, the rate of wilting does not depend on the angle of the deformed roots. This result also proves that even after entirely decaying, the roots can still have a theoretical shear strength of about 3 kPa, because, the decayed roots of wilted plants are still within the soil. Although these decayed roots are brittle and they can still contribute to the shear strength of soil, so irrespective of their angle of deformation, decayed roots still contribute much the same shear strength. To observe the optimum angle of deformed roots, the results of root induced shear strength predicted by the model in regard to the angle of deformed roots to the horizontal direction is shown in Figure 5.16.

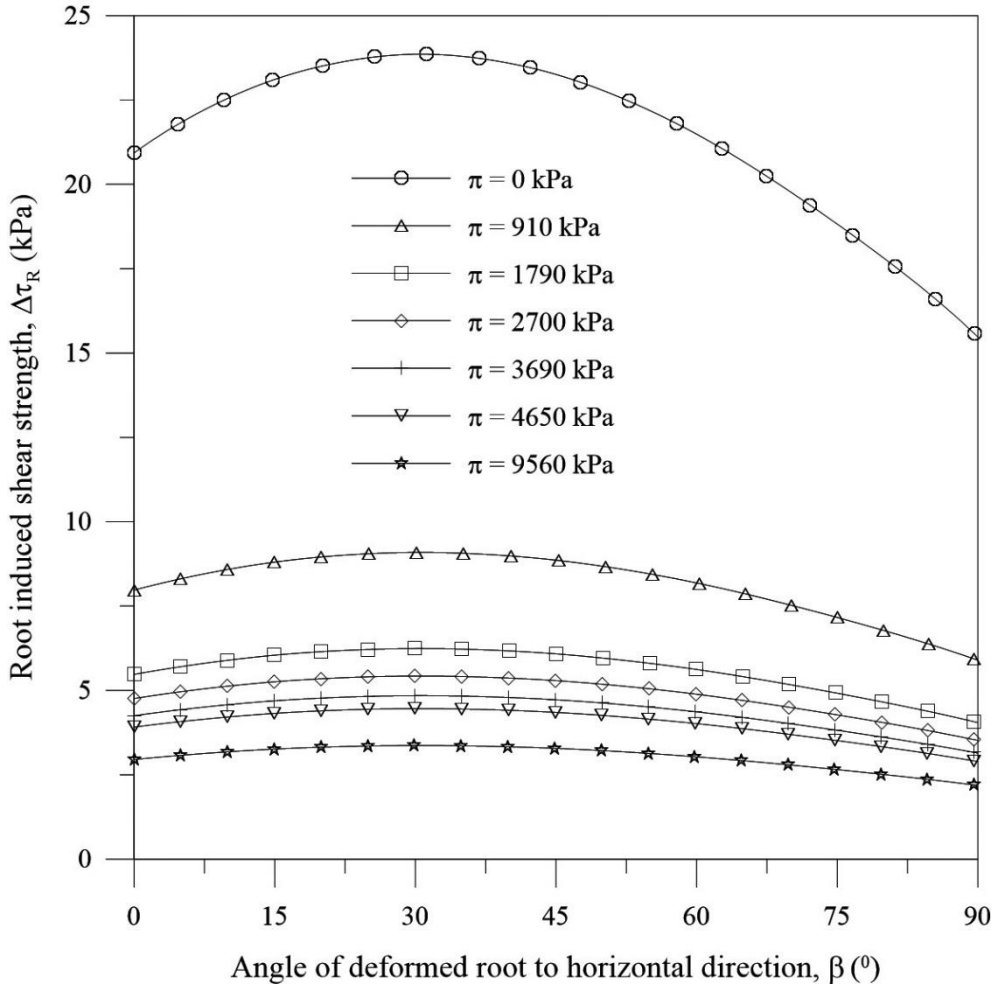

Figure 5.16 Model prediction of root induced shear strength with the angle of deformed root for different osmotic stresses

Figure 5.16 shows that the lower the root angle is to the horizontal, the higher the root induced shear strength, and when the roots are vertical, the root induced shear strength takes its lowest. This behaviour is common under all the conditions of osmotic stress. As the angle of deformed roots increases, the root induced shear strength increases until it reaches a maximum angle of deformation of almost 30^0. Therefore, irrespective of the amount of osmotic stress a plant experiences, the maximum increase in shear strength due to tree roots can be expected when the angle of deformed roots is 30^0.

The influence of ECR on root induced shear strength for different root diameters is shown in Figure 5.17. The model results indicate that the root induced shear strength decreased

with increasing ECR for all root diameters; the main reason for this behaviour is the osmotic stress that is generated in the roots due to salinity in pore water. It is evident that the osmotic stress influences not only the small roots but also the larger diameter roots. Figure 5.17 shows that the induced shear strength changes more in larger diameters roots than smaller diameter roots.

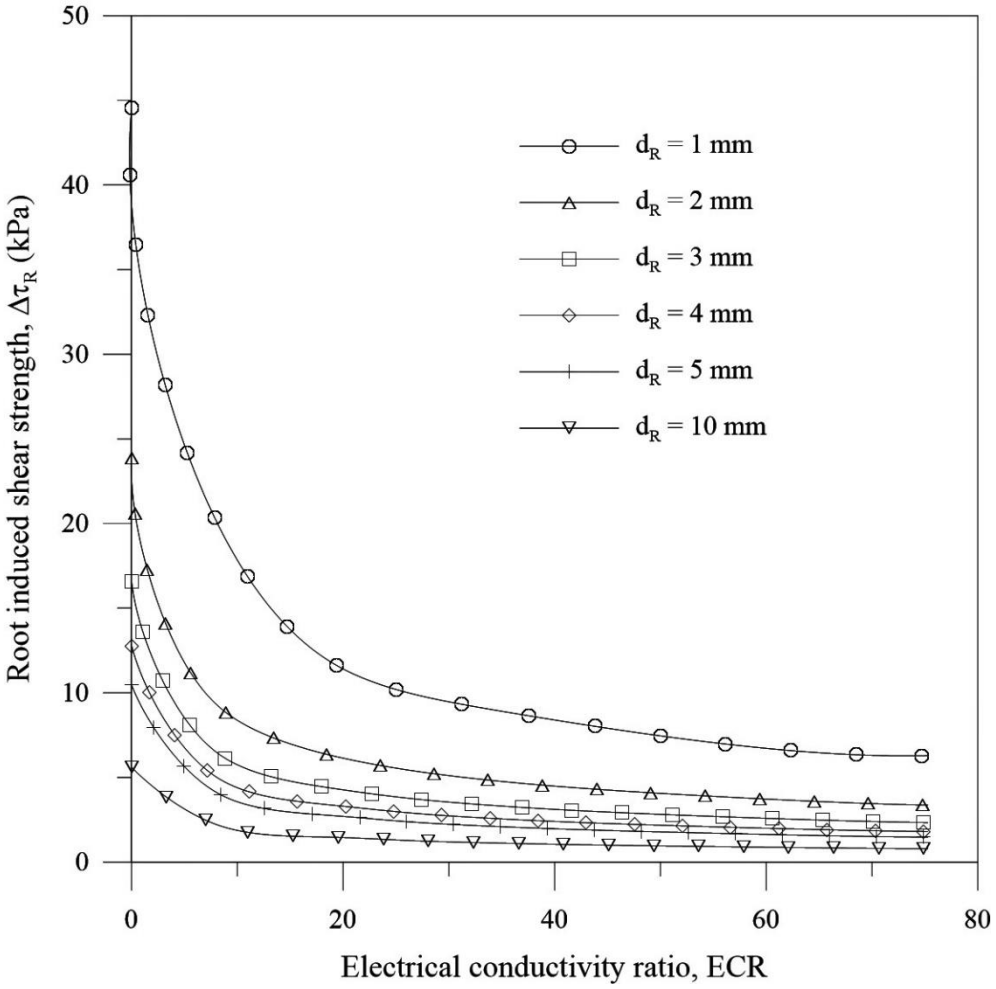

Figure 5.17 Model prediction of root induced shear strength with ECR for different root diameters

As expected, the model results indicate that the root induced shear strength decreases as the root diameter increases. While, this is common for all osmotic stresses, at lower levels of osmotic stress, the change of root induced shear strength is higher than for elevated

levels of osmotic stress. It is evident that irrespective of root diameter, the effect of osmotic stress is dominant at very high levels of osmotic stress; this behaviour is illustrated in Figure 5.18.

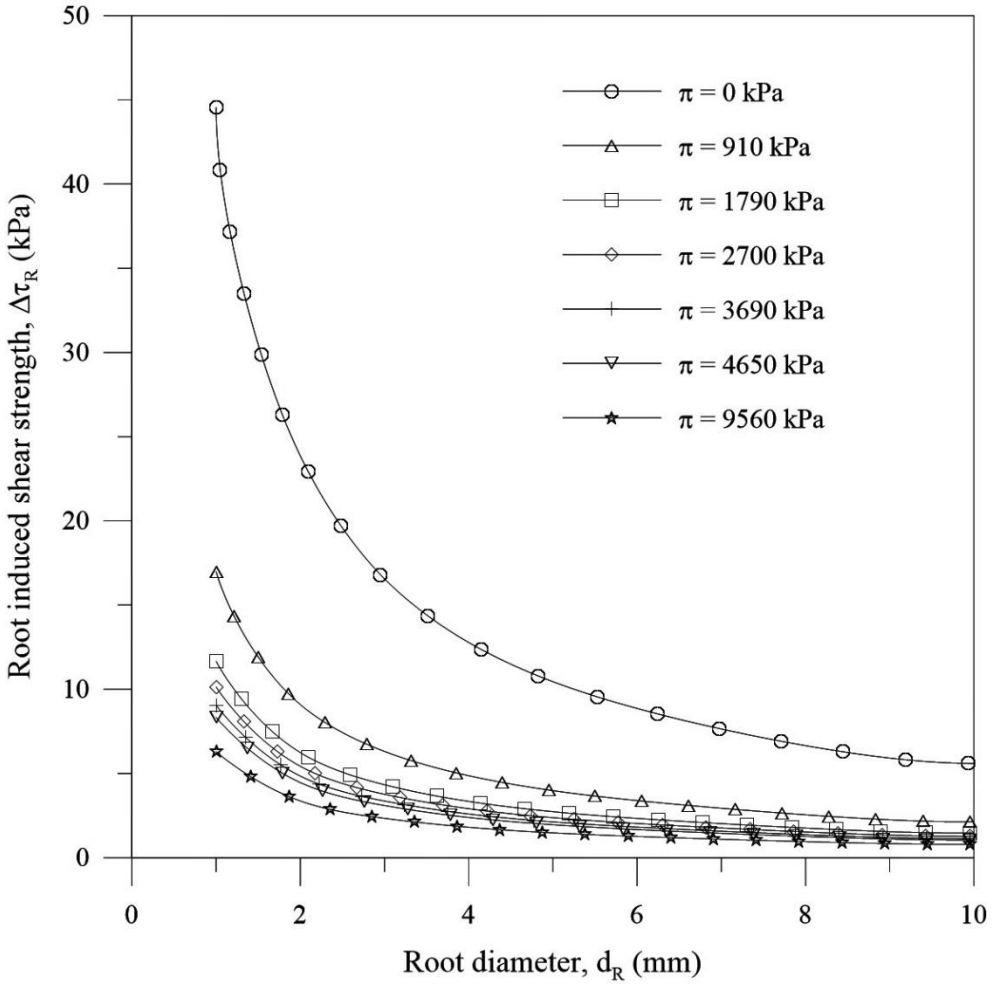

Figure 5.18 Model prediction of root induced shear strength with root diameters for different osmotic stresses

5.3.3 Model calibration and validation

Based on these observations, the model results were compared with the experimental results when the matric suction of the soil was 200 kPa, where the highest root influenced an increase in shear strength was observed (Figure 5.19). Based on this model calibration, the values for λ_1 and λ_2 can be determined.

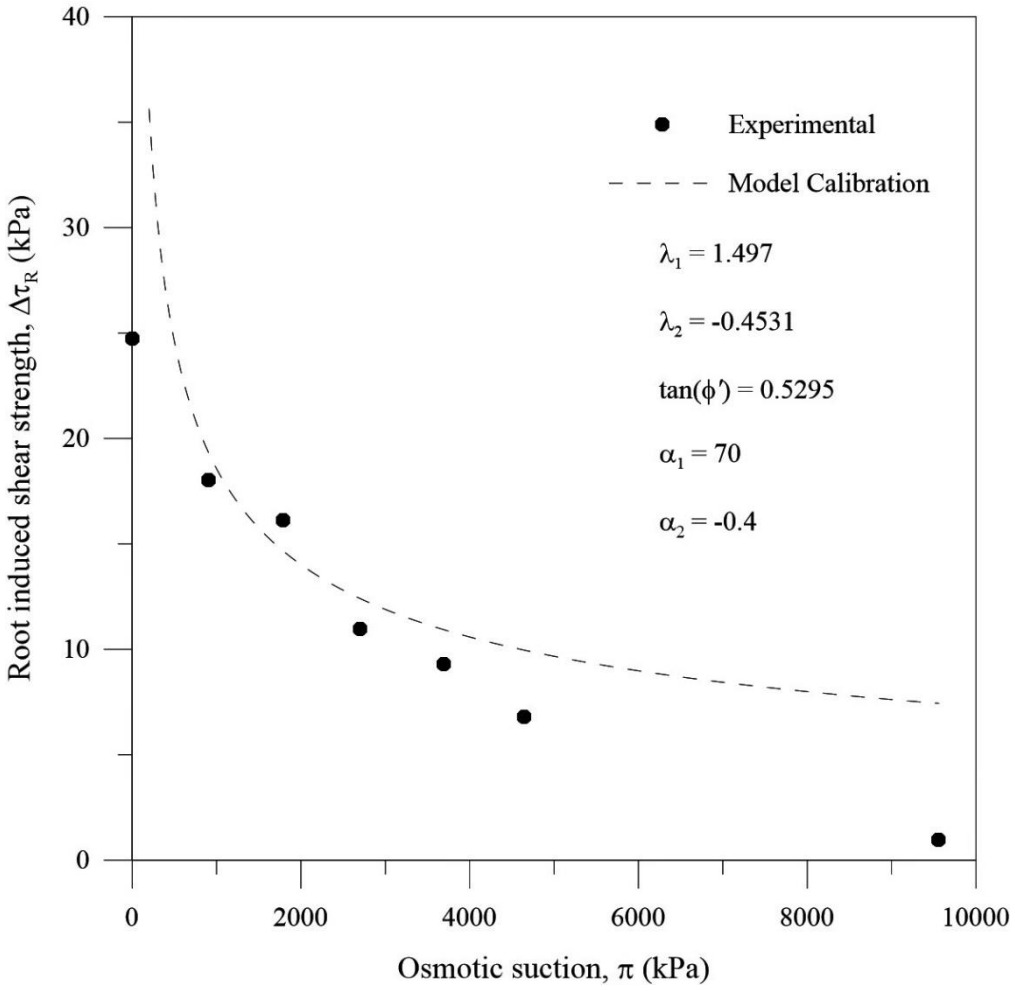

Figure 5.19 Comparison of experimental and model results of root induced shear strength

Figure 5.19 shows that the proposed model can satisfactorily predict the actual behaviour of root induced shear strength until about 4000 kPa of osmotic stress, but when the osmotic stress is very high (9560 kPa), the model shows a significant deviation from the

experimental results. This deviation occurs because at very high levels of osmotic stress, the roots have not grown across the shear plane, and therefore they have almost no effect on the shear strength of the soil. The calibrated model was then used to predict the root induced shear strength with saturated and 100 kPa matric suction (Figure 5.20), using $B_{r/sl}$ (the bond stress between root and soil of the root system during pure slipping) and $B_{r/sa}$ (bond stress between root and soil of the root system during pulling out with a soil annulus).

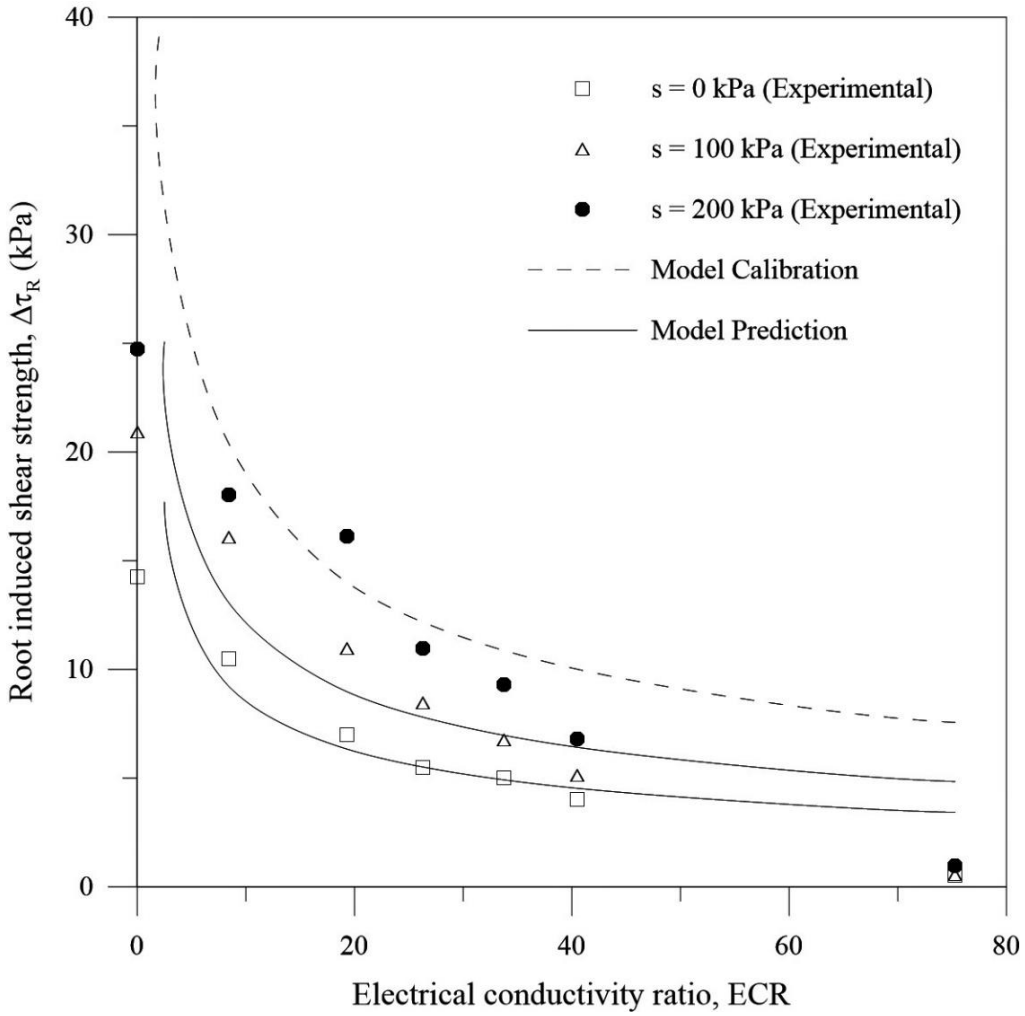

Figure 5.20 Experimental and model prediction of root induced shear strength

Figure 5.20 shows that the proposed new model predicted the experimental results satisfactorily, and therefore, the proposed new model for $\Delta\tau_R$ can be used to predict the shear strength induced by tree roots under unsaturated conditions even with the influence of osmotic stress due to salinity in the pore water.

5.3.4 Limitations of the model

The proposed new model can satisfactorily predict the actual behaviour of shear strength induced by tree roots within certain limitations, as stated below.

- It cannot predict the exact behaviour of root induced shear strength at very high levels of osmotic stresses, because, at these levels the roots may deteriorate or drastically decrease the growth. Also, the proposed model does not consider the growth of roots, because it is a time-dependent variable.
- It does consider a cylindrical shape root with an average diameter (d_R), but in reality, roots are not exactly cylindrical.

5.4 Summary

This study has introduced two new models to predict the shear strength of soil while considering the role of osmotic suction with and without roots. The development of the shear strength model was based on the Mohr-Coulomb failure criterion with a single effective friction angle. The osmotically induced shear strength was successfully characterised by the new osmotic stress parameter (χ_2) which depends on osmotic suction. Osmotic suction is mainly due to salinity in the pore water, which increases the concentration of ions in the pore water. Therefore, to capture the variations of shear strength due to changes in osmotic suction, electrical conductivity was used as a parameter. The electrical conductivity ratio (ECR) was developed based on fully-saturated conditions where the matric suction cannot influence the osmotic suction. The

proposed new model for osmotically induced shear strength (τ'_{US}) using χ_2 can successfully predict the actual behaviour of unsaturated soil under the influence of osmotic suction. Although the root induced shear strength has been broadly discussed by previous research, the influence of osmotic stress has on shear strength induced by roots is still not well established, and it lacks sufficient theoretical depth. The experimental results from Chapter 3 reveal that the tensile strength of an individual root is not affected by the influence of osmotic stress, whereas the RAR is significantly affected by osmotic stress. This is why a new model called osmotically induced RAR or RAR_π was developed in terms of ECR. This new RAR_π was then used in the existing shear strength equation proposed earlier by Gray and Leiser (1982) to calculate the contribution made by roots induced shear strength. The proposed new model can satisfactorily predict the experimental behaviour of root induced shear strength.

CHAPTER 6: Numerical simulation on a practical application

6.1 Background

This chapter looks at the slope stability of a rail embankment (Figure 6.1). Numerical simulation of the influence of osmotic suction and native vegetation on the stress-strain behaviour of soil was carried out for a field-based application. A commercially available finite element modelling software PLAXIS 2D (2018) was used for this analysis. A two-dimensional plain strain model was developed for an integrated layer system consisting of rails, sleepers, sub-ballast, ballast, an embankment and three layers of subgrade. The settlement and corresponding deformation of the embankment resulting from the load applied by a train were analysed to obtain the factor of safety for stability. This analysis took place with various osmotic suctions under saturated and unsaturated conditions, and with and without roots. The model was also extended to observe how the clearance length (distance between the toe of the embankment fill and the centre of the tree) affected the stress-strain behaviour of soil.

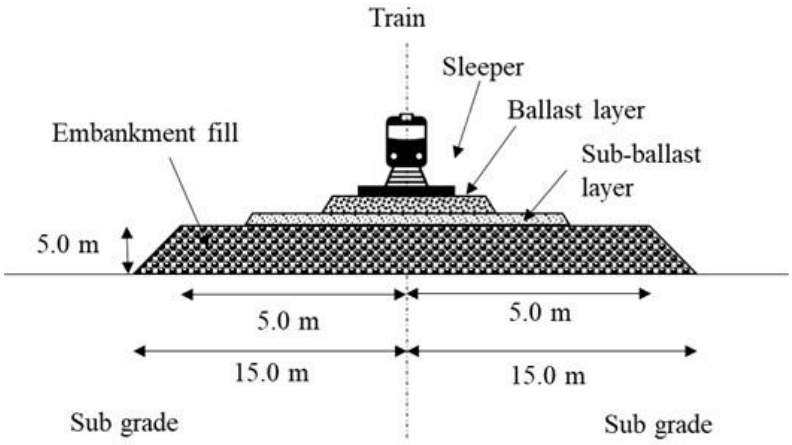

Figure 6.1 Schematic diagram of the rail section of the study

6.2 Analysis using PLAXIS

Determining the complex and unforeseen behaviour of geotechnical applications by numerical simulation has become common practice for a decade or so. Within the bounds of numerical simulation, finite element modelling plays a crucial role in solving geotechnical engineering related problems. In finite element analysis, a series of partial differential equations with two or three space variables are solved mathematically to obtain an approximated solution with which to interpret the response generated from elements. These elements are called finite elements and they are created by discretising the entire space of the domain into smaller segments by constructing a mesh. Domain discretisation has several advantages;

- The total solution can be easily represented
- Even complex geometries can be accurately analysed
- Dissimilar material properties can be included
- Local effects can be captured accurately

In this study, the finite element software called PLAXIS 2D was used to observe the behaviour of unsaturated and saturated soil under different osmotic suctions for vegetated and non-vegetated conditions. The latest version is PLAXIS 2D (2018) which does not consider the influence of matric suction, osmotic suction or the root reinforcement effect of tree roots; thus it can only be considered as an early attempt to model the coupled contribution of unsaturated, saline, and rooted conditions on the behaviour of an embankment using PLAXIS 2D. The stability of the embankment was interpreted using the factor of safety ($\sum M_{SF}$), and embankment settlement was interpreted using the vertical deformation (u_y).

6.2.1 Material model in FEM

The new shear strength model proposed in Chapter 5 is an extension of the Mohr-Coulomb model, so the Mohr-Coulomb (MC) model available in PLAXIS 2D (2018) was used for this numerical study. The Mohr-Coulomb model is a first order linear elastic perfectly plastic model where the effective stress state at failure is generally described in terms of the effective stress parameters *c'* and ϕ'. The Mohr-Coulomb model involves five major input parameters, i.e. Young's modulus (E), Poisson's ratio (ν), friction angle (ϕ'), cohesion (c') and dilatancy angle (ϕ_d). Even the latest versions of PLAXIS cannot simulate the behaviour of unsaturated soil or changes in its geo-chemistry; therefore this study can be considered as an early prototype for modelling the stability of an embankment over the influence of osmotic suction in unsaturated soil with and without the influence of roots.

6.2.2 Generation of element mesh in PLAXIS 2D

In finite element analysis the ground section is divided into smaller segments (in PLAXIS 2D, these segments are triangular) called elements, this collection of all the elements is called a mesh. Generating element meshes in PLAXIS is fully automatic but the density of the elements (number of elements) or the size of the elements for a considered area can be manually controlled as shown in Figure 6.2.

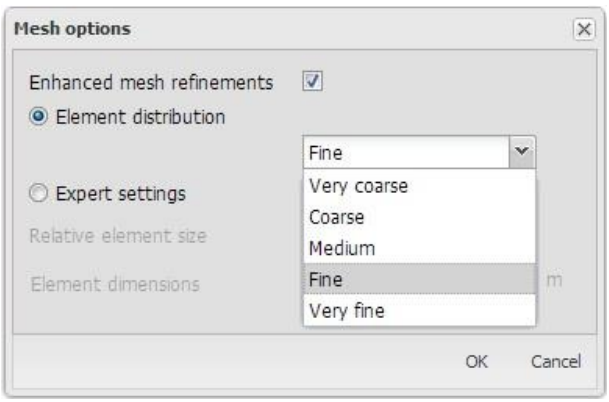

Figure 6.2 Mesh options in PLAXIS

In PLAXIS 2D, an element consists of nodes and Gaussian integration points or stress points (Figure 6.3). The nodes are mainly used to determine primary variables such as displacement and the stress points determine secondary variables such as stress. In PLAXIS 2D the nodes of the triangular elements can be either 15 or 6 (Figure 6.3), so for a single 15 node element there are 12 stress points, and for a single 6 node element there are 3 stress points. The magnitudes of the nodes are continuous along the boundaries of the elements, so the deformation within the element is determined by polynomial interpolation. The accuracy of the results depends on the number of nodes for an element. Increasing the number of nodes for an element means having to solve a high order polynomial equation, which is time-consuming. However, 15 nodded elements were selected for this study.

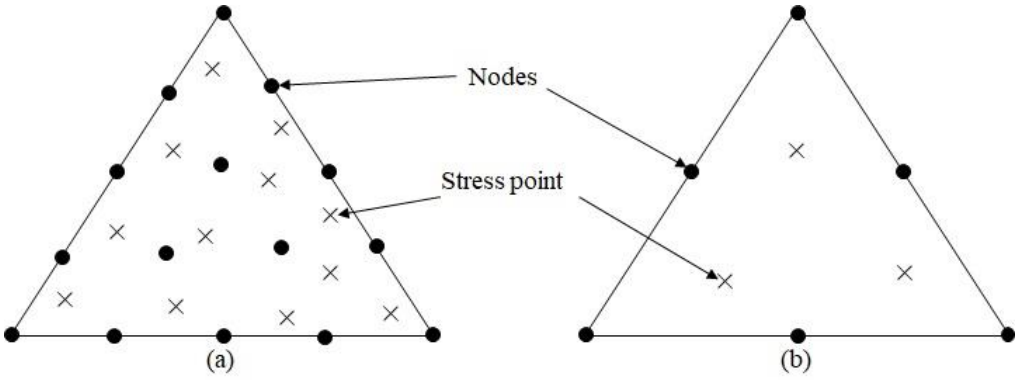

Figure 6.3 Types of elements in PLAXIS 2D, (a) 15 nodes elements, and (b) 6 nodes elements

6.2.3 Root simulation

In this study, the roots are simulated using geogrids with a unit thickness. Geogrids are line elements with two translational degrees of freedom in each node (u_x,u_y). For a 15 node soil element, each geogrid element is defined with five nodes (Figure 6.4). Based on the PLAXIS 2D (2018) manual, geogrids can sustain a tensile force and can be used

as a reinforcing tool in soil modelling. The only material property used for geogrids is axial stiffness (EA). Moreover, tension failure can be simulated by assigning a maximum value for the tension force.

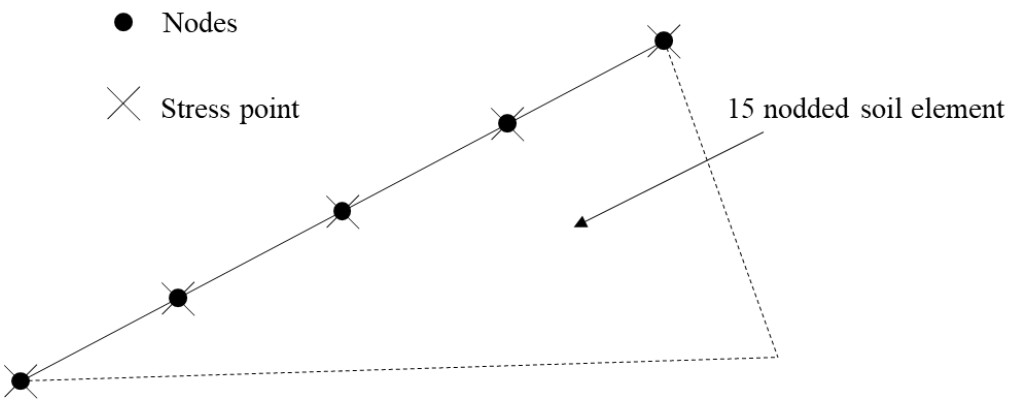

Figure 6.4 Nodes and stress points in a geogrid element

6.3 Rail embankment simulation using PLAXIS 2D

A section of embankment on subgrade soil was modelled in PLAXIS 2D, and then the settlement and factor of safety were compared for different degrees of saturation and salinity, and in vegetated and non-vegetated conditions. The root system for this analysis was assumed to be constant, so the same type of root system was modelled out of geo-grid. The model is described in detail in the following sub-sections.

6.3.1 Model geometry

The symmetry of this model geometry meant that only half of the soil section was considered for this analysis. The model has an embankment and a subgrade soil, so it was defined by the Mohr-Coulomb soil model. The unsaturated flow properties of soil were based on the user-defined van Genuchten model. The geo-grid option under structures in PLAXIS 2D was used to model the effect of tree root reinforcement. The graphical input of the soil model and the corresponding finite element mesh are shown in Figure 6.5.

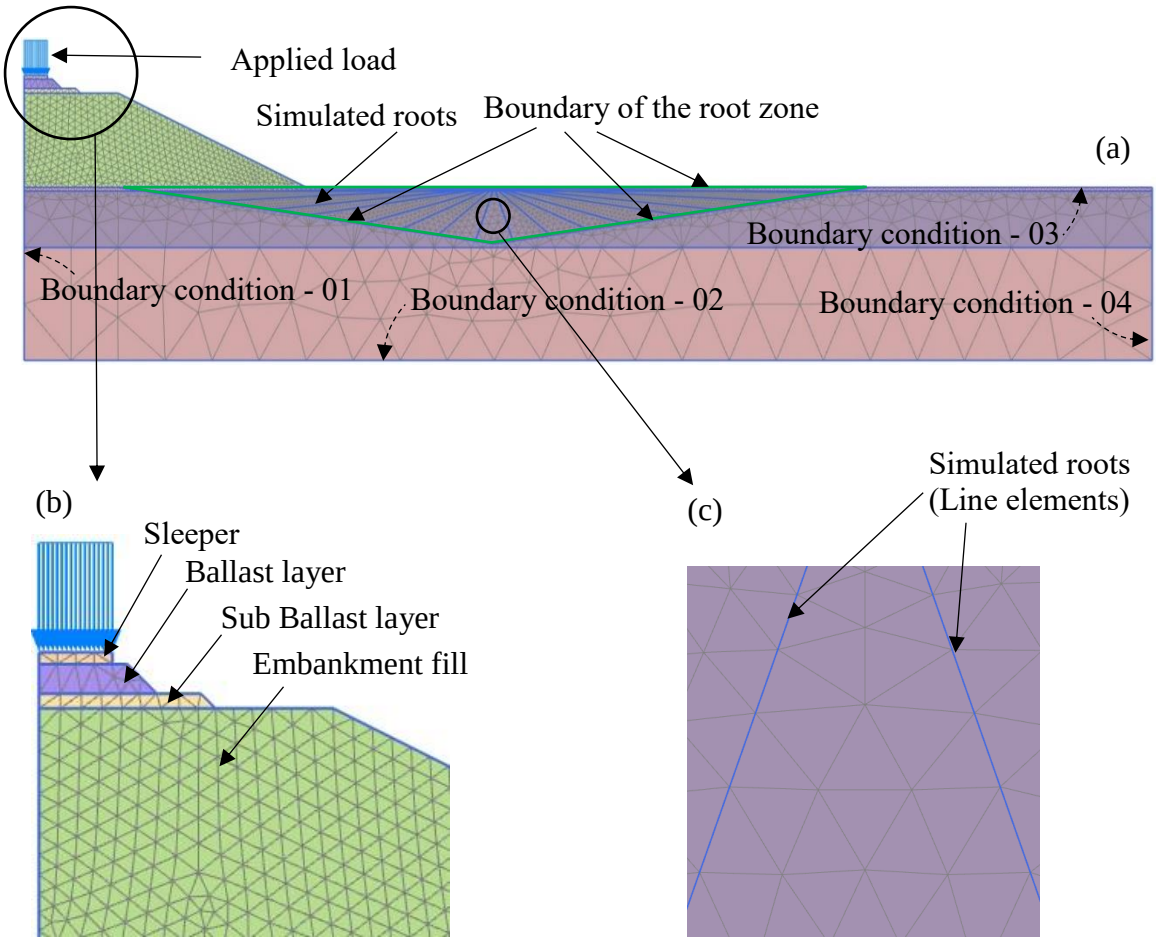

Figure 6.5 Diagram of PLAXIS 2D model

The coarseness factor of the finite element mesh close to roots was reduced to 0.5, but it remained at 1.0 for the other sections which is why the density of the finite element mesh close to roots was much higher than the other areas. The boundary conditions for ground-water flow were defined by keeping 'Open' for boundary conditions no - 02, 03 and 04, to accommodate any seepage during settlement. However, the boundary condition no - 01 remained 'Closed' due to the symmetry of the model. The boundary conditions for deformation were defined according to the free movement of the soil boundaries. Boundary conditions no - 01 was set as symmetrical for deformation, but boundary conditions no - 02 and 03 were fixed for horizontal movement and vertical movement. Modelling each and every root for a particular root system in PLAXIS is never easy and

it is also time-consuming. Therefore, only eight geo-grid lines were selected to simulate the behaviour of the overall root system within the soil. The material type for the geo-grid was defined as elastic. The experimentally measured tensile strength of tree roots was used as an input parameter to define the geo-grids.

6.3.2 Initial calibration of the model

The direct shear test can be modelled and run in PLAXIS 2D 2018 as per the input material properties; this function is available as 'Soil Test' under 'Material sets'. The Mohr-Coulomb (MC) model was used as the deformation model, and the results of the direct shear test from PLAXIS 2D was compared to the experiment results. The equivalent parameters to characterise the influence due to the change in matric suction, osmotic suction and tree root reinforcement were calculated separately based on the new models proposed in Chapter 5 and introduced to the numerical model as necessary. The properties of the material used for this analysis are summarised in Table 6.1.

The results of the shear stress vs horizontal displacement taken from the proposed numerical model were compared with the results for different soil conditions, as shown in Figure 6.6. The elastic parameters were calibrated to match the initial small strain stiffness of the shear stress vs displacement plot in Figure 6.6. These parameters were then used for a field application proposed by Fatahi et al. (2010) and Esmaeili et al. (2013).

Table 6.1 Properties of input parameters for the DSS test in PLAXIS 2D

Material Property	Values used for initial analysis	Calibrated values
Material model	Mohr-Coulomb model	Mohr-Coulomb model
γ_{sat}	19.82 kN/m^3	20 kN/m^3
γ_{unsat}	15.58 kN/m^3	16 kN/m^3
c'	6.056 kN/m^2	6 kN/m^3
ϕ'	27.9^0	28 kN/m^3
E	5 x 10^3 kN/m^2	8 x 10^3 kN/m^2
ν	0.3	0.32
Ground water model	Van Genuchten (User-defined)	Van Genuchten (User-defined)
S_{res}	0.042	0.042
S_{sat}	1.0	1.0
g_n	1.44	1.44
g_a	0.008	0.008
g_l	-0.306	-0.306
Type of test	Undrained	Undrained
Consolidation	Isotropic	Isotropic

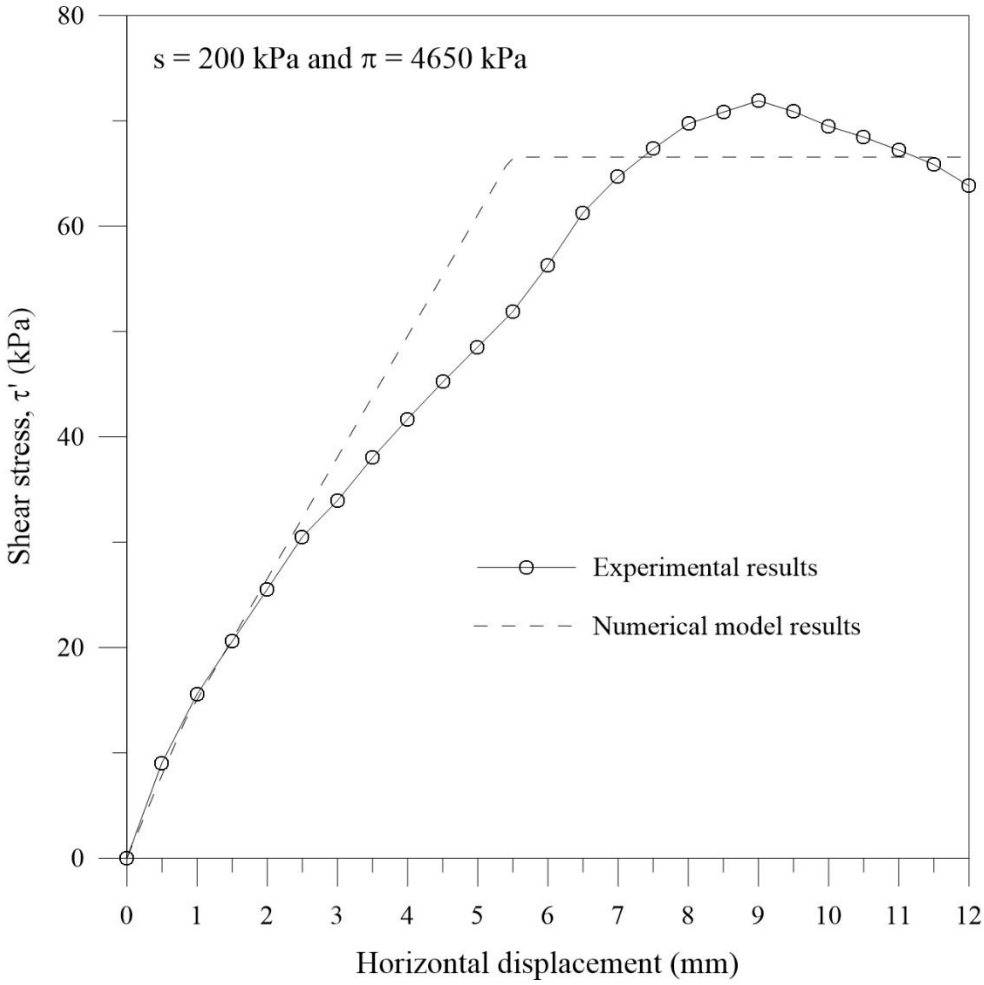

Figure 6.6 Shear stress distribution of numerical model vs experimental results

(s = 200 kPa and π = 4650 kPa)

6.4 Simulating the field application

A section of the green corridor along the railway line in Miram, Australia (Fatahi et al. 2010) was used for this analysis. In Fatahi et al. (2010)'s observations, the vegetation was only along a single side, but in this study it was assumed to be on both sides. A 5 m high section of the embankment was also introduced to the model, so the influence of tree roots and osmotic suction was determined by the stability of the embankment. A sectional view of the rail line is shown in Figures 6.7 and 6.8. The main challenges in this study were to successfully model the effects of tree roots and osmotic suction for different unsaturated conditions.

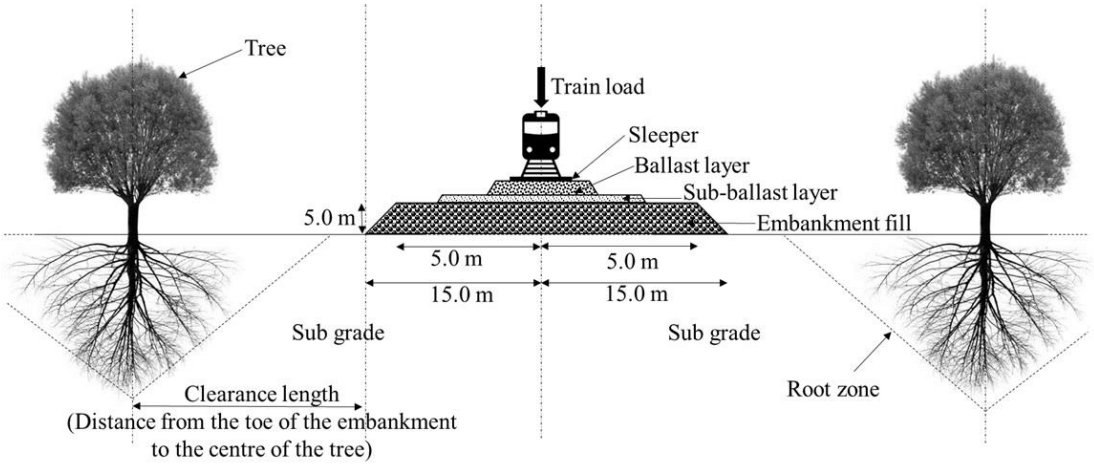

Figure 6.7 Schematic diagram of a typical section of rail with the user defined embankment section

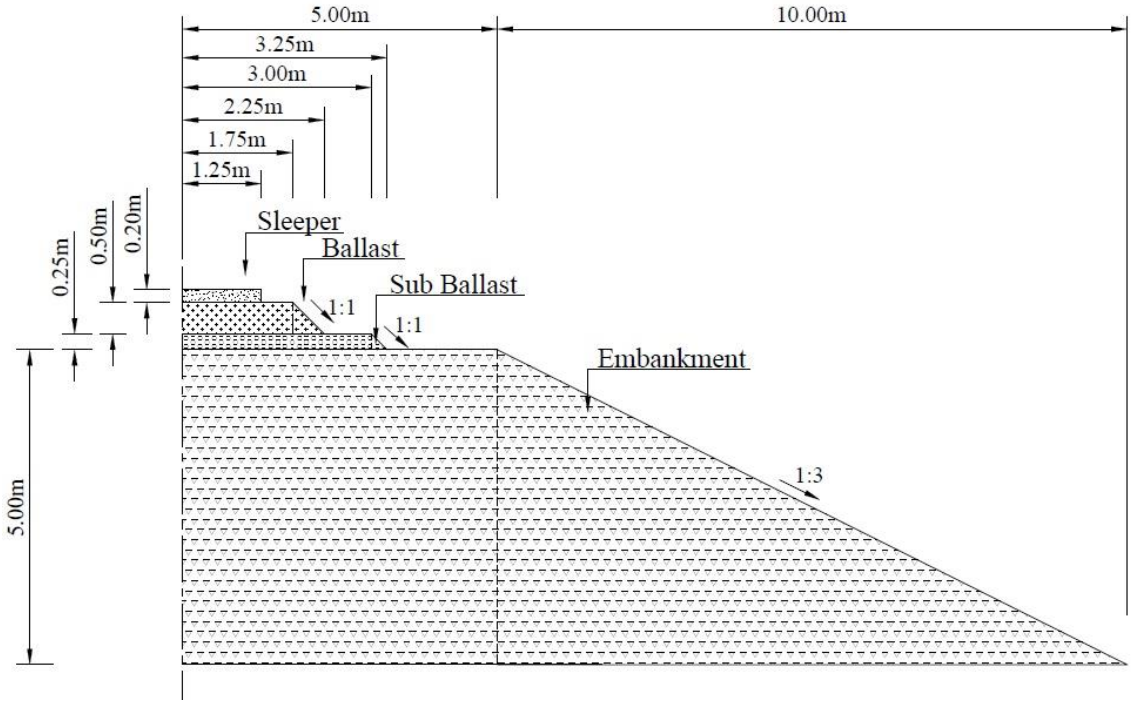

Figure 6.8 Schematic diagram of the super structure and the embankment

6.4.1 Properties of tree roots

Docker and Hubble (2008) investigated the increase in shear strength due to root reinforcement by four common Australian species. The tensile strength of a single root in

each species was measured. The tensile properties of *Eucalyptus Amplifolia* measured by Docker and Hubble (2008) were used for this study. The root geometry is summarised in Table 6.2.

Table 6.2 Parameters for the root zone

Parameter	Value	Reference
r_{max} (m)	20	Fatahi et al. (2010)
z_{max} (m)	3	Fatahi et al. (2010)
T_r (MPa)	55.39	
d_R (mm)	2.56	

6.4.2 Properties of subgrade soil and the embankment

The geotechnical conditions for the subgrade soil were selected based on Fatahi et al. (2010), the soil properties are summarised in Table 6.3. The Van Genutchen (User-defined) model is available in PLAXIS so it was used as the ground water flow model. A fully-saturated condition was maintained in the model by keeping the head level at the top of the subgrade layer and using the same value for the saturated (γ_{sat}) and unsaturated (γ_{unsat}) densities. Unsaturated conditions in the model were achieved by keeping the head level at the bottom of the subgrade layer. Modelling micro-scale influences such as the pore water chemistry and the subsequent increase in van der Wall's forces is challenging with PLAXIS, so to incorporate the effect of osmotic suction, the shear strength as influenced by osmotic suction was calculated based on Equations 5.5 and 5.6. Hence, the overall shear strength was calculated based on Equation 5.4. The embankment section for this study was modelled based on the Mohr-Coulomb model, and the parameters for the embankment were based on an experimental study by Esmaeili et al. (2013). The parameters are summarised in Table 6.4.

Table 6.3 Properties of the subgrade soil (After Fatahi et al. (2010))

Parameter	Layer No 01	Layer No 02	Layer No 03
γ_d (kN/m^3)	16.6	17.3	17.8
e_0	0.61	0.52	0.47
E (MPa)	25.0	40.0	56.0
ν	0.30	0.33	0.32
c' (kPa)	12.0	10.0	13.5
ϕ' (degree)	25.0	26.5	31
S_{res}	0.060	0.055	0.081
S_{sat}	1.0	1.0	1.0
g_n	1.560	1.560	1.525
g_a	0.030	0.040	0.072
g_l	0.359	0.359	0.352

Table 6.4 Properties of the embankment (Esmaeili et al. 2013)

Parameter	Value
γ_{dmax} (kN/m^3)	17.5
γ_b (kN/m^3)	18.1
E (MPa)	49.891
c' (kPa)	25.0
ϕ' (degree)	32.0

6.4.3 Track geometry and material properties of the super structure

Conventional track geometry was used in this study. The concrete sleepers were embedded with a coarse granular layer called Ballast. The sleeper was 2.5 m in length

and 0.21 m in height. The ballast layer had a maximum length of 2.5 m and a maximum height of 0.5 m. A 3.0 m long by 0.25 m high layer of sub-ballast was placed under the ballast. The material properties used for the super structure are given in Table 6.5.

Table 6.5 Material properties for the super structure (Indraratna et al. 2017)

Parameter	Value			
	Rail	Sleeper	Ballast	Sub-ballast
γ (kN/m^3)	19.62	19.62	15.0	20.6
E (MPa)	500,000	30,000	2.0	2.0
ν	0.3	0.25	0.3	0.3
e_o	0.25	0.3	0.77	0.5
ϕ (^{o})			45	39
c (kPa)			1.0	1
ψ_d (^{o})			15	5

6.4.4 Loading

This analysis was based on a typical freight car used by Australian railways which would generate an axle load of 25 tonnes. According to Indraratna et al. (2017), this axle load corresponds to a static wheel load of 122.5 kN. The load applied by a moving train onto the underlying soil layers is generally cyclic, so the principal axis rotation and the dynamic amplification of load should be considered; in this study, they were not considered.

6.5 Results and discussion

6.5.1 Vertical deformation

The vertical deformation of a section of embankment on a subgrade was analysed based on PLAXIS 2D. The change in vertical deformation was compared with the changing osmotic suction and matric suction, with and without roots.

Here the influence of osmotic suction on vertical deformation was also compared under saturated and unsaturated conditions without roots (Figure 6.9).

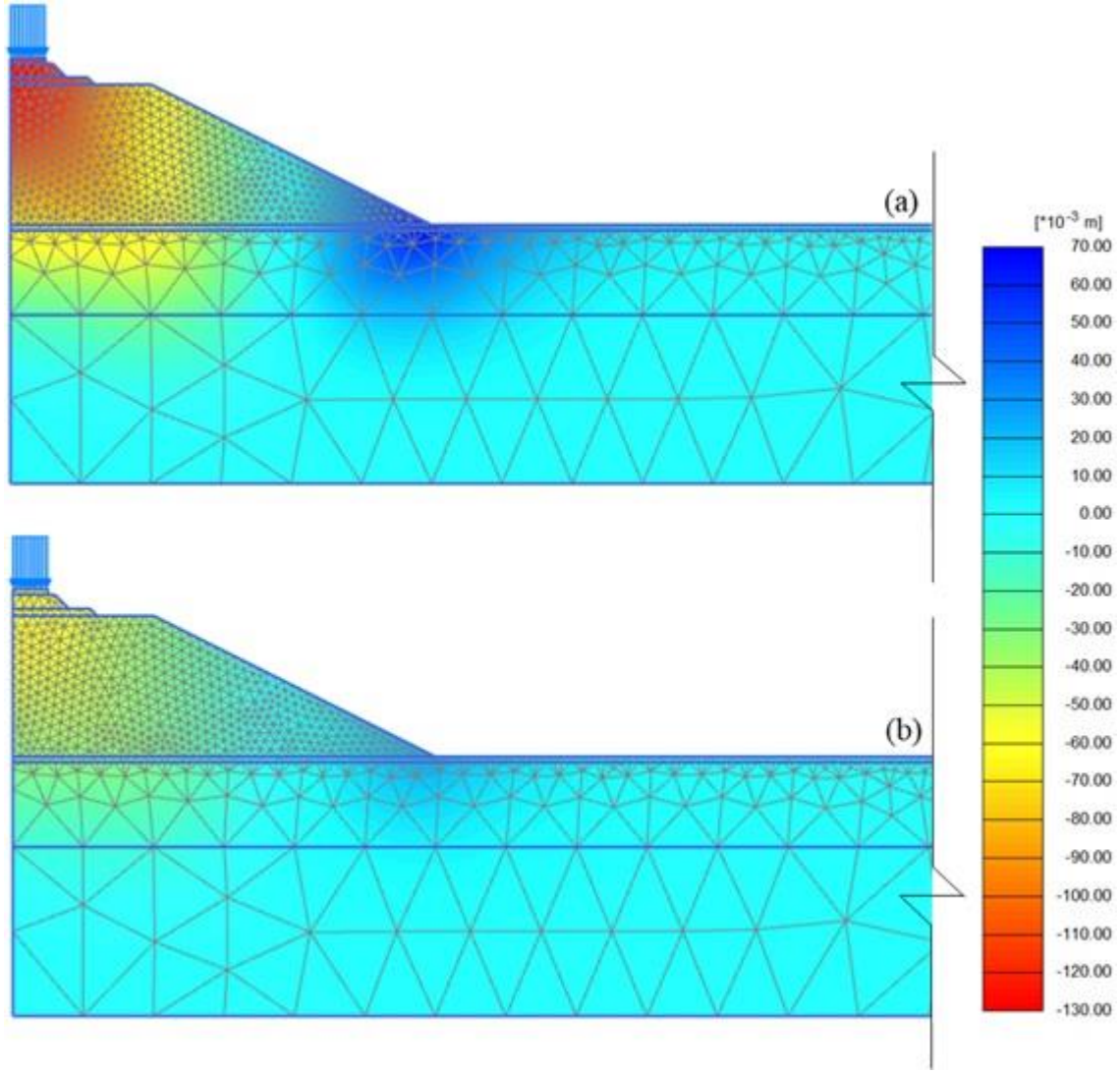

Figure 6.9 Graphical view of the distribution of vertical deformation,

(a) π = 0 kPa and (b) π = 9560 kPa, for fully saturated conditions (without roots)

Figure 6.9 (a) and Figure 6.9 (b), shows the decrease in vertical deformation due to osmotic suction. As the osmotic suction increased, the vertical deformation decreased significantly; this behaviour was shown experimentally in Chapter 3 as the maximum vertical displacement that resulted from the direct shear tests. In Chapter 3 the influence of osmotic suction on unsaturated soil was significant, so to numerically prove the influence of osmotic suction on unsaturated soil the distributions of vertical deformation are shown in Figures 6.10 and 6.11 for 100 kPa and 200 kPa of matric suction without roots.

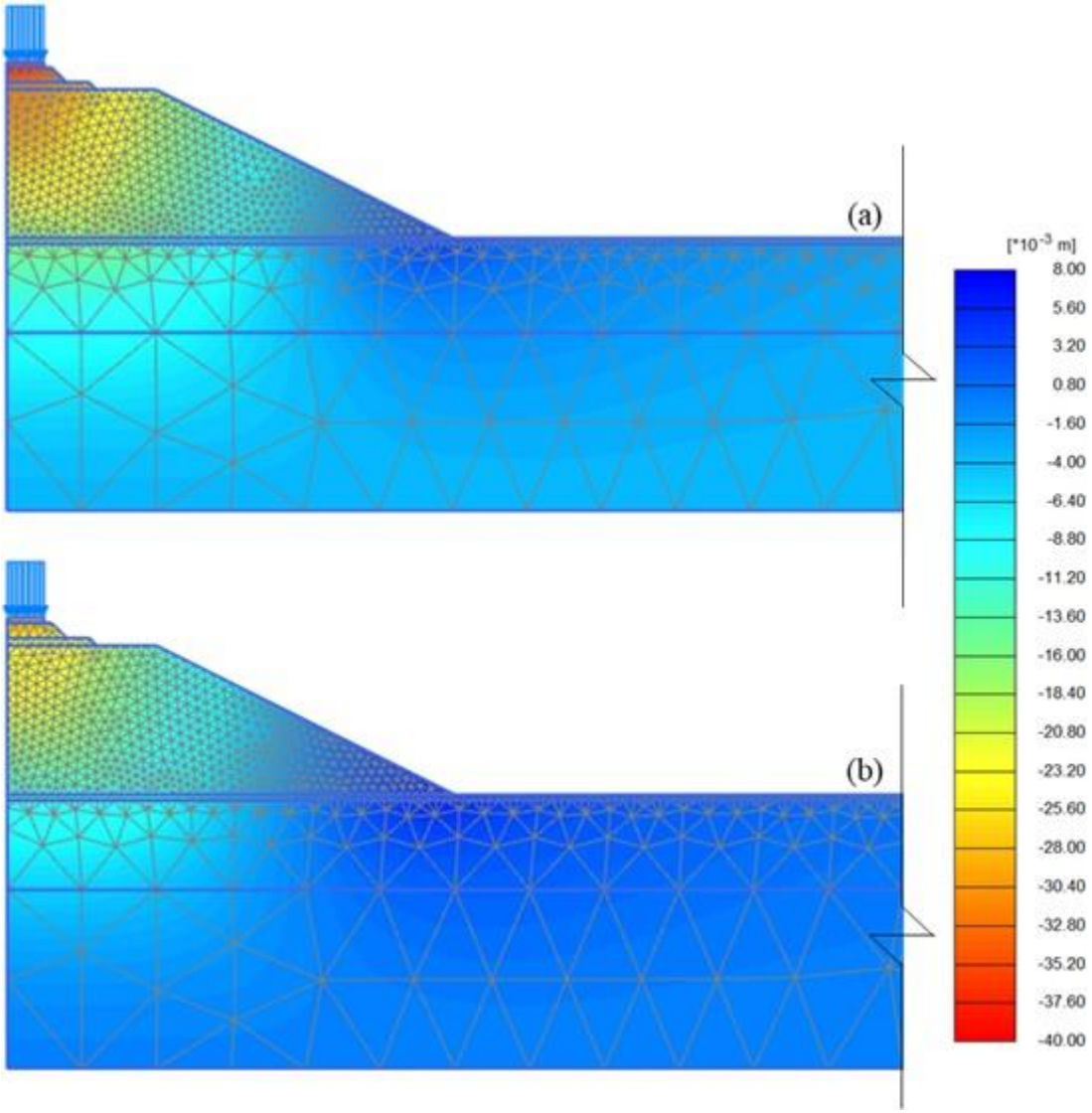

Figure 6.10 Graphical view of the distribution of vertical deformation,

(a) π = 0 kPa and (b) π = 9560 kPa, for s = 100 kPa (without roots)

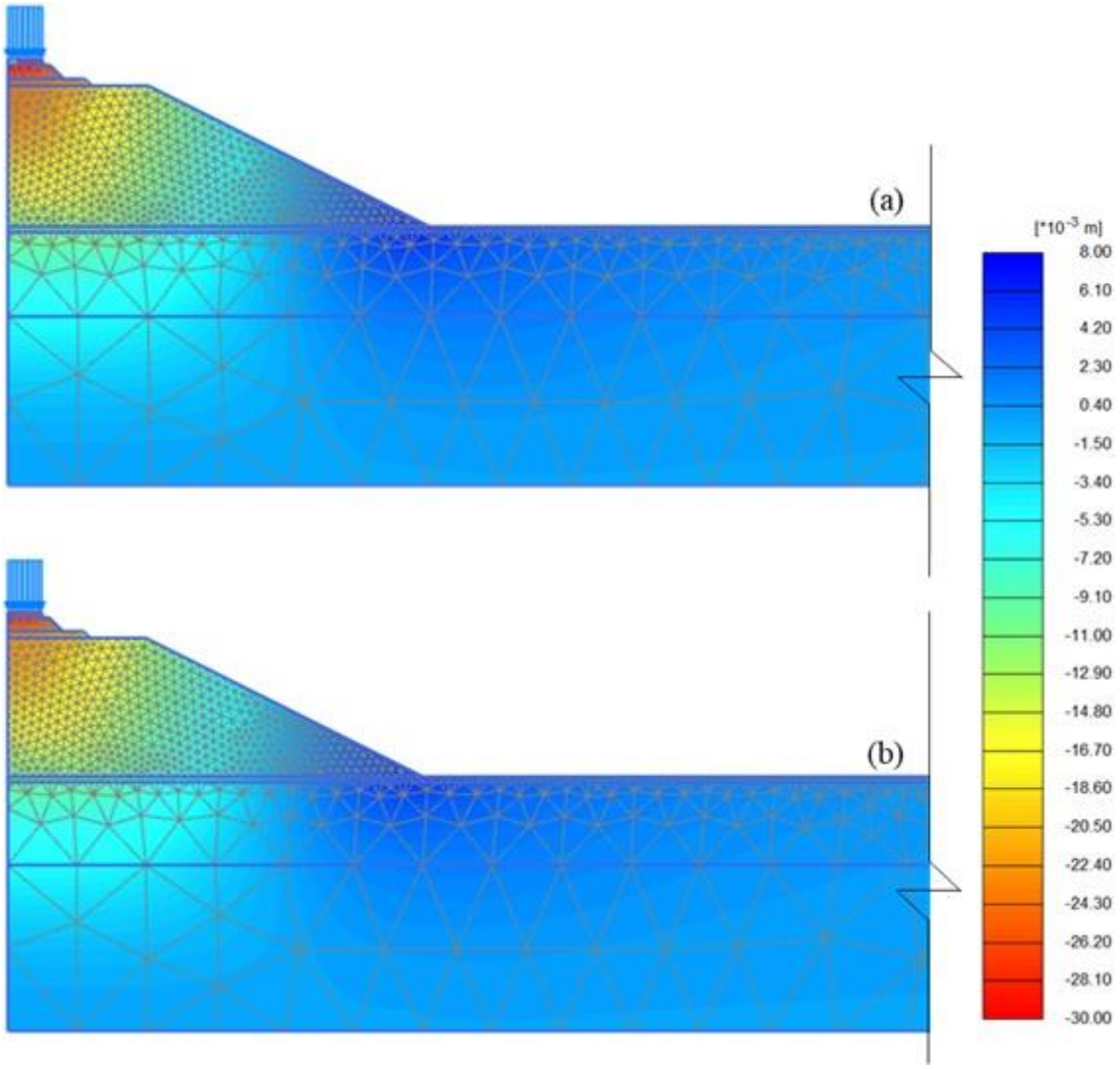

Figure 6.11 Graphical view of the distribution of vertical deformation, (a) π = 0 kPa and (b) π = 9560 kPa, for s = 200 kPa (without roots)

The maximum vertical deformation from the PLAXIS 2D model is shown in Figure 6.12 with various degree of saturation; here, the vertical deformation decreased as the osmotic suction increased under saturated conditions, and as expected, the change in maximum vertical deformation decreased due to matric suction. However, under every matric suction condition, the maximum vertical deformation decreased with the osmotic suction. This kind of behaviour was discussed in Chapter 3.

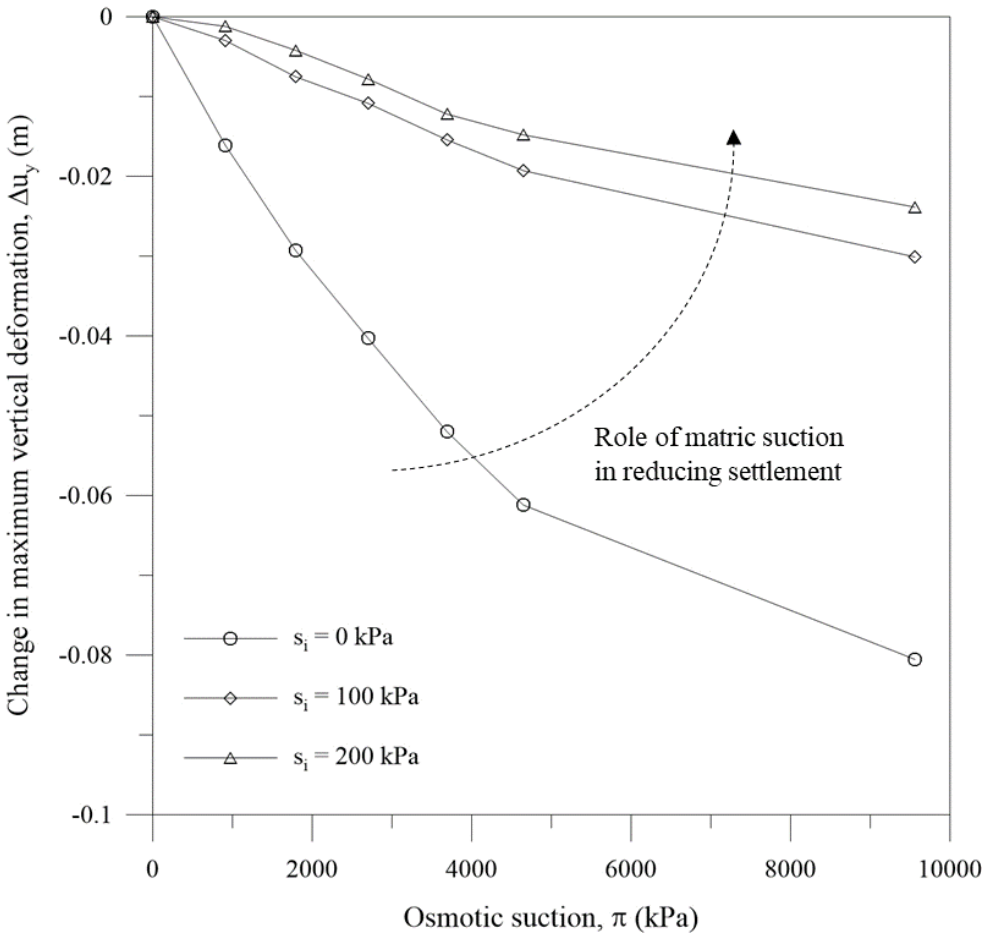

Figure 6.12 Change in maximum vertical deformation with respect to osmotic suction for different matric suctions (without roots)

Tree roots can reduce settlement, as shown by previous studies and by this study using the large scale direct shear apparatus described in Chapter 4. Finite element modelling the actual behaviours of roots is extremely challenging, so only the reinforcement effect by tree roots into the soil stratum was considered in this study. Figure 6.13 shows the change of vertical deformation without the influence of roots and with varying amounts of osmotic suction under vegetated conditions. The vertical deformation clearly decreased due to the influence of roots [Figure 6.13 (a) and (b)], and decreased further due to osmotic suction [Figure 6.13 (c)].

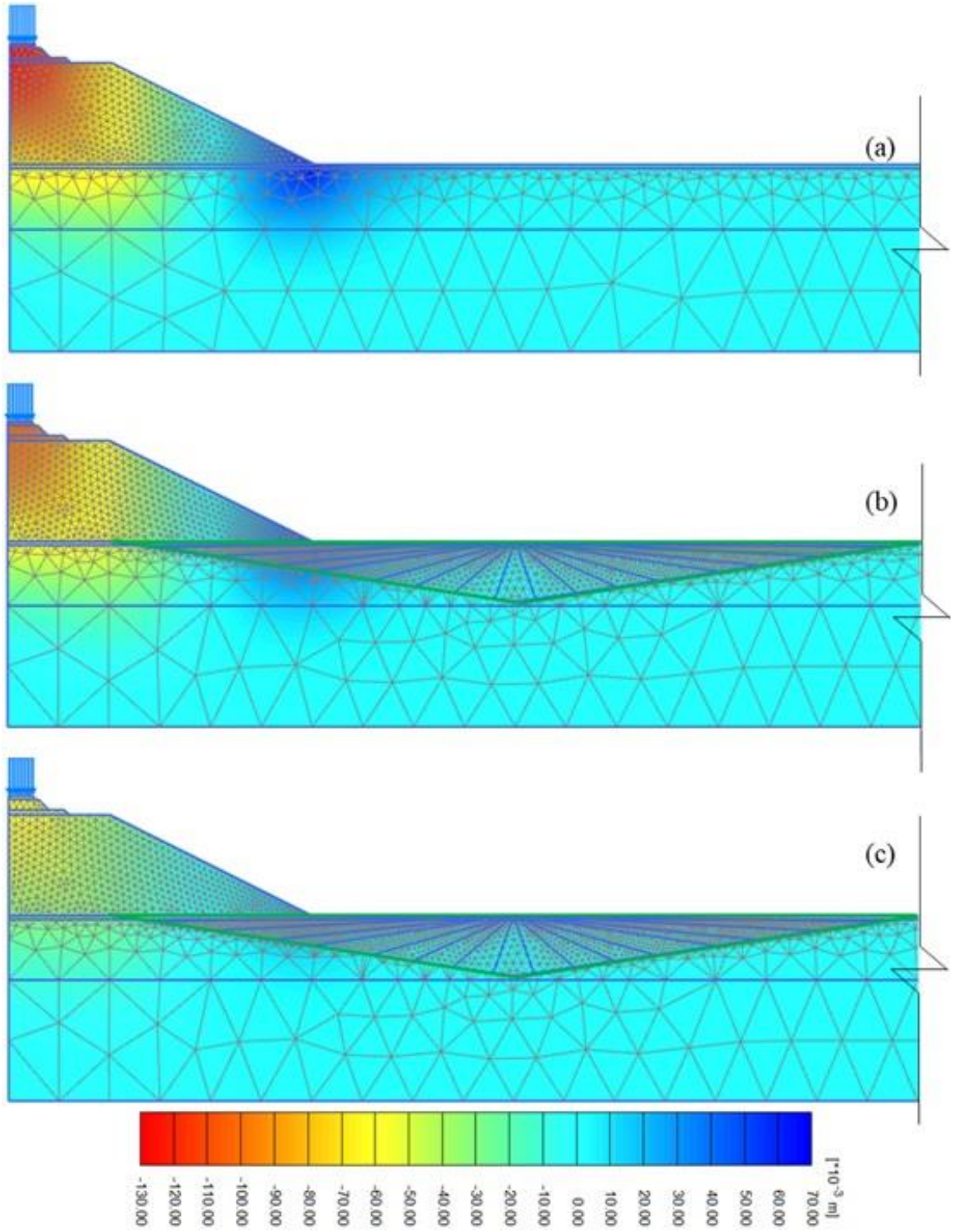

Figure 6.13 Graphical view of vertical deformation (Fully-saturated), (a) without roots (π = 0 kPa), (b) with roots (π = 0 kPa) and (c) with roots (π = 95600 kPa)

Figure 6.14 shows the maximum vertical deformation due to osmotic suction. The figure shows, there was no significant difference in maximum vertical deformation between vegetated and non-vegetated conditions until the osmotic suction reached 4650 kPa.

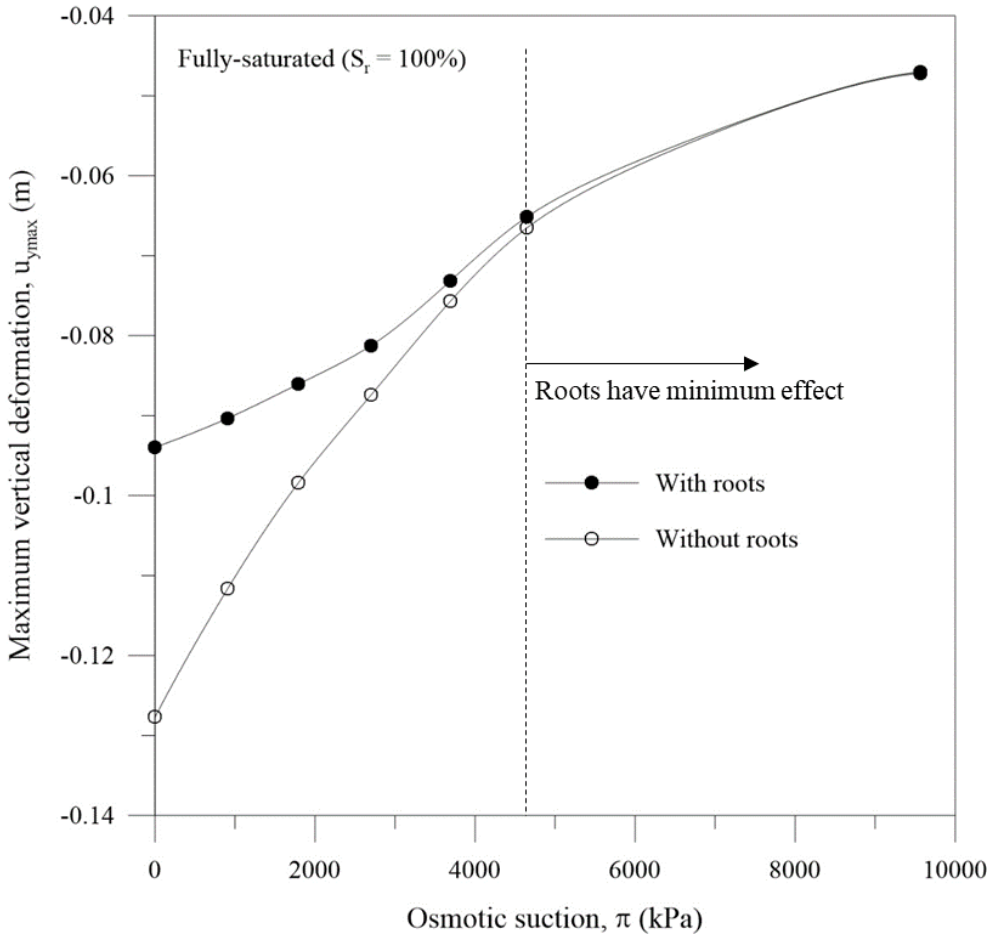

Figure 6.14 Distribution of maximum vertical deformation (Fully-saturated) due to osmotic suction with and without roots

The conclusion is that the tree roots deteriorated due to salinity in the pore water, as is shown by the maximum vertical deformation. This vertical deformation was also analysed for different matric suctions with roots; the PLAXIS 2D output results are shown in Figures 6.15 and 6.16.

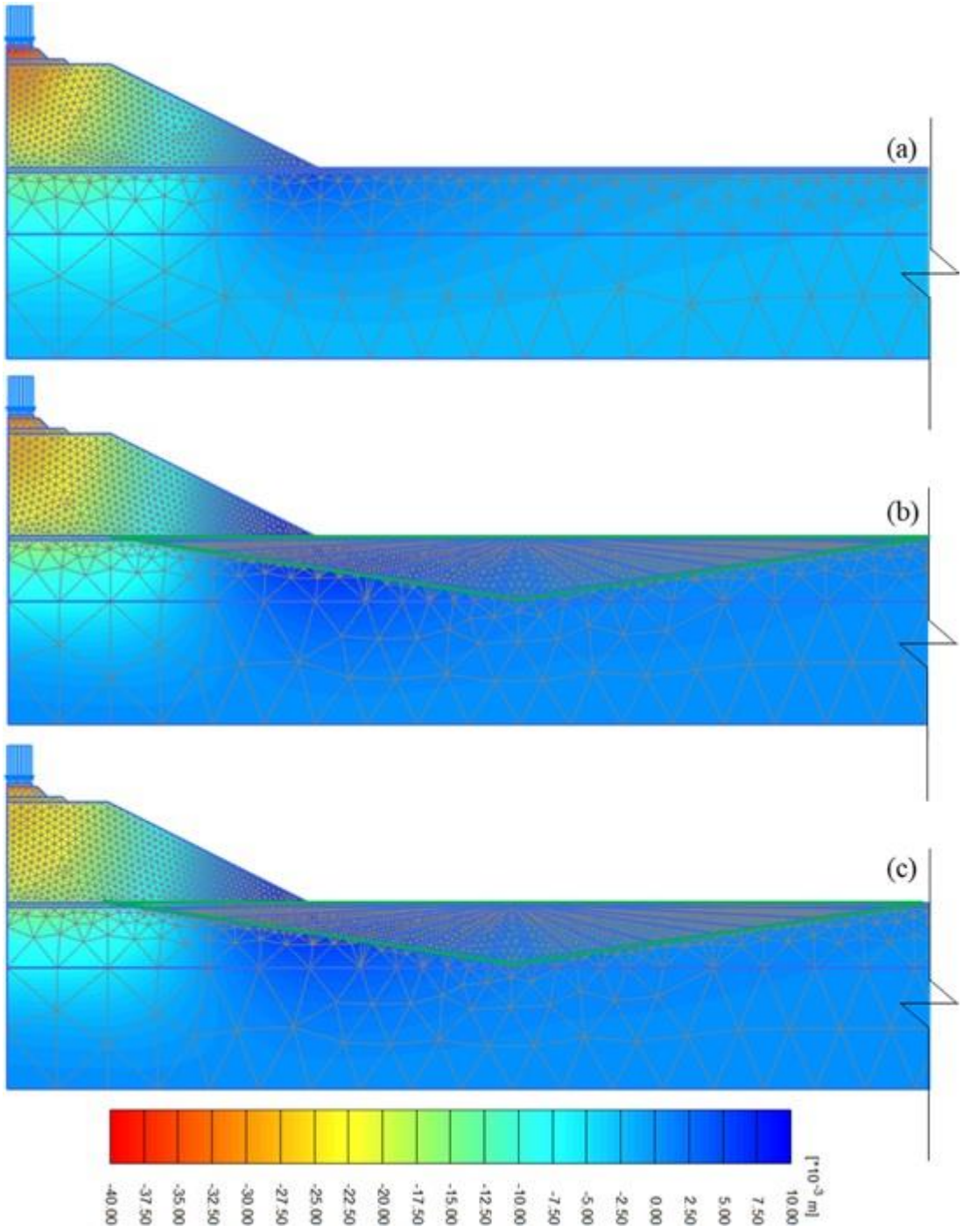

Figure 6.15 Graphical view of vertical deformation (s = 100 kPa),

(a) without roots (π = 0 kPa), (b) with roots (π = 0 kPa),

and (c) with roots (π = 95600 kPa)

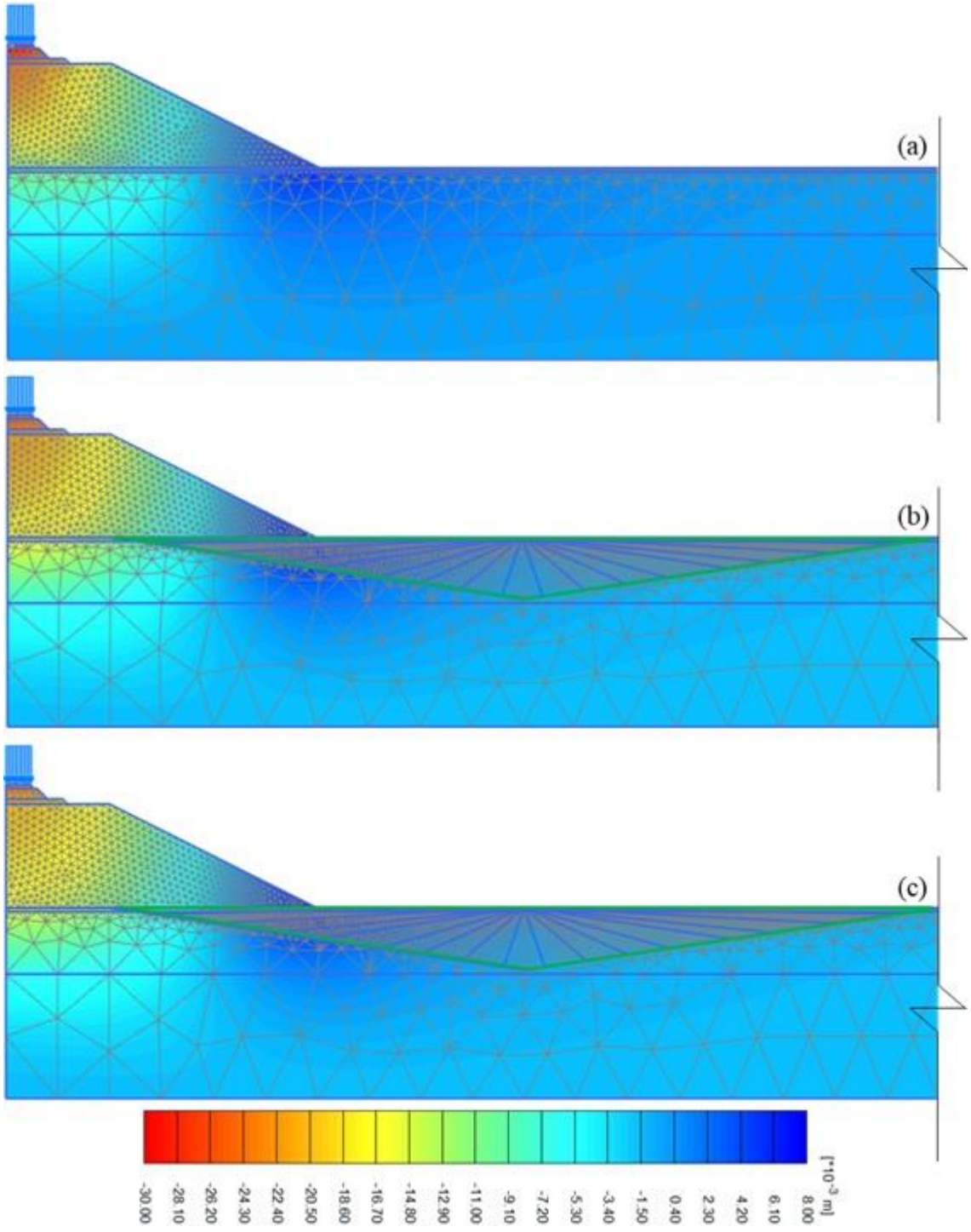

Figure 6.16 Graphical view of vertical deformation (s = 200 kPa),

(a) without roots (π = 0 kPa), (b) with roots (π = 0 kPa),

and (c) with roots (π = 95600 kPa)

Maximum vertical deformation in unsaturated conditions was compared with and without roots with varying amounts of osmotic suction (Figure 6.17). The maximum vertical deformation under unsaturated conditions was similar to saturated conditions. Figure 6.17 shows that the maximum vertical deformation decreased with increasing matric suction with and without roots. Furthermore, Figure 6.14 and Figure 6.17 show that the change of maximum vertical deformation due to roots decreased as the matric suction increased, particularly when the osmotic suction was 0 kPa.

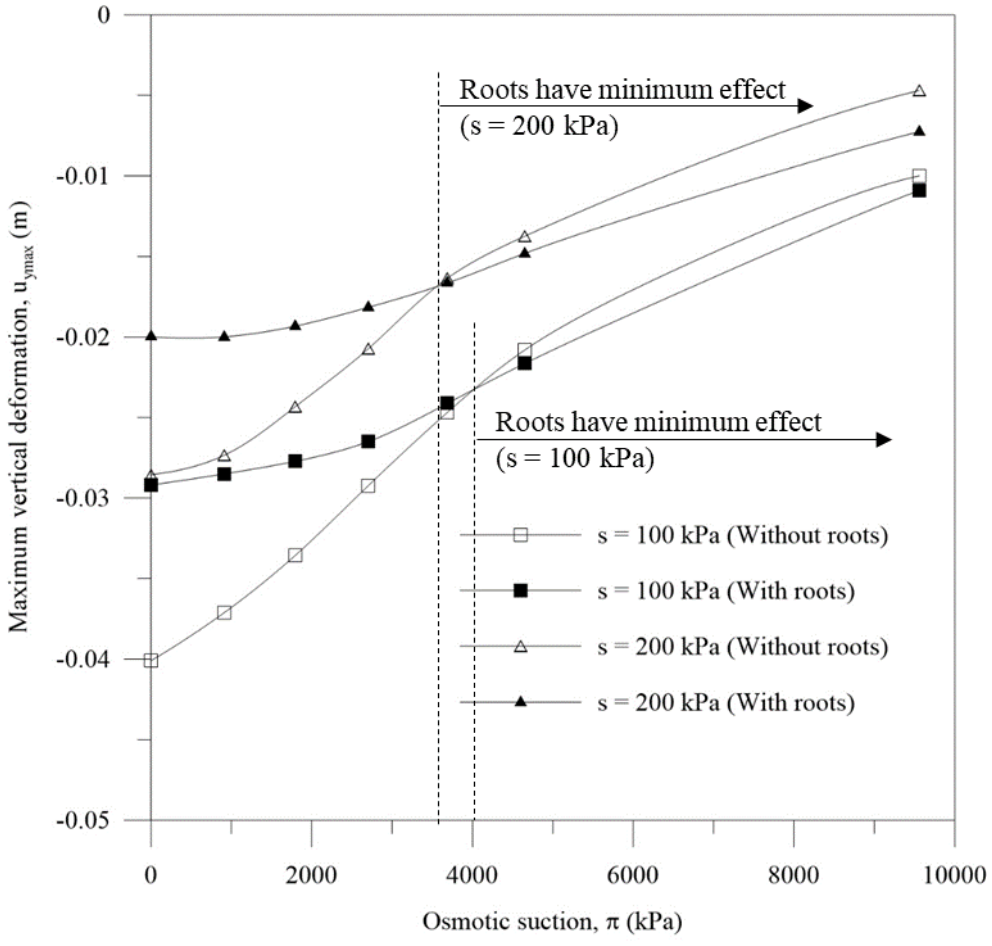

Figure 6.17 Distribution of maximum vertical deformation due to osmotic suction with and without roots

6.5.2 Factor of safety

The most common parameters used in PLAXIS to analyse the strength or stability of an embankment is the factor of safety. Here, the factor of safety of the embankment was calculated at the point of maximum total deformation. This factor of safety for the embankment was compared for various osmotic suctions and matric suctions with and without roots. The factor of safety can be graphically interpreted using the incremental deformation in PLAXIS. Figure 6.18 shows the decrease of incremental deformation ($|\Delta u|$) along the slipping surface as the osmotic suction increases under fully-saturated conditions without the influence of roots.

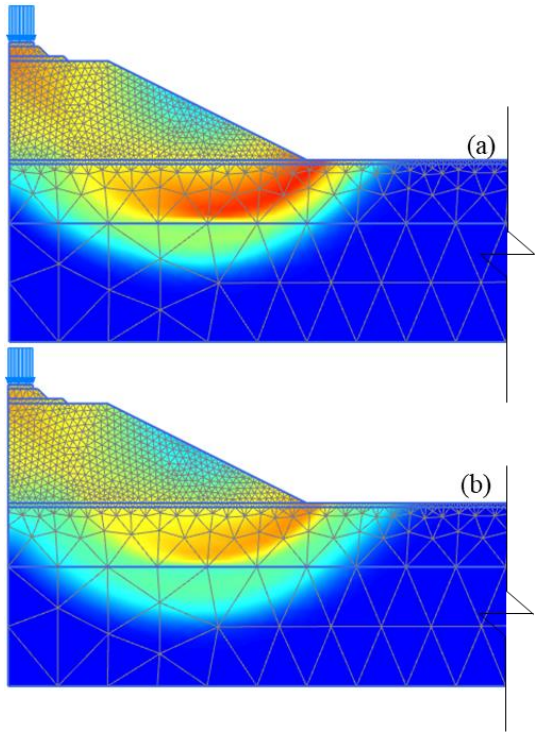

Figure 6.18 Graphical view of the variation of incremental deformation ($|\Delta u|$) without roots (Fully-saturated), π = 0 kPa and (b) π = 9560 kPa

Similarly, the variation of total deformation was compared for different matric suctions (100 kPa and 200 kPa) without roots and with changing osmotic suction. The factor of safety with respect to matric suction varied under different amounts of osmotic suction

(without the influence of roots), as shown in Figure 6.19; basically, the factor of safety increased as the matric suction increased. As an example, the factor of safety (at π = 0 kPa) increased to almost 2.829 as the matric suction increased to 200 kPa and for the same increase in matric suction the factor of safety (at π = 9560 kPa) increased to almost 3.504. However, the rate at which the factor of safety increased was decreased at higher matric suctions such as 200 kPa.

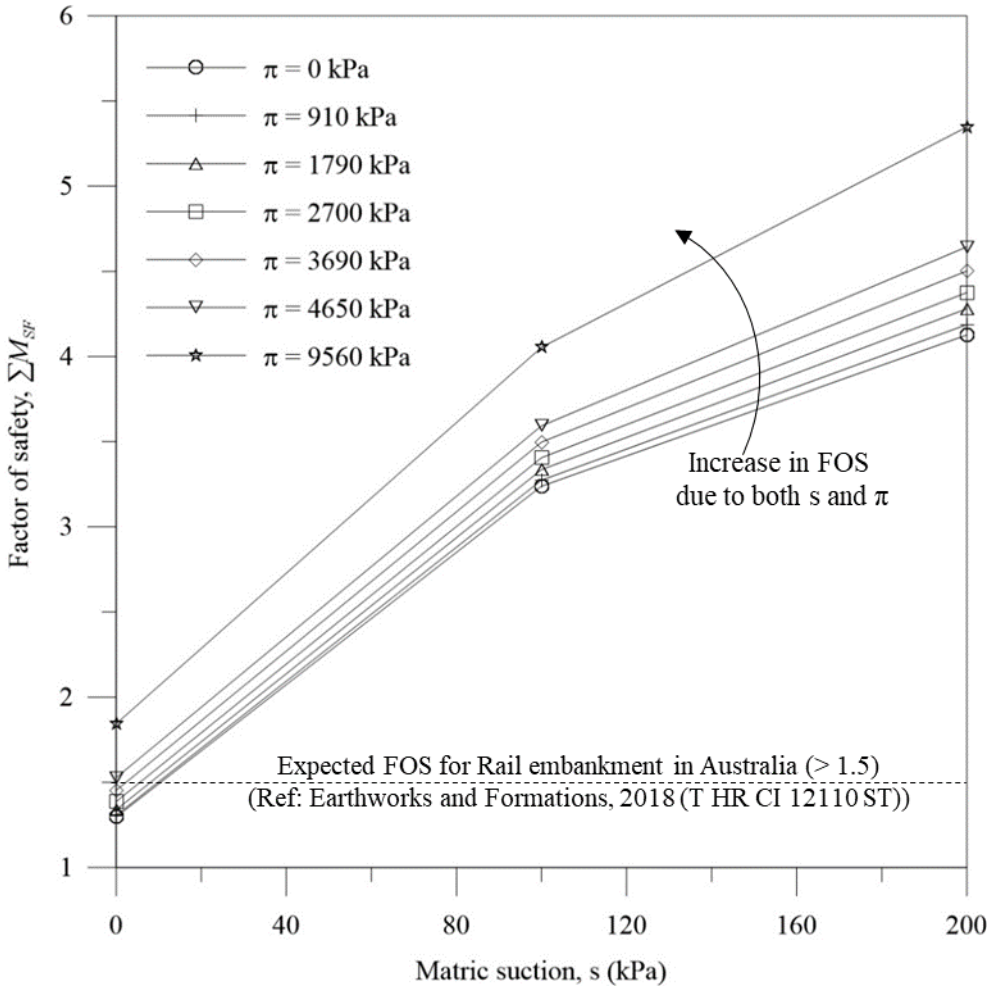

Figure 6.19 Distribution of factor of safety with respect to matric suction for various osmotic suctions (Without roots)

Furthermore, the factor of safety due to osmotic suction increased with the matric suction, but when the soil was fully-saturated and had 200 kPa of matric suction, the highest

increase in the factor of safety was 0.547 and 1.221 respectively. Therefore, the factor of safety increases with increasing osmotic suction for all matric suctions.

The stability of embankments or the bearing capacity of subgrade soil can be increased by the influence of root reinforcement. This change in the factor of safety was analysed and compared numerically with PLAXIS 2D with and without roots.

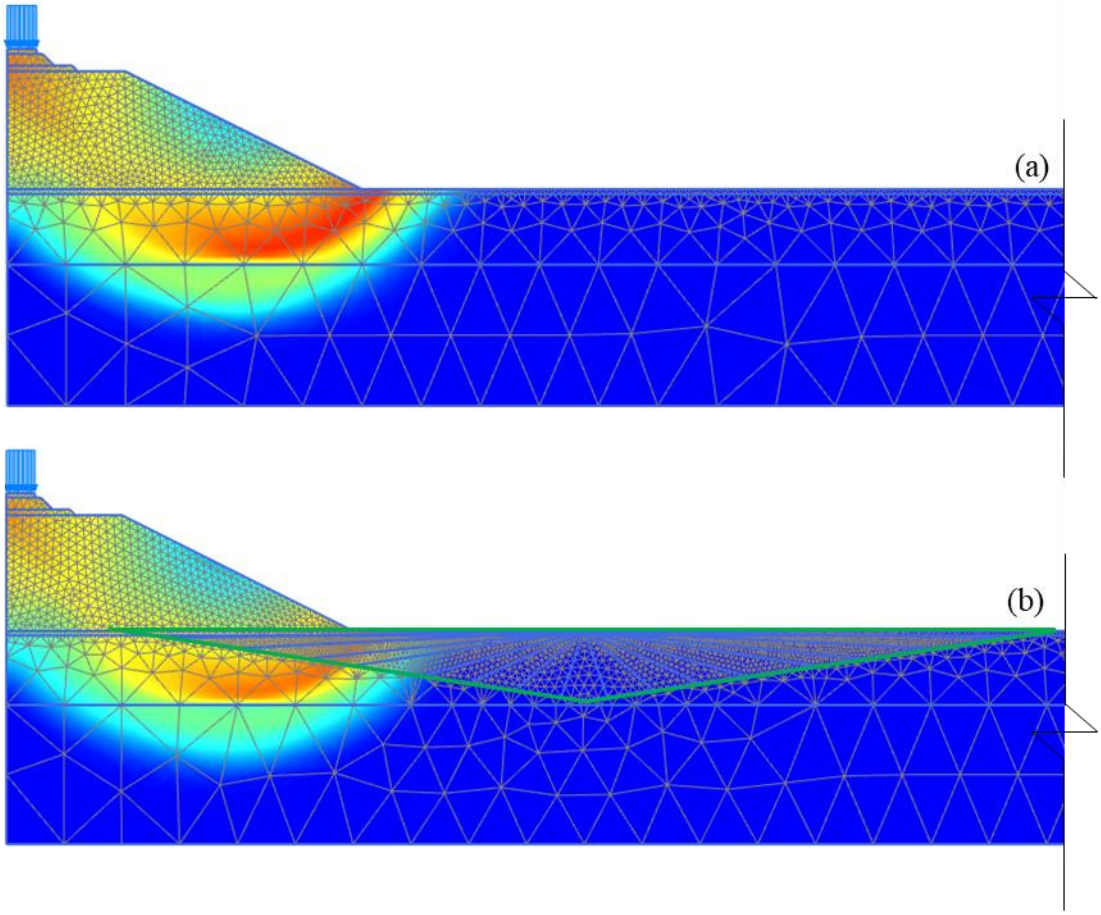

Figure 6.20 Graphical view of the change of $|\Delta u|$ (Fully-saturated),

(a) without roots and (b) with roots

Figure 6.20 shows that the stability of the embankment increased due to the root reinforcement under fully-saturated conditions. This behaviour is similar even with matric suctions (100 kPa and 200 kPa). A graphical view of the change of $|\Delta u|$ for 100 kPa and 200 kPa of matric suctions is shown in Figures 6.21 and 6.22, respectively.

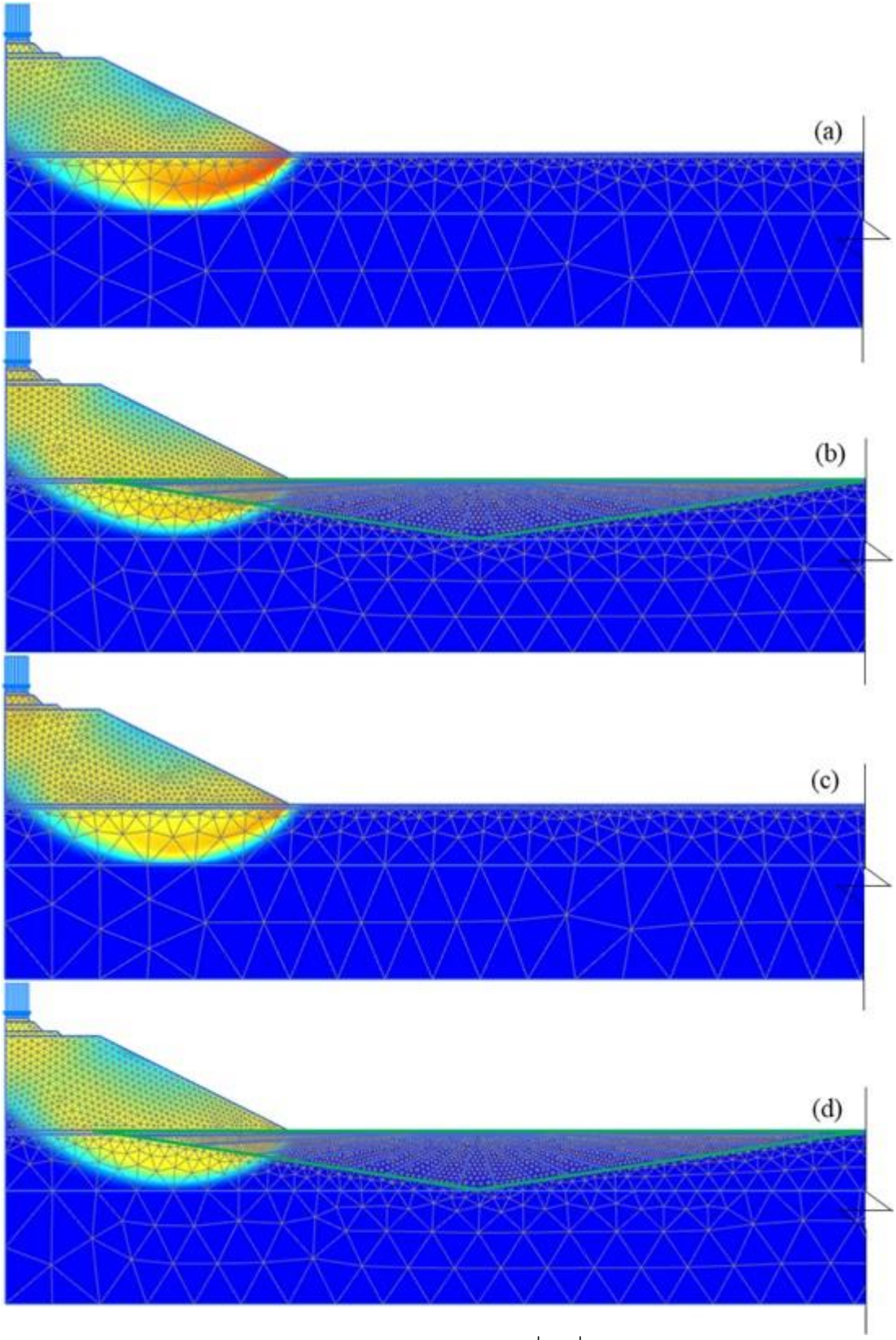

Figure 6.21 Graphical view of the distribution of $|\Delta u|$ (s = 100 kPa), (a) π = 0 kPa (without roots), (b) π = 0 kPa (with roots), (c) π = 9560 kPa (without roots) and (d) π = 9560 kPa (With roots)

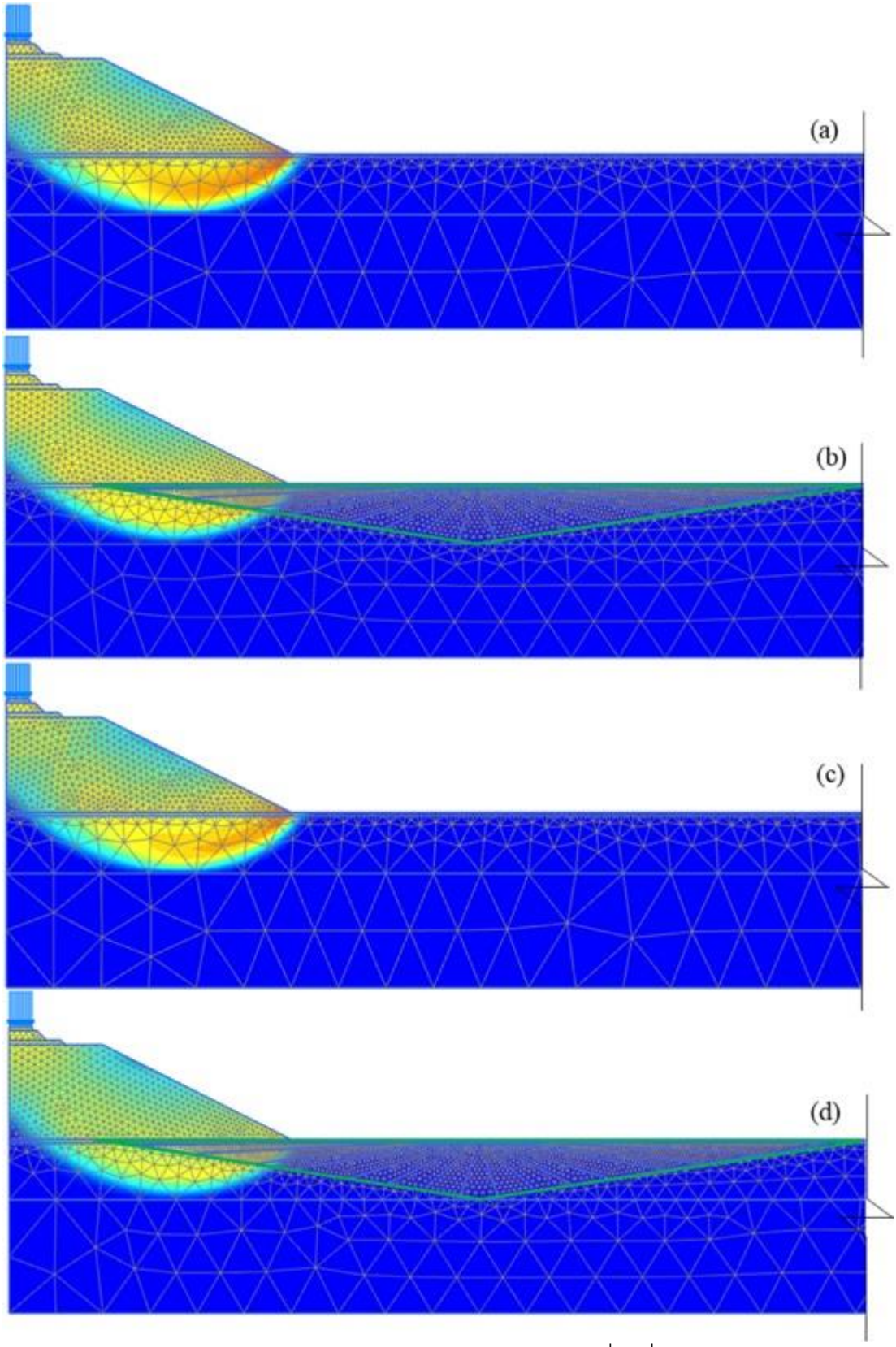

Figure 6.22 Graphical view of the distribution of $|\Delta u|$ (s = 200 kPa),

(a) π = 0 kPa (without roots), (b) π = 0 kPa (with roots),

(c) π = 9560 kPa (without roots) and (d) π = 9560 kPa (With roots)

Figures 6.21 and 6.22 show the incremental deformation changed significantly due to the influence of osmotic suction, matric suction and roots. As anticipated, tree roots increased the factor of safety (Figure 6.23). The factor of safety also increased as the osmotic suction increased with and without roots, a common occurrence for all three matric suctions (Figure 6.23). However, Figure 6.24 shows the osmotic suction had a negative effect on the factor of safety by reducing it due to osmotic stress. The main possible reason for this decrease in the factor of safety would be due to the deterioration of the existing roots or a control of the growth of the plant due to salinity in the pore water; this kind of behaviour was observed experimentally in Chapter 4. The new model has successfully captured this behaviour. Furthermore, the factor of safety seems to reach a minimum value for all matric suctions as the osmotic suction increased further.

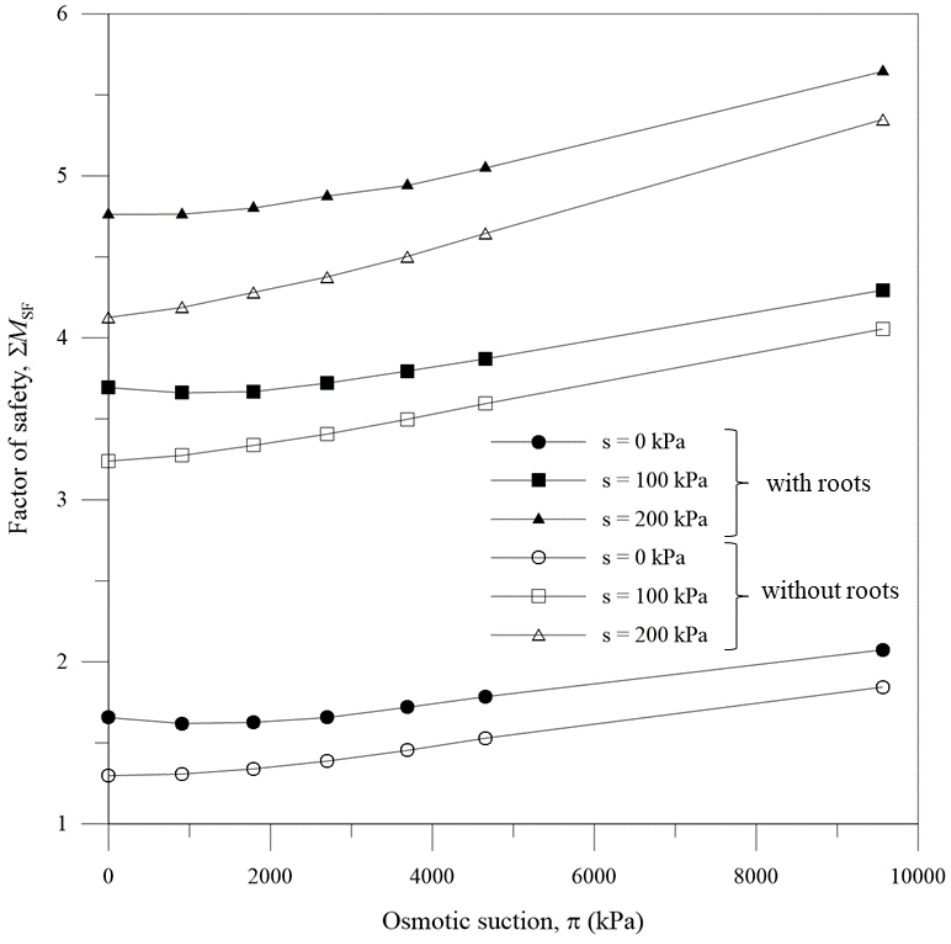

Figure 6.23 Factor of safety with respect to osmotic suction with and without roots

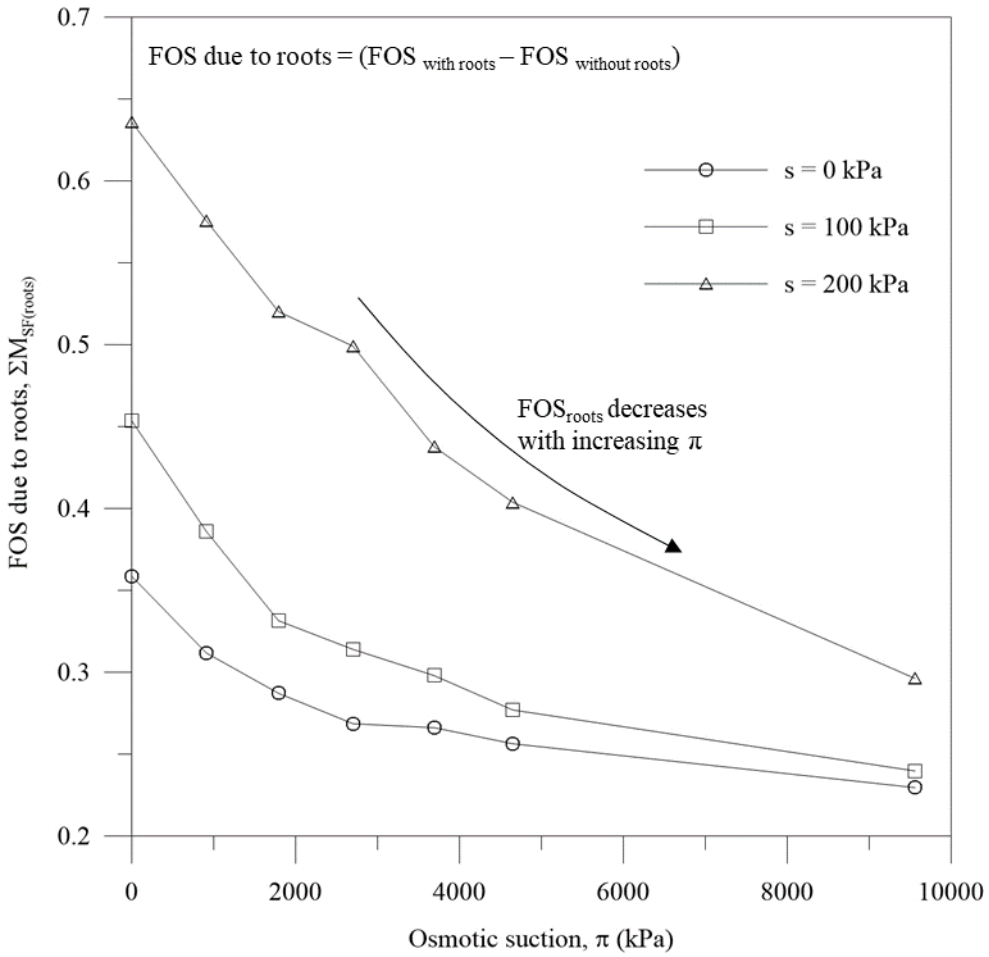

Figure 6.24 Factor of safety due to roots with respect to osmotic suction for various matric suctions

6.5.3 Influence of clearance length to the tree

The investigation of the influence of clearance length (distance between the toe of the embankment fill and the centre of the tree) was challenging and time-consuming. In this investigation, 5 m, 10 m, 15 m and 25 m clearance lengths were selected. A schematic diagram of the field conditions and relevant dimensions is shown in Figure 6.25. The dimensions for the embankment and the superstructure remain unchanged (as shown in Figures 6.7 and 6.8), and under all conditions, the same root-structure was considered. The corresponding mesh for each stage is shown in Figure 6. 26.

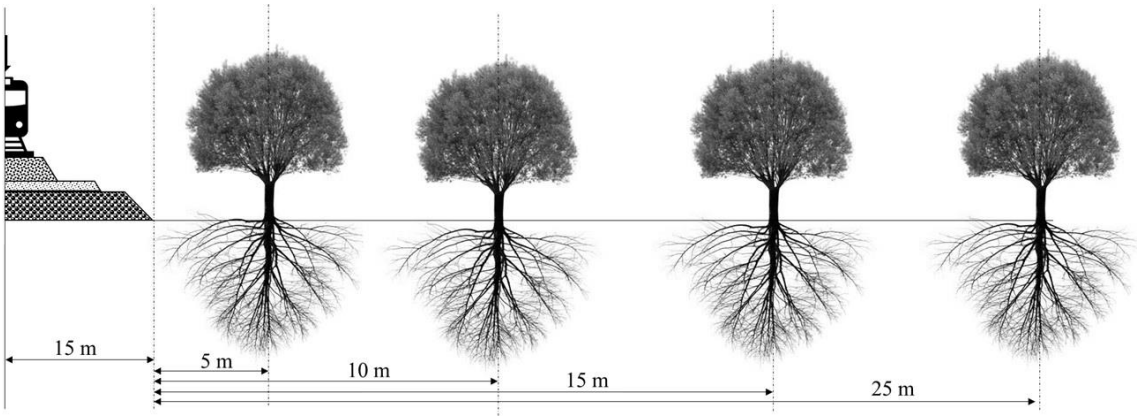

Figure 6.25 Schematic diagram of a rail track with different clearance lengths

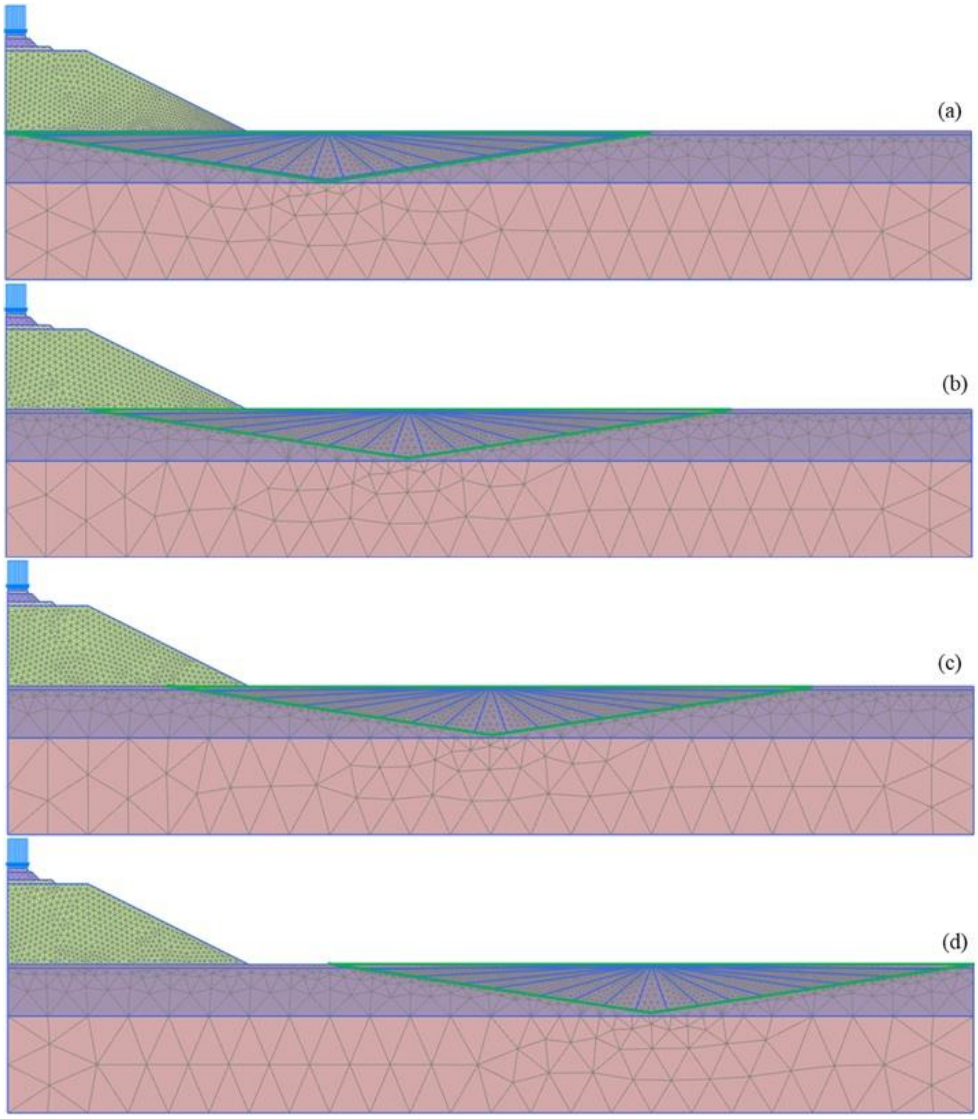

Figure 6.26 Generated mesh diagram for various clearance lengths,

(a) 5 m (b) 10 m (c) 15 m and (d) 25 m

6.5.3.1 Change in vertical deformation due to clearance length

The influence of the clearance length (i.e. 5 m, 10 m, 15 m and 25 m) on vertical deformation was analysed numerically, exactly on top of the top subgrade layer (Layer No: 01) as shown in Figure 6.27.

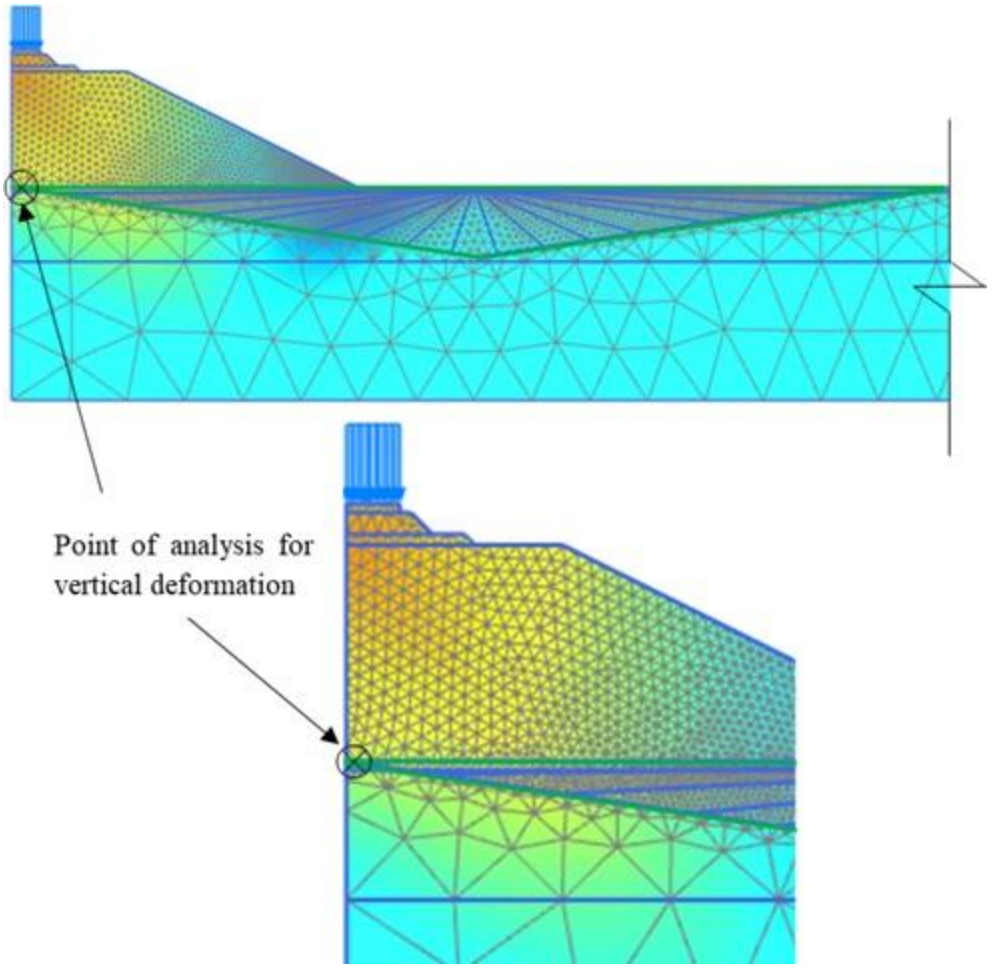

Figure 6.27 The point of analysis for vertical deformation while determining the influence of clearance length

A graphical view of vertical deformation with varying clearance lengths for saturated (s = 0 kPa) and non-saline (π = 0 kPa) soil is shown in Figure 6.28. Also, the 3D distribution of vertical deformation with respect to the clearance length and osmotic suction (based on numerical observations) is shown in Figure 6.29.

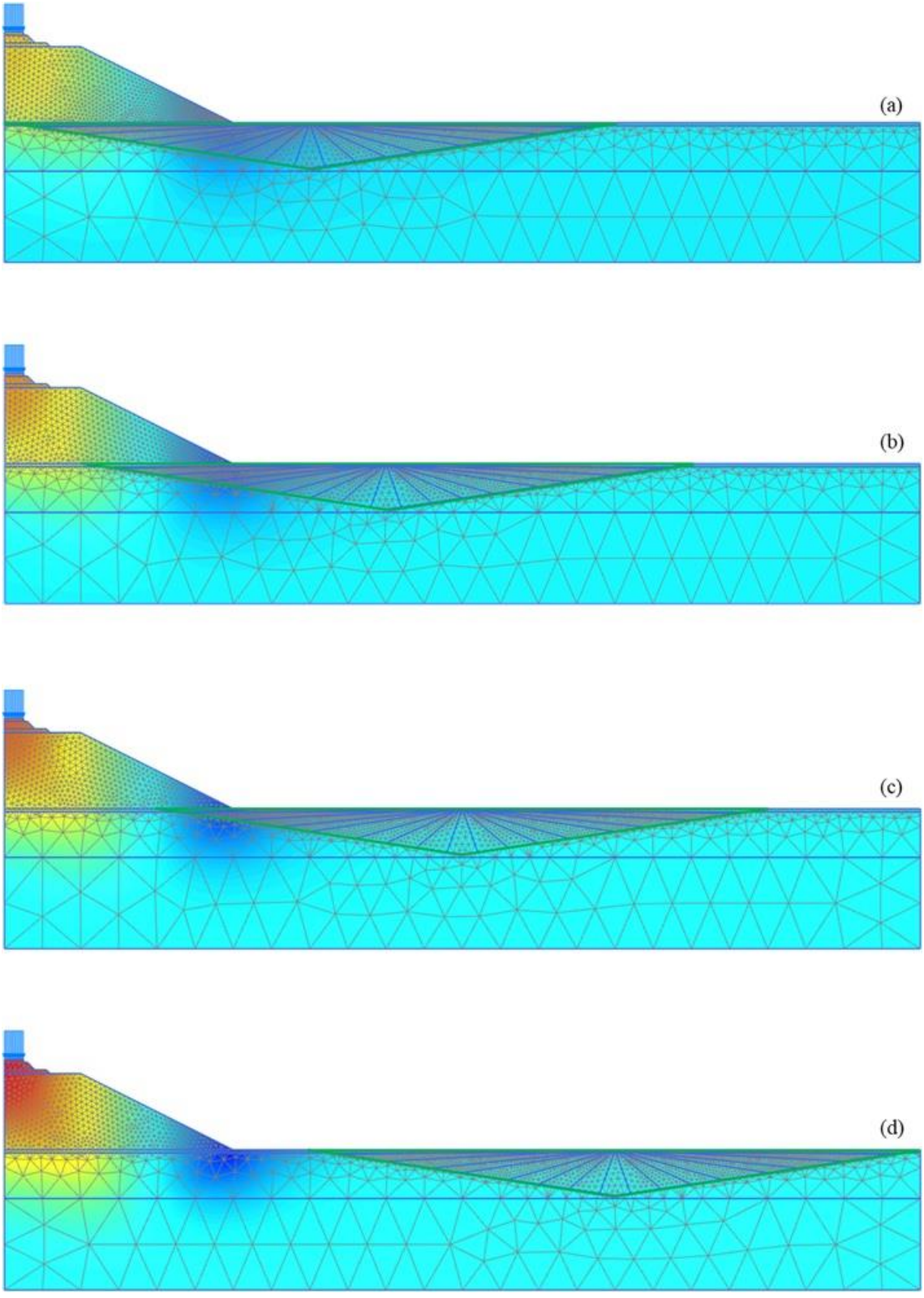

Figure 6.28 Graphical view of the distribution of vertical deformation (when s = 0 kPa and (kPa= 0 kPa) for various clearance lengths, (a) 5 m (b) 10 m (c) 15 m and (d) 25 m

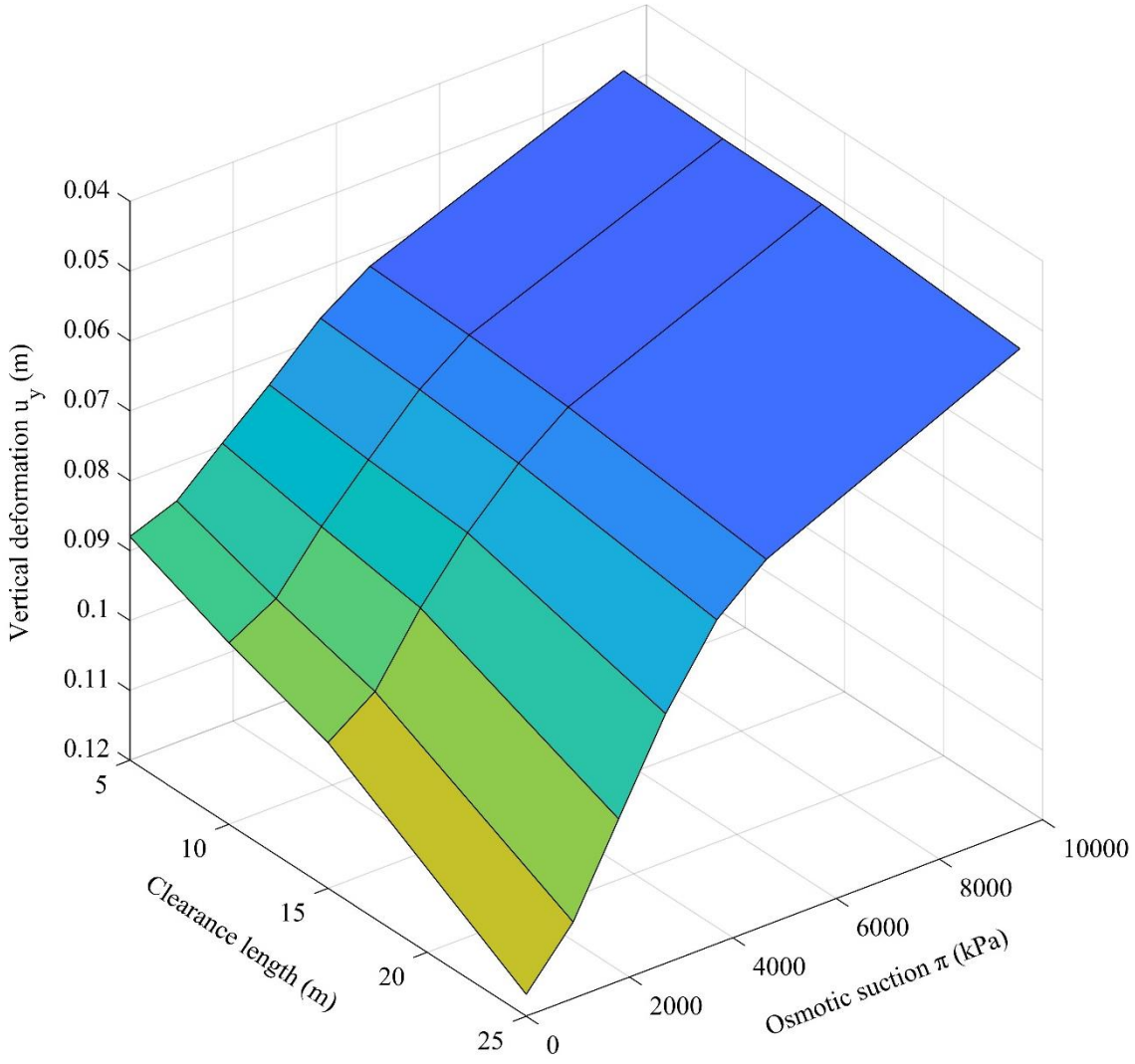

Figure 6.29 3D distribution of vertical deformation with respect to clearance length and osmotic suction (Saturated)

These observations indicate that vertical deformation increased as the clearance length increased, because the root influenced zone moved away from the structure, and hence the bearing capacity provided by the tree roots decreased. This would lead to an increase in vertical deformation, whilst increasing the clearance length from the point of the applied load. However, the influence of the clearance length became negligible as the osmotic suction increased (Figure 6.30), because of the decrease in RAR with increasing osmotic suction; this was discussed in Chapter 4. It is therefore evident that an increase

in the clearance length has a negative influence on the stability of the soil. However, safety analysis of the same conditions was carried out for further clarification.

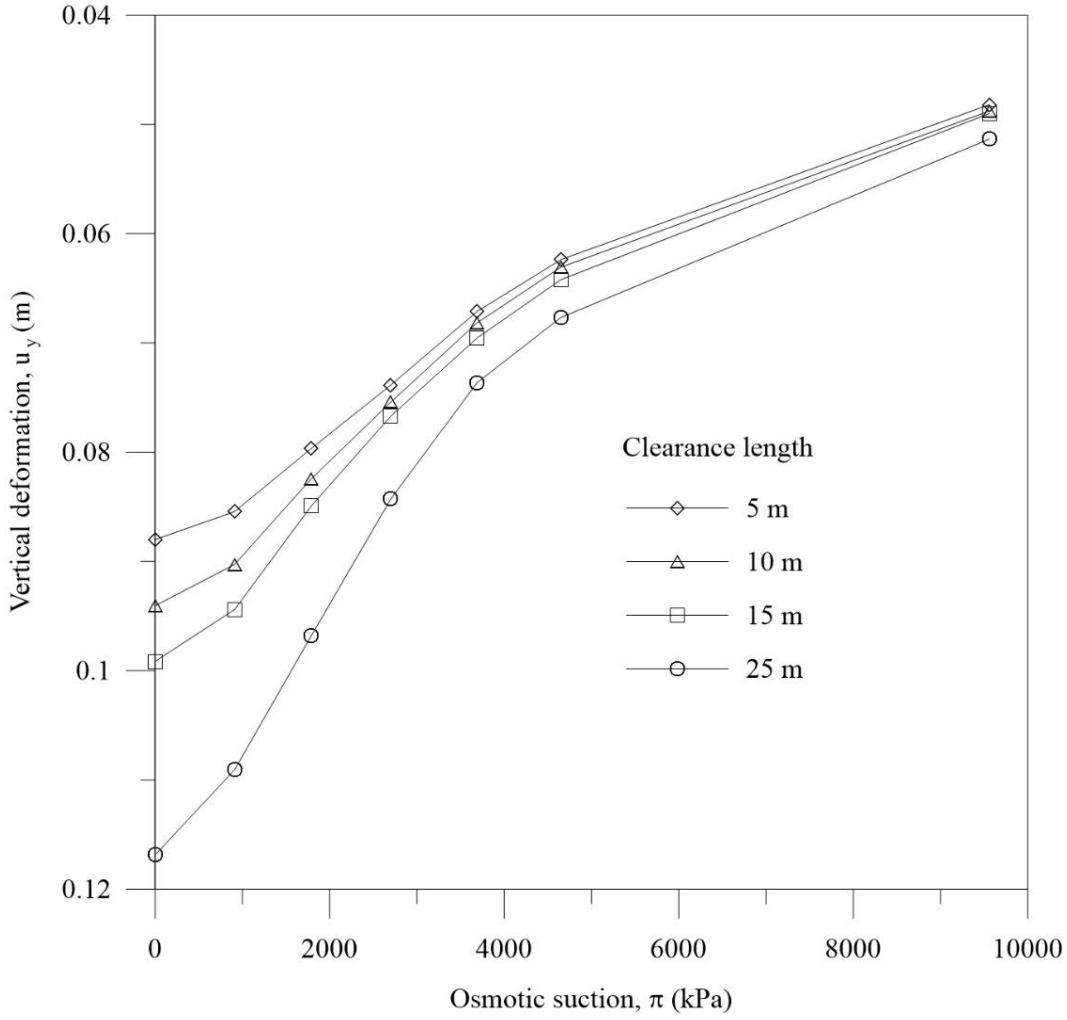

Figure 6.30 Distribution of maximum vertical deformation with respect to osmotic suction for various clearance lengths (Saturated)

6.5.3.2 Change in the factor of safety due to clearance length

A graphical view of the distribution of incremental deformation ($|u|$) with varying clearance length for saturated (s = 0 kPa) and non-saline (π = 0 kPa) is shown in Figure 6.31.

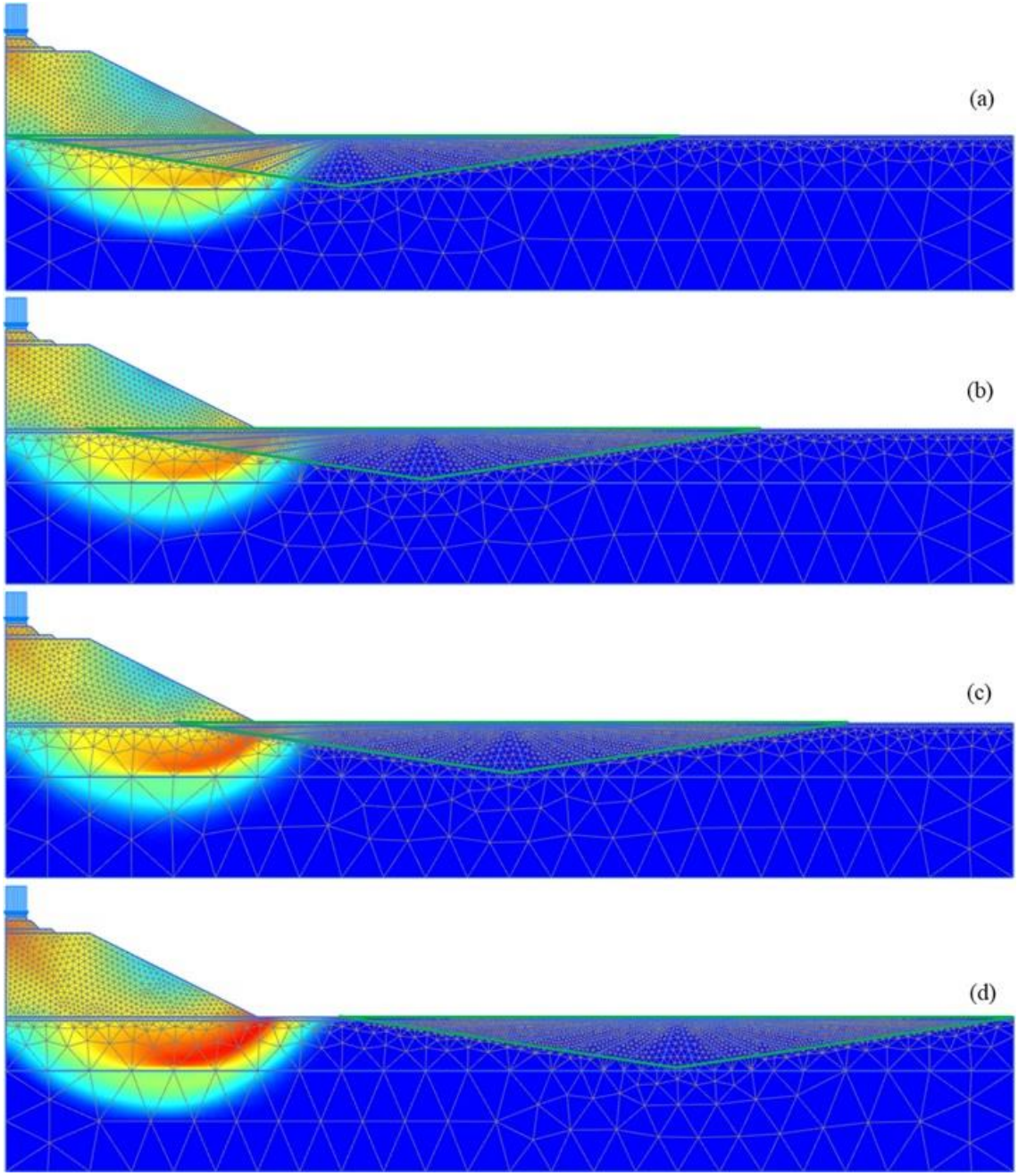

Figure 6.31 Graphical view of the distribution of $|u|$ (when s = 0 kPa and π = 0 kPa) due to changing clearance length, (a) 5 m (b) 10 m (c) 15 m and (d) 25 m

Figure 6.31 shows how tree roots have stabilised the slope of the embankment by providing additional resistance to the slope surface. However, the increase in clearance length significantly reduced the stability of the embankment, and therefore the closer the trees are to the rail track, the higher the stability of the structure. This is clearly shown in

Figure 6.32, which gives the factor safety with respect to the clearance length. Figure 6.32 shows that the factor of safety decreased with the clearance length for both levels of osmotic suction; therefore it is evident that the increase in the clearance length reduced the stability of the embankment.

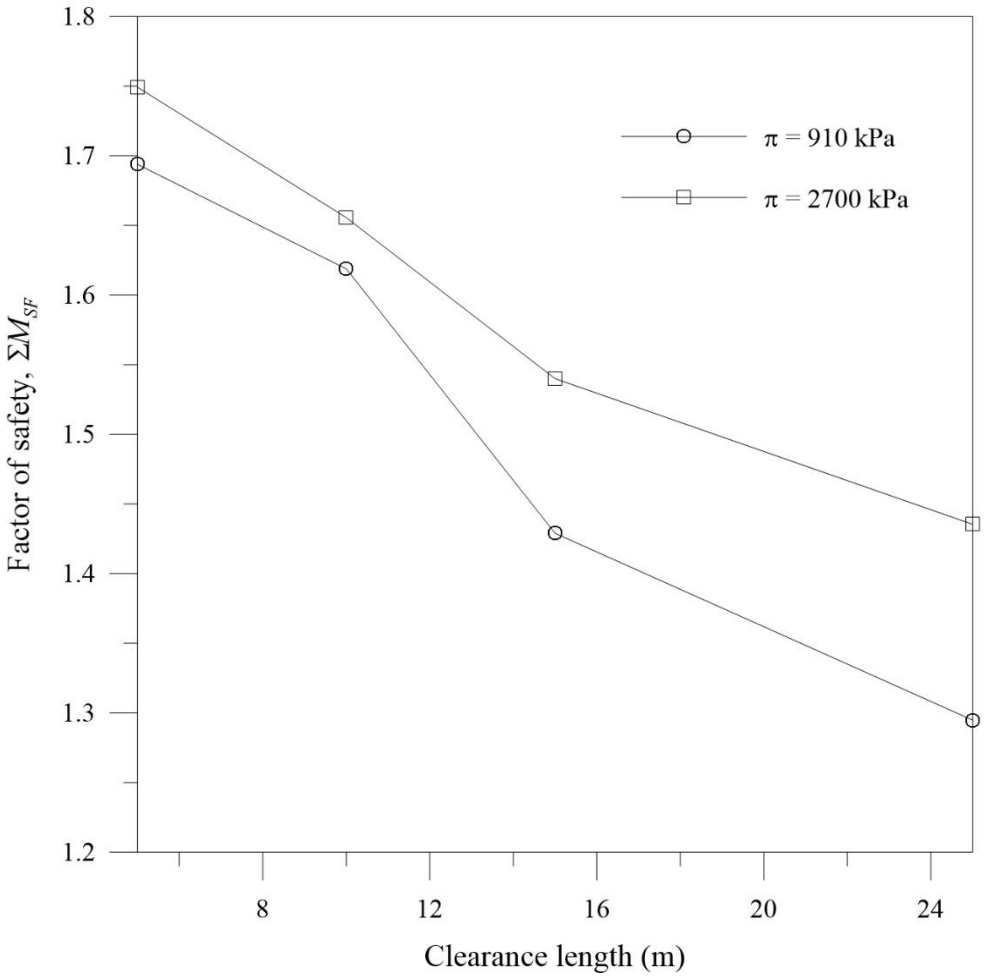

Figure 6.32 Distribution of factor of safety with respect to the clearance length (Fully-saturated)

Furthermore, at higher clearance lengths, the factor of safety of vegetated soil is almost equal to the factor of safety of bare soil (without roots) (Figure 6.33). This is because, at higher clearance lengths, the influence of roots when calculating the stability of a rail track is negligible.

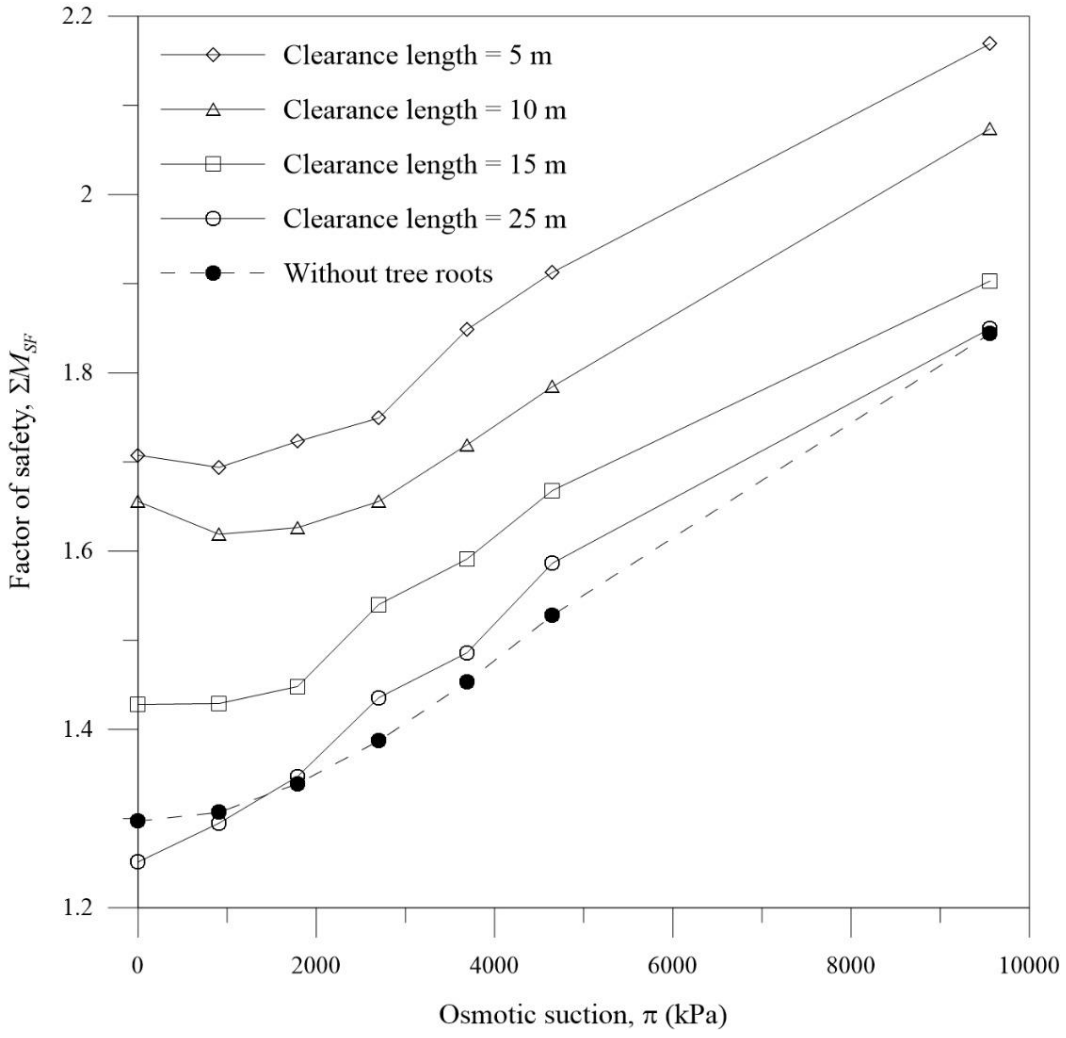

Figure 6.33 Distribution of factor of safety with respect to osmotic suction (Fully-saturated)

6.6 Summary

The performance of an embankment was monitored against the influence of osmotic suction and tree roots using the PLAXIS 2D (2018) finite element package. The equivalent parameters due to the increase in peak shear stress due to matric suction, osmotic suction and roots were estimated based on the proposed new models. The rail track and the subgrade were modelled based on previous research carried out by Potter (2006) and Fatahi et al. (2010). The tree roots were modelled using the geogrid function in PLAXIS. For this analysis, a typical modern freight car that can generate an axle load

of 25 tonnes was considered. All these analyses were carried out on a plain strain model under static loading conditions, so the cyclic loading parameters were converted to static loading conditions as necessary. The vertical deformation and the factor of safety of the embankment were analysed with variable osmotic suctions with and without the influence of roots. It was found that due to the influence of osmotic suction and roots, the vertical deformation decreased and the factor of safety increased, and the clearance length had a marked effect on vertical deformation and the factor of safety. With higher clearance lengths, the influence of roots on the stability of soil under the rail track was less, and therefore the optimum clearance length would be up to about 5 m. The influence of root water uptake was not considered during this study, because this mechanism could intensify the observed results and result in more stable soil under the same conditions due to the induced suction.

CHAPTER 7: Conclusions and recommendations

7.1 Background

As most types of infrastructure are built and remain above the groundwater table for most of their service life, the soil remains in an unsaturated condition where the capillary stresses or suction play an important role. In addition to the conventional suction components (i.e. matric and osmotic suction), the influence that native vegetation has on the shear strength of soil has now been identified as a potential soil stabilisation technique. While the effect of matric suction on the shear strength is relatively well established, only a limited number of studies have focussed on the influence of osmotic suction combined with tree roots.

A novel osmotic stress parameter (χ_2) and an osmotically induced root area ratio (RAR_π) were introduced in this study to capture the stress-strain behaviour of a vegetated soil realistically. Both parameters were defined based on the electrical conductivity which depends on the level of salinity or osmotic suction of the pore water. These two parameters were used to develop new models that can successfully predict the shear strength of unsaturated-saline-rooted soil accurately. These models were calibrated and validated for independent loading conditions using two different series of direct shear tests (i.e. small scale (60 x 60 x 40 mm) and large scale (300 x 300 x 200 mm)). The direct shear tests were carried out to investigate how the mechanical reinforcement of tree roots influences the shear strength of the soil and the change in shear strength due to the influence of osmotic suction. The direct shear tests showed that the peak shear stress increases as the osmotic suction increases and due to the mechanical strengthening induced by the tree roots. The results also showed that the contribution to the soil shear

strength provided by root reinforcement decreases as osmotic suction increases. Numerical modelling using the finite element tool (PLAXIS 2D) was also carried out to compare the variation in the factor of safety and deformation of a rail embankment based on proposed new models. The numerical model was further extended to observe the optimum clearance length between a rail embankment and the tree line adjoining the rail track.

7.2 Specific observations

7.2.1 Development of a new model (χ_2) on saline shear strength

The conventional Mohr-Coulomb criterion was extended and incorporated in a new model to capture the shear strength behaviour of unsaturated soil considering the influence of osmotic suction by introducing a new osmotic stress parameter (χ_2). This proposed model was calibrated and validated for independent loading conditions through a series of small scale direct shear box tests, which were conducted at constant water content conditions with varying values of osmotic suction (0, 910, 1790, 2700, 3690, 4650, and 9560 kPa) and matric suction (0, 25, 100, 200, 500, 1000, and 1500 kPa). The direct shear tests were carried out at three different levels of normal stress (10, 20, and 40 kPa) and at a very low strain of about 0.006 mm/min to accommodate any redistribution of suction induced by shearing. The salient findings of this proposed model and tests are summarised below:

1. The existing methods to determine osmotic suction are often challenging. However, the proposed new technique (i.e. electrical conductivity) was successfully used for disturbed soil specimens.

2. Osmotic suction is present in both saturated and unsaturated conditions, therefore incorporating the degree of saturation into the model enabled the variations in osmotic suction as they pertain to changes in moisture to be captured.
3. In this study, the proposed model was formulated using the new osmotic stress parameter (χ_2) to capture the increase of peak shear stress due to an increase in osmotic suction (e.g. caused by NaCl). The combination of Equations 5.4, 5.5, and 5.6 represents the proposed shear strength model incorporating the influence of osmotic suction within the framework of the Mohr-Coulomb criterion.
4. Depending on pore water NaCl concentration (pore water chemistry) the critical electrical conductivity ratio (ECR_c) and maximum χ_2 ($\chi_{2_{max}}$) may reach different values. For instance, when the soil is fully saturated, ECR_c and $\chi_{2_{max}}$ are 900 and 0.003 respectively, but when the matric suction is 1500 kPa these values change to 225 and 0.023, respectively.
5. Except for slight deviations at high osmotic suctions (i.e. $\pi > 4650$ kPa) and high matric suctions (i.e. $s_i > 500$ kPa), the proposed χ_2 model can satisfactorily predict the experimental results (i.e. for $a = 0.003$, $b = 0.0375$ and $c = 2$).
6. The results presented herein show that osmotic suction can influence the stress-strain behaviour of soil and this influence is more significant at higher levels of matric suction than under saturated or relatively low matric suction values.
7. This study also showed that the peak shear stress increases with the level of osmotic suction and further increases are observed for larger matric suction levels. For instance, the peak shear stress increased by 121.64 kPa when the osmotic suction increased from 0 kPa to 9560 kPa under fully saturated conditions. However, when the matric suction was 1500 kPa, the peak shear stress increased by 207.12 kPa for the same increase in osmotic suction.

8. The proposed model retains the fundamental Mohr-Coulomb framework whereby an equivalent friction angle (ϕ) was considered. While it matched the experimental results well at lower levels of osmotic suction (< 4650 kPa), a significant discrepancy was shown at higher osmotic suctions. For this reason, the writer recommends cautious optimism when using the combined (χ_1 and χ_2) shear strength equation for saline soils at osmotic levels exceeding 4650 kPa.
9. The results indicate that under all matric suction conditions, the maximum vertical deformation decreased with respect to osmotic suction. Furthermore, the increase in osmotic suction resulted in a lower contraction of the specimen under both saturated and unsaturated conditions, and as expected, at higher matric suctions the specimens exhibited lower contraction than in saturated conditions.

7.2.2 Development of a new model (RAR_π) to characterise the influence of osmotic stress on root growth

Most previous studies used the root area ratio (RAR) to indicate the distribution of roots, so a new osmotically influenced root area ratio (RAR_π) was introduced in this study to determine the influence of osmotic suction on the geometric shape of a root system. For plant related applications, the term osmotic stress was used instead of osmotic suction. This enabled the change in the shear strength of vegetated soil with respect to osmotic stress to be determined. The proposed new model was calibrated and validated for independent loading conditions through a series of large scale direct shear box tests using an *Acacia Stenophylla* (River Cooba) species in each box. These tests were carried out at constant water content with varying values of osmotic stress (0, 910, 1790, 2700, 3690, 4650 and 9560 kPa) and different levels of matric suction (0, 100 and 200 kPa) at three predetermined normal stresses (10, 20 and 40 kPa). The findings of the proposed model in relation to large scale direct shear box tests are as follows:

1. The influence of osmotic stress on the growth of the root system means the root area ratio was characterised by combining the electrical conductivity ratio (ECR) and the initial root area ratio (RAR^0) with two other experimental coefficients.
2. The initial root area ratio (RAR^0) was determined when the osmotic stress was zero, hence when the osmotic stress is negligible (i.e. π = 0 kPa), $RAR_\pi = RAR^0$, according to Equation 5.18.
3. This study showed that the root area ratio decreased as the osmotic stress increased, and the distribution of root area ratio with respect to osmotic stress could be described using a power decay model (i.e. for l_1=1.497 and l_2=-0.4531).
4. The contribution to the shear strength of soil made by the tree roots decreased due to osmotic stress, irrespective of the soil matric suction. The proposed model could satisfactorily capture the shear strength of unsaturated soil where the influence of osmotic stress and root effect was considered.
5. The post-peak behaviour was significantly increased by the tensile strength of tree roots, compared to the soil specimens without tree roots.
6. There is no doubt that the presence of tree roots assists in the reduction of settlement. While the influence of osmotic suction can adversely affect the growth of tree roots, the experimental results show that settlement due to tree roots still decreases with osmotic suction. This is because although osmotic stress can hinder the growth of roots, they still act as physical reinforcement.
7. It is anticipated that the root tensile strength decreases with increasing root diameter, but based on observed results, the root tensile strength was not influenced by osmotic suction. Therefore, for a given root diameter the root tensile strength can be independent of osmotic suction.

8. The growth of the root system was influenced by the levels of osmotic suction. Due to salinity in the pore water generated within the root system, the osmotic stress-controlled the growth of roots, and therefore, the root diameter also decreases as the osmotic suction decreases. Therefore, according to the experimental study, the maximum root diameter of the root system decreases with increasing salinity based osmotic suction.
9. The proposed model can satisfactorily predict the experimental results of specimens having roots, but it deviates at very high osmotic suctions. It is anticipated that at very high levels of salinity the growth of roots can be impacted, and the corresponding contribution from root-influenced shear strength decreases. This root decaying process at larger salinity levels was not within the scope of this study.

7.2.3 Suction variation in a saline-vegetated environment

Trees roots can generate additional matric and osmotic suction by inducing a variation of moisture content driven by the mechanisms of root water uptake followed by transpiration. However, the presence of salt in pore water can influence the amount of water extracted by the tree roots and hence the variation of matric and osmotic suction. Similar size *Acacia Stenophylla* (River Cooba) species were planted in seven different soil boxes (300x300x400 mm) having seven different soil pore water salinities. An MPS2 matric suction sensor and EC5 moisture sensor were used to determine the change of matric suction and moisture due to transpiration. The plants were allowed to grow for twelve months in a temperature and humidity-controlled (20±2^{o}C, 30% RH) room, during which time, the variations of soil matric suction and the moisture content were monitored. The findings of this experimental study are as follows:

1. Soil retains a significantly higher soil matric suction in the vegetated ground due to the amount of water extracted by root water uptake and transpiration. Results also show that a larger air entry value (AEV) is observed for soil having roots. For instance, the AEV of root permeated soil was about 70 kPa whereas for soil with no roots was about 50 kPa. This is due to the presence of roots in soil pores, i.e. the effective void ratio decreases.
2. The slope of the SWCC within the transition zone or the rate of desorption remained unchanged. This is because the root water uptake and transpiration had not influenced the rate of desorption.
3. The SWCC of root permeated soil shifted down along the moisture content axis due to osmotic stress that affects the growth of the tree roots.

7.2.4 Numerical modelling with a FEM software PLAXIS 2D

A section of a rail embankment was numerically simulated using PLAXIS 2D (2018). The equivalent parameters in relation to the increase in peak shear stress caused by matric suction, osmotic stress, and root reinforcement were calculated based on the proposed models described in Chapter 5, and incorporated in the finite element analysis. The stability of the embankment was studied with emphasis on the change in deformation and the factor of safety of the embankment subjected to an applied vertical load. The analysis was then extended to observe the influence of clearance length between the embankment and tree line. The following conclusions can be made:

1. The maximum vertical deformation (without considering roots) decreased significantly as the osmotic stress increased under saturated conditions and decreased even more as the matric suction continued to increase. In contrast, the reinforcement from tree roots further reduced the maximum vertical deformation for all levels of matric and osmotic suction. When the osmotic stress was high the

contribution made by tree roots on the maximum vertical deformation was negligible for a given matric suction, and with the increase of matric suction, this was observed at lower levels of osmotic stress. For instance, this minimum osmotic stress decreased from 4650 to 3800 kPa, when the soil matric suction increased from 0 to 200 kPa.

2. The factor of safety increased as the osmotic stress and matric suction increased with and without tree roots. For instance, under fully saturated conditions, the factor of safety increased from 1.3 to 1.8 as the osmotic stress increased from 0 to 9560 kPa. Moreover, the contribution made by tree roots on the factor of safety decreased as the osmotic stress increased; this change in the factor of safety due to roots alone under saturated conditions was less than at increased levels of matric suction when the soil was unsaturated.
3. The clearance length significantly influenced the deformation and the factor of safety of the rail embankment. The maximum vertical deformation increased as the clearance length increased for a given osmotic stress. For instance, when the clearance length increased from 5 to 25 m, the maximum vertical deformation increased by 0.033 m while the osmotic stress was 0 kPa and soil was fully saturated.
4. The increase in osmotic stress retarded the growth of the roots (Chapter 4) and hence reduced the contribution that the tree roots have on vertical deformation for a given clearance length and matric suction. As an example, when the osmotic stress increased from 0 to 9560 kPa, the maximum vertical deformation decreased by 0.047 m while the clearance length was 5 m and the soil was fully saturated.

5. The increase in clearance length reduced the factor of safety for given osmotic stress and matric suction. For instance, when the clearance length was 25 m the factor of safety for both with and without root conditions was almost equal.
6. The highest factor of safety and the least deformation was observed when the roots were exactly underneath the rail embankment, i.e. clearance length = 5 m.

7.3 Limitations of the study

1. Due to the technical difficulties in obtaining identical undisturbed soil samples in terms of soil microstructure and salt concentration, disturbed soil samples were used for this study.
2. The model proposed in this study is based on electrical conductivity and NaCl was the only influencing parameter of salinity. However, the model can deviate further from the experimental results when the soil solution contains other electrically charged ions such as Fe^{3+} or Fe^{2+}. Furthermore, at very high matric suctions where the degree of saturation is almost zero, the influence that salt crystallisation has on the shear strength of soil could not be predicted accurately by this model.
3. The selected box size for the direct shear test with plants can limit the roots spread, and hence may not represent the real field conditions. However, this is the largest direct shear test facility in the geotechnical laboratory in University of Wollongong.
4. The numerical study was conducted for a 2D plain stain model. However, the real root system contributes in a 3D environment.

7.4 Recommendations for future work

The following items are recommended for future extensions in this of this research work:

1. Most of the trees beside a rail track are fully grown and established. However, the tree root system studied was not grown enough for a comprehensive study. It is recommended that the role of plant growth to be considered to simulate more realistic field conditions.
2. It is suggested that electrical resistivity analysis in the field to be conducted in future studies to map the water retention behaviour of soil throughout the year and at different tree maturation stages. In addition, the 3D profiles of electrical resistivity in the field and along the rail track can be used to capture any uncertainties such as unexpected settlement or undrained soil failure under heavy haul traffic.
3. Only a single tree species (i.e. *Acacia Stenophylla*, River Cooba) was selected for calibration of the proposed new model RAR_{π}; it is therefore recommended that this model be validated for other species under similar conditions.
4. The mechanism of evapotranspiration was not fully modelled in this finite element analysis. Therefore, an extended numerical model with a more complete root uptake and transpiration model is recommended as a future extension.
5. The finite element analysis presented focussed on quasi-static loading conditions, whereas the loading mechanism from a moving train is dynamic. It is therefore recommended that the numerical model be extended for considering the effect of 3D moving wheel dynamics.
6. Root water uptake that takes place can be understood from a micromechanical standpoint. Therefore, a coupled DEM-CFD approach for a more insightful in-depth study is recommended.

REFERENCES

Abu-Hassanein, ZS, Benson, CH & Blotz, LR 1996, 'Electrical resistivity of compacted clays', Journal of Geotechnical Engineering, vol. 122, no. 5, pp. 397-406.

Agus, SS & Schanz, T 2005, 'Comparison of four methods for measuring total suction', Vadose Zone Journal, vol. 4, no. 4, pp. 1087-95.

Aitchison, GD 1964, 'Engineering concepts of moisture equilibria and moisture changes in soils', In Moisture Equilibria and Moisture Changes in Soil Beneath Covered Areas, pp. 7-21.

Arulanandan, K & Muraleetharan, KK 1988, 'Level ground soil-liquefaction analysis using in situ properties: I', Journal of Geotechnical Engineering, vol. 114, no. 7, pp. 753-70.

AS1289.3.1.1 2009, 'Determination of the liquid limit of a soil - Four-point Casagrande method', Standards Australia.

AS1289.3.5.2 2009, 'Determination of the soil particle density of combined soil fractions – Vacuum pycnometer method', Standards Australia.

AS1289.3.6.1 2009, 'Determination of the particle size distribution of a soil - standard method of analysis by sieving', Standards Australia.

AS1289.5.1.1 2009, 'Determination of the dry density/moisture content relation of a soil using standard compaction effort', Standards Australia.

AS1289.6.2.2 2009, 'Determination of the shear strength of a soil-Direct shear test using a shear box', Standards Australia.

ASTM_D5298 2003, ‘Standard Test Method for Measurement of Soil Potential (Suction) Using Filter Paper’, Annual Book of ASTM Standards, Soil and Rock.

ASTM_D2487 2010, ‘Standard practice for classification of soils for engineering purposes (Unified Soil Classification System)’, Annual Book of ASTM Standards. ASTM, International West Conshohocken, PA.

Australian Railway Association 2014. Available in: https://icn.org.au/sites/default/files/1%20Australasian%20Railway%20Association%20Perth%20Industry%20Briefing%20Presentation.pdf, Accessed on: 10.05.2020

Ayenu-Prah, AY 2004, ‘Effect of the chemical composition of compaction water on the performance of soil subgrades and embankments’, Doctoral dissertation, Texas Tech University.

Babu, GS, Gartung, E, Peter, J & Mukesh, M 2005, ‘Significance of soil suction and soil water characteristic curve parameters’. Geotechnical Testing Journal, 28(1), pp.102-107.

Bai, F & Liu, S 2012, ‘Measurement of the shear strength of an expansive soil by combining a filter paper method and direct shear tests’. Geotechnical Testing Journal, 35(3), pp.451-459.

Baker, R & Frydman, S 2009, ‘Unsaturated soil mechanics: Critical review of physical foundations’, Engineering Geology, vol. 106, no. 1, pp. 26-39.

Barber, D & Martin, J 1976, ‘The release of organic substances by cereal roots into soil’, New Phytologist, vol. 76, no. 1, pp. 69-80.

Bernstone, C, Dahlin, T, Ohlsson, T & Hogland, H 2000, 'DC-resistivity mapping of internal landfill structures: two pre-excavation surveys', Environmental geology, vol. 39, no. 3-4, pp. 360-71.

Bishop, AW 1959, The principles of effective stress, Teknisk ukeblad, 39, pp.859-863.

Boldrin, D, Leung, A & Bengough, A 2017, 'Root biomechanical properties during establishment of woody perennials', Ecological Engineering, vol. 109, pp. 196-206.

Boxshall, D & Jenkyn, T 2001, 'Eumong - River Cooba, Acacia stenophylla. Farm Forestry Species Profile for North Central Victoria', Department of Primary Industries, Victoria.

Bulut, R & Leong, EC 2008, 'Indirect measurement of suction', Geotechnical and Geological Engineering, vol. 26, no. 6, pp. 633-44.

Busscher, W & Fritton, D 1978, 'Simulated flow through the root xylem', Soil Science, vol. 125, no. 1, pp. 1-6.

Butterfield, R & Johnston, I 1980, 'The influence of electro-osmosis on metallic piles in clay', Géotechnique, vol. 30, no. 1, pp. 17-38.

Chattopadhyay, PK 1972, 'Residual shear strength of some pure clay minerals', PhD Thesis thesis, University of Alberta, Edmonton.

Colmer, T, Munns, R & Flowers, T 2006, 'Improving salt tolerance of wheat and barley: future prospects', Australian Journal of Experimental Agriculture, vol. 45, no. 11, pp. 1425-43.

Czyż, EA & Dexter, AR 2013, 'Plant wilting can be caused either by the plant or by the soil', Soil Research, vol. 50, no. 8, pp. 708-13.

Di Maio, C, Santoli, L & Schiavone, P 2004, 'Volume change behaviour of clays: the influence of mineral composition, pore fluid composition and stress state', Mechanics of materials, vol. 36, no. 5, pp. 435-51.

Di Maio, C & Scaringi, G 2016, 'Shear displacements induced by decrease in pore solution concentration on a pre-existing slip surface', Engineering Geology, vol. 200, pp. 1-9.

Docker, B & Hubble, T 2001, 'Strength and distribution of casuarinas glauca roots in relation to slope stability', Geotechnical Engineering (HO KKS and LI KS (eds)). Swets & Zeitlinger, Lisse, pp. 745-9.

Docker, B & Hubble, T 2008, 'Quantifying root-reinforcement of river bank soils by four Australian tree species', Geomorphology, vol. 100, no. 3-4, pp. 401-18.

El-Aal, AKA 2017, 'Effect of salinity of groundwater on the geotechnical properties of some Egyptian clay', Egyptian journal of petroleum, vol. 26, no. 3, pp. 643-8.

Esmaeili, M, Nik, MG & Khayyer, F 2013, 'Experimental and numerical study of micropiles to reinforce high railway embankments', International Journal of Geomechanics, vol. 13, no. 6, pp. 729-44.

Fan, CC & Chen, YW 2010, 'The effect of root architecture on the shearing resistance of root-permeated soils', Ecological Engineering, vol. 36, no. 6, pp. 813-26.

Fan, CC & Su, CF 2008, 'Role of roots in the shear strength of root-reinforced soils with high moisture content', Ecological Engineering, vol. 33, no. 2, pp. 157-66.

Fatahi, B, Khabbaz, H & Indraratna, B 2010, 'Bioengineering ground improvement considering root water uptake model', Ecological Engineering, vol. 36, no. 2, pp. 222-9.

Fatahi, B, Khabbaz, H & Indraratna, B 2014, 'Modelling of unsaturated ground behaviour influenced by vegetation transpiration', Geomechanics and Geoengineering, vol. 9, no. 3, pp. 187-207.

Fatahi, B, Pathirage, U, Indraratna, B, Pallewattha, M & Khabbaz, MH 2015, 'The role of native vegetation in stabilizing formation soil for transport corridors: an Australian experience'. In Ground Improvement Case Histories (pp. 591-628). Butterworth-Heinemann.

Feddes, RA, Kowalik, P, Kolinska-Malinka, K & Zaradny, H 1976, 'Simulation of field water uptake by plants using a soil water dependent root extraction function', Journal of Hydrology, vol. 31, no. 1-2, pp. 13-26.

Feddes, RA, Kowalik, PJ & Zaradny, H 1978, 'Simulation of field water use and crop yield', Centre for Agricultural Publishing and Documentation. Simulation monographs. Pudoc, Wageningen, pp.9-30.

Fiscus, EL 1975, 'The interaction between osmotic-and pressure-induced water flow in plant roots', Plant physiology, vol. 55, no. 5, pp. 917-22.

Fiscus, EL & Kramer, PJ 1975, 'General model for osmotic and pressure-induced flow in plant roots', Proceedings of the National Academy of Sciences, vol. 72, no. 8, pp. 3114-8.

Fredlund, D, Morgenstern, NR & Widger, R 1978, 'The shear strength of unsaturated soils', Canadian Geotechnical Journal, vol. 15, no. 3, pp. 313-21.

Fredlund, DG & Rahardjo, H 1993, 'An overview of unsaturated soil behaviour', Geotechnical special publication, pp. 1-1.

Fredlund, DG, Rahardjo, H & Fredlund, MD 2012, Unsaturated soil mechanics in engineering practice, John Wiley & Sons.

Fredlund, DG, Sheng, D & Zhao, J 2011, 'Estimation of soil suction from the soil-water characteristic curve', Canadian Geotechnical Journal, vol. 48, no. 2, pp. 186-98.

Fritz, SJ & Marine, IW 1983, 'Experimental support for a predictive osmotic model of clay membranes', Geochimica et Cosmochimica Acta, vol. 47, no. 8, pp. 1515-22.

Frydman, S & Baker, R 2009, 'Theoretical soil-water characteristic curves based on adsorption, cavitation, and a double porosity model', International Journal of Geomechanics, vol. 9, no. 6, pp. 250-7.

Fu, J-t, Hu, X-s, Li, X-l, Yu, D-m, Liu, Y-b, Yang, Y-Q, Qi, Z-x & Li, S-x 2019, 'Influences of soil moisture and salt content on loess shear strength in the Xining Basin, northeastern Qinghai-Tibet Plateau', Journal of Mountain Science, vol. 16, no. 5, pp. 1184-97.

Fuentesc, W & Triantafyllidisc, T 2013, 'On the effective stress for unsaturated soils with residual water'. Géotechnique, 63(16), pp.1451-1455.

Fukue, M, Minato, T, Horibe, H & Taya, N 1999, 'The micro-structures of clay given by resistivity measurements', Engineering Geology, vol. 54, no. 1-2, pp. 43-53.

Galpathage, SG, Indraratna, B, Heitor, A & Rujikiatkamjorn, C 2019, 'Pull-out behaviour of simulated tree roots embedded in compacted soil', Proceedings of the Institution of Civil Engineers-Ground Improvement, pp. 1-11.

Ghestem, M, Sidle, RC & Stokes, A 2011, 'The influence of plant root systems on subsurface flow: implications for slope stability', Bioscience, vol. 61, no. 11, pp. 869-79.

Gidigasu, M 1974, 'Degree of weathering in the identification of laterite materials for engineering purposes—a review', Engineering Geology, vol. 8, no. 3, pp. 213-66.

Gleason, MH, Daniel, DE & Eykholt, GR 1997, 'Calcium and sodium bentonite for hydraulic containment applications', Journal of geotechnical and geoenvironmental engineering, vol. 123, no. 5, pp. 438-45.

Gouy, M 1910, 'Sur la constitution de la charge electrique a la surface d'un electrolyte', J. Phys. Theor. Appl., vol. 9, no. 1, pp. 457-68.

Gray, DH & Leiser, AT 1982, Biotechnical slope protection and erosion control, Van Nostrand Reinhold Company Inc.

Gray, DH & Sotir, RB 1996, Biotechnical and soil bioengineering slope stabilization: a practical guide for erosion control, John Wiley & Sons.

Guimarães, LDN, Gens, A, Sánchez, M & Olivella, S 2013, 'A chemo-mechanical constitutive model accounting for cation exchange in expansive clays', Géotechnique, vol. 63, no. 3, pp. 221-34.

Gunnink, BW & El-Jayyousi, J 1993, 'Soil-fabric measurement using phase transition porosimetry', Journal of Geotechnical Engineering, vol. 119, no. 6, pp. 1019-36.

Gwenzi, W, Veneklaas, EJ, Holmes, KW, Bleby, TM, Phillips, IR & Hinz, C 2011, 'Spatial analysis of fine root distribution on a recently constructed ecosystem in a water-limited environment', Plant and soil, vol. 344, no. 1-2, pp. 255-72.

Herman, R 2001, ‘An introduction to electrical resistivity in geophysics’, American Journal of Physics, vol. 69, no. 9, pp. 943-52.

Higginbottom, I 1976, ‘The use of geophysical methods in engineering geology. Part 2: Electrical resistivity, magnetic and gravity methods’, Ground Engineering, vol. 9, no. 2, pp. 34-8.

Hillel, D & Talpaz, H 1976, ‘Simulation of root growth and its effect on the pattern of soil water uptake by a nonuniform root system’, Soil Science, vol. 121, no. 5, pp. 307-12.

Hopkins, WG 1999, Introduction to plant physiology (No. Ed. 2), John Wiley and Sons.

Indraratna, B, Fatahi, B & Khabbaz, H 2006, ‘Numerical analysis of matric suction effects of tree roots’, Proceedings of the Institution of Civil Engineers: Geotechnical Engineering, 159(2), pp.77-90.

Indraratna, B, Sun, Q & Grant, J 2017, ‘Behaviour of subballast reinforced with used tyre and potential application in rail tracks’, Transportation Geotechnics, vol. 12, pp. 26-36.

Jiao-Jun, Z, Hong-Zhang, K & Gonda, Y 2007, ‘Application of Wenner configuration to estimate soil water content in pine plantations on sandy land’, Pedosphere, vol. 17, no. 6, pp. 801-12.

Kalinski, RJ & Kelly, WE 1993, ‘Estimating water content of soils from electrical resistivity’, Geotechnical Testing Journal, vol. 16, no. 3, pp. 323-9.

Karube, D & Kawai, K 2001, ‘The role of pore water in the mechanical behavior of unsaturated soils’, Geotechnical & Geological Engineering, vol. 19, no. 3-4, pp. 211-41.

Keller, GV & Frischknecht, FC 1966, Electrical methods in geophysical prospecting. Pergamon Press Inc., Oxford.

Khalili, N & Khabbaz, M 1998, 'A unique relationship for chi for the determination of the shear strength of unsaturated soils', Géotechnique, vol. 48, no. 5, pp. 681-7.

Khamehchiyan, M, Charkhabi, AH & Tajik, M 2007, 'Effects of crude oil contamination on geotechnical properties of clayey and sandy soils', Engineering Geology, vol. 89, no. 3, pp. 220-9.

Kleidon, A & Heimann, M 1998, 'Optimised rooting depth and its impacts on the simulated climate of an atmospheric general circulation model', Geophysical research letters, vol. 25, no. 3, pp. 345-8.

Konrad, J-M & Lebeau, M 2015, 'Capillary-based effective stress formulation for predicting shear strength of unsaturated soils', Canadian Geotechnical Journal, vol. 52, no. 12, pp. 2067-76.

Krahn, J & Fredlund, D 1972, 'On total, matric and osmotic suction', Soil Science, 114(5), pp.339-348.

Kramer, PJ 1932, 'The absorption of water by root systems of plants', American Journal of Botany, pp. 148-64.

Kutílek, M & Nielsen, DR 1994, Soil hydrology: texbook for students of soil science, agriculture, forestry, geoecology, hydrology, geomorphology and other related disciplines, Catena Verlag.

Landsberg, J & Fowkes, N 1978, 'Water movement through plant roots', Annals of Botany, vol. 42, no. 3, pp. 493-508.

Leong, E, Widiastuti, S, Lee, C & Rahardjo, H 2007, 'Accuracy of suction measurement', Géotechnique, vol. 57, no. 6, pp. 547-56.

Leung, A, Garg, A, Coo, J, Ng, C & Hau, B 2015, 'Effects of the roots of Cynodon dactylon and Schefflera heptaphylla on water infiltration rate and soil hydraulic conductivity', Hydrological processes, vol. 29, no. 15, pp. 3342-54.

Leung, AK, Garg, A & Ng, CWW 2015, 'Effects of plant roots on soil-water retention and induced suction in vegetated soil', Engineering Geology, vol. 193, pp. 183-97.

Leung, FT, Yan, W, Hau, BC & Tham, L 2015, 'Root systems of native shrubs and trees in Hong Kong and their effects on enhancing slope stability', Catena, vol. 125, pp. 102-10.

Li, J, Sun, Da, Sheng, D, Sloan, S & Fredlund, D 2007, 'Preliminary study on soil water characteristics of Maryland clay', in Proceedings of the 3rd Asian Conference on Unsaturated Soils, Nanjing, China, pp. 569-74.

Liang, Y, Hilal, N, Langston, P & Starov, V 2007, 'Interaction forces between colloidal particles in liquid: Theory and experiment', Advances in colloid and interface science, vol. 134, pp. 151-66.

Likos, WJ & Lu, N 2003, 'Automated humidity system for measuring total suction characteristics of clay'. Geotechnical Testing Journal, 26(2), pp.179-190.

Likos, WJ & Lu, N 2004, Unsaturated soil mechanics, John Wiley and Sons Inc., New Jersey.

Lu, N, Godt, JW & Wu, DT 2010, 'A closed-form equation for effective stress in unsaturated soil', Water Resources Research, vol. 46, no. 5., W05515.

Lynch, J 1995, 'Root architecture and plant productivity', Plant physiology, vol. 109, no. 1, p. 7.

Maas, EV & Hoffman, GJ 1977, 'Crop salt tolerance-current assessment', Journal of the irrigation and drainage division, vol. 103, no. 2, pp. 115-34.

Mansouri, H, Ajalloeian, R & Sadeghpour, AH 2013, 'The Investigation of Salinity Effects on Behavioral Parameters of Fine-Grained Soils', Seventh International Conference on Case Histories in Geotechnical Engineering, USA, 2013, pp 1-10.

Mao, Z, Saint-André, L, Genet, M, Mine, F-X, Jourdan, C, Rey, H, Courbaud, B & Stokes, A 2012, 'Engineering ecological protection against landslides in diverse mountain forests: choosing cohesion models', Ecological Engineering, vol. 45, pp. 55-69.

Maps of World 2013, Available in: https://www.mapsofworld.com/australia/states/new-south-wales/, Accessed on: 15.05.2020.

Marcar, N, Crawford, D, Leppert, P, Jovanovic, T, Floyd, R & Farrow, R 1995, Trees for saltland: a guide to selecting native species for Australia, Csiro Publishing.

Marinho, FA 2005, 'Nature of soil–water characteristic curve for plastic soils', Journal of geotechnical and geoenvironmental engineering, vol. 131, no. 5, pp. 654-61.

Mattia, C, Bischetti, GB & Gentile, F 2005, 'Biotechnical characteristics of root systems of typical Mediterranean species', Plant and soil, vol. 278, no. 1-2, pp. 23-32.

McCarter, W 1984, 'The electrical resistivity characteristics of compacted clays', Géotechnique, vol. 34, no. 2, pp. 263-7.

McCollum, B & Logan, KH 1913, 'Electrolytic corrosion of iron in soils', Proceedings of the American Institute of Electrical Engineers, vol. 32, no. 7, pp. 1515-75.

McElrone, AJ, Choat, B, Gambetta, GA & Brodersen, CR 2013, 'Water uptake and transport in vascular plants', Nature Education Knowledge, vol. 4, no. 6.

Memon, SA, Hou, X & Wang, LJ 2010, 'Morphological analysis of salt stress response of pak Choi', Electronic Journal of Environmental, Agricultural & Food Chemistry, vol. 9, no. 1, pp. 248-54.

Michot, D, Benderitter, Y, Dorigny, A, Nicoullaud, B, King, D & Tabbagh, A 2003, 'Spatial and temporal monitoring of soil water content with an irrigated corn crop cover using surface electrical resistivity tomography', Water Resources Research, vol. 39, no. 5, doi:10.1029/2002WR001518.

Milly, P 1997, 'Sensitivity of greenhouse summer dryness to changes in plant rooting characteristics', Geophysical research letters, vol. 24, no. 3, pp. 269-71.

Minhas, P, Ramos, TB, Ben-Gal, A & Pereira, LS 2020, 'Coping with salinity in irrigated agriculture: Crop evapotranspiration and water management issues', Agricultural water management, vol. 227, p. 105832.

Mishra, AK, Ohtsubo, M, Li, LY, Higashi, T & Park, J 2009, 'Effect of salt of various concentrations on liquid limit, and hydraulic conductivity of different soil-bentonite mixtures', Environmental geology, vol. 57, no. 5, pp. 1145-53.

Moore, R 1991, 'The chemical and mineralogical controls upon the residual strength of pure and natural clays', Géotechnique, vol. 41, no. 1, pp. 35-47.

Mori, Y, Hopmans, J, Mortensen, A & Kluitenberg, G 2003, 'Multi-functional heat pulse probe for the simultaneous measurement of soil water content, solute concentration, and heat transport parameters', Vadose Zone Journal, vol. 2, no. 4, pp. 561-71.

Mualem, Y & Friedman, S 1991, 'Theoretical prediction of electrical conductivity in saturated and unsaturated soil', Water Resour. Res, vol. 27, no. 10, pp. 2771-7.

Murray, EJ & Sivakumar, V 2010, Unsaturated soils: a fundamental interpretation of soil behaviour, John Wiley & Sons.

Newman, EI 1976, 'Interaction between osmotic-and pressure-induced water flow in plant roots', Plant physiology, vol. 57, no. 5, pp. 738-9.

Ng, C, Kamchoom, V & Leung, A 2016, 'Centrifuge modelling of the effects of root geometry on transpiration-induced suction and stability of vegetated slopes', Landslides, vol. 13, no. 5, pp. 925-38.

Ng, CW & Pang, Y 2000, 'Experimental investigations of the soil-water characteristics of a volcanic soil', Canadian Geotechnical Journal, vol. 37, no. 6, pp. 1252-64.

Ng, CWW, Garg, A, Leung, A & Hau, B 2016, 'Relationships between leaf and root area indices and soil suction induced during drying–wetting cycles', Ecological Engineering, vol. 91, pp. 113-8.

Ng, CWW, Leung, AK & Woon, K 2013, 'Effects of soil density on grass-induced suction distributions in compacted soil subjected to rainfall', Canadian Geotechnical Journal, vol. 51, no. 3, pp. 311-21.

Ng, CWW, Ni, J, Leung, A, Zhou, C & Wang, Z 2016, 'Effects of planting density on tree growth and induced soil suction', Géotechnique, vol. 66, no. 9, pp. 711-24.

Nobel, P 2009, Physiochemical dan Environmental Plant Physiology, Academic Press, London, UK.

Oloo, S & Fredlund, D 1996, 'A method for determination of φ b for statically compacted soils', Canadian Geotechnical Journal, vol. 33, no. 2, pp. 272-80.

Operstein, V & Frydman, S 2000, 'The influence of vegetation on soil strength', Proceedings of the Institution of Civil Engineers-Ground Improvement, vol. 4, no. 2, pp. 81-9.

Pallewattha, M, Indraratna, B, Heitor, A & Rujikiatkamjorn, C 2019, 'Shear strength of a vegetated soil incorporating both root reinforcement and suction', Transportation Geotechnics, vol. 18, pp. 72-82.

Parkhomenko, EI 2012, Electrical properties of rocks, Springer Science & Business Media.

Pasha, AY, Khoshghalb, A & Khalili, N 2016, 'Pitfalls in interpretation of gravimetric water content–based soil-water characteristic curve for deformable porous media', International Journal of Geomechanics, vol. 16, no. 6, p. D4015004.

Pathirage, U, Indraratna, B, Pallewattha, M & Heitor, A 2017, 'A theoretical model for total suction effects by tree roots', Environmental Geotechnics, pp. 1-8.

Perez, N, Garnica, P, Landaverde, N, Hamza, M, Shahien, M & El-Mossallamy, Y 2009, 'Measurement of soil suction using soil's resistivity', in Proceedings of the 17th International Conference on Soil Mechanics and Geotechnical Engineering: The academia and practice of geotechnical engineering, Alexandria, Egypt, 5-9 October 2009., pp. 245-8.

Perrochet, P 1987, ‘Water uptake by plant roots—A simulation model, I. Conceptual model’, Journal of Hydrology, vol. 95, no. 1-2, pp. 55-61.

Pham, HQ, Fredlund, DG & Barbour, SL 2005, ‘A study of hysteresis models for soil-water characteristic curves’, Canadian Geotechnical Journal, vol. 42, no. 6, pp. 1548-68.

Potter, W 2006, ‘The feasibility of improving rail infrastructure by using native vegetation on clay soils’, Doctoral dissertation, University of South Australia, Adelaide, Australia.

Prasad, R 1988, ‘A linear root water uptake model’, Journal of Hydrology, vol. 99, no. 3-4, pp. 297-306.

Protopapas, AL & Bras, RL 1993, ‘Effects of weather variability and soil parameter uncertainty on the soil-crop-climate system’, Journal of climate, vol. 6, no. 4, pp. 645-56.

Qados, AMA 2011, ‘Effect of salt stress on plant growth and metabolism of bean plant Vicia faba (L.)’, Journal of the Saudi Society of Agricultural Sciences, vol. 10, no. 1, pp. 7-15.

Radcliffe, D, Hayden, T, Watson, K, Crowley, P & Phillips, R 1980, ‘Simulation of soil water within the root zone of a corn crop’, Agronomy Journal, vol. 72, no. 1, pp. 19-24.

Rahardjo, H, Satyanaga, A, Leong, E, Santoso, V & Ng, Y 2014, ‘Performance of an instrumented slope covered with shrubs and deep-rooted grass’, Soils and foundations, vol. 54, no. 3, pp. 417-25.

Rao, SM & Thyagaraj, T 2007, ‘Role of direction of salt migration on the swelling behaviour of compacted clays’, Applied clay science, vol. 38, no. 1, pp. 113-29.

Reshma, A, Singh, D & Sreedeep, S 2004, 'Measuring soil electrical resistivity using a resistivity box and a resistivity probe'. Geotechnical testing journal, 27(4), pp.411-415.

Reynolds, JM 2011, An introduction to applied and environmental geophysics, John Wiley & Sons.

Rhoades, J, Raats, P & Prather, R 1976, 'Effects of liquid-phase electrical conductivity, water content, and surface conductivity on bulk soil electrical conductivity', Soil Science Society of America Journal, vol. 40, no. 5, pp. 651-5.

Ribeiro Heitor, AP 2013, 'Assessment of post-compaction characteristics of an unsaturated silty sand', PhD thesis, University of Wollongong.

Ridley, A, Dineen, K, Burland, J & Vaughan, P 2003, 'Soil matrix suction: some examples of its measurement and application in geotechnical engineering', Géotechnique, vol. 53, no. 2, pp. 241-53.

Rodriguez, P, Dell'Amico, J, Morales, D, Blanco, MS & Alarcón, J 1997, 'Effects of salinity on growth, shoot water relations and root hydraulic conductivity in tomato plants', The Journal of Agricultural Science, vol. 128, no. 04, pp. 439-44.

Sanderson, J 1983, 'Water uptake by different regions of the barley root. Pathways of radial flow in relation to development of the endodermis', Journal of Experimental Botany, vol. 34, no. 3, pp. 240-53.

Scarth, P, Armston, J, Lucas, R & Bunting, P 2019, 'A Structural Classification of Australian Vegetation Using ICESat/GLAS, ALOS PALSAR, and Landsat Sensor Data', Remote Sensing, vol. 11, no. 2, p. 147.

Schmitz, RM 2006, ‘Can the diffuse double layer theory describe changes in hydraulic conductivity of compacted clays?’, Geotechnical & Geological Engineering, vol. 24, no. 6, pp. 1835-44.

Shackelford, CD, Benson, CH, Katsumi, T, Edil, TB & Lin, L 2000, ‘Evaluating the hydraulic conductivity of GCLs permeated with non-standard liquids’, Geotextiles and Geomembranes, vol. 18, no. 2, pp. 133-61.

Shalhevet, J & Bernstein, L 1968, ‘Effects of vertically heterogeneous soil salinity on plant growth and water uptake’, Soil Science, vol. 106, no. 2, pp. 85-93.

Shea, P & Luthin, J 1961, ‘An investigation of the use of the four-electrode probe for measuring soil salinity in situ’, Soil Science, vol. 92, no. 5, pp. 331-9.

Sheets, KR & Hendrickx, JM 1995, ‘Noninvasive soil water content measurement using electromagnetic induction’, Water Resources Research, vol. 31, no. 10, pp. 2401-9.

Siau, J 1984, Transport processes in wood, Springer, Berlin, Germany.

Skaggs, TH, van Genuchten, MT, Shouse, PJ & Poss, JA 2006, ‘Macroscopic approaches to root water uptake as a function of water and salinity stress’, Agricultural water management, vol. 86, no. 1, pp. 140-9.

Sreedeep, S & Singh, D 2008, ‘A critical review of the methodologies employed for suction measurement for developing the SWCC’, The 12th International Conference of International Association for Computer Methods and Advances in Geomechanics (IACMAG), Goa, India, pp. 1988-1993.

Sudduth, KA, Kitchen, N, Bollero, G, Bullock, D & Wiebold, W 2003, 'Comparison of electromagnetic induction and direct sensing of soil electrical conductivity', Agronomy Journal, vol. 95, no. 3, pp. 472-82.

Sudnitsyn, I, Smagin, A & Shvarov, A 2012, 'The theory of Maxwell-Boltzmann-Helmholtz-Gouy about the double electric layer in disperse systems and its application to soil science (on the 100th anniversary of the paper published by Gouy)', Eurasian Soil Science, vol. 45, no. 4, pp. 452-7.

Sumner, ME & Naidu, R 1998, Sodic soils: distribution, properties, management and environmental consequences, No. 631.416 S6, Oxford University Press.

Tang, G, Graham, J & Fredlund, D 1997, 'Effects of osmotic suction on strength of unsaturated highly plastic clays', in Proceedings of the 50th Canadian Geotechnical Conference, Golden Jubilee, Ottawa, pp. 641-8.

Taylor, HM & Klepper, B 1975, 'Water uptake by cotton root systems: an examination of assumptions in the single root model', Soil Science, vol. 120, no. 1, pp. 57-67.

Telford, WM, Geldart, LP & Sheriff, RE 1990, Applied geophysics, vol. 1, Cambridge University press.

Terzaghi, Kv 1936, 'The shearing resistance of saturated soils and the angle between the planes of shear', in Proceedings of the 1st international conference on soil mechanics and foundation engineering, vol. 1, pp. 54-6.

Thakur, VK, Sreedeep, S & Singh, DN 2006, 'Laboratory investigations on extremely high suction measurements for fine-grained soils', Geotechnical & Geological Engineering, vol. 24, no. 3, pp. 565-78.

Thevanayagam, S 1993, ‘Electrical response of two-phase soil: theory and applications’, Journal of Geotechnical Engineering, vol. 119, no. 8, pp. 1250-75.

Thu, TM, Rahardjo, H & Leong, E-C 2007, ‘Soil-water characteristic curve and consolidation behavior for a compacted silt’, Canadian Geotechnical Journal, vol. 44, no. 3, pp. 266-75.

Thyagaraj, T & Rao, SM 2010, ‘Influence of osmotic suction on the soil-water characteristic curves of compacted expansive clay’, Journal of geotechnical and geoenvironmental engineering, vol. 136, no. 12, pp. 1695-702.

Thyagaraj, T & Salini, U 2015, ‘Effect of pore fluid osmotic suction on matric and total suctions of compacted clay’, Géotechnique, vol. 65, no. 11, pp. 952-60.

Tiwari, B & Ajmera, B 2014, ‘Reduction in fully softened shear strength of natural clays with NaCl leaching and its effect on slope stability’, Journal of geotechnical and geoenvironmental engineering, vol. 141, no. 1, p. 04014086.

Van Olphen, H 1977, An introduction to clay colloid chemistry: for clay technologists, geologists, and soil scientists, 2nd ed., Wiley Interscience, New York.

Vanapalli, SK, Fredlund, D & Pufahl, D 1999, ‘The influence of soil structure and stress history on the soil-water characteristics of a compacted till’. Geotechnique, 49(2), pp.143-159.

Vanapalli, SK, Fredlund, D, Pufahl, D & Clifton, A 1996, ‘Model for the prediction of shear strength with respect to soil suction’, Canadian Geotechnical Journal, vol. 33, no. 3, pp. 379-92.

Vanapalli, SK, Fredlund, DG & Pufahl, DE 1996, 'The relationship between the soil-water characteristic curve and the unsaturated shear strength of a compacted glacial till', Geotechnical Testing Journal, vol. 19, no. 3, pp. 259-68.

Wagner, A-M, Houston, SL & Houston, WN 1994, 'Laboratory filter paper suction measurements'. Geotechnical Testing Journal, 17(2), pp.185-194.

Waldron, L 1977, 'The shear resistance of root-permeated homogeneous and stratified soil', Soil Science Society of America Journal, vol. 41, no. 5, pp. 843-9.

Ward, SH 1990, 'Resistivity and induced polarization methods', Geotechnical and environmental geophysics, vol. 1, pp. 147-89.

Weatherley, P 1970, 'Some aspects of water relations', Advances in botanical research, vol. 3, pp. 171-206.

Wissmeier, L & Barry, D 2008, 'Reactive transport in unsaturated soil: Comprehensive modelling of the dynamic spatial and temporal mass balance of water and chemical components', Advances in Water Resources, vol. 31, no. 5, pp. 858-75.

Woon, KX, Leung, AK, Ng, CW, Chu, L & Hau, B 2011, 'An experimental investigation on suction influence zone induced by plant transpiration', Unsaturated Soils: Theory and Practice, Proceeding of the 5 Asia-Pacific Conference on Unsaturated Soils, Dusit Thani Pattaya, Thailand. Vol II, pp. 861-866.

Wu, TH 1976, 'Investigation of landslides on prince of Wales Island, Alaska, Ohio State University', Geotechnical Engineering Report 5, Department of Civil Engineering, Ohio State University, Columbia, Ohio, Geotechnical Engineering Report N5, pp. 93.

Xiao, M, Reddi, LN & Steinberg, SL 2009, 'Variation of water retention characteristics due to particle rearrangement under zero gravity', International Journal of Geomechanics, vol. 9, no. 4, pp. 179-86.

Xu, Y 2004, 'Fractal approach to unsaturated shear strength', Journal of geotechnical and geoenvironmental engineering, vol. 130, no. 3, pp. 264-73.

Yan, M, Miao, L & Cui, Y 2012, 'Electrical resistivity features of compacted expansive soils', Marine Georesources & Geotechnology, vol. 30, no. 2, pp. 167-79.

Yilmaz, H & Kina, A 2008, 'The influence of NaCl salinity on some vegetative and chemical changes of strawberries (Fragaria x ananssa L.)', African Journal of Biotechnology, vol. 7, no. 18, pp. 3299-3305.

Yong, RN, Mohamed, A-MO & Warkentin, BP 1992, Principles of contaminant transport in soils, Elsevier Science Publishers.

Zeng, X, Dai, YJ, Dickinson, RE & Shaikh, M 1998, 'The role of root distribution for climate simulation over land', Geophysical research letters, vol. 25, no. 24, pp. 4533-6.

Zhang, L, Sun, Da & Jia, D 2016, 'Shear strength of GMZ07 bentonite and its mixture with sand saturated with saline solution', Applied clay science, vol. 132, pp. 24-32.

Zhou, A, Huang, R & Sheng, D 2016, 'Capillary water retention curve and shear strength of unsaturated soils', Canadian Geotechnical Journal, vol. 53, no. 6, pp. 974-87.

APPENDIX A: Previous models for the shear strength of unsaturated soil

Reference	Equation
Bishop (1959)	$\tau' = c' + [(\sigma - u_a) + \chi(u_a - u_w)] \tan \phi'$
Greacen (1960)	$\tau' = [\sigma + (u_a - u_w)] \tan \phi' (1 - n_a)$
Sridharan (1970)	$\tau' = f[\sigma - u_w - R - A]$
Fredlund et al. (1978)	$\tau' = c' + (\sigma - u_a) \tan \phi' + (u_a - u_w) \tan \phi^b$
Satija (1978)	$[\frac{(\sigma_1 - \sigma_3)_f}{2}] = c' + (\sigma_3 - u_a)_f \tan \alpha + (u_a - u_w) \tan \beta$
Lamborn (1986)	$\tau' = c' + (\sigma - u_a) \tan \phi' + (u_a - u_w)\theta_w \tan \phi'$
Karube (1988)	$q = M'[p + f(u_a - u_w)]$
Peterson (1988)	$\tau' = c' + (\sigma - u_a) \tan \phi' + C_\psi$
Abramento and Carvalho (1989)	$\tau' = c' + (\sigma - u_a) \tan \phi' + \alpha(u_a - u_w)^\beta$

Toll (1990)	$q = M_a(p - u_a) + M_w(u_a - u_w)$
Lu (1992)	$\tau' = c' + (\sigma - u_a)\tan\phi' + P_s \tan\phi'$
Wheeler and Sivakumar (1995)	$q = Mp' + \mu(u_a - u_w)$
Rohm and Vilar (1995)	$q = c^{"} + (p - u_a)\, tan\alpha'$
Shen and Yu (1996)	$\tau' = c' + (\sigma - u_a)\tan\phi' + (u_a - u_w)\left[\frac{1}{1 + d(u_a - u_w)}\right]\tan\phi'$
Vanapalli, et al. (1996)	$\tau' = c' + (\sigma - u_a)\tan\phi' + (u_a - u_w)\left(\frac{\theta_w - \theta_r}{\theta_s - \theta_r}\right)\tan\phi'$
	$\tau' = c' + (\sigma - u_a)\tan\phi' + (u_a - u_w)\Theta^K \tan\phi'$
Öberg and Sällfors (1997)	$\tau' = c' + (\sigma - u_a) + (u_a - u_w)S\tan\phi'$

Chenggang et al. (1998)	$\tau' = c' + (\sigma - u_a)\tan\phi' + (u_a - u_w)\left(\frac{log(u_a - u_w)_r - log(u_a - u_w)}{log(u_a - u_w)_r - log(u_a - u_w)_b}\right)\tan\phi'$
Khalili and Khabbaz (1998)	$\tau' = c' + (\sigma - u_a)\tan\phi' + (u_a - u_w)\left[\frac{(u_a - u_w)}{(u_a - u_w)_b}\right]^{\eta}\tan\phi'$
Shenggang et al. (1998)	$\tau' = c' + (\sigma - u_a)\tan\phi' + (u_a - u_w)\left[\frac{1}{\frac{1}{tan\alpha} + \frac{(u_a - u_w)}{\beta}}\right]$
Rassam and Williams (1999b)	$\tau' = c' + \sigma\tan\phi' + (u_a - u_w)\tan\phi' - \phi'[(u_a - u_w) - (u_a - u_w)_b]^{\beta}$
Xu and Sun (2002)	$\tau' = c' + (\sigma - u_a)\tan\phi' + m^{(1-\zeta)}(u_a - u_w)^{\zeta}\tan\phi'$
Miao et al. (2002)	$\tau' = c' + (\sigma - u_a)\tan\phi' + \left[\frac{a_1(u_a - u_w)}{1 + \frac{1 - a_1}{p_a}(u_a - u_w)}\right]$

Rassam and Williams (1999a)	$\tau' = c' + (\sigma - u_a)\tan\phi' + (u_a - u_w)\tan\phi' - \left[\frac{(u_a - u_w)_r \tan\phi' - \tau_{S_r}}{[(u_a - u_w)_r - (u_a - u_w)_b]^{\beta}}\right] * [(u_a - u_w)_r - (u_a - u_w)_b]^{\frac{(\tan\phi'[(u_a - u_w)_r - (u_a - u_w)_b)}{\tan\phi'(u_a - u_w)_r - \tau_{S_r}}}$
Aubeny and Lytton (2003)	$\tau' = c' + (\sigma - u_a)\tan\phi' + f_1(u_a - u_w)\theta\tan\phi'$
Lee et al. (2003)	$\tau' = c' + (\sigma - u_a)\tan\phi' + \frac{(u_a - u_w)}{a_2 + b_3(u_a - u_w)}$
Schick (2004)	$\tau' = c' + (\sigma - u_a)\tan\phi' + \frac{(u_a - u_w)}{a_2 + b_2(u_a - u_w)}$
Tekinsoy et al. (2004)	$\tau' = c' + (\sigma - u_a)\tan\phi' + [(u_a - u_w)_b + p_a]\tan\phi' * \ln\left[\frac{(u_a - u_w) + p_a}{p_a}\right]$
Xu (2004)	$\tau' = c' + (\sigma - u_a)\tan\phi' + (u_a - u_w)_b{}^{(1-\zeta)}(u_a - u_w)^{\zeta}\tan\phi'$

Jiang et al. (2004)	$\tau' = c' + (\sigma - u_a)\tan\phi' + \left[\frac{(u_a - u_w)}{a + d(u_a - u_w)}\right]\tan\phi'$
	$\tau' = c' + (\sigma - u_a)\tan\phi' + \left[1 - \frac{S - S_r}{100 - S_r}\right]\sigma_{eqm}\tan\phi'$
Lee et al. (2005)	$\tau' = c' + (\sigma - u_a)\tan\phi' + (u_a - u_w)_b \tan\phi' + [(u_a - u_w) - (u_a - u_w)_b]\Theta^K[1 + \lambda(\sigma - u_a)]\tan\phi'$
Matsushi and Matsukura (2006)	$\tau' = \sigma'\tan\phi' + Ce^{-\mu\theta_w}$
Vilar (2006)	$\tau' = c' + (\sigma - u_a)\tan\phi' + \frac{(u_a - u_w)}{\left[\frac{1}{\tan\phi'} + \left(\frac{1}{\tau_m - c'} - \frac{1}{(u_a - u_w)_m \tan\phi'}\right)\right]}$
Sheng et al. (2008)	$\tau' = c' + (\sigma - u_a)\tan\phi' + s\tan\phi' \ : \ s \le s_{sa}$ $\tau' = c' + (\sigma - u_a)\tan\phi' + \tan\left(\phi' s_{sa} + (s_{sa} + 1)\ln\left(\frac{s + 1}{s_{sa} + 1}\right)\right) : s \le s_{sa}$

Hamid and Miller (2009)	$\tau_f{}' = c_a{}' + (\sigma_{nf} - u_{af}) \tan \delta' + (u_{af} - u_{wf}) \tan \delta^b$
	$\tau_f{}' = c_a{}' + (\sigma_{nf} - u_{af}) \tan \delta' + (u_{af} - u_{wf})(\frac{\theta - \theta_r}{\theta_s - \theta_r}) \tan \delta'$
Alonso et al. (2010)	$\tau' = c' + (\sigma - p_g) \tan \phi' + S_r{}^e s \tan \phi'$
Lu et al. (2010)	$\tau' = c' + (\sigma - u_a + (u_a - u_w)) \tan \phi' \quad : (u_a - u_w) \leq 0$ $\tau' = c' + \left(\sigma - u_a + \frac{(u_a - u_w)}{(1 + [\alpha(u_a - u_w)]^n)^{(\frac{n-1}{n})}} \right) \tan \phi' \quad : (u_a - u_w) > 0$
Oh et al. (2011)	$\tau' = c' + \left(\sigma - u_a + \frac{1}{\alpha} \left(\frac{\theta - \theta_r}{\theta_s - \theta_r} \right) \left[\left(\frac{\theta - \theta_r}{\theta_s - \theta_r} \right)^{\left(\frac{n}{n-1}\right)} - 1 \right]^{\frac{1}{n}} \right) \tan \phi'$

Konrad and Lebeau (2015)	$\tau' = c' + (\sigma - u_a + S_{r,c}s)\tan\phi'$
Zhou et al. (2016)	$\tau' = c' + \left[(\sigma - u_a) + (u_a - u_w)\frac{A_w{}^{cap}}{A}\right]\tan\phi'$
	$\tau' = c' + \left[(\sigma - u_a) + (u_a - u_w)\frac{A_w}{A}\right]\tan\phi'$
Wang et al. (2017)	$\tau' = (\sigma - u_a)\,tan\,\phi' + \left[1 + \left(\frac{d_{60}(u_a - u_w)}{C_2\gamma}\right)^{\frac{C_1}{log_{10}(C_u)}+1}\right]^{\frac{-C_1}{C_1+log_{10}(C_u)}} * (u_a - u_w)\theta\,tan\,\phi'$

APPENDIX B: Determination of optimum electrode spacing

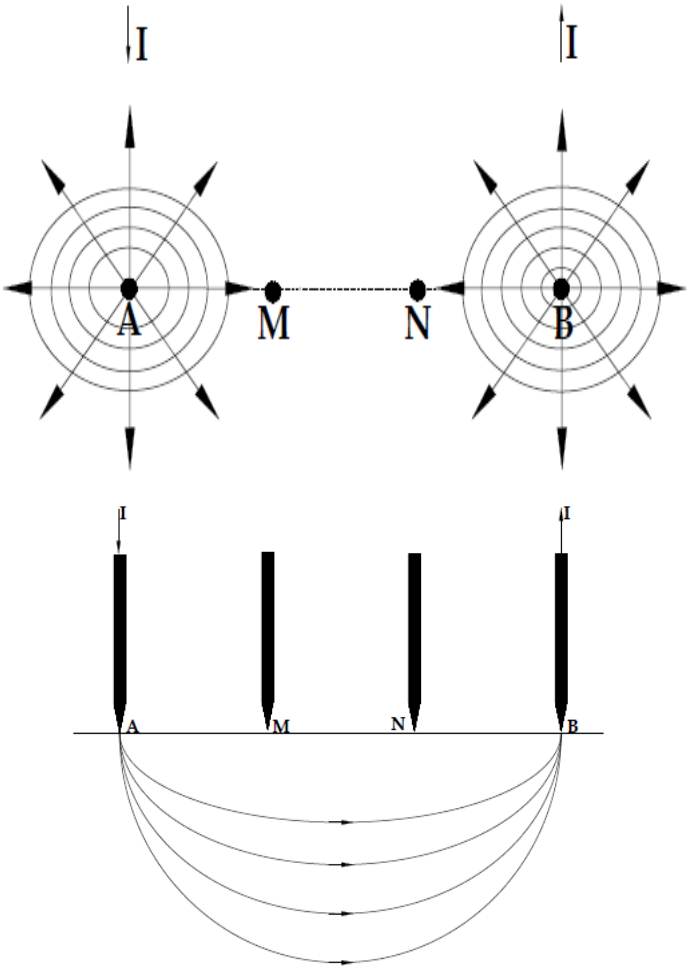

Figure B: 1 Current flow patterns through electrodes into soil

Based on current flow, the potential;

$$V = \frac{I\rho}{2\pi S_{el}} \tag{B.1}$$

Here, the distances AM = MN = NB = S_{el};

According to Schuetze et al. (2004)

$$V_M = V_M I_A + V_M I_B + V_M I_A' + V_M I_B' \quad \text{(B.2)}$$

$$V_N = V_N I_A + V_N I_B + V_N I_A' + V_N I_B' \quad \text{(B.3)}$$

Where, V_M and V_N are the electric potentials at point M and N respectively. I_A and I_B are the current flows through the point A and point B respectively. I_A' and I_B' are the current flow due to reflection (virtual current).

The electrical resistivity of soil has to be calculated in the laboratory. So, in such cases, the space for distribution of current within the soil is very limited, since the soil is packed into a box or any other container. When current flows into the soil, it can be reflected upon obstacles such as walls of the box; thus the reflected current behaves as formed from another source (electrode) which is called as virtual electrode (Figure B: 2). This is an error; therefore this effect has to be omitted by selecting the optimum electrode spacing.

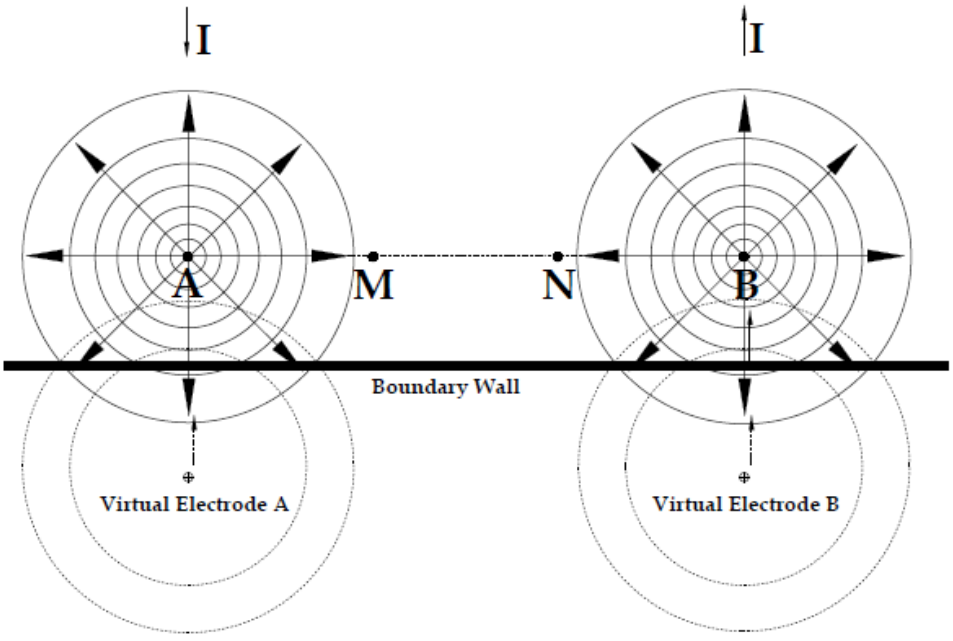

Figure B: 2 Formation of virtual electrodes with boundary walls

(After Schuetze et al. (2004))

Schuetze et al. (2004) figured out this effect and came up with an equation and electrode spacing, by analysing only a single boundary wall. But when the resistivity experiments are carried out in lab scale boxes, the reflection of current upon the wall and formation of virtual electrodes are taken place due to each boundary wall.

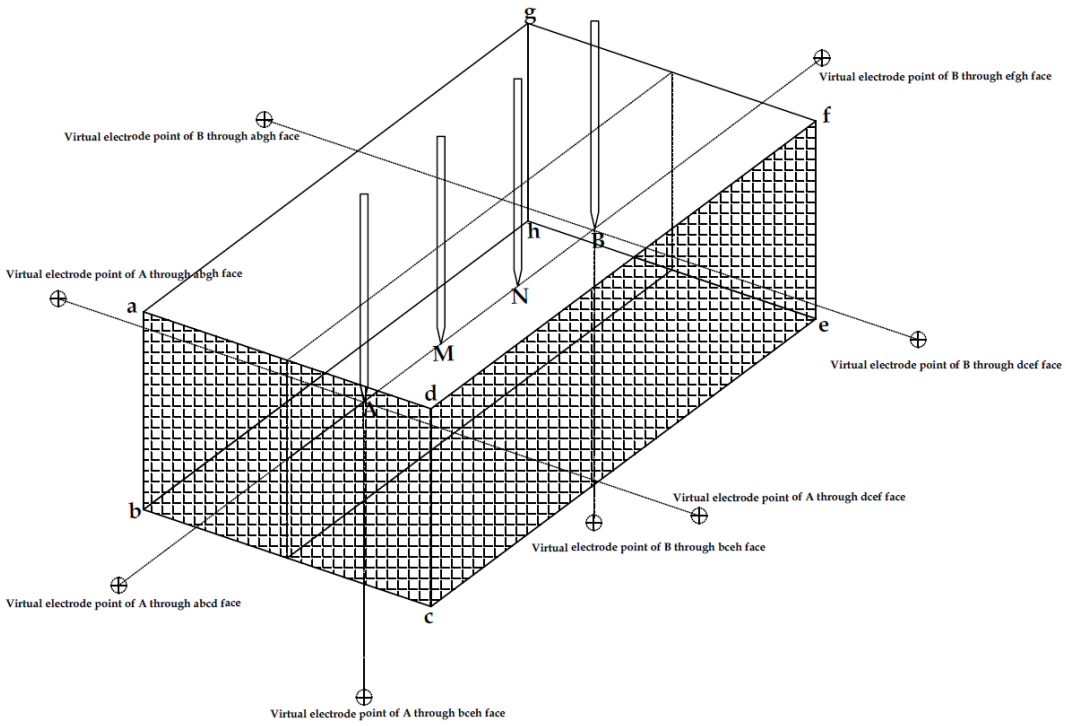

Figure B: 3 Virtual electrodes of a box shaped set up

The Schuetze et al. (2004)'s work can be extended to all boundary conditions as reference to the Figure B: 3;

$$V_M = V_M I_A + V_M I_B + V_M {I_1}^A + V_M {I_2}^A + V_M {I_3}^A + V_M {I_4}^A + V_M {I_5}^A \quad \text{(B.4)}$$
$$+ V_M {I_1}^B + V_M {I_2}^B + V_M {I_3}^B + V_M {I_4}^B + V_M {I_5}^B$$

Where, ${I_1}^A$ to ${I_5}^A$ are the virtual current generated with respect to I_A from each wall face respectively and ${I_1}^B$ to ${I_5}^B$ are the virtual current generated with respect to I_B from each wall face respectively. Theoretically, the values of ${I_3}^A$ and ${I_1}^B$ will be negligible, due to the longer flow distance compared to other faces.

Therefore the above equation can be re-written as follows;

$$V_M = V_M I_A + V_M I_B + V_M {I_1}^A + V_M {I_2}^A + V_M {I_4}^A + V_M {I_5}^A + V_M {I_2}^B + V_M {I_3}^B + V_M {I_4}^B + V_M {I_5}^B \quad \text{(B.5)}$$

Where, the distance from abcd face to the virtual electrode of A through abcd face is x_1, the distance from dcef face to the virtual electrode of A through dcef face is x_2, the distance from dcef face to the virtual electrode of B through dcef face is x_2, the distance from efgh face to the virtual electrode of B through efgh face is x_3, the distance from abgh face to the virtual electrode of B through abgh face is x_4, the distance from abgh face to the virtual electrode of A through abgh face is x_4, the distance from bceh face to the virtual electrode of A through bceh face is x_5 and the distance from bceh face to the virtual electrode of B through bceh face is x_5.

According to the Equation (B.5) at Point M;

$$V_M I_A = -\frac{I\rho}{2\pi S_{el}} \quad \text{(B.6)}$$

$$V_M I_B = \frac{I\rho}{4\pi S_{el}} \quad \text{(B.7)}$$

$$V_M {I_1}^A = -\frac{I\rho}{2\pi(S_{el} + 2x_1)} \quad \text{(B.8)}$$

$$V_M {I_2}^A = -\frac{I\rho}{2\pi\sqrt{{S_{el}}^2 + 4{x_2}^2}} \quad \text{(B.9)}$$

$$V_M {I_4}^A = -\frac{I\rho}{2\pi\sqrt{{S_{el}}^2 + 4{x_4}^2}} \quad \text{(B.10)}$$

$$V_M {I_5}^A = -\frac{I\rho}{2\pi\sqrt{{S_{el}}^2 + 4{x_5}^2}} \quad \text{(B.11)}$$

$$V_M {I_2}^B = \frac{I\rho}{2\pi\sqrt{4{S_{el}}^2 + 4{x_2}^2}} \quad \text{(B.12)}$$

$$V_M {I_3}^B = \frac{I\rho}{2\pi(2S_{el} + 2x_3)} \quad \text{(B.13)}$$

$$V_M {I_4}^B = \frac{I\rho}{2\pi\sqrt{4{S_{el}}^2 + 4{x_4}^2}} \quad \text{(B.14)}$$

$$V_M {I_5}^B = \frac{I\rho}{2\pi\sqrt{4{S_{el}}^2 + 4{x_5}^2}} \quad \text{(B.15)}$$

The Equation (B.5) can be re-written with respect to point N as follows;

$$V_N = V_N I_A + V_N I_B + V_N {I_1}^A + V_N {I_2}^A + V_N {I_4}^A + V_N {I_5}^A + V_N {I_2}^B + V_N {I_3}^B + V_N {I_4}^B + V_N {I_5}^B \quad \text{(B.16)}$$

Then, according to the Equation (B.16) at Point N;

$$V_N I_A = -\frac{I\rho}{4\pi S_{el}} \quad \text{(B.17)}$$

$$V_N I_B = \frac{I\rho}{2\pi S_{el}} \quad \text{(B.18)}$$

$$V_N {I_1}^A = -\frac{I\rho}{2\pi(2S_{el} + 2x_1)} \tag{B.19}$$

$$V_N {I_2}^A = -\frac{I\rho}{2\pi\sqrt{4{S_{el}}^2 + 4{x_2}^2}} \tag{B.20}$$

$$V_N {I_4}^A = -\frac{I\rho}{2\pi\sqrt{4{S_{el}}^2 + 4{x_4}^2}} \tag{B.21}$$

$$V_N {I_5}^A = -\frac{I\rho}{2\pi\sqrt{4{S_{el}}^2 + 4{x_5}^2}} \tag{B.22}$$

$$V_N {I_2}^B = \frac{I\rho}{2\pi\sqrt{{S_{el}}^2 + 4{x_2}^2}} \tag{B.23}$$

$$V_N {I_3}^B = \frac{I\rho}{2\pi(S_{el} + 2x_3)} \tag{B.24}$$

$$V_N {I_4}^B = \frac{I\rho}{2\pi\sqrt{{S_{el}}^2 + 4{x_4}^2}} \tag{B.25}$$

$$V_N {I_5}^B = \frac{I\rho}{2\pi\sqrt{{S_{el}}^2 + 4{x_5}^2}} \tag{B.26}$$

Further, the potential difference between point M and point N can be estimated;

$$V_{MN} = (V_M - V_N) \tag{B.27}$$

By adding Equations B.6 – B.15 and B.17 – B.26 to B.27;

$$V_{MN} = \frac{I\rho}{2\pi} * \frac{1}{K'} \tag{B.28}$$

Where, K' is a parameter depends on the spacing between electrodes and the boundary wall of the container.